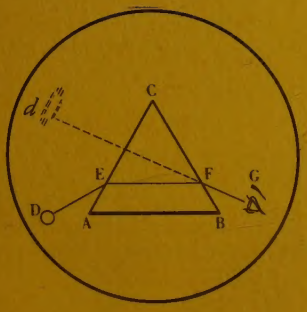

UNIVERSITY OF ILLINOIS
LIBRARY
JUN 27 1961
CHICAGO

optics and spectroscopy

volume x
number 3
march 1961

OPTICAL SOCIETY OF AMERICA

USSR ACADEMY OF SCIENCES

RUSSIAN EDITORIAL STAFF FOR
OPTIKA I SPEKTROSKOPIYA sponsored by
USSR ACADEMY OF SCIENCES

Editor: S. E. FRISH

Assistant Editor: P. P. FEOFILOV
Corresponding Secretary: L. S. SAZONOV

Associate Editors:

M. M. GUREVICH M. A. EL'IASHEVICH A. A. LEBEDEV V. P. LINNIK
S. L. MANDEL'SHTAM I. V. OBREIMOV V. K. PROKOF'EV
N. N. SOBOLEV A. N. TERENIN A. I. TUDOROVSKII

Translated from *OPTIKA I SPEKTROSKOPIYA* on the initiative of THE OPTICAL SOCIETY OF AMERICA, INC. with a grant-in-aid from THE NATIONAL SCIENCE FOUNDATION. *Optics and Spectroscopy* is a cover-to-cover translation of *Optika i Spektroskopiya* and no attempt is made to edit the material other than to correct obvious misprints. The views are those of the original authors and do not represent the Optical Society of America.

TRANSLATION EDITORIAL STAFF

Scientific Editors

CYRUS FELDMAN, *Oak Ridge National Laboratory*

CARL W. GARLAND, *Massachusetts Institute of Technology*

MATHEW G. GIBBONS, *Oakland, California*

Administrative Editor: PATRICIA R. WAKELING, *OSA*

Published monthly by the Optical Society of America, Inc. Executive office: 1155 Sixteenth Street, N.W., Washington, D.C. Subscriptions for one year to members of the Society: Associates $13.00; Regular members and Fellows $17.00. Subscriptions for non-members of the Society: One year U. S. and Possessions, $25.00; Foreign $28.00. Back numbers: $3.00 per copy. Subscriptions, changes of address and undeliverable copies should be referred to the Executive offices in Washington, D.C. The office of publication is 2500 South State Street, Ann Arbor, Michigan. Second class postage paid at Ann Arbor, Michigan.

Printed in the U.S.A. by Edwards Brothers, Inc., Ann Arbor, Michigan.

ON THE QUANTUM THEORY OF THE VAVILOV-CHERENKOV RADIATION EMITTED BY A PARTICLE WITH A MAGNETIC MOMENT

A. B. Kukanov (pp. 289-296)

Received 21 April 1960

The methods of relativistic quantum electrodynamics are used to investigate the emission of Vavilov-Cherenkov radiation by a particle having a magnetic moment, moving in a ferrodielectric medium. Two possible forms of the interaction (μ_0; **B**, **E**, and μ_0; **H**, **D**) between the magnetic moment and the quantized electromagnetic field in the medium are considered. The polarization of the radiation is studied. The character of the radiation and the quantum mechanism of the emission process are considered in detail in the extreme relativistic case ($\beta \to 1$), and also for $\cos\theta = 1$.

1. The emission of Vavilov-Cherenkov radiation by a particle with a magnetic moment has been considered in a number of papers;[1-15] both classical and quantum theoretical methods have been used. However, the formulas obtained by different authors for the intensity of the radiation emitted in a direction perpendicular to the velocity vector of the moving particle do not agree.

Ginzburg and Eidman[11] (see also refs. 4 and 13) pointed out that some authors[3,7,8] use a model of the magnetic moment consisting of magnetic poles, while other authors start from the concept of a currentlike moment. Since a moving "true" magnetic moment is equivalent to a currentlike moment in empty space only, the above-mentioned differences in the corresponding formulas are to be expected.

Vavilov-Cherenkov radiation is not the only physical phenomenon which can reveal the "nature" of the magnetic moment. In the formulation of a theory of the magnetic scattering of neutrons, models have been considered in which the neutron is replaced either by a point-dipole or by an element of current.[16-18] But magnetic scattering experiments have shown that neutrons behave like current elements, not like point-dipoles.

2. In this paper, the methods of relativistic quantum electrodynamics are used to investigate the emission of Vavilov-Cherenkov radiation by neutral Dirac particles ($e = 0$) possessing a magnetic moment μ_0. For brevity, we shall henceforth speak of the motion and emission of radiation by magnetic moments.

The Dirac equation for a magnetic moment has the form:[19,20]

$$-\frac{\hbar}{i}\frac{\partial}{\partial t}\psi = \left(\frac{c\hbar}{i}(\alpha\nabla) + U + \rho_3 m_0 c^2\right)\psi. \tag{1}$$

where, as usual, $\hbar$ is Planck's constant divided by 2π, c is the velocity of light in vacuo, m_0 is the mass of the magnetic moment, α and ρ_3 are the familiar Dirac matrices, and U is the operator of the energy of interaction of the magnetic moment with the electromagnetic field in the medium. We shall assume that the magnetic moment moves in a transparent ferrodielectric medium with the characteristics $\varepsilon(\omega)$ (dielectric susceptibility) and $\mu(\omega)$ (magnetic susceptibility).

We consider two possible forms of the interaction of the magnetic moment with the electromagnetic field in the medium, corresponding to two different expressions for the operator of the interaction energy:

$$U^{B,E} = -\mu_0[\rho_3(\sigma B) + \rho_2(\sigma E)] \tag{2}$$

and

$$U^{H,D} = -\mu_0[\rho_3(\sigma H) + \rho_2(\sigma D)]. \tag{3}$$

In Eqs. (2) and (3) σ and ρ_2 are Dirac matrices. The expression for the vector potential **A** of the quantized transverse electromagnetic field in the ferrodielectric medium is written in the form:

$$\mathbf{A} = L^{-\frac{3}{2}}\sum_{\varkappa}\left(\frac{2\pi c''\hbar}{\varkappa}\right)^{\frac{1}{2}} \times[\mathbf{a}\exp(-ic'\varkappa t + i\varkappa\mathbf{r}) + \mathbf{a}^{+}\exp(ic'\varkappa t - i\varkappa\mathbf{r})], \tag{4}$$

where L^3 is the volume of the basic parallelepiped,

$$c' = \frac{c}{n} = \frac{c}{\sqrt{\varepsilon\mu}}, \quad c'' = c'\mu$$

and $\hbar\kappa$ is the momentum of the photon. The amplitudes **a** and $\mathbf{a}^+$ obey the commutation relations:

$$a_{\varkappa n}a'^{+}_{\varkappa' n'} - a'^{+}_{\varkappa' n'}a_{\varkappa n} = \delta_{x_1x_1'}\delta_{x_2x_2'}\delta_{x_3x_3'}\left(\delta_{nn'} - \frac{\varkappa_n\varkappa_{n'}}{\varkappa^2}\right), \quad n, n' = 1, 2, 3. \tag{5}$$

In particular, if photons are not initially present (which we shall hereinafter assume to be the case), one can write

$$\left.\begin{aligned} a'^{+}_{\varkappa' n'}a_{\varkappa n} &= 0, \\ a_{\varkappa n}a'^{+}_{\varkappa' n'} &= \delta_{x_1x_1'}\delta_{x_2x_2'}\delta_{x_3x_3'}\left(\delta_{nn'} - \frac{\varkappa_n\varkappa_{n'}}{\varkappa^2}\right) \end{aligned}\right\}. \tag{6}$$

In order to investigate the polarization of the radiation, we resolve the amplitude **a** of the vector potential **A** into components characterizing the different states of polarization. In investigating linear polarization we resolve **a** into two mutually perpendicular components as follows:[19,22]

$$\mathbf{a} = \mathbf{a}_2 + \mathbf{a}_3 = \beta_2 q_2 + \beta_3 q_3, \tag{7}$$

$$\left.\begin{aligned} \beta_2 &= [\mathbf{x}^0\mathbf{k}^0](1 - (\mathbf{x}^0\mathbf{k}^0)^2)^{-\frac{1}{2}}, \\ \beta_3 &= [\mathbf{x}^0\beta_2]. \end{aligned}\right\} \tag{8}$$

κ^0 is the unit vector in the direction κ, and $\mathbf{k}^0$ is the unit vector along the direction of motion of the magnetic moment.

In investigating circular polarization, we represent the amplitude **a** by two components in the following way:

$$\mathbf{a} = \mathbf{a}_1 + \mathbf{a}_{-1} = \beta_1 q_1 + \beta_{-1} q_{-1}, \tag{9}$$

$$\beta_j = \frac{\beta_2 + ij\beta_3}{\sqrt{2}}, \quad j = -1, 1. \tag{10}$$

Following the tradition of classical optics, we should assume that $j = +1$ corresponds to left-handed circular polarization, and $j = -1$ to right-handed polarization.[19,23,24] In Eqs. (7) and (9), the quantized parts of the amplitudes

obey the following relations:

$$q_{j'}^{+}=0, \quad q_j q_{j'}^{+}=\delta_{jj'}, \qquad (11)$$
$$j,\ j'=-1,\ 1,\ 2,\ 3.$$

Considering that

$$\mathbf{B}=\operatorname{rot}\mathbf{A}, \qquad (12)$$

$$\mathbf{E}=-\frac{1}{c}\frac{\partial \mathbf{A}}{\partial t}, \qquad (13)$$

$$\mathbf{D}=\varepsilon\mathbf{E}, \quad \mathbf{B}=\mu\mathbf{H}, \qquad (14)$$

and that there are no photons present initially, we obtain the following expression for the operator of the energy of interaction of the magnetic moment with the electromagnetic field in the medium:

$$U_j^{(N)+}=i\mu_0 L^{-\frac{3}{2}}\sum_{\varkappa}(2\pi c'\hbar\varkappa)^{\frac{1}{2}}\mu^{\frac{N}{2}}\left\{\rho_3(\sigma[\mathbf{x}^0\mathbf{a}_j^{+}])+n^{-N}\rho_2(\sigma\mathbf{a}_j^{+})\right\} \times\exp(ic'\varkappa t-i\varkappa\mathbf{r}). \qquad (15)$$

From here on, we should use N = +1 for the interaction μ_0; B, E [Eq. (2)], and N = −1 for the interaction μ_0; H, D [Eq. (3)]. Using perturbation theory, it is not difficult to obtain an expression for the probability of emission of radiation by the magnetic moment:

$$w_j^{(N)}(ss')=\frac{2\pi}{c\hbar^2}\sum_{\mathbf{k}'}\sum_{\varkappa}R_j^{(N)+}(ss')\,R_j^{(N)}(ss')\,\delta_{\mathbf{k},\,\mathbf{k}'+\varkappa}\times\left(K'+\frac{\varkappa}{n}-K\right), \qquad (16)$$

where

$$R_j^{(N)}(ss')=i\mu_0 L^{-\frac{3}{2}}(2\pi c'\hbar\varkappa)^{\frac{1}{2}}\mu^{\frac{N}{2}}b'^{+}\left\{\rho_3(\sigma[\mathbf{x}^0\mathbf{a}_j^{+}])+n^{-N}\rho_2(\sigma\mathbf{a}_j^{+})\right\}b. \qquad (17)$$

In Eq. (16), $\mathbf{k}$, $\mathbf{k}'$ denote the momenta ($\hbar\mathbf{k}$), ($\hbar\mathbf{k}'$) of the magnetic moment before and after the emission process, while $K=\sqrt{k^2+k_0^2}$, $K'=\sqrt{k'^2+k_0^2}$ are the corresponding energies, ($\hbar cK$), ($\hbar ck'$), ($k_0=m_0c/\hbar$). In Eq. (17), b = b($\hbar$k; ($\hbar$/2)s; +1) and b′ = b($\hbar$k′; ($\hbar$/2)s′; +1) are fourth order Dirac matrices which are determined by the momentum of the magnetic moment and by the value of the projection ($\hbar$/2 or −$\hbar$/2) of its spin on the direction of the momentum. Evaluating the matrix elements required in Eqs. (16) and (17), carrying out the summation over $\mathbf{k}'$, and making the transition to the continuous spectrum in κ,

$$\left(\frac{1}{L^3}\sum_{\varkappa}\to\frac{1}{8\pi^3}\int d^3\varkappa\right),$$

we obtain the following expression for the probability of emission of radiation by the magnetic moment:

$$w_j^{(N)}(ss')=\frac{\mu_0^2}{8\pi\hbar}\int\frac{\mu^N}{n}\Pi_j^{(N)}(ss')\,\delta\left(K'+\frac{\varkappa}{n}-K\right)\varkappa d^3\varkappa, \qquad (18)$$

where

$$\Pi_j^{(N)}(ss')=\left(1-ss'\frac{kk'}{KK'}+\frac{k_0^2}{KK'}\right)\left\{\left(1-ss'\frac{(\mathbf{kk}')}{kk'}\right)([\mathbf{x}^0\mathbf{a}_j][\mathbf{x}^0\mathbf{a}_j^{+}])+\frac{i}{kk'}(sk'\mathbf{k}-s'k\mathbf{k}')[[\mathbf{x}^0\mathbf{a}_j][\mathbf{x}^0\mathbf{a}_j^{+}]]+ss'\frac{(\mathbf{k}'[\mathbf{x}^0\mathbf{a}_j])(\mathbf{k}'[\mathbf{x}^0\mathbf{a}_j^{+}])+(\mathbf{k}'[\mathbf{x}^0\mathbf{a}_j])(\mathbf{k}[\mathbf{x}^0\mathbf{a}_j^{+}])}{kk'}\right\}$$
$$+n^{-2N}\left(1-ss'\frac{kk'}{KK'}-\frac{k_0^2}{KK'}\right)\left\{\left(1-ss'\frac{(\mathbf{kk}')}{kk'}\right)(\mathbf{a}_j\mathbf{a}_j^{+})+\frac{i}{kk'}(sk'\mathbf{k}-s'k\mathbf{k}')[\mathbf{a}_j\mathbf{a}_j^{+}]+ss'\frac{(\mathbf{ka}_j)(\mathbf{k}'\mathbf{a}_j^{+})+(\mathbf{k}'\mathbf{a}_j)(\mathbf{ka}_j^{+})}{kk'}\right\}$$
$$+\frac{2n^{-N}}{i}\left(\frac{sk}{K}-\frac{s'k'}{K'}\right)\left\{\left(1-ss'\frac{(\mathbf{kk}')}{kk'}\right)([\mathbf{x}^0\mathbf{a}_j]\mathbf{a}_j^{+})+\frac{i}{kk'}(sk'\mathbf{k}-s'k\mathbf{k}')[[\mathbf{x}^0\mathbf{a}_j]\mathbf{a}_j^{+}]+ss'\times\frac{(\mathbf{k}[\mathbf{x}^0\mathbf{a}_j])(\mathbf{k}'\mathbf{a}_j^{+})+(\mathbf{k}'[\mathbf{x}^0\mathbf{a}_j])(\mathbf{ka}_j^{+})}{kk'}\right\}.$$

The formula for $w_j^{(N)}(ss')$ takes into account both the initial value (s), and the final value (s′) of the spin state of the magnetic moment. The intensity of radiation per unit length can be evaluated with the aid of the formula

$$W_j^{(N)}(ss')=\frac{\hbar}{\beta}\int\frac{\varkappa}{n}dw_j^{(N)}(ss'), \qquad (19)$$

where

$$\beta=\frac{k}{K}. \qquad (20)$$

When we investigate the linear polarization of the radiation we obtain the following formulas for the intensity:

$$W_j^{\mathbf{B},\mathbf{E}}(ss')=\frac{\mu_0^2}{2\beta^2c^4}\int_0^{\omega_m}\mu n^2\omega^3\left(1-\frac{1}{n^2}\right)\{\beta^2(j-2)(1-\cos^2\theta)+(1-\beta^2$$
$$+ss'Z^{-1}[\beta^2(j-2)(1-\cos^2\theta)-(1-\beta^2)][2n\cos\theta-\beta(n^2+1)]-2\beta ss'Z^{-1}(n^2+1)(j-2)(1-\beta^2)(1-\cos^2\theta)\}d\omega,$$
$$j=2,\ 3; \qquad (21)$$

$$W_j^{\mathbf{H},\mathbf{D}}(ss')=\frac{\mu_0^2}{2c^4}\int_0^{\omega_m}\frac{n^4\omega^3}{\mu}\left(1-\frac{1}{n^2}\right)\times(3-j)(1-\cos^2\theta)\{1+ss'Z^{-1}[2n\cos\theta-\beta(n^2+1)]\}d\omega,$$
$$j=2,\ 3. \qquad (22)$$

Investigating the circular polarization we obtain the formula

$$W_j^{\mathbf{B},\mathbf{E}}(ss')=\frac{\mu_0^2}{4\beta^2c^4}\int_0^{\omega_m}\mu n^2\omega^3\left(1-\frac{1}{n^2}\right)\{\beta^2(1-\cos^2\theta)+2(1-\beta^2)$$
$$+ss'Z^{-1}[2n\cos\theta-\beta(n^2+1)][\beta^2(1-\cos^2\theta)-2(1-\beta^2)]-2\beta ss'Z^{-1}(n^2+1)(1-\beta^2)(1-\cos^2\theta)+2js(1-\beta^2)\cos\theta-2js'Z^{-1}(1-\beta^2)[2n-\beta(n^2+1)\cos\theta]\}d\omega,$$
$$j=-1,\ 1; \qquad (23)$$

$$W_j^{\mathbf{H},\mathbf{D}}(ss')=\frac{\mu_0^2}{4c^4}\int_0^{\omega_m}\frac{n^4\omega^3}{\mu}\left(1-\frac{1}{n^2}\right)\times(1-\cos^2\theta)\times\{1+ss'Z^{-1}[2n\cos\theta-\beta(n^2+1)]\}d\omega,$$
$$j=-1,\ 1. \qquad (24)$$

In Eqs. (21) to (24),

$$Z=\{[2n-\beta(n^2+1)\cos\theta]^2+\beta^2(n^2-1)^2(1-\cos^2\theta)\}^{\frac{1}{2}}$$
$$=\{[2n\cos\theta-\beta(n^2+1)]^2+4n^2(1-\beta^2)(1-\cos^2\theta)\}^{\frac{1}{2}}; \qquad (25)$$

$$\cos\theta=\frac{1}{\beta n}+\frac{n\omega\hbar}{2pc}\left(1-\frac{1}{n^2}\right), \quad p=\hbar k, \qquad (26)$$

where θ, the angle between the vectors κ and $\mathbf{k}$, can be determined from the conditions

$$\mathbf{k}'=\mathbf{k}-\mathbf{x}; \quad K'=K-\frac{\varkappa}{n}. \qquad (27)$$

The maximum frequency of the radiation, ω_m, is obtained from Eq. (26) if one sets $\cos\theta = 1$.

3. Let us now analyze the results obtained. To obtain formulas for the intensity of the radiation emitted

by longitudinally polarized particles (s fixed), one has to carry out the summation over the final spin states[24] In Eqs. (21) to (24):

$$W_j^{\mathbf{B},\mathbf{E}}(s)=\frac{\mu_0^2}{\beta^2c^4}\int_0^{\omega_m}\mu n^2\omega^3\left(1-\frac{1}{n^2}\right)$$

$$\times\{\beta^2(j-2)(1-\cos^2\theta)+1-\beta^2\}\,d\omega, \qquad (28)$$

$$j=2,\ 3;$$

$$W_j^{\mathbf{H},\mathbf{D}}(s)=\frac{\mu_0^2}{c^4}\int_0^{\omega_m}\frac{n^4\omega^3}{\mu}\left(1-\frac{1}{n^2}\right)(3-j)(1-\cos^2\theta)\,d\omega, \qquad (29)$$

$$j=2,\ 3;$$

$$W_j^{\mathbf{B},\mathbf{E}}(s)=\frac{\mu_0^2}{2\beta^2c^4}\int_0^{\omega_m}\mu n^2\omega^3\left(1-\frac{1}{n^2}\right)\{2(1-\beta^2)+\beta^2(1-\cos^2\theta)$$

$$+2js(1-\beta^2)\cos\theta\}\,d\omega, \qquad (30)$$

$$j=-1,\ 1;$$

$$W_j^{\mathbf{H},\mathbf{D}}(s)=\frac{\mu_0^2}{2c^4}\int_0^{\omega_m}\frac{n^4\omega^3}{\mu}\left(1-\frac{1}{n^2}\right)(1-\cos^2\theta)\,d\omega, \qquad (31)$$

$$j=-1,\ 1.$$

If the particle beam is not polarized, one has still to average Eqs. (28) to (31) over the initial spin states. It is obvious that

$$W_j^{\mathbf{B},\mathbf{E}}=W_j^{\mathbf{B},\mathbf{E}}(s), \qquad (32)$$

$$j=2,\ 3;$$

$$W_j^{\mathbf{B},\mathbf{E}}=\frac{\mu_0^2}{2\beta^2c^4}\int_0^{\omega_m}\mu n^2\omega^3\left(1-\frac{1}{n^2}\right)[\beta^2(1-\cos^2\theta)+2(1-\beta^2)]\,d\omega, \qquad (33)$$

$$j=-1,\ 1;$$

$$W_j^{\mathbf{H},\mathbf{D}}=W_j^{\mathbf{H},\mathbf{D}}(s), \qquad (34)$$

$$j=-1,\ 1,\ 2,\ 3.$$

For the μ_0; **B, E** interaction, it is easily seen that the radiation from longitudinally polarized particles turns out to be eliptically polarized;[10] the radiation from nonpolarized particles consists of two parts—a linearly polarized part [with the vector **E** perpendicular to the plane $(\kappa^0, \kappa^0\times k^0)$], and a nonpolarized additional part.[9]

For the μ_0; **H, D** interaction, the radiation shows strong linear polarization [the vector **D** is perpendicular to the plane (κ^0, k^0)] regardless of the particle velocity (as long as emission of radiation is possible), this polarization does not depend upon the initial spin state.

Let us now consider Eqs. (21) to (24) in the extreme relativistic case ($\beta\to 1$). It follows from these equations that for $\beta\to 1$, the emission of radiation by the magnetic moment involves the complete reversal of the spin direction, since

$$W_j^{(N)}(ss'=1)\to 0, \qquad (35)$$

$$N=-1,\ 1,$$

$$j=-1,\ 1,\ 2,\ 3,$$

For the μ_0; **B, E** interaction, this radiation is linearly polarized

$$W_j^{\mathbf{B},\mathbf{E}}(ss'=-1)\to\frac{\mu_0^2(j-2)}{c^4}\int_0^{\omega'_m}\mu n^2\omega^3\left(1-\frac{1}{n^2}\right)^2 d\omega, \qquad (36)$$

$$j=2,\ 3;$$

$$W_j^{\mathbf{H},\mathbf{D}}(ss'=-1)\to\frac{\mu_0^2(3-j)}{c^4}\int_0^{\omega_m}\frac{n^4\omega^3}{\mu}\left(1-\frac{1}{n^2}\right)^2 d\omega, \qquad (37)$$

$$j=2,\ 3.$$

In the derivation of these formulas we have put $\cos\theta = 1/n$; this is obvious (for $\beta\to 1$) for photons of limited energy.

The upper limit of the integrals ω'_m (the maximum energy of the emitted photons) is finite, since for a real medium the refractive index rapidly drops to unity as the frequency increases; that is, $n(\omega'_m) = 1$.

It is important to note that for the interaction μ_0; **H, D** the vector **D** is perpendicular to the generatrix (κ^0) of the radiation cone, and lies within the plane which is tangential to the cone along this generatrix, while for the μ_0; **B, E** interaction, in the extreme relativistic case, the vector **E** is perpendicular to this tangential plane.

Let us consider Eqs. (21) to (24) for $\cos\theta = 1$. It is obvious that

$$W_j^{\mathbf{B},\mathbf{E}}(ss')=\frac{\mu_0^2}{2\beta^2c^4}\int_0^{\omega m}\mu n^2\omega^3\left(1-\frac{1}{n^2}\right)(1-\beta^2)(1-ss')\,d\omega, \qquad (38)$$

$$j=2,\ 3;$$

$$W_j^{\mathbf{B},\mathbf{E}}(ss')=\frac{\mu_0^2}{2\beta^2c^4}\int_0^{\omega_m}\mu n^2\omega^3\left(1-\frac{1}{n^2}\right)$$

$$(1-\beta^2)[1-ss'+j(s-s')]\,d\omega, \qquad (39)$$

$$j=-1,\ 1;$$

$$W_j^{\mathbf{H},\mathbf{D}}(ss')=0, \qquad (40)$$

$$j=-1,\ 1,\ 2,\ 3.$$

Thus, for the μ_0; **B, E** interaction and $\cos\theta = 1$, the emission of radiation is due to quantum transitions with spin reversal. If the particle beam is nonpolarized, then this radiation is also unpolarized. The radiation from longitudinally polarized particles ($s = -1$ or $s = +1$), as was first mentioned in ref. 10, is circularly polarized for $\cos\theta = 1$ (right-handedly or left-handedly, respectively). We mention further that for $\cos\theta = 1/(\beta n) = 1$ (radiation threshold) the integrals (38) and (39) vanish, since $\omega_m = 0$.

Finally, let us obtain the classical approximations to the formulas (21)-(24). We should then obviously let $s = s'$, and go to the limit $\hbar\to 0$, that is, we should put $\cos\theta = 1/(\beta n)$. This leads to the formulas:

$$W_j^{\mathbf{B},\mathbf{E}\,(\text{class.})}=\frac{\mu_0^2(1-\beta^2)(3-j)}{\beta^2c^4}\int_0^{\omega''_m}\mu n^2\omega^3\left(1-\frac{1}{n^2\beta^2}\right)d\omega, \qquad (41)$$

$$j=2,\ 3;$$

$$W_j^{\mathbf{B},\mathbf{E}\,(\text{class.})}=\frac{1}{2}W_2^{\mathbf{B},\mathbf{E}\,(\text{class.})}, \qquad (42)$$

$$j=-1,\ 1;$$

$$W_j^{\mathbf{H},\mathbf{D}\,(\text{class.})}=\frac{\mu_0^2(1-\beta^2)(3-j)}{\beta^2c^4}\int_0^{\omega''_m}\frac{n^2\omega^3}{\mu}\left(1-\frac{1}{n^2\beta^2}\right)d\omega, \qquad (43)$$

$$j=2,\ 3;$$

$$W_j^{\mathbf{H},\mathbf{D}\,(\text{class.})}=\frac{1}{2}W_2^{\mathbf{H},\mathbf{D}\,(\text{class.})}, \qquad (44)$$

$$j=-1,\ 1.$$

ω''_m should be determined from the condition $\beta n(\omega''_m) = 1$. For $\mu = 1$, the formulas (41) to (44) become identical

with the known results of Ginzburg and Frank.[1-3]

4. The formulas for the intensity of Vavilov-Cherenkov radiation from unpolarized Dirac electrons moving in a ferrodielectric medium are of the form[9,26]

$$W_j^e = \frac{e^2}{c^2}\int_0^{\omega_m} \mu\omega\,(j-2)\,(1-\cos^2\theta)\,d\omega + I_j; \qquad (45)$$

$$I_j = \frac{e^2}{c^2}\int_0^{\omega_m} \frac{\mu n^2\omega^3\hbar^2}{4p^2c^2}\left(1-\frac{1}{n^2}\right)d\omega; \qquad (46)$$

$$j = 2,\ 3.$$

The quantities I_j represent the unpolarized part of the radiation, and can also be written in the form

$$I_j = \frac{\mu_B^2}{\beta^2c^4}\int_0^{\omega_m} \mu n^2\omega^3\,(1-\beta^2)\left(1-\frac{1}{n^2}\right)d\omega, \qquad (47)$$

where $\mu_B = |e|\hbar/2m_0c$ is the Bohr magneton.

For $\cos\theta = 1$, the intensity of the radiation is given by Eq. (47) where, in this case, I_j is determined solely by quantum transitions with spin reversal. One can easily see that for $\cos\theta = 1$, the formulas for the intensity of the radiation emitted by Dirac electrons coincide with the corresponding formulas (see ref. 38) for the intensity of the radiation emitted by a magnetic moment. In the extreme relativistic case $I_j \to 0$, and the expression for W_j^e coincides with the classical expression,[27] in full agreement with refs. 1 and 28.

In conclusion, I wish to express my gratitude to A. A. Sokolov for his interest in this work, and to Yu. M. Loskutov for friendly discussions.

REFERENCES

1. V. L. Ginzburg, Zhur. Eksptl. i Teoret. Fiz. 10, 589 (1940).
2. I. M. Frank, Izvest. Akad. Nauk SSSR, Ser. Fiz. 6, 3 (1942).
3. I. M. Frank, Sb. Pamyati S. I. Vavilova (Collection in memory of S. I. Vavilov). Izd. Akad. Nauk SSSR, Moscow, 1952.
4. V. L. Ginzburg, Sb. Pamyati S. I. Vavilova (Collection in memory of S. I. Vavilov). Izd. Akad. Nauk SSSR, Moscow, 1952.
5. K. Tanaka, Phys. Rev. 90, 358 (1953).
6. K. Tanaka, Sb. Millimetrovye i submillimetrovye volny (Collection: Millimeter and sub-millimeter waves). Izd. Inostrannoi Lit., Moscow, 1959.
7. V. Ya. Eidman, Uchenye Zapiski Gor'kovsk. Univ., Ser. Fiz. 30, 229 (1956).
8. N. L. Balazs, Phys. Rev. 104, 1220 (1956).
9. Yu. M. Loskutov and A. B. Kykanov, Zhur. Eksptl. i Teoret. Fiz. 34, 477 (1958), Soviet Phys.—JETP 7, 328 (1958).
10. Yu. M. Loskutov, Kand. Diss. Moskov. Gosudarst. Univ., 1959.
11. V. L. Ginzburg and V. Ya. Eidman, Zhur. Eksptl. i Teoret. Fiz. 35, 1508 (1958), Soviet Phys.—JETP 8, 1055 (1959).
12. G. A. Begiashvili and E. V. Gedalin, Zhur. Eksptl. i Teoret. Fiz. 36, 1939 (1959), Soviet Phys.—JETP 9, 1379 (1959).
13. V. L. Ginzburg, Uspekhi Fiz. Nauk 69, 537 (1959), Soviet Phys.—Uspekhi 2, 874 (1960).
14. B. M. Bolotovskii and E. M. Leikin, Uspekhi Fiz. Nauk 69, 693 (1959), Soviet Phys.—Uspekhi 2, 987 (1960).
15. J. V. Jelley, "Cherenkov Radiation and Its Applications," Pergamon Press, London, 1958.
16. Sb. Fizika ferromagnitnikh oblastei (Collection: Physics of Ferromagnetic Domains). Izd. Inostrannoi Lit., Moscow, 1951.
17. D. Hughes, "Neitronnaya Optika" (Neutron Optics). Izd. Inostrannoi Lit., Moscow, 1955. (Interscience tracts on physics and astronomy, vol. 1.) Interscience New York, 1953.
18. J. Bacon, "Diffraktsiya neitronov" (Neutron Diffraction). Izd. Inostrannoi Lit., Moscow, 1957. Oxford Univ. Press, 1955.
19. A. A. Sokolov, "Vvedenie v kvantovuyu elektrodinamiku" (Introduction to Quantum Electrodynamics). Fizmatgiz, Moscow, 1958.
20. A. I. Akhiezer and V. B. Berestetskii, "Kvantovaya elektrodinamika" (Quantum Electrodynamics). Fizmatgiz, Moscow, 1959.
21. A. A. Sokolov and V. N. Tsytovich, Zhur. Eksptl. i Teoret. Fiz. 30, 136 (1956), Soviet Phys.—JETP 2 94 (1956).
22. A. A. Sokolov and I. M. Ternov, Zhur. Eksptl. i Teoret. Fiz. 31, 473 (1956), Soviet Phys.—JETP 4, 396 (1957).
23. F. I Fedorov, "Optika anizotropnykh sred" (Optics of Anisotropic Media). Izd. Akad. Nauk Beloruss. SSR Minsk, 1958.
24. A. A. Sokolov and Yu. M. Loskutov, Zhur. Eksptl. i Teoret. Fiz. 34, 1022 (1958), Soviet Phys.—JETP 7, 706 (1958).
25. L. D. Landau and E. M. Lifshits, "Elektrodinamika sploshnykh sred" (Electrodynamics of Continuous Media). Fizmatgiz, Moscow, 1957. Addison Wesley, Reading, Mass., 1960.
26. A. A. Sokolov and Yu. M. Loskutov, Zhur. Eksptl. i Teoret. Fiz. 32, 630 (1957), Soviet Phys.—JETP 5, 523 (1957).
27. I. M. Frank and I. E. Tamm, Doklady Akad. Nauk SSSR 14, 109 (1937).
28. I. M. Frank, Uspekhi Fiz. Nauk 30, 149 (1946).

DETERMINATION OF THE NUCLEAR MAGNETIC MOMENT OF Hg^{199} FROM THE HYPERFINE STRUCTURE OF THE HgI 5461 A LINE

I. I. Agarbiceanu, L. Blanaru, V. Draganescu, N. J. Ionesco-Pallas, N. Komanichu, and V. Tatu (pp. 297-300)

Received 27 June 1960

The hyperfine structure of the 5461 A line of natural mercury has been completely resolved using a Fabry-Perot etalon and cooled light sources of different types. The nuclear magnetic moment of Hg^{199} was determined from the experimental data by using theoretical formulas with certain corrections. The value obtained ($\mu_{199} = 0.51\mu_N$) is in good agreement with the value $\mu_{199} = 0.504\mu_N$ obtained from magnetic resonance experiments.

1. The hyperfine structure (hfs) of the λ 5461 line $[6s6p^3P_2 - 6s7s^3S_1]$ has been studied in detail by a number of researchers.[1-5] Almost all of the components have been resolved, including both isotopic components and those due to nuclear spin. However, despite the fact that the wavelengths given by the authors coincide almost perfectly, the values of the nuclear magnetic moments of the odd isotopes vary considerably (for example, according to the data of ref. 1, $\mu_{199} = 0.45\mu_N$, whereas ref. 3 gives $\mu_{199} = 0.53\mu_N$).

This paper is devoted to a further study of the question.

2. A high frequency discharge, a liquid nitrogen-cooled Schüler tube, and a Korolev[6] tube were used as sources of optical excitation. Both the cooled Schüler tube and the Korolev tube were used as sources for resolving the central part of the line, which covered almost 0.12×10^{-3} cm^{-1} and contained 7 components. A Fabry-Perot etalon, made in our laboratory, was used for the measurements. The high reflection coefficient of the metallic films (vacuum-deposited silver[7-9]) required that parasitic rings be eliminated from the interference pattern. In order to do this, the rear surface of the plate was inclined[10,11] (the angle of inclination is determined from the relationship $D = 2nf\varepsilon$, where D is the distance between the centers of the primary and parasitic rings, n is the index of refraction of the glass, f is the focal length, and ε is the angle of inclination. In our case this angle is about 3°).

3. If one considers that inaccurate placement of the photographic plate in the focal plane of the objective leads to a dependence of the radii of interference rings of a given order on the distance between the etalon and the camera; i.e.,

$$R(L) = \bar{R}\left[1 + \frac{\delta f}{f}\left(1 - \frac{L}{f}\right)\right],$$

the total relative error for the whole spectral interval will be

$$\frac{\delta|\Delta\nu|}{|\Delta\nu|} \sim 2\left\{\frac{\delta L}{R}\left(\frac{\partial R}{\partial L}\right) + \frac{\delta\bar{R}}{|R_2 - R_1|}\right\};\quad \bar{R} = \frac{1}{2}(R_1 + R_2),$$

where δL is the random variation in the measured values of L, and $2\delta\bar{R}$ is the error in measurement of the radius of a ring (a typical value of this error is on the order of 0.002×10^{-3} cm^{-1}).

4. The results of hfs measurements of the 5461 A line of natural mercury are shown in the Table. The data obtained by Korolev,[2] Blaise and Chantrel,[3] and Murakawa[4] are also shown for comparison. Photographs of the interference pattern of the λ 5461 A line hfs are presented in the Figure.

Hg isotope	Transition F	Symbol	Intensity %	$\Delta\nu$ (cm^{-1}) Ref. 2 data	Ref. 3 data	Ref. 4 data	Our data
201	2/5 3/2	*a*	0.13	−0.723	−0.7247	−0.7244	−0.726
201	5/2 5/2	*b*	0.19	−0.436	−0.4363	−0.4365	−0.436
199	1/2 3/2	*A*	5.68	−0.289	−0.2876	−0.2883	−0.287
201	3/2 1/2	*d*	0.22	−0.240	−0.2413	−0.2404	−0.240
201	3/2 3/2	*e*	1.40	−0.057	−0.0613	−0.0610	−0.057
201	3/2 7/2	*c*	5.27	−0.057	−0.0573	−0.0568	−0.057
198	"Fine" transition	I	10.12	−0.028	−0.0280	−0.0276	−0.028
200	"Fine" transition	II	23.25	0.000	−0.0000	0.0000	0.0000
202		III	29.54	+0.030	+0.0310	+0.0311	+0.031
199	3/2 5/2	*B*	10.23	+0.030	+0.0305	+0.0321	+0.031
204	"Fine" transition	IV	6.72	+0.060	+0.0610	+0.0620	+0.060
201	1/2 1/2	*g*	1.09	+0.157	+0.1567	+0.1576	+0.157
201	3/2 5/2	*f*	2.76	+0.226	+0.2271	+0.2269	+0.226
201	1/2 3/2	*h*	1.09	+0.336	+0.3367	+0.3370	+0.337
199	3/2 3/2	*C*	1.14	+0.787	+0.7878	+0.7883	+0.787

The frequency intervals $\Delta\nu$ are calculated from the formula

$$\Delta\nu = \nu_0 \frac{\bar{R}}{f^2}(R_2 - R_1);\quad \bar{R} = \frac{1}{2}(R_1 + R_2).$$

The intensity of the center (unresolved in earlier measurements) amounts to 86.53% of the total intensity of the green line and has a maximum at a distance of +0.0115 cm^{-1} from the Hg^{200} component. The center was resolved with a Fabry-Perot etalon which had a distance of 30 mm between the reflecting surfaces (its dispersion range was 0.166 cm^{-1}).

Once the hyperfine splitting intervals have been obtained the interval factors of the levels can be derived with the aid of Casimir's formula. The discrepancies among the values of the interval factors derived from different components is explained by perturbation of the $^3P_2$ level by other levels.

5. Inasmuch as the $6s7s^3S_1$ level is not perturbed, the experimental value of the quantity A ($^3S_1$) can be used to calculate the nuclear magnetic moment of the isotope Hg^{199}. The well-known formula for determining the value of the interval factor is employed for this calculation; it has the form

A B

Interference pattern of the hfs of HgI λ 5461 A. A—outer components of the line; B—central part of the line.

$$A(^3S_1)=\frac{1}{2}Y\left(a^0_{6S_{1/2}}+a^0_{7S_{1/2}}\right).$$

The factor Y is a correction for the finite size and structure of the nucleus. The expression

$$a^0_{S_{1/2}}=\frac{8}{3}R_\infty\alpha^2 g_I\frac{Z_i Z_0^2}{1836}\frac{\left(1-\frac{d\sigma}{dn}\right)}{n_*^3}\chi\left(\frac{1}{2},\ Z_i\right)(\text{см}^{-1}).$$

is used for $a^0_{S_{1/2}}$.

Application of the Fermi-Segré formula to atoms with two valence electrons is to a certain degree unjustified, although it has definite meaning in this case if it is remembered that the value of $(1/n_*^3)(dn_*/dn)$ is still determined from a single-electron spectral series.

For the case of the Hg atom, in which the spectral series are known up to terms of fairly high order, a computation of the finite differences

$$\left(1-\frac{d\sigma}{dn}\right)=\ln(1+\Delta)\,n_*,$$

can be successfully used for calculating the differential $d\sigma/dn$, extrapolating the series obtained with the help of the d'Alembert convergence criterion.

We obtain the following values in this way:

$$n_{*6S}=1.1418;\quad n_{*7S}=2.2419;$$

$$\left(1-\frac{d\sigma}{dn}\right)_{6S}=1.4206;\quad \left(1-\frac{d\sigma}{dn}\right)_{7S}=1.0582.$$

A few comments regarding the multiplier Y are in order here. It is made up of two corrections—the Breit-Crawford-Schawlow $Q = 1 - \delta$ and the Bohr and Weisskopf $\Lambda = 1 - \varepsilon$. The latest value for the nuclear radius should be taken when using this multiplier, and the correction then derived from the formula

$$Y(R_2)=1-\{1-Y(R_1)\}\left(\frac{R_2}{R_1}\right)^{2\rho-1};\quad \rho=\left(1-\frac{Z^2}{137^2}\right)^{1/2}.$$

We assumed that the Hg^{199} nucleus was incompressible, had its nucleons homogeneously distributed, and was not deformed. It was also assumed that there were no nuclear currents.

A precise calculation based on the abovementioned assumptions yielded[12]

$$Y_{Hg^{199}} = 0.8798$$

The value of the nuclear moment which we obtained from the experimental and theoretical data was

$$\mu_{199} = +0.51\mu_N$$

which is very close to the value $\mu_{199} = +0.504\mu_N$ measured by the magnetic resonance method in ref. 12.

REFERENCES

1. H. Schüler and T. Schmidt, Z. Physik **98**, 239 (1936).
2. F. Korolev and V. Odintsov, Opt. i Spektr. **1**, 17 (195
3. J. Blaise and H. Chantrel, J. phys. radium **18**, 193 (1957).
4. K. Murakawa, J. Phys. Soc. Japan **14**, 1624 (1959).
5. I. Agarbiceanu, Compt. rend. acad. sci. **250**, 317 (1960).
6. F. Korolev, Vestnik Moskov. Univ. **3**, 101 (1953).
7. L. Holland, "Vacuum Deposition and Properties of Thin Films." Wiley, New York, 1958.
8. R. S. Sennett and G. D. Scott, J. Opt. Soc. Am. **40**, 203 (1950).
9. H. Huhn and Wilson, Proc. Phys. Soc. (London) **B63**, 750 (1950).
10. S. Tolansky, Phil. Mag. **35**, 229 (1944).
11. C. Dufour, Ann. phys. **6**, 5 (1951).
12. N. J Ionesco-Pallas, Phys. Rev. **117**, 505 (1960).
13. W. Proctor and F. Yu, Phys. Rev. **76**, 1728 (1949).

DETERMINATION OF THE NUCLEAR MAGNETIC MOMENT OF Na^{23} FROM THE HYPERFINE STRUCTURE OF THE ABSORPTION LINES D_1 AND D_2

V. Draganescu (pp. 301-307)

Received 27 June 1960

The hfs (hyperfine structure) of the D_1 and D_2 absorption lines of sodium was measured using an atomic beam and was found to be $\Delta\nu(D_1) = 0.058\ cm^{-1}$. With the aid of the current, more accurate theory the magnetic moment of Na^{23} was determined and the value $\mu = 1.97 \pm 0.02$ n.m. (nuclear magnetons) was obtained. Taking into account the polarization of the electron shells of the atom by the optical electron, a more accurate value of $\mu = 2.32 \pm 0.02$ n.m. was obtained for the magnetic moment. Within the limits of experimental error, this corresponds to the value $\mu = 2.217$ n.m. measured by the magnetic resonance method.

INTRODUCTION

The D_1 and D_2 lines of sodium have a very narrow hfs, which can be resolved only under special experimental conditions.

The first determinations of the hfs of sodium lines were made in 1928 by Schüler[1] using a hollow cathode, and by Dobrezoff and Terenin,[2] who investigated it with a tube containing an optically excited atomic beam. Their results agreed. In 1933 Granath and van Atta[3] studied the hyperfine structure using a hollow-cathode cooled by liquid air. Using data on the magnitude of the splitting of the hyperfine structure obtained, they calculated the magnitude of the nuclear magnetic moment. In 1935 Jackson and Kuhn,[4] using an atomic beam, also determined the hf in absorption and from it the nuclear magnetic moment. Finally, in 1937, Meissner and Luft,[5] using a hollow-cathode, determined the hfs in emission and calculated the magnetic moment of Na^{23}.

The values obtained by the abovementioned authors are very close to one another; however, because of the insufficiencies of the theory of nuclear magnetic momen existing at that time, they differ strongly from the value obtained by direct magnetic resonance measurements.

However, it is necessary to emphasize once more that the authors mentioned above, in spite of differences in experimental technique, obtained identical results. The fact that Jackson, working with an atomic beam (the most accurate optical method), obtained results agreeing with the results of the other authors confirms the accuracy of the experimental data.

The present paper is also devoted to the study of the hfs of the sodium D_1 and D_2 absorption lines. The magnitude of the magnetic moment of Na^{23} is determined using the data obtained and the modern theory of magnetic moments,[6] improved by N. Ionescu-Pallas,[7] and also considering the effect of electron shell polarization caused by the optical electron—an important effect in light and medium weight atoms.

EXPERIMENTAL ARRANGEMENT

The experimental arrangement shown in Fig. 1 was used to obtain the hyperfine structure of absorption.

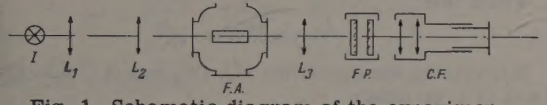

Fig. 1. Schematic diagram of the experimental arrangement. I—light source; L_1, L_2, L_3—lenses; F.A.—atomic beam lamp; F.P.—Fabry-Perot etalon; C.F.—camera.

A sodium vapor lamp, water-cooled to eliminate self-absorption, served as the light source The temperature of the lamp was such that in the spectrum, each of the emitted lines (D_1 and D_2) appeared as a constant emission background of width $\Delta\nu \approx 0.180$ cm^{-1}. Superimposed on this was the hfs of just those absorption lines caused by the atomic beam of sodium. The latter was obtained from an atomic beam source which was built by us (Fig. 2) and was considerably better than the previous ones.[8] In this version, operation of the lamp is greatly simplified because the oven can be filled by removing only one closure (13 in Fig. 2). As a result of the improvement in the construction of this lamp, it is possible to obtain a vacuum of the order of $1\text{-}2 \times 10^{-6}$ mm Hg.

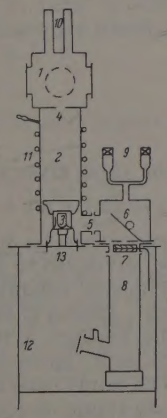

Fig. 2. Schematic diagram of the atomic beam source. 1—upper chamber; 2—lower chamber; 3—oven; 4—slit; 5—tube for pumping out gas; 6—vacuum valve; 7—liquid nitrogen-cooled trap; 8—diffusion pump; 9—manometers; 10—trap with liquid nitrogen; 11—water-filled spiral; 12—lamp support; 13—oven door for filling oven.

The equivalent temperature of the atoms in the beam was about 1.15°K, corresponding to a Doppler half-width of about 0.0013°K at an oven temperature of 500°K.

The high resolution instrument was a Fabry-Perot etalon whose silvered glass plates were spaced 7.15 mm apart.

RESULTS

(a) **The hyperfine structure.** Figure 3 is a photograph of the hfs of the sodium D_1 and D_2 lines. The separation between the hfs components was determined with the help of the relation

$$\Delta\nu = \frac{\nu_0}{2f^2}(R_1 + R_2)(R_1 - R_2) = \frac{\nu_0}{f^2}\bar{R}\Delta R, \qquad (1)$$

where ν_0 is the frequency of the center of gravity, R_1 and R_2 are the radii of the interference rings of the two hfs components of the lines, and f is the focal length of the camera. The data obtained are presented below in Table 2 and are in very good agreement with the data of other authors.

(b) **Calculation of the magnetic moment.** Figure 4 is a schematic diagram of the transitions for the hyperfine structure of the D_1 and D_2 lines consistent with the selection rules. Since the magnitude of the splitting of the $^2P_{1/2}$ and $^2P_{3/2}$ hfs terms is approximately ten times less than the splitting of the $^2S_{1/2}$ term, only two groups of hfs lines can be resolved for each D line. In order to calculate the hfs constant, which is necessary in order to determine the magnetic moment, the influence of the $^2P_{1/2}$ and $^2P_{3/2}$ terms should also be taken into account.

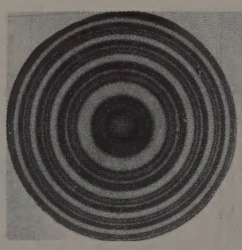

Fig. 3

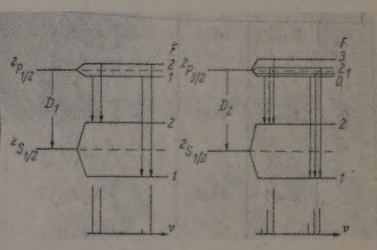

Fig. 4

Fig. 3. Interference pattern of the hfs of the sodium D_1 and D_2 lines.

Fig. 4. Schematic diagram of the transitions which lead to the appearance of hfs in the sodium D_1 and D_2 lines.

Table 1 presents the assignments of the hfs lines, their relative intensities, expressions for the energy, the centers of gravity of the unresolved groups, and the separations between them. For the determination of these quantities, the following energy relations were used:

$$\delta W = \frac{1}{2}A[F(F+1) - I(I+1) - J(J+1)], \qquad (2)$$

where A is the hfs constant, F is the "hyperfine" quantum number, I is the nuclear spin, and J is the total angular momentum of the electrons.

For the hfs constant A ($^2S_{1/2}$) we obtain two expressions in which the quantities $\Delta\nu(D_1)$ and $\Delta\nu(D_2)$ and the ratio of the corresponding constants for the levels between which transitions take place:

$$A(^2S_{1/2}) = \frac{1}{2}\frac{\Delta\nu(D_1)}{\left[1 + \frac{1}{3}\frac{A(^2P_{1/2})}{A(^2S_{1/2})}\right]} \qquad (3)$$

and

$$A(^2S_{1/2}) = \frac{1}{2}\frac{\Delta\nu(D_2)}{\left[1-\frac{5}{3}\frac{A(^2P_{3/2})}{A(^2S_{1/2})}\right]}. \qquad (3')$$

The expression for the hfs constant of the $^2S_{1/2}$ term has the form:

$$A(^2S_{1/2}) = \frac{8\pi}{3} R_\infty a_H^3 \frac{\alpha^2}{1836} g_I \times \left[\frac{Z_i Z_0^2}{\pi a_H^3 n_{*S_{1/2}}^3}\left(1-\frac{d\sigma}{dn}\right)\right] \chi\left(\frac{1}{2},\ Z_i\right) Y\ (\text{cm}^{-1}), \qquad (4)$$

where $n_{*S_{1/2}} = 1.6271$, $\alpha = 1/137$, $\chi(1/2, Z_i) = 1.0119$, $R_\infty = 109{,}737\ \text{cm}^{-1}$, $Y = 0.9980$, $Z_i = 11$, $Z_0 = 1$, $(1 - d\sigma/dn) = 1.033$, and a_H is the Bohr radius. The value of the quantity $(1 - d\sigma/dn)$ was calculated accurately by Ionescu-Pallas,[7] starting from the expressions

$$T = R_\infty \frac{Z_0^2}{n_*^2};\quad n_* = n - \sigma(n);\quad \sigma(n) = A + \frac{B}{n_*^2}. \qquad (5)$$

From this we get

$$\left(1-\frac{d\sigma}{dn}\right)^{-1} = 1 - 2\frac{T_1^{3/2}}{T_1 - T_2}\left[\left(T_2^{-1/2} - T_1^{-1/2}\right) - \frac{1}{Z_0\sqrt{R_\infty}}\right], \qquad (6)$$

where $T_1 = 41{,}449.463\ \text{cm}^{-1}$ and $T_2 = 15{,}709.59\ \text{cm}^{-1}$.

Table 1

Transition		Relative intensity, %	Energy	Center of gravity	$\Delta\nu$
Fine	Hyperfine				
$D_1\ (^2P_{1/2} - {}^2S_{1/2})$	1 → 2	50	$-\frac{5}{4}A(^2P_{1/2}) - \frac{3}{4}A(^2S_{1/2})$	$-\frac{1}{4}A(^2P_{1/2}) - \frac{3}{4}A(^2S_{1/2})$	$\frac{2}{3}A(^2P_{1/2}) + 2A(^2S_{1/2})$
	2 → 2	50	$+\frac{3}{4}A(^2P_{1/2}) - \frac{3}{4}A(^2S_{1/2})$		
	1 → 1	16.67	$-\frac{5}{4}A(^2P_{1/2}) - \frac{5}{4}A(^2S_{1/2})$	$+\frac{5}{12}A(^2P_{1/2}) + \frac{5}{4}A(^2S_{1/2})$	
	2 → 1	83.33	$+\frac{3}{4}A(^2P_{1/2}) + \frac{5}{4}A(^2S_{1/2})$		
$D_2\ (^2P_{3/2} - {}^2S_{1/2})$	1 → 2	4.97	$-\frac{11}{4}A(^2P_{3/2}) - \frac{3}{4}A(^2S_{1/2})$	$+\frac{5}{4}A(^2P_{3/2}) - \frac{3}{4}A(^2S_{1/2})$	$-\frac{10}{3}A(^2P_{3/2}) + 2A(^2S_{1/2})$
	2 → 2	25.02	$-\frac{3}{4}A(^2P_{3/2}) - \frac{3}{4}A(^2S_{1/2})$		
	3 → 2	70.01	$+\frac{9}{4}A(^2P_{3/2}) - \frac{3}{4}A(^2S_{1/2})$		
	0 → 1	16.66	$-\frac{15}{4}A(^2P_{3/2}) + \frac{5}{4}A(^2S_{1/2})$	$-\frac{25}{12}A(^2P_{3/2}) + \frac{5}{4}A(^2S_{1/2})$	
	1 → 1	41.67	$-\frac{11}{4}A(^2P_{3/2}) + \frac{5}{4}A(^2S_{1/2})$		
	2 → 1	41.67	$-\frac{3}{4}A(^2P_{3/2}) + \frac{5}{4}A(^2S_{1/2})$		

Substituting all the numerical data into Eq. (4), we obtain the quantity $A(^2S_{1/2})$ as a function of g_I:

$$A(^2S_{1/2}) = 0.0227 \cdot g_I. \qquad (7)$$

For the hfs constant of the term $^2P_{1/2}$, using the expression

$$A(^2P_{1/2}) = \frac{8}{9} R_\infty \alpha^2 \frac{Z_i - 4}{n_{*P_{1/2}}^3 \cdot 1836} g_I \chi\left(\frac{1}{2},\ Z_i - 4\right), \qquad (8)$$

where $n_{*P_{1/2}} = 2.1168$, and $\chi(1/2, Z_i - 4) = 1.0048$, we obtain

$$A(^2P_{1/2}) = 0.0021 \cdot g_I, \qquad (9)$$

that is, approximately 10 times less than for the $^2S_{1/2}$ term. The expression for the hfs constant of the $^2P_{3/2}$ term has the form:

$$A(^2P_{3/2}) = \frac{8}{45} R_\infty \alpha^2 \frac{Z_i - 4}{n_{*P_{3/2}}^3 \cdot 1836} g_I \chi\left(\frac{3}{2},\ Z_i - 4\right), \qquad (10)$$

where $n_{*P_{3/2}} \approx n_{*P_{1/2}} = 2.1168$, and $\chi(3/2, Z_i - 4) = 1.0010$.

From this,

$$A(^2P_{3/2}) = 0.00042 \cdot g_I. \qquad (11)$$

Introducing the quantities (7), (9), and (11) into Eqs. (3) and (3′), we obtain

$$A(^2S_{1/2}) = 0.485 \cdot \Delta\nu(D_1), \qquad (12)$$

$$A(^2S_{1/2}) = 0.515 \cdot \Delta\nu(D_2). \qquad (12')$$

The quantity g_I can now be easily determined from (7), (12), and (12′). We have

$$g_I(D_1) = 21.39 \cdot \Delta\nu(D_1), \qquad (13)$$

$$g_I(D_2) = 22.74 \cdot \Delta\nu(D_2). \qquad (13')$$

Substituting the experimental values of $\Delta\nu$ from Table 2 into (13) and (13′), we obtain the magnetic moments

$$\mu(D_1) = (1.96 \pm 0.02)\ \text{n.m.},$$
$$\mu(D_2) = (1.98 \pm 0.02)\ \text{n.m.}$$

It is easily seen that the two values are very similar. Taking experimental error into account, it can be said that they practically coincide, so that the mean value of the magnetic moment is

$$\mu = (1.97 \pm 0.02)\ \text{n.m.} \qquad (14)$$

DISCUSSION

Upon comparing the value given in (14) with

$$\mu = 2.217\ \text{n.m.}, \qquad (15)$$

obtained by magnetic resonance,[9] a difference is observed which cannot be attributed to experimental error (improvement of experimental conditions does not decrease this discrepancy). Hence, it is necessary to look for the source of the discrepancy in the theoretical expression for the hfs constant. Since all of the corrections to it are determined with fairly good accuracy, it remains only to proceed in the direction of making the wave function more accurate. In 1959, Cohen et al.[10] calculated the wave function for sodium, taking into account the effect of polarization of the electron shell by the optical electron. Using this function, he determined the isotopic shift and obtained very good results. This shows that the polarization effect is significant for light and medium weight atoms. If this effect is taken into account, the expression for the hfs constant takes the form

$$\Delta A(^2S_{1/2}) = \frac{8\pi}{3} R_\infty a_H^3 \frac{\alpha^2}{1836} g_I^{(p)} \left[\psi^2_{3s\uparrow}(0) + (\psi^2_{2s\uparrow}(0) - \psi^2_{2s\downarrow}(0)) + (\psi^2_{1s\uparrow}(0) - \psi^2_{1s\downarrow}(0))\right] \times \chi\left(\frac{1}{2}, Z_i\right) Y. \quad (16)$$

The ratio of Eqs. (4) and (16) becomes a correction factor for the magnetic moment given in Eq. (14).

Obviously

$$\mu^{(p)} = \mu \frac{\frac{Z_i Z_0^2}{\pi a_H^3 n_*^3}\left(1 - \frac{d\sigma}{dn}\right)}{\psi^2_{3s\uparrow}(0) + \left[\psi^2_{2s\uparrow}(0) - \psi^2_{2s\downarrow}(0)\right] + \left[\psi^2_{1s\uparrow}(0) - \psi^2_{1s\downarrow}(0)\right]}, \quad (17)$$

where[10]

$$\frac{Z_i Z_0^2}{\pi a_H^3 n_*^3}\left(1 - \frac{d\sigma}{dn}\right) = \frac{0.840}{a_H^3}$$

and

$$\psi^2_{3s\uparrow}(0) = \frac{0.671}{a_H^3}; \quad \left[\psi^2_{2s\uparrow}(0) - \psi^2_{2s\downarrow}(0)\right] = -\frac{0.013}{a_H^3}; \quad \left[\psi^2_{1s\uparrow}(0) - \psi^2_{1s\downarrow}(0)\right] = \frac{0.050}{a_H^3}.$$

From this we obtain

$$\mu^{(p)} = 1.18 \cdot \mu = (2.32 \pm 0.02) \text{ n. m.}, \quad (18)$$

This value is in relatively good agreement with the value obtained by magnetic resonance, (15).

Table 2 gives a summary of our results in comparison with the results of other authors.

The author expresses his deep gratitude to I. Agîrbiceanu for suggesting this investigation, and for his constant encouragement toward its realization, and also to Ionescu-Pallas for his assistance in the theoretical part of the paper.

Table 2

Author and year	$\Delta\nu(D_1)$ (cm^{-1})	$\Delta\nu(D_2)$ (cm^{-1})	$A(^2S_{1/2})$ (cm^{-1})	μ (n. m.)	Method
Granath, 1933	0.0612	0.0555	0.02915	2.02	Hfs
Jackson, 1935	0.0610	0.0565	0.02950	2.05	Hfs
Meissner, 1937	0.0607	0.0572	0.02970	2.08	Hfs
Kopfermann, 1955	—	—	0.029549	1.958	Deflection of atomic beam
Kusch, 1949	—	—	—	2.217	Magnetic resonance
Draganescu, 1960	0.061	0.058	0.0286	2.32	Hfs

REFERENCES

1. H. Schüler, Naturwissenschaften **16**, 512 (1928).
2. L. N. Dobrezoff and A. N. Terenin, Naturwissenschaften **16**, 656 (1928).
3. L. P. Granath and C. M. van Atta, Phys. Rev. **44**, 935 (1933).
4. D. A. Jackson and H. G. Kuhn, Proc. Roy. Soc. (London) **A148**, 335 (1935).
5. K. W. Meissner and K. F. Luft, Ann. Physik **28**, 667 (1937).
6. H. Kopfermann, Kernmomente, 1955.
7. N. Ionescu-Pallas, private communication.
8. I. Agîrbiceanu, V. Drăgănescu, and A. Chetroiu, Studii si cercetări de Fizică **2**, 247 (1959).
9. P. Kusch et al., Phys. Rev. **75**, 1477 (1949).
10. M. H. Cohen and D. A. Goodings, Proc. Phys. Soc. (London) **73**, 473, 811 (1959).

CALCULATION OF THE PROBABILITY OF AUTOIONIZATION IN He^- AND Be^+ IONS

R. Kh. Propin (pp. 308-311)

Received 27 April 1960

The probability of autoionization in He^- and Be^+ ions is calculated for the $1s2s^2\ ^2S$, $1s2s2p\ ^2P$, $1s2p^2\ ^2S$, and $1s2p^2\ ^2D$ states. The approximate wave functions and energies of these states are found. The probability of autoionization is estimated for an ion with nuclear charge $Z \gg 1$.

The probability of autoionization is given by the equation:

$$w = \frac{2\pi}{\hbar}\left|\int \Psi_i^* \left(\sum_{k\neq l}\frac{e^2}{r_{kl}}\right)\Psi_f d\tau\right|^2, \quad (1)$$

where Ψ_i and Ψ_f are the wave functions of the initial and final states of the system, respectively, and r_{kl} is the distance between electrons (summation and integration are carried out over all the electrons).

The functions of the initial state were evaluated by the variational method. For trial functions we used:

$$\Psi = N^{-1}[\psi_1 + C\psi_2], \quad (2)$$

where N is a normalizing constant and ψ_1 and ψ_2 describe the states of the system with definite values of L, L_z, and S.

In the case of He^-, the ψ functions were built up from one-electron Coulomb functions, the 1s electron being treated as if it was in the field of a 2μ charge, and the remaining electrons in the field of a 1μ charge (in atomic units). In the case of Be^+, the 1s electron was treated as being in the field of a 4μ charge and the remaining electrons in the field of a 3μ charge. The coefficient C and the scale factor μ were determined from the minimum energy condition. The quantum numbers ψ_1 should correspond to the state of interest to us; ψ_2 is a correction to ψ_1, ψ_2 describing the state closest in energy to ψ_1.

Since there exists an infinite set of states with energy lower than those being considered, it is not possible to satisfy all the orthogonality conditions required by the variational method. Indeed, one cannot be certain that the energy obtained is not lower than the true energy. If we replace ψ_1 and ψ_2 by symbols of the states to which they correspond, the wave functions of the initial states are written as follows:

For He^-

(1) $1s2s^2\ ^2S$ state:

$$\Psi = N^{-1}[\psi(1s\,2s^2\,^2S) + C\psi(1s\,2p^2\,^2S)],$$

$$\mu = 0.988; \quad C = 0.481; \quad N^2 = 1.189; \quad E = -2.1476;$$

(2) $1s2s2p\ ^2P$ state:

$$\Psi = N^{-1}[\psi(1s\,2s\,2p^2\,P) + C\psi(1s\,2s\,3p^2\,P)],$$
$$\mu = 0.956;\ C = 0.498;\ N^2 = 1.222;\ E = -2.0666;$$

(3) $1s2p^2\ ^2S$ state:

$$\Psi = N^{-1}[\psi(1s\,2p^2\,^2S) + C\psi(1s\,2s^2\,^2S)];$$
$$\mu = 0.950;\ C = -0.510;\ N^2 = 1.250;\ E = -2.0190;$$

(4) $1s2p^2\ ^2D$ state:

$$\Psi = N^{-1}[\psi(1s\,2p^2\,^2D) + C\psi(1s\,2p\,3p^2\,D)];$$
$$\mu = 0.942;\ C = 0.939;\ N^2 = 1.881;\ E = -2.0434;$$

For Be^+

(1) $1s2s^2\ ^2S$ state:

$$\Psi = N^{-1}[\psi(1s\,2s^2\,^2S) + C\psi(1s\,2p^2\,^2S)];$$
$$\mu = 1.012;\ C = 0.381;\ N^2 = 1.129;\ E = -10.0582;$$

(2) $1s2s2p\ ^2P$ state:

$$\Psi = N^{-1}[\psi(1s\,2s\,2p^2\,P) + C\psi(1s\,2s\,3p^2\,P)];$$
$$\mu = 0.998;\ C = -0.131;\ N^2 = 1.009;\ E = -9.8019;$$

(3) $1s2p^2\ ^2S$ state:

$$\Psi = N^{-1}[\psi(1s\,2p^2\,^2S) + C\psi(1s\,2s^2\,^2S)];$$
$$\mu = 0.971;\ C = -0.406;\ N^2 = 1.162;\ E = -9.5966;$$

(4) $1s2p^2\ ^2D$ state:

$$\Psi = N^{-1}[\psi(1s\,2p^2\,^2D) + C\psi(1s\,2p\,3p^2\,D)];$$
$$\mu = 0.995;\ C = -0.235;\ N^2 = 1.055;\ E = -9.7707.$$

The wave functions of an ion with a shell of three electrons and a nuclear charge $Z \gg 1$ were built up from single-electron Coulomb functions for a field of charge Z. In this case, the expelled electron was treated as being in the field of a charge Z.

The wave function of the final state was chosen in the form:

$$\Psi_f = \frac{1}{\sqrt{6}}\begin{vmatrix} \psi_{100}(1)\,\eta_+(1); & \psi_{100}(2)\,\eta_+(2); & \psi_{100}(3)\,\eta_+(3) \\ \psi_{100}(1)\,\eta_-(1); & \psi_{100}(2)\,\eta_-(2); & \psi_{100}(3)\,\eta_-(3) \\ \psi_{E_{lm}}(1)\,\eta_+(1); & \psi_{E_{lm}}(2)\,\eta_+(2); & \psi_{E_{lm}}(3)\,\eta_+(3) \end{vmatrix}, \quad (3)$$

where η_+ and η_- are spin functions.

For He^-:

$$\psi_{100} = \sqrt{\frac{8\mu^3}{\pi}} \cdot e^{-2\mu r},$$

where the variational parameter $\mu = 0.84375$; $\psi_{E_{lm}}$ is the wave function of the expelled electron for a field with Z = 0 (the wave function corresponds to definite values of l and m and is normalized to a δ-function of the energy).

For Be^+

$$\psi_{100} = 8\sqrt{\frac{\mu^3}{\pi}} \cdot e^{-4\mu r}$$

(the variational parameter $\mu = 0.92187$), $\psi_{E_{lm}}$ is the Coulomb function of a continuous spectrum for the field with charge Z = 2.

The quantum numbers of the wave function of the final state are determined by the condition of conservation of energy E, angular momentum L, its projection on the z-axis L_z, spin S, and parity.

The Table gives the computed values of the probability. Similar values for lithium, from the data of ref. 1, are also given for comparison. The Table shows that the probability of autoionization of an atom or an ion with a shell of three electrons varies relatively slowly with nuclear charge. Autoionization from the $1s2p^2\ ^2S$ state is an exception to this. However, for this state, the matrix elements of the transition for the Li atom, and especially for the Be^+ ion, are the differences of large quantities. The computational error is therefore large in this case, and the result can only be regarded as qualitative.

State	w (sec^{-1})			
	He^-	Li	Be^+	Ion with Z > 1
$1s\,2s^2\,^2S$	$1.11 \cdot 10^{15}$	$8.03 \cdot 10^{14}$	$6.04 \cdot 10^{14}$	$1.03 \cdot 10^{14}$
$1s\,2s\,2p\,^2P$	$1.15 \cdot 10^{15}$	$2.55 \cdot 10^{14}$*	$2.44 \cdot 10^{14}$	$1.01 \cdot 10^{14}$
$1s\,2p^2\,^2S$	$9.30 \cdot 10^{13}$	$2.8 \cdot 10^{12}$	$0.9 \cdot 10^{12}$	$7.84 \cdot 10^{13}$
$1s\,2p^2\,^2D$	$2.48 \cdot 10^{13}$	$2.18 \cdot 10^{13}$	$5.50 \cdot 10^{13}$	$1.86 \cdot 10^{14}$

* For this case, an incorrect value of the transition probability was given in ref. 1. The correct value is given here.

For all the calculations we treated the expelled electron as being in the Coulomb field of an atomic or ionic residue, the charge of the residue being equal to the nuclear charge minus the charge of all of the electrons. This should have the greatest effect on the He^- results. As a check on the importance of this factor, we made the following calculation for the He^- ion.

The emitted electron was treated as being in the field:

$$V = -\frac{Z_p}{r}, \quad (4$$

where

$$Z_p = (2 + 4\mu r) \cdot e^{-4\mu r};\quad \mu = 0.84\,375.$$

These expressions correspond to the approximation for the static field of an He atom.

To simplify the calculation of the effective charge Z_p the following relationships were defined:

$$\left.\begin{array}{lll} Z_p = 0 & \text{for} & r \geqslant 1.258; \\ Z_p = 0.9181 - 0.7298r & \text{"} & 0.652 \leqslant r \leqslant 1.258; \\ Z_p = 1.5369 - 1.6791r & \text{"} & 0.356 \leqslant r \leqslant 0.652; \\ Z_p = 1.9141 - 2.7399r & \text{"} & 0.120 \leqslant r \leqslant 0.356; \\ Z_p = 2.0130 - 3.5741r & \text{"} & 0 \leqslant r \leqslant 0.120. \end{array}\right\} \quad (5)$$

The value of Z_p defined by the relationships (5) does not deviate by more than 0.1 from the values obtained from (4); in the most important region ($0 \leqslant r \leqslant 1.0$) this discrepancy does not exceed 0.025. The solution in each interval is expressed by a confluent hypergeometric function (Kummer function).

The extra contribution to the matrix element of the transition is evaluated by numerical integration according to Eq. (1); it originates in the static field of the He atom. The following result was obtained: for the $1s2s^2\ ^2S$, $1s2s2p\ ^2P$, and $1s2p^2\ ^2D$ states, the probability of a transition increases by 0.34, 1.14, and 0.05%, respectively; for the $1s2p^2\ ^2S$ state the probability is reduced by 30.0%; the exact value $w = 6.51 \times 10^{13}$ sec^{-1}. We may suppose that the corresponding corrections for He, Li, and Be^+ would be still smaller.

Experimentally, the autoionization of Be^+ appears as the absence of the corresponding spectral line. The possibility of forming the He^- ion, and its subsequent decay

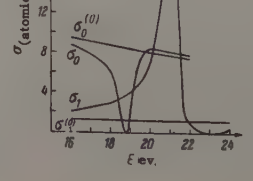

as a result of autoionization, should lead to a resonance in the scattering of slow electrons by He atoms.[2] The Figure shows how the effective scattering cross section σ_0 of electrons with $l = 0$ and the cross section σ_1 of electrons with $l = 1$ changes as a function of their energies ($\sigma_0^{(0)}$ and $\sigma_1^{(0)}$ correspond to potential scattering).[3]

As far as we know, calculations and experiments to determine the probability of autoionization in these ions have not been made previously.

In conclusion I wish to thank B. T. Geilikman for his valuable advice.

REFERENCES

1. P. Kh. Propin, Opt. i Spektr. 8, 300 (1960), Optics and Spectroscopy 8, 158 (1960).
2. L. D. Landau and E. M. Lifshitz, "Kvantovaya Mekhanika" (Quantum Mechanics) 1948. Addison Wesley, Reading, Mass., 1958.
3. H. S. W. Massey and E. H. S. Burhop, "Elektronnye i ionnye stolknoveniya" (Electrons and Ionic Impact Phenomena). Izd. Inostrannoi Lit., Moscow, 1958. Oxford Univ. Press, 1952.

STUDY OF THE STATE OF KRYPTON BEHIND A SHOCK WAVE

A. P. Dronov, A. G. Sviridov, and N. N. Sobolev (pp. 312-321)

Received 13 May 1960

The state of krypton between a shock wave (M = 10-15) was studied by computation and experimentally by means of the light emission of hydrogen present as an impurity. It was found that a temperature determination from the relative intensities of the Balmer lines of hydrogen was complicated by the great width of H_β and H_γ lines and by the intense continuous spectrum which occurred in the region of these lines. It was shown that a determination of the concentration of charged particles is possible from a study of the profiles of the H_α and H_β lines. The experimental data on the concentrations of charged particles differ from calculated values by a factor not greater than two.

The number of investigations devoted to the spectroscopic study of the state of the rare gases behind a shock wave and the processes which occur in the gas is not very large;[1-7] they deal for the most part with argon and xenon. Only one paper,[8] which has appeared recently, contains an account of results obtained in a pyrometric study of the state of neon using chromium lines, and one paper deals with a study of krypton behind a reflected shock wave. Alyamovskii and Kitaeva,[10] using the broadening of the H_β line of hydrogen, determined the concentration of charged particles in argon behind a shock wave reflected from the end of the shock tube. Faizullov, Sobolev, and Kudryavtsev[11] carried out a pyrometric investigation of argon at temperatures in the range 4000-5000°K, and demonstrated a deviation from equilibrium population for the levels of ionic barium at pressures of about one atmosphere in the shock tube. It was found that the generalized reversal method of measuring the temperature of the argon could be used only for pressures higher than 12 atm.

The present investigation deals with a spectroscopic study of krypton behind a shock wave and constitutes a continuation of the investigations cited above [10,11] An attempt was made to study the state of krypton by means of the line emission of hydrogen, present in the gas under study as a natural impurity or purposely added in quantities which did not change significantly the thermodynamical properties of the gas under study.

STATE OF THE PLASMA BEHIND A SHOCK WAVE IN KRYPTON

To obtain some idea of the values of the parameters specifying the state of the plasma behind a shock wave in krypton, a calculation of the temperature, density, pressure, and degree of ionization behind the shock wave was carried out assuming single ionization. Up to a temperature of 20,000°K double ionization of krypton is very small and can be neglected, since the second ionization potential of krypton (26.4 ev) is almost twice as high as the first (13.94 ev). It should be noted that in our calculations no account was taken of radiation losses, which increase with increasing temperature of the gas. Radiation losses for the rare gases begin to play an important role at temperatures higher than 15,000°K. Moreover, in the calculations there was no account taken of the lowering of the ionization potential of krypton, which can reach 0.5-1.0 ev for concentrations of charged particles of the order of 10^{17}-10^{18} cm^{-3}. It was assumed that thermodynamic equilibrium is established behind the shock wave.

The calculation of the state of krypton behind a shock wave was carried out on the basis of the laws of conservation of mass, momentum, and energy:

$$\rho_1 U_S = \rho_2 (U_S - u_2), \tag{1}$$

$$p_1 + \rho_1 U_S^2 = p_2 + \rho_2 (U_S - u_2)^2, \tag{2}$$

$$H_1 + \frac{1}{2} U_S^2 = H_2 + \frac{1}{2} (U_S - u_2)^2, \tag{3}$$

and also the equation of state of the gas

$$\frac{p_2}{\rho_1} = (1 + \alpha_2) \frac{RT_2}{\mu} \tag{4}$$

and the Saha equation

$$\frac{\alpha_2^2}{1 - \alpha_2^2} p_2 = K(T_2). \tag{5}$$

In this system of equations

$$H = \frac{5}{2} (1 + \alpha) \frac{R}{\mu} T + \alpha \frac{N\chi_0}{\mu}$$

is the enthalpy of unit mass, and

$$K(T_2) = \frac{2g^+}{g_0} k \left(\frac{2\pi m_e k}{h^2} \right)^{\frac{3}{2}} T_2^{\frac{5}{2}} e^{-\frac{\chi_0}{kT_2}}.$$

The following designations are used: the index 1 refers to the gas up to the time of passage of the shock wave; the index 2 refers to the gas behind the shock wave; p is the pressure; ρ is the density; U_s is the speed of

the shock wave; u_2 is the speed of the gas particles; α is the degree of ionization; χ_0 is the ionization potential; g_0 is the statistical weight of the neutral atom; g^+ is the statistical weight of the ion; e, k, m_e, h, π have their usual meanings. If the initial state of the gas is known, that is, if ρ_1, p_1, and T_1 are known, and if U_s the speed of the shock wave is known, the equations (1)-(5) allow one to find u_2, ρ_2, p_2, α_2, and T_2.

We can transform the system of equations (1)-(5) into a single equation relating the degree of ionization α_2 to the temperature T:

$$\frac{1-\alpha_2^2}{\alpha_2^2}\cdot\frac{1}{\rho}K-\frac{p_1}{\rho_1}-4(1+\alpha_2)\frac{R}{\mu}T_2-\frac{\alpha_2^2}{1-\alpha_2}\frac{R}{\mu}T_2\frac{p_1}{K}-2\alpha_2\frac{N\chi_0}{\mu}+\frac{5RT_1}{\mu}=0, \quad (6)$$

where N is Avogadro's number and μ is the molecular weight. If the value of T_2 is given it is possible to calculate the corresponding degree of ionization α_2.

In this way, knowing T_2 and α_2 one can easily calculate the pressure p_2, the density ρ_2, and the speed U_s of the shock wave from the formulas

$$p_2=\frac{1-\alpha_2^2}{\alpha_2^2}K, \quad (7)$$

$$\rho_2=\frac{p_2}{\frac{R}{\mu}T_2(1+\alpha_2)}, \quad (8)$$

$$U_s=\left(\frac{p_2}{\rho_1}\cdot\frac{p_2-p_1}{\rho_2-\rho_1}\right)^{\frac{1}{2}}, \quad (9)$$

which are obtained from Eqs. (1)-(5). Having thus determined α_2, p_2, ρ_2, and U_s as functions of T_2, one can construct graphs of the variation of T_2, α_2, p_2, ρ_2, with U_s or with $M = U_s/c_1$, where c_1 is the velocity of sound in krypton (218 meters/sec).

The calculation of the state of krypton behind a shock wave was carried out according to the method described on a "Ural" electronic calculating machine with M varying in the range from 5 to 30; T_2 was assumed to be equal to 293°K, $g_0 = 1$, and $g_1 = 6$. The parameters specifying the state of the krypton behind the shock wave were obtained for six initial pressures p_1, namely 1.0, 2.0, 5.2, 7.0, 10.0, and 15 mm Hg.

The results of the calculation are given graphically in Figs. 1 and 2. As is seen from Fig. 1, the temperature of the krypton plasma for $p_1 = 5.2$ mm increases from 2000 to 17000°K when M rises from 5 to 30. Up to $M = 9$ ($T_2 = 7000$°K) the ionization is negligible (Fig. 2); therefore the temperature of the plasma is also independent of the initial pressure p_1. For $M > 9$ ionization begins to play a significant role. The value of the degree of ionization α_2 is higher for small values of p_1 (and thus also for small p_2) than for high values of p_1; thus all the curves for T vs M are lower for small values of p_1 than for large values of p_1. When M changes from 9 to 30 the degree of ionization rises from 10^{-4} to 0.9, a particularly sharp rise occurring in the region $M = 9$ to $M = 15$.

These are the essential features of the state of krypton behind a shock wave. It is only necessary to note that in view of the neglect of radiation losses and of second ionization, the results of the calculation given should be used with caution for $M > 20$. It can in fact be shown that the parameters for krypton between a shock wave for $M > 20$ are smaller than the calculated values.

DESCRIPTION OF THE APPARATUS

A cylindrical shock tube of constant cross section and 30 mm internal diameter (Fig. 3) was used to produce

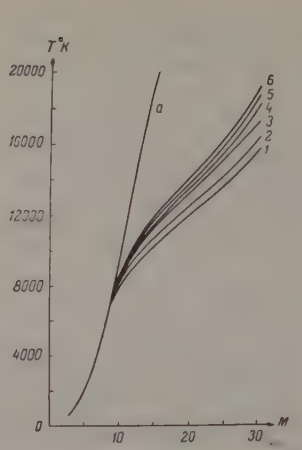

Fig. 1

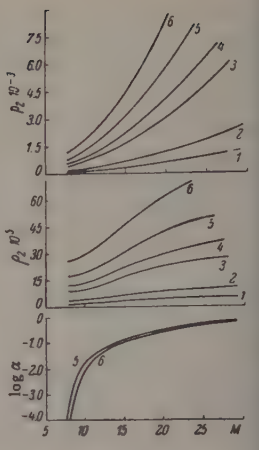

Fig. 2

Fig. 1. Variation of the plasma temperature T_2 behind a shock-wave front in krypton with the M number for different values of the initial pressure p_1 (in mm Hg). Curve 1—p_1 = 1.0; curve 2—p_1 = 2.0; curve 3—p_1 = 5.2; curve 4—p_1 = 7.0; curve 5—p_1 = 10.0; curve 8—p_1 = 15.0.

Fig. 2. Variation of the degree of ionization α_2, the density ρ_2, and the pressure p_2 behind the shock-wave front with the M number for various values of the initial pressure p_1 (in mm Hg). Curve 1—p_1 = 1.0; curve 2—p_1 = 2.0; curve 3—p_1 = 5.2; curve 4—p_1 = 7.0; curve 5—p_1 = 10.0; curve 6—p_1 = 15.0.

the shock waves. A glass tube with thick walls (4-5 mm) served as the low pressure chamber K. The use of a glass tube as the low pressure chamber has notable advantages. There is in fact a large effect on the thermodynamic properties of the gas behind a shock wave due to traces of foreign matter, which inevitably come away from the walls of metal tubes even when these are very carefully cleaned. In work with a glass shock tube the degree of cleanliness can be considerably enhanced.

The low and high pressure chambers were separated by diaphragms made of copper, brass, or aluminum foil 0.1-0.2 mm thick. To obtain strong shock waves the diaphragms were prepared from several layers of foil. Least scatter in the shock wave speeds was obtained by using diaphragms of copper foil which had been annealed beforehand. Hydrogen was used as the driver gas.

The speed of the shock wave was measured by recording on a double-beam OK-17 oscillograph the light signals from the luminous part of the shock wave received by two photomultipliers located 50 cm apart. The sweep of the OK-17 M oscilloscope on which the photomultiplier signals were recorded was triggered with a third photomultiplier.

As an example, Fig. 4 illustrates the appearance of an oscillogram used for the determination of the speed of the shock wave. The spectra were recorded with an ISP-51 spectrograph. A series of measurements was also made with an ISP-51 spectrograph provided with a double-beam photoelectric attachment.

THE SPECTRUM OF THE KRYPTON EMISSION BEHIND A SHOCK WAVE

Emission observable with photographic recording appeared for M values of about 9 and for initial pres-

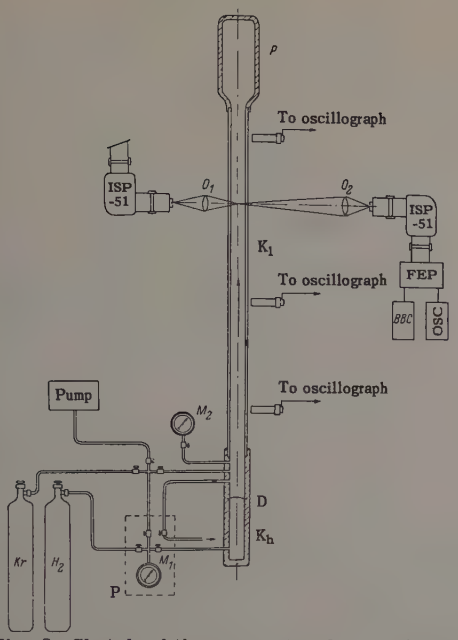

Fig. 3. Sketch of the apparatus for producing and studying shock waves. K_h and K_1 are the high and low pressure chambers, respectively, D the diaphragm, R the receiver, M_1 and M_2 gauges for measuring the pressures in K_h and K_1, P the control panel, Kr and H_2 krypton and hydrogen storage cylinders, O_1 and O_2 lenses, FEP a photoelectric attachment, BBC a high-voltage stabilized rectifier, OSC a double-beam oscillograph with retarded sweep. Also shown are the photomultipliers (ISP-51) which furnish the signals for measuring the shock-wave speeds.

sures of a few mm Hg. The intensity of the emission increased steadily in approaching more extreme conditions. Figure 5 shows a photograph of the spectrum of the emission. In the region 3900-6500 A, 20 krypton lines and 15 xenon lines were observed. The sodium D lines and the calcium resonance line at 4227 A were very weak or, on some spectrograms, not present at all. The Ca^+ lines at 3968 and 3933 A were intense. A continuous spectrum was observed under all conditions, its intensity increasing with increasing M. In addition to the Kr, Xe, Ca, and Na lines the H_α and H_β lines were always present on the spectrograms, even when hydrogen was not purposely introduced into the low pressure chamber. A mass-spectrographic analysis of the krypton used for filling the low pressure chanber showed that the following gases were present as impurities: xenon 2.28% (by pressure), hydro-

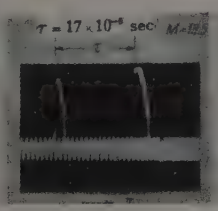

Fig. 4. Oscillogram for determining the shock-wave speed. $\tau = 17 \times 10^{-5}$ sec; M = 13.5.

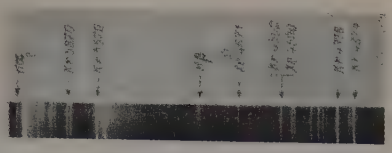

Fig. 5. Spectrum of the emission of krypton behind a shock wave.

gen 0.11%, hydrocarbons 0.11%, nitrogen 0.52%, oxygen 0.04%, and carbon dioxide 0.09%. Thus, we can assume that the concentration of hydrogen atoms in the krypton used in the investigation was less than 1%.

The H_α, H_β, and H_γ lines were broadened. In the center of H_β a gap was observed. H_γ was observed only up to M = 11.5; at higher values it was greatly broadened and blended with the background. H_δ was not observed at all. We note that because of the presence of the strong continuous spectrum the Inglis-Teller method[12] of estimating the concentration of charged particles by the disappearance of the hydrogen lines is quite unsuitable for studying the state of krypton behind a shock wave, since its use would always overestimate the concentration.

MEASUREMENT OF THE TEMPERATURE BY THE RELATIVE INTENSITIES OF THE H_α AND H_β LINES

An attempt was made to measure the plasma temperature using the relative intensities of the hydrogen H_α and H_β lines. It was found that the natural hydrogen impurity was not sufficient to obtain line intensities which were markedly greater than the background. Hydrogen amounting to 8-10% was therefore added to the low pressure chamber; this gave increased intensities for the H_α and H_β lines and reduced the continuous background.

Two series of experiments were carried out under these conditions to measure the temperature of the krypton behind the shock wave. The working conditions of the shock tube were such that, according to the calculations, one could expect a temperature of 9000° in the first series and 9800°K in the second series.

The first series of experiments gave a temperature of 5500° ± 400°K and the second 7000° ± 250°K. Thus, in both series of experiments the temperature was lower than that calculated. This discrepancy in the temperature can be related to two circumstances. In the first place, as the experiments mentioned below showed (Table 3), the half-width of the H_β line could reach 20 A; thus for a slit width of 0.4 mm and a linear dispersion of 40 A/mm in the region of H_β not all wavelengths contributed to the intensity so that the line intensity was reduced, whereas the intensity of the H_α line would have been measured correctly. This could have lead to a reduced value of the temperature. In the second place, the calculated values of the temperature, with which the experimental temperatures were compared, were obtained assuming pure krypton. The addition of 8-10% hydrogen to the krypton could lower considerably the temperature of the mixture studied and lead to the observed discrepancy.

Thus, the experiments showed with certainty that the use of hydrogen lines for the measurement of the temperature of krypton behind a shock wave is unsatisfactory because of the large width of the H_β line and the presence of an intense background which prevented a reliable measurement of its intensity by integrating over the profile.

DETERMINATION OF THE CONCENTRATION OF CHARGED PARTICLES IN THE KRYPTON FROM THE WIDTHS OF H_α AND H_β

The method of determining the concentration of charged particles from the profiles of hydrogen lines has been widely used in the study of the arc plasma.[13] Kitaeva and Alyamovskii[10] have also used this method for investigating the plasma existing behind a reflected shock wave in argon.

We have applied the method of determining the concentration of charged particles by the H_α and H_β lines to the plasma in krypton behind a progressive shock wave in a comparatively wide range of shock wave velocities (10-15 M).

Spectrograms for the study of the profile of H_α were obtained with an ISP-51 spectrograph with a long focal length camera and collimator (F = 800 mm). In studying the profile of H_β the exposures were made with the ISP-51 spectrograph with medium cameras (f = 270 and 300 mm).

The H_α line was photographed on Aerofoto plates, and H_β on Flyuorapid plates. In constructing the intensity contour of the H_β line it was necessary in view of its large width to take the variation of the plate sensitivity with wavelength into account. Figures 6 and 7 show profiles of the H_α and H_β lines for two sets of experimental conditions.

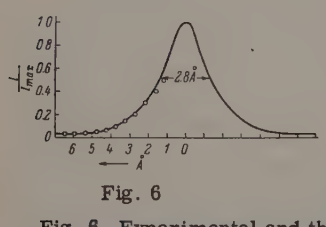

Fig. 6

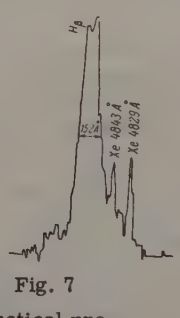

Fig. 7

Fig. 6. Experimental and theoretical profiles of the H_α line. Experimental conditions: M = 10.8; T = 9160°K; $N_i = 2.2 \times 10^{16}$ cm^{-3}.

Fig. 7. Microphotometer trace of the profile of H_β. Experimental conditions: M = 11.5; T = 9600°K; $N_i = 2.0 \times 10^{16}$ cm^{-3}.

The determination of the concentration of charged particles was carried out by comparing the experimental profiles of H_α and H_β with profiles predicted by the Holtsmark theory. This was done by choosing theoretical profiles which agreed best with the experimental profiles (Fig. 6). The comparison was of course made in the wings of the lines, for which the Holtsmark theory is valid. As may be seen from Fig. 6, for H_α the agreement of theory and experiment is entirely satisfactory. In view of the marked background and the xenon lines at 4843 and 4829 A which occur in the region of H_β, more accurate data on the concentration N_i were obtained from this line by using its half-width $\Delta\lambda$ in the formula[14]

$$N_i = \left(\frac{\Delta\omega}{15.6\alpha}\right)^{\frac{3}{2}}, \qquad (10)$$

After substituting the value of the effective Stark constant for H_β, $\bar{\alpha} = 10.5$, and going over from the half-width expressed in cyclic frequencies $\Delta\omega$ to the half-width expressed in Angstrom units, one obtains the form more suitable for calculations:

$$N_i = 3.4 \cdot 10^{14} (\Delta\lambda)^{\frac{3}{2}}. \qquad (11)$$

On the other hand it is not feasible to determine the concentration from the half-width of H_α, since this line has a central component the broadening of which is not given by the Holtsmark theory. The results of the determination of the concentration of charged particles by H_α and H_β lines for the initial krypton pressure $p_1 = 5.2$ mm Hg, with natural hydrogen impurity, are given in Tables 1 and 2 and in Fig. 7. Tables 1 and 2 are set up in the same way. The first column gives the hydrogen pressure at which the diaphragm burst, the second the number of experiments required to obtain one spectrogram, the third the M number with an indication of the scatter of the combined experiments, the fourth the measured half-width, and the fifth the concentration of charged particles determined from the profile of H_α and from the half-width of H_β. The three following columns give respectively the temperature, the degree of ionization α, and the concentration of charged particles calculated from the experimental measurements of the shock wave velocities (cf. Figs. 1 and 2).

Table 1. Results of the Determination of the Concentration of Charged Particles from the Width of the H_α Line

Pressure of H_2 (atm)	No. of experiments to obtain one spectrogram	M	$\Delta\lambda$ (in Å)	$N_i \cdot 10^{-16}$	T °K	α	$N_i \cdot 10^{-16}$ (theor.)
24	5	10.8 ± 0.2	2.3	1.5	9160	0.025	2.1
25	5	10.8 ± 0.2	2.8	2.2	9160	0.025	2.1
33	4	11.2 ± 0.2	2.9	1.7	9440	0.032	2.8
35	2	11.5 ± 0.1	3.9	2.4	9600	0.037	3.2
46	2	12.0 + 0.1	4.0	3.2	10000	0.054	5.1
46	2	12.0 ± 0.1	4.0	3.8	10000	0.054	5.1
48	1	12.3	4.7	4.3	10100	0.057	6.0
49	1	12.6	4.2	4.1	10360	0.070	7.0
49	1	12.6	4.7	4.7	10360	0.070	7.0
47	1	13.4	6.5	8.5	10700	0.089	10.0
74	1	13.5	6.8	5.5	10800	0.095	10.5
74	1	13.5	6.9	7.0	10800	0.095	10.5
100	1	14.0	7.2	10.4	11000	0.10	12.2
98	1	14.0	7.2	10.1	11000	0.10	12.2
100	1	14.0	7.1	11.2	11000	0.10	12.2
127	1	14.3	9.5	12.8	11160	0.11	13.4
132	1	14.3	9.8	10.7	11160	0.11	13.4

Table 2. Results of the Determination of the Concentration of Charged Particles from the Width of the H_β Line

Pressure of H_2 (atm)	No. of experiments to obtain one spectrogram	M	$\Delta\lambda$ (in Å)	$N_i \cdot 10^{-16}$	T °K	α	$N_i \cdot 10^{-16}$ (theor.)
19	5	9.7 ± 0.1	9.6 ± 0.4	1.0	8300	0.010	0.66
22	9	10.1 ± 0.4	13.2 ± 0.4	1.6	8600	0.015	1.1
29	4	11.1 ± 0.2	14.4 ± 0.3	1.9	9200	0.026	2.6
35	2	11.5 ± 0.1	15.2 ± 0.4	2.0	9600	0.037	3.5
39	2	11.8 ± 0.1	19.0 ± 0.3	2.8	9920	0.050	4.5
40	2	11.8 ± 0.1	18.8 ± 0.3	2.8	9920	0.050	4.5
44	1	12.0	20.0 ± 0.2	3.0	10000	0.054	5.1
58	1	12.5	22.0 ± 0.2	3.5	10300	0.070	7.0
67	1	13.0	26.0 ± 0.2	4.5	10600	0.079	8.4

As can be seen from the tables and Fig. 8 the agreement between the experimental and the theoretical data is quite satisfactory. The discrepancy never exceeds a factor of 1.5-2. However, a more careful examination of the figure shows that most of the experimental points lie lower than the theoretical curve. This can be due to two circumstances: firstly, the reduced value of the gas temperature as compared with the calculated value resulting from the presence of hydrogen and other impurities in the krypton and, secondly, the neglect of various radiation losses in the calculation. An effect in the same direction can be due to the fact that the emission recorded by the photographic plate is integrated over the nonhomogeneous luminous portion of the shock wave.

If all of these circumstances are taken into account we can consider that there is adequate agreement be-

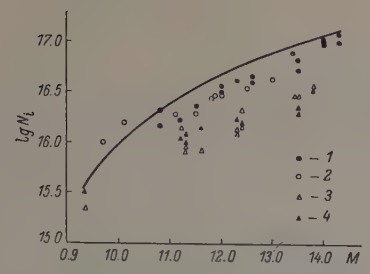

Fig. 8. Results of the experimental determination of the concentration of charged particles by the H_α and H_β lines of hydrogen. 1—H_α; 2—H_β; 3—H_α with added H_2; 4—H_β with added H_2. The solid curve is calculated.

tween theory and experiment and thus corroborate that the initial simplifying assumptions of the gas-dynamical calculations are permissible.

In addition to the experiments on the determination of the concentration of charged particles in krypton with the natural impurity of hydrogen, we carried out a similar series of experiments with the addition of larger concentrations of hydrogen to the krypton. The results of these experiments are given in Table 3 and Fig. 8. The experiments showed that the addition to the krypton of hydrogen impurities up to 5% by pressure lowers the shock wave speed by a negligible amount. However, the character of the emission changes: the intensity of the continuous spectrum decreases relatively to the line intensities, but the absolute intensities of the hydrogen lines also decrease.

Table 3. Results of the Determination of the Concentration of Charged Particles from the Widths of the H_α and H_β Lines with Added H_2

Pressure of H_2 (atm)	No. of experiments	H_2 content (%)	M	H_α		H_β	
				$\Delta\lambda$ (в Å)	$N_i \cdot 10^{-16}$	$\Delta\lambda$ (в Å)	$N_i \cdot 10^{-16}$
25	3	3	9.35 ± 0.4	1.68	0.22	4.4	0.32
33	4	1.7	11.2 ± 0.1	3.1	1.4	10.0	1.1
32	2	1.6	11.3	2.8	0.83	9.6	1.0
33	2	1.5	11.3	2.8	0.9	10.6	1.2
40	1	1.6	11.8	2.8	0.82	12.0	1.4
48	1	3.3	12.3	4.1	1.3	14.0	1.8
48	1	3.3	12.3	3.7	1.6		
48	1	3.3	12.4	3.5	2.2	13.0	1.6
48	1	3.3	12.4	3.8	1.5		
77	1	5	13.5	5.2	3.0	—	—
77	1	4	13.5	4.7	3.1	15.8	2.0
77	1	3.3	13.5	—	—	17.2	2.4
94	1	4	13.8	5.4	3.6	22.4	3.6

As is seen from Table 3 and Fig. 8, the concentration of charged particles is also markedly decreased. All these facts are quite understandable, since according to calculations the addition of hydrogen should show a negligible effect on the shock wave velocity in a mixture of krypton and hydrogen, but the temperature of the gas behind the shock wave, and consequently also the concentration of charged particles, should be markedly reduced.

CONCLUSION

The experiments which were carried out showed that the determination of the temperature from the relative intensities of the H_α and H_β lines behind a shock wave in krypton is hampered by the great width of the H_β line and by the continuous spectrum which surrounds this line. On the other hand the determination of the concentration of charged particles from the half-widths of the H_α and H_β lines can be recommended for the study of the krypton plasma.

In considering further work on the study of the rare gases behind a shock wave, it would clearly be expedient to try to use for temperature measurement a method based on the absolute intensity of the hydrogen H_α line. A study of the continuous spectrum also offers important possibilities.

The authors express their gratitude to G. V. Kazakova for her assistance in the investigation.

Note added in proof:

In the calculation of the state of krypton behind a shock wave we used for the statistical weight of the ion in Saha's formula the sum of the statistical weights ($g^+ = g_1^+ + g_2^+ = 4 + 2 = 6$) of the two lowest states which are separated from one another by $\Delta E = 5371\ cm^{-1}$. It would have been more correct to use the statistical sum of these two states, $g_1^+ + g_2^1 \exp(-\Delta E)kT = 4 + 2\exp(-\Delta E/kT)$. For temperatures of 10,000-15,000°K this statistical sum would be equal to 4.9-5.1, and not 6. Substitution of g^+ for the statistical sum in the expression for $k(T_2)$ leads to a decrease in the value of α_2 calculated by formula (5) by only 8%. Thus the calculated curve in Fig. 8 for the concentration of charged particles should be lowered by about 1 mm. As a result the agreement between theory and experiment is still more satisfactory.

REFERENCES

1. E. L. Resler, Shao-Shi Lin, and A. Kantrowitz, J. Appl. Phys. 23, 1390 (1952).
2. H. E. Petschek, P. H. Rose, H. S. Glick, A. Kane, and A. Kantrowitz, J. Appl. Phys. **26**, 83 (1955).
3. H. Petschek and S. Byron, Ann. of Phys. **1**, 270 (1957).
4. W. Roth and P. Gloersen, J. Chem. Phys. **29**, 820 (1958).
5. W. Roth, J. Chem. Phys. **31**, 720 (1959).
6. W. Lochte-Holtgreven, Izvest. Akad. Nauk SSSR, Ser. Fiz. **22**, 1297 (1958).
7. S. R. Kholev, Voprocy magnitnoi gidrodinamiki i dinamiki plazmy (Problems in the magneto-hydrodynamics and the dynamics of plasma). Trudy Konf., Riga (Transactions of the Riga conference), 1958, p. 93.
8. G. Charutis and T. D. Wilkerson, Phys. Fluids **2**, No. 5, 578 (1959).
9. O. Weber, Z. Physik **152**, 3, 281 (1958).
10. V. N. Alyamovskii and V. F. Kitaeva, Opt. i Spektr. **8**, 152 (1960), Optics and Spectroscopy **8**, 80 (1960).
11. F. S. Faizullov, N. N. Sobolev, and E. M. Kudryavtsev, Opt. i Spektr. **8**, 761 (1960), Optics and Spectroscopy **8**, 400 (1960).
12. D. R. Inglis and E. Teller, Astrophys. J. **90**, 439 (1939).
13. W. Lochte-Holtgreven, Repts. Progr. in Phys. **21**, 312 (1958).
14. V. I. Kogan, "Fizika plazmy i problema upravlyaemykh termoyadernykh reaktsii" (Plasma Physics and the Problem of Controlled Thermonuclear Reactions), IV p. 295, Izd. Akad. Nauk SSSR, Moscow, 1958.

VIBRATIONAL SPECTRA OF AROMATIC COMPOUNDS
VIII. Characteristic Vibrations of 1,2-Orthodisubstituted Benzenes

A. M. Bogomolov (pp. 322-327)

Received 16 May 1960

A classification of the characteristic vibrations of 1,2-orthodisubstituted benzenes has been carried out on the basis of a calculation of the frequencies. vibration forms, and atomic displacements of ortho-xylene during its vibrations.

RESULTS OF THE CALCULATION

The procedure for the calculation of the characteristic (specific) vibrations of substituted benzenes has been set forth in the preceding article of this series.[1] In the present work, this procedure is applied to the determination of the characteristic vibrations of 1,2-orthodisubstituted benzenes. In our article,[2] an interpretation of the vibrational spectra of ortho-xylene was carried out on the basis of a calculation of the frequencies and vibration forms, and a correlation of the vibrations of ortho-xylene with the vibrations of benzene was given. Here this correlation is confirmed by a calculation of the atomic displacements of ortho-xylene during its vibrations. The fundamental results of the calculations are presented in Tables 1-4 and in the Figure. In Tables 1-3 are given the atomic displacements of ortho-xylene for vibration types A_1, B_1, B_2, and A_2 in Angstroms along the coordinate axes. The total displacement of an atom is obtained by vector addition of the coordinate displacements. Each column of the table gives the components of the displacements of all atoms during the vibration with the frequency indicated at the head of the column ($\nu_{obs.}$, $\nu_{calc.}$). Each row of the table gives the components of the displacements of equivalent atoms, with their signs, for all vibrations represented in the table. Only the atomic displacements during vibrations of the ring are shown in the table; the displacements during vibrations of the methyl groups are not included in the table, as being of no interest.

The designations of the atoms of ortho-xylene and

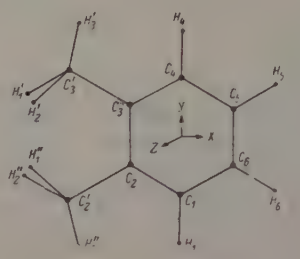

The atomic displacements of the methyl groups durin planar vibrations of the ring have negligibly small components along the OZ axis and are therefore not shown in Tables 1 and 2. Atoms lying in the plane of the molecule have zero displacements along the OZ axis for types A_1 and B_1, and zero displacements along the OX and OY axes for types A_2 and B_2.
the positive directions of the coordinate axes are shown in the Figure. The atoms of the methyl groups are denoted by primes, and the atoms H'_3 and H''_3 are located in the plane of the ring.

In Table 4 are presented the vibration frequencies of 1,2-orthodisubstituted benzenes, divided into three groups—frequencies of completely characteristic vibrations, of vibrations characteristic in frequency, and of noncharacteristic vibrations. CH valence vibrations are not included in the table. The experimental frequency values in Table 4 are based on the results given in numerous literature sources.[3-20]

Table 1. Displacements (in A) of the Atoms of Ortho-Xylene During Planar Vibrations

	Representation A_1										
$\nu_{obs.}$	180	582	735	1054	1159	1223	1300	1500	1584	3030	3045
$\nu_{calc.}$	211	564	729	1085	1153	1239	1306	1518	1610	3052	3067
xC_1, xC_4	−0.002	0.008	0.010	−0.005	0.005	−0.001	−0.012	0.010	0	0	0
xC_2, xC_3	0.016	−0.008	0.005	−0.006	−0.003	−0.015	0.004	−0.007	−0.003	0	0
xC_6, xC_5	0	0.020	−0.001	0.012	0.002	0.002	0.005	−0.001	0.004	−0.001	0.004
xH_1, xH_4	−0.013	0.011	0.021	−0.029	0.028	0.039	0.019	−0.031	−0.001	0	0
xC'_2, xC'_3	−0.005	−0.017	−0.014	0	−0.001	0.007	0.001	0.002	0	0	0
xH_6, xH_5	0.001	0.016	0.007	0.008	−0.032	0.018	−0.012	−0.012	−0.009	0.013	−0.040
yC_1, $-yC_4$	−0.011	0.016	−0.021	−0.008	−0.002	−0.004	0	0	−0.006	−0.004	−0.001
yC_2, $-yC_3$	0.021	0.004	−0.005	0.005	0.003	−0.004	−0.013	−0.011	0.012	0	0
yC_6, $-yC_5$	−0.013	0.001	0.002	−0.006	−0.006	0.001	0.012	0.003	0.013	0.001	−0.002
yH_1, $-yH_4$	−0.011	0.016	−0.021	−0.008	−0.003	−0.004	−0.001	0	−0.005	0.047	0.015
yC'_2, $-yC'_3$	0.054	−0.008	−0.009	0.009	0.002	0.003	0.001	0.003	−0.001	0	0
yH_6, $-yH_5$	−0.011	−0.007	0.014	−0.010	−0.061	0.024	−0.020	−0.008	−0.009	−0.008	0.023
$y(H'_1, H''_1, H'_2, H''_2)$	−0.041	−0.018	−0.013	−0.004	0.011	0.003	−0.001	0.017	0.005	0	0
xH'_3, xH''_3	−0.099	−0.013	0.001	0.030	0.007	0.001	0.002	−0.010	−0.010	0	0
$x(H'_1, -H''_1, H'_2, -H''_2)$	0.076	−0.007	−0.014	−0.014	−0.005	0.010	0.001	−0.003	0	0	0
yH'_3, $-yH''_3$	0.031	−0.002	−0.003	0.011	0.003	0.002	0.001	0	−0.003	0	0

Table 2. Displacements (in A) of the Atoms of Ortho-Xylene During Planar Vibrations

	Representation B_1									
$\nu_{obs.}$	406	506	830	1118	1223	1290	1448	1609	3045	—
$\nu_{calc.}$	371	508	803	1114	1227	1275	1448	1617	3055	3071
xC_1, $-xC_4$	0.013	0.013	0.006	0.006	0.005	—0.006	0	0.015	0	0
xC_2, $-xC_3$	0.002	0.016	—0.001	—0.002	0.009	—0.011	0.010	—0.011	0	0
xC_6, $-xC_5$	0.003	0.012	0.019	—0.003	—0.007	0.001	—0.010	—0.006	—0.004	—0.001
xH_1, $-xH_4$	0.035	0.008	—0.008	0.041	0.037	0.052	0.005	—0.014	0	0
xC'_2, $-xC'_3$	—0.045	0.019	—0.016	0.003	—0.010	0.005	—0.002	0.002	0	0
xH_6, $-xH_5$	0.012	0.017	0.025	—0.022	—0.014	0.020	0.015	0	0.040	0.014
yC_1, yC_4	—0.006	—0.009	0.007	0.011	—0.007	—0.001	0.005	0	—0.001	0.004
yC_2, yC_3	—0.014	0.001	—0.010	—0.003	0.012	0	—0.001	0.002	0	0
yC_6, yC_5	0.017	—0.009	—0.010	—0.002	0.003	—0.001	—0.007	—0.004	0.002	0.001
yH_1, yH_4	—0.006	—0.009	0.007	0.012	—0.008	—0.001	0.007	—0.016	0.016	—0.046
yC'_2, yC'_3	0.028	0.025	—0.008	0	—0.002	0.002	—0.002	0	0	0
yH_6, yH_5	0.028	0	0.002	—0.041	—0.013	0.024	0.036	0.007	—0.023	—0.008
$x(H'_1, -H''_1, H'_2, -H''_2)$	0.030	—0.010	0.010	—0.004	0.010	0.001	—0.022	—0.005	0	0
xH'_3, $-xH''_3$	0.057	0.001	—0.001	—0.016	0.014	0.002	0.012	0.003	0	0
$y(H'_1, H''_1, H'_2, H''_2)$	—0.016	—0.022	0.012	0.007	—0.001	—0.007	0.009	—0.001	0	0
yH'_3, yH''_3	—0.001	—0.013	0.003	—0.007	0.007	0.001	0.001	0	0	0

Table 3. Displacements (in A) of the Atoms of Ortho-Xylene During Nonplanar Vibrations

	Representation A_2					Representation B_2			
$\nu_{obs.}$	180	505	710	862	986	250	433	740	940
$\nu_{calc.}$	183	486	704	869	978	228	425	746	946
zC_1, zC_4	0.027	0.011	—0.013	—0.013	—0.006	—0.020	0.025	—0.007	—0.012
zC_2	0.020	—0.025	0.010	—0.005	0.010	—0.035	—0.021	0.005	0.001
zC_3	—0.030	0.020	—0.015	0.004	—0.011	—0.046	—0.025	0.007	0.004
zC_5, zC_6	—0.031	—0.020	—0.023	—0.004	—0.008	0.022	0.002	—0.010	0.008
zH_1, zH_4	0.048	—0.009	—0.037	0.074	0.035	—0.016	0.065	0.051	0.063
zC'_2	—0.008	0.001	0.004	0.002	—0.001	0.019	0	0.001	0.002
zC'_3	0.041	0.010	0.003	0.001	0.003	0.049	0.008	—0.004	—0.003
zH_5, zH_6	0.090	0.071	—0.007	—0.014	0.035	0.062	—0.016	0.077	—0.044
$z(H'_1, H''_1, H'_2, H''_2)$	—0.044	—0.010	—0.005	—0.002	—0.001	—0.034	—0.007	0.003	0.003
zH'_3, zH''_3	—0.045	—0.012	—0.007	—0.003	—0.003	—0.035	—0.008	0.005	0.006
$z(H'_1, H''_1, -H'_2, -H''_2)$	0.001	0.012	0.015	0.004	0.004	0.017	0.011	—0.006	—0.008
$y(H'_1, -H''_1, -H'_2, H''_2)$	0.002	—0.006	—0.007	—0.002	—0.001	—0.008	—0.006	0.002	0.003

Table 4. Vibrations of 1,2-Orthodisubstituted Benzenes, Their Correlation with the Vibrations of Benzene, and Their Specificity Properties

Vibrations characteristic in frequency, form, and atomic displacements for the C_6H_4 coordinate group						
No. of the vibration	$\nu_{obs.}$ IR	$\nu_{obs.}$ Ram.	$\nu_{calc.}$	Symmetry	Benzene vibrations	
1	750 ± 6	745 ± 10	746	B_2	849	10a
2	865 ± 10	854 ± 7	869	A_2	849	10b
3	940 ± 10	—	946	B_2	970	17a
4	1156 ± 8	1158 ± 5	1153	A_1	1178	9a
5	1310 ± 12	—	1306	A_1	1310	14
6	1581 ± 9	1585 ± 6	1610	A_1	1596	8a
7	1610 ± 8	1606 ± 10	1617	B_1	1596	8b
Vibrations characteristic in frequency						
8	430 ± 5	410 ± 10	425	B_2	405	16a
9	—	482 ± 10	486	A_2	970	17b
10	580 ± 12	585 ± 8	564	A_1	606	6a
11	—	698 ± 10	704	A_2	703	4
12	750 ± 6	745 ± 10	729	A_1	992	1
13	827 ± 5	820 ± 10	803	B_1	1010	12
14	977 ± 10	990 ± 5	978	A_2	985	5
15	1036 ± 6	1030 ± 10	1085	A_1	1037	18b
16	1130 ± 8	1120 ± 12	1114	B_1	1037	18a
17	1292 ± 8	1285 ± 6	1275	B_1	1326	3
18	1445 ± 5	1452 ± 7	1448	B_1	1485	19a
19	1500 ± 3	1496 ± 8	1518	A_1	1485	19b

Noncharacteristic vibrations

No. of the vibration	Orthoxylene $\nu_{obs.}$	Orthoxylene $\nu_{calc.}$	Symmetry	Substituent group I (R_1R_2=C_nH_m)	Substituent group II (R_1R_2=O,N,S,Cl,Br,I,F)	Benzene vibrations	
20	180	183	A_2	150 — 200	100 — 200	405	16b
21		211	A_1	180 — 250	150 — 230	1150	15
22	250	228	B_2	220 — 300	200 — 320	671	11
23	406	371	B_1	350 — 400	250 — 400	1178	9b
24	506	508	B_1	450 — 510	430 — 550	606	6b
25	1223	1227	B_1	1220 ± 12	1170 — 1210		
26		1239	A_1	Characteristic for the $C_6H_4C_2$ group	1210 — 1270		

Note: Frequency in cm^{-1}. Symbols: Ram. – Raman spectra; IR – infrared absorption spectra.

The determination of the specificity of the vibrations was carried out on the basis of calculation of the frequencies and form coefficients of the vibrations. The criteria for complete specificity of a vibration are: for frequency, the nonspecificity coefficient;[21] for the forms of the vibrations, the smallness of that portion of the vibration form coefficients corresponding to coordinates of the substituents (methyl and ethyl group); for the displacements, the smallness of the components of the atomic displacement vectors of the substituent during a given vibration.

The values of the form coefficients and components of the displacements are considered small if their ratio to the maximum coefficient or component amounts to not more than 5%. This quantity is just comparable with the rounding-off error in the computations of the form coefficients and atomic displacements. For determination of the specificity of a vibration with respect to frequency only, we carried out a diagonalization of the submatrices of the ortho-xylene and ortho-diethylbenzene rings and compared their diagonal elements to determine the nonspecificity coefficient. If the nonspecificity coefficient did not exceed 10%, the vibration was considered specific with respect to frequency.

We make the following notes with regard to individual normal vibrations:

Nos. 1, 12. The intense band with the frequency 750 cm^{-1} observed in the Raman and infrared spectra is a

superposition of two normal vibrations—the nonplanar type B_2 vibration 10a and the planar totally symmetric A_{1g} vibration.

No. 15. In ortho-xylene, the vibration has the frequency 1054 cm^{-1}. As the substituents grow heavier, the frequency drops by 15 to 20 cm^{-1} and thereafter does not depend on the nature and mass of the substituents.

Nos. 16, 23. The correlation of these vibrations of orthosubstituted benzenes with the vibrations of benzene has been changed in comparison with ref. 2. This change is based on calculation of the atomic displacements of ortho-xylene and comparison of them with the atomic displacements of benzene and toluene[1] during the vibrations.

No. 21. The benzene vibration 15 (B_{2u}) is very sensitive to any type of substitution in the benzene ring. On substitution, the frequency of the vibration is abruptly lowered to the 200-300 cm^{-1} interval.

Nos. 25, 26. Valence vibrations of the C—X bonds connecting the ring with the substituents. Both vibrations are characteristic in frequency for the $C_6H_4C_2$ coordinate group, and in the spectra a single intense band with the frequency 1220 ± 12 cm^{-1} corresponds to them. For group II substituents, there is no specificity with respect to frequency, and two bands in different regions of the spectrum correspond to the two vibrations.

The conclusions reached in ref. 1 concerning the character of the removal of degeneracy for the degenerate benzene vibrations on monosubstitution, and concerning the connection of the specificity of the vibrations with the atomic displacements, are also confirmed for 1,2-orthodisubstituted benzenes, as follows from Table 4.

In conclusion, the author thanks M. A. Kovner for his interest in the work and for discussions.

REFERENCES

1. A. M. Bogomolov, Opt. i Spektr. **9**, 311 (1960), Optics and Spectroscopy **9**, 162 (1960).
2. M. A. Kovner and A. M. Bogomolov, Opt. i Spektr. **7**, 751 (1959), Optics and Spectroscopy **7**, 444 (1959).
3. G. S. Landsberg, P. A. Bazhulin, and M. M. Sushchinskii, "Osnovnye parametry spektrov kombinatsionnogo rasseyaniya" (Fundamental Parameters of Raman Spectra). Izd. Akad. Nauk SSSR, Moscow, 1956.
4. R. R. Randle and D. H. Whiffen, Molec. Spectrosc. 7, 111 (1955).
5. M. M. Sushchinskii, Izvest. Akad. Nauk SSSR, Ser. Fiz. **17**, 608 (1953).
6. G. S. Landsberg, B. A. Kazanskii, P. A. Bazhulin, T. F. Bulanova, A. L. Liberman, E. A. Mikhailova, A. F. Plate, Kh. E. Sterin, M. M. Sushchinskii, G. A. Tarasova, and S. A. Ukholin, "Opredelenie individual'nogo uglevodorodnogo sostava benzinov pryamoi gonki kombinirovannym metodom" (Determination of the Individual Hydrocarbon Composition of Straight-Run Gasolines by the Raman Method). Izd. Akad. Nauk SSSR, Moscow, 1959.
7. K. Kohlrausch, "Spektry kombinatsionnogo rasseyaniya" (Raman Spectra). Izd. Inostrannoi Lit., Moscow, 1952. Edwards, Ann Arbor, Michigan.
8. Landolt-Börnstein Zahlenwerte und Funktionen, Vol. 1, Pt. II, 1951.
9. E. G. Treshchova and V. I. Tatevskii, Doklady Akad. Nauk SSSR **61**, 841 (1948).
10. E. K. Plyler, Discuss. Faraday Soc. No. 9, 100 (1950).
11. H. L. McMurry and V. Thornton, Anal. Chem. **24**, 318 (1952).
12. M. R. Freske, W. G. Braun, R. V. Wiegand, D. Quiggle, R. H. McCormick, and R. H. Rank, Anal. Chem. **19**, 700 (1947).
13. E. A. Glebovskaya, A. A. Zakharov, I. K. Lapina, and Z. G. Kaplan, Trudy Vsesoyuz. Nauch.-Issledovatel. Geol.-Razved. Inst. **105**, Geokhim. Sbornik No. 4, 23 (1957).
14. D. C. Biswas, Indian J. Phys. **29**, 179 (1955); Ibid. **28**, 303 (1954).
15. A. Hidalgo and J. Bellanato, Anales real soc. españ. fis. y quím. (Madrid) **51B**, 227 (1955).
16. J. Lecomte, Cahiers phys. No. **77**, 1 (1957).
17. S. L. N. G. Krishnamachari and Rao V. Ramakrishna, Indian J. Phys. **29**, 254 (1955).
18. R. B. Barnes, R. C. Gore, U. Liddel, and V. Z. Williams, "Infrared Spectroscopy." Reinhold, New York, 1944.
19. N. A. Narasimham, J. Chem. Phys. **24**, 420 (1956).
20. J. Lecomte, "Infrakrasnoe izluchenie" (Infrared Radiation). Fizmatgiz, Moscow, 1958.
21. L. S. Mayants, Trudy Fiz. Inst. Akad. Nauk SSSR **5**, 65 (1950).

VIBRATIONAL SPECTRA OF ATOMATIC COMPOUNDS
IX. Theoretical Calculation of Intensities in the Infrared Spectra of Benzene and Certain Deuteriobenzenes

M. A. Kovner and B. N. Snegirev (pp. 328-334)

Received 16 May 1960

The forms of all the infrared-active normal vibrations of the molecules C_6H_6, p-$C_6H_4D_2$, C_6H_5D, and C_6D_6 have been calculated. These data have been used to calculate the intensities in the infrared spectra of the designated substances, in the first approximation of the valence-optical theory. The computed intensity values are in good agreement with their experimental values. The dipole moment of the C—H bond in benzene has been unequivocally determined and equals 0.65D.

In ref. 1, a calculation of the intensities in the infrared spectra of benzene and certain deuteriobenzenes was carried out (in the zero-order approximation of the valence-optical theory). As a result of the calculation of the intensities of lines corresponding to planar and nonplanar vibrations, the values 0.31 and 0.61D were obtained for the dipole moment of the CH bond. It is evident that this ambiguity is devoid of physical meaning. It has been shown in a series of works[2] that difficulties of this sort are eliminated if the calculation of the intensities is carried out not in the zero-order, but in the first-order approximation of the valence-optical theory.[3]

In the present work, the experimental data[1] on intensities in the infrared spectra of the C_6H_6, p-$C_6H_4D_2$, and C_6H_5D molecules are used to determine the electro-optical parameters of benzene in the first-order approximation of the valence-optical theory. With the help of the electro-optical parameters thus found, the intensities in the infrared spectrum of C_6D_6 are theoretically calculated in advance. For the calculation of the forms of the vibrations, we used the results of the solution of the mechanical problem[4] for the planar and nonplanar vibrations of benzene and the deuteriobenzenes, with certain changes proceeding from ref. 5.

The following linearly independent symmetry coordinates of the planar vibrations (see Figure) were used in the calculation:

for C_6H_6, C_6D_6

$$E_u^{-I}:\ Q=\frac{1}{\sqrt{3}}\left(-\frac{1}{2}\,Q_1-Q_2-\frac{1}{2}Q_3+\frac{1}{2}Q_4+Q_5+\frac{1}{2}Q_6\right);$$

$$q=\frac{1}{2}\,(-q_2-q_3+q_5+q_6);$$

$$\beta_a=\frac{1}{\sqrt{6}}\left(-\beta_1+\frac{1}{2}\beta_2-\frac{1}{2}\beta_3-\frac{1}{2}\beta_4+\frac{1}{2}\beta_5-\beta_6+\beta_7-\frac{1}{2}\beta_8+\frac{1}{2}\beta_9+\frac{1}{2}\beta_{10}-\frac{1}{2}\beta_{11}+\beta_{12},\right).$$

for p-$C_6H_4D_2$

$$B_{2u}:\ Q=\frac{1}{2}\,(Q_1-Q_3-Q_4+Q_6);$$

$$q'=\frac{1}{2}\,(q_2-q_3-q_5+q_6);\quad q''=\frac{1}{\sqrt{2}}\,(q_1-q_4);\quad \gamma=\frac{1}{\sqrt{2}}\,(\gamma_1-\gamma_4);$$

$$\beta=\frac{1}{2}\,(\beta_3-\beta_4-\beta_9+\beta_{10});$$

$$B_{3u}:\ Q'=\frac{1}{2}\,(Q_1+Q_3-Q_4-Q_6);\qquad Q''=\frac{1}{\sqrt{2}}\,(Q_2-Q_5);$$

$$q=\frac{1}{2}\,(q_2+q_3-q_5-q_6);$$

$$\beta'=\frac{1}{2}\,(\beta_1+\beta_6-\beta_7-\beta_{12});\qquad \beta''=\frac{1}{2}\,(\beta_3+\beta_4-\beta_9-\beta_{10}).$$

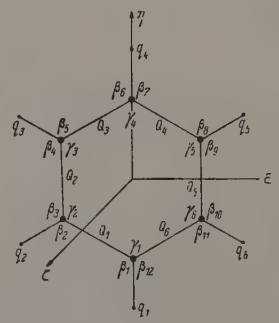

For C_6H_5D, the symmetry coordinates of the A_1 and B_1 planar vibrations have been presented in Table 1 of ref. 6 and are used here with the same designations.

The mechanical problem for the nonplanar vibrations has been solved for all the molecules considered here in the D_{6h} approximate symmetry coordinates (see Table 1 of ref. 6).

The calculation of the vector components of the derivatives of the dipole moment with respect to the k-th normal coordinate, p'_{uk} (u = ξ, η, ζ), was carried out according to formula (1) of ref. 7. Using transformations analogous to those described in ref. 6, we have obtained the following computation formulas:

for C_6H_6, C_6D_6

$$E_u^{-I}:\ p'_{\xi k}=\sqrt{3}\,AL_k^q-\frac{3}{2s}\,BL_k^Q-\frac{1}{a}\sqrt{\frac{3}{2}}\,C\cdot L_k^{\beta a};$$

$$p'_{\eta k}=p'_{\zeta k}=0;\qquad A=\mu'_q-\left(\frac{\partial\mu_q}{\partial q}\right)_m-\left(\frac{\partial\mu_q}{\partial q}\right)_p;$$

$$B=\mu_q-\frac{1}{\sqrt{3}}\left[2\,\frac{\partial\mu_q}{\partial\beta}+\left(\frac{\partial\mu_q}{\partial\beta}\right)_0^{(1)}+\left(\frac{\partial\mu_q}{\partial\beta}\right)_0^{(2)}-\left(\frac{\partial\mu_q}{\partial\beta}\right)_m^{(1)}-\left(\frac{\partial\mu_q}{\partial\beta}\right)_m^{(2)}-2\left(\frac{\partial\mu_q}{\partial\beta}\right)_p\right];$$

$$C=\mu_q-\sqrt{3}\left[\left(\frac{\partial\mu_q}{\partial\beta}\right)_0^{(1)}-\left(\frac{\partial\mu_q}{\partial\beta}\right)_0^{(2)}+\left(\frac{\partial\mu_q}{\partial\beta}\right)_m^{(1)}-\left(\frac{\partial\mu_q}{\partial\beta}\right)_m^{(2)}\right];$$

Table 1. Normalized Vibration Form Coefficients, L

		C_6H_6			C_6D_6		
E_u^{-I}	$\nu_{obs.}$ (cm^{-1})	1038	1486	3080	813	1333	2294
	$\nu_{calc.}$ (cm^{-1})	1030	1476	3074	817	1320	2306
	Q	0.251	—0.256	—0.086	0.145	—0.313	—0.133
	q	0.017	—0.029	1.044	0.018	—0.075	0.773
	β_a	0.575	1.474	0.104	0.689	1.015	0.180
A_{2u}			1.108			0.612	

Table 1. (Continued)

p-$C_6H_4D_2$

B_{2u}	$\nu_{obs.}(cm^{-1})$	992	1034	1475	2278	3060
	$\nu_{calc.}(cm^{-1})$	987	1019	1466	2301	3065
	Q	—0.084	0.230	0.242	—0.111	—0.051
	q'	0.003	0.011	0.016	—0.013	1 044
	q''	—0.033	0.021	0.060	0.773	0.008
	γ	0.467	0.010	—0.136	0.190	—0.081
	β	0.389	—0.199	1.113	—0.062	—0.135
B_{3u}	$\nu_{obs.}(cm^{-1})$	823	1107	—	1414	3080
	$\nu_{calc.}(cm^{-1})$	823	1107	1301	1413	3075
	Q'	0.100	—0.047	—0.453	—0.078	—0.0 0
	Q''	0.085	0.230	0.192	—0.281	—0.070
	q	0.007	0.012	—0.010	—0.029	1.044
	β'	0.767	—0.337	0.568	0.637	0.084
	β''	0.022	0.679	—0.359	0.706	0.008

B_{1u}	$\nu_{obs.}(cm^{-1})$	367	597	874
	$\nu_{calc.}(cm^{-1})$	365	595	875
	$\rho^{A_{2u}}$	—0.109	0.875	0.406
	$\rho_u^{E^{+I}}$	0.209	0.337	—1.245
	$\varkappa_u^{E^{+I}}$	0.677	0.345	—0.559

C_6H_5D

A_1	$\nu_{obs.}(cm^{-1})$	601	973	1000	1032	1178	1475	1590	2277	3070	3070	3070
	$\nu_{calc.}(cm^{-1})$	588	977	1001	1022	1172	1471	1589	2288	3054	3061	3069
	1. $Q_2+Q_5^*$	—0.190	0.146	—0.061	0.027	0.104	—0.018	0.374	0.006	—0.040	—0.041	—0.017
	2. Q_1+Q_6	0.009	0.122	—0.061	0.200	—0.053	—0.174	—0.192	0.006	0.008	—0.027	—0.076
	3. Q_3+Q_4	0.006	0.177	—0.059	—0.150	—0.054	0.178	—0.172	—0.105	—0.015	—0.042	0.021
	4. q_3+q_5	—0.004	0.005	—0.006	—0.006	—0.004	0.012	—0.002	—0.012	0.272	0.947	—0.34
	5. q_2+q_6	—0.004	0.006	0.002	0.008	—0.004	—0.012	—0.003	0.000	0.756	0.031	0.725
	6. q_1	0.006	0.002	—0.004	0.010	0.005	—0.016	0.003	0.015	—0.667	0.438	0.675
	7. q_4	0.000	0.026	0.009	—0.019	0.007	0.043	—0.019	0.773	0.009	0.003	—0.009
	8. γ_1	0.267	0.150	0.301	—0.096	0.030	0.104	0.239	—0.010	—0.135	0.048	0.020
	9. γ_4	0.274	—0.128	—0.292	0.087	0.032	—0.108	0.216	0.180	—0.014	—0.076	0.021
	10. $\beta_4+\beta_9$	0.157	—0.104	—0.202	0.220	0.818	0.796	—0.350	—0.047	0.028	—0.055	0.075
	11. $\beta_3+\beta_{10}$	0.153	0.125	0.211	—0.231	0.613	—0.768	—0.399	0.015	—0.021	—0.056	—0.076

C_6H_5D

B_1	$\nu_{obs.}(cm^{-1})$	603	859	1078	1159	1291	—	1462	1590	3044	3079
	$\nu_{calc.}(cm^{-1})$	594	859	1074	1155	1287	1315	1446	1586	3049	3075
	1. Q_1-Q_6	—0.016	0.036	—0.076	0.181	0.142	—0.223	—0.052	0.334	0.027	—0.035
	2. Q_3-Q_4	0.013	0.085	—0.006	0.077	0.224	—0.216	—0.131	—0.312	—0.027	—0.035
	3. q_3-q_5	0.007	0.002	—0.013	0.005	0.001	0.000	—0.019	0.008	0.739	0.738
	4. q_2-q_6	—0.008	0.006	—0.007	—0.003	0.007	0.001	—0.022	—0.004	—0.738	0.739
	5. $\gamma_3-\gamma_5$	0.336	—0.038	0.110	0.006	—0.060	—0.006	0.176	0.267	0.119	0.047
	6. $\gamma_2-\gamma_6$	—0.333	—0.084	0.121	—0.032	—0.011	—0.002	0.115	—0.296	—0.119	0.048
	7. $\beta_5-\beta_8$	—0.206	0.066	0.335	0.141	0.534	0.731	—0.457	0.167	—0.037	—0.054
	8. $\beta_2-\beta_{11}$	0.203	0.013	0.151	0.526	—0.695	0.015	—0.639	—0.096	0.037	—0.054
	9. $\beta_1-\beta_{12}$	0.072	0.056	—0.388	0.782	0.063	0.686	0.899	—0.586	—0.045	0.061
	10. $\beta_6-\beta_7$	—0.109	0.837	0.401	—0.101	—0.469	0.024	0.453	0.338	0.042	0.057

B_2	$\nu_{obs.}(cm^{-1})$	380	607	698	778	926	995
	$\nu_{calc.}(cm^{-1})$	384	606	699	777	924	979
	$\rho_g^{E^{-II}}$	—0.048	0.268	—0.102	0.866	—0.555	0.044
	$\rho^{B_{2g}}$	0.014	—0.006	—0.510	—0.417	—0.666	1.270
	$\varkappa^{B_{2g}}$	0.022	—0.272	1.281	0.550	0.435	—0.682
	$\rho^{A_{2u}}$	—0.064	0.808	0.411	—0.428	—0.136	0.015
	$\rho_u^{E^{+I}}$	0.259	0.265	—0.071	0.362	1.040	0.723
	$\varkappa_u^{E^{+I}}$	0.734	0.260	—0.051	0.208	0.416	0.256

*The factor $1/\sqrt{2}$ is omitted.

(the meaning of the symbols introduced is clear from the Figure: for example, for the dipole moment μ_q of the CH bond with the vibrational coordinate q_1,

$$\left(\frac{\partial\mu_q}{\partial\beta}\right)_0^{(1)} = \frac{\partial\mu_q}{\partial\beta_2}; \qquad \left(\frac{\partial\mu_q}{\partial\beta}\right)_0^{(2)} = \frac{\partial\mu_q}{\partial\beta_3}$$

and analogously for the derivatives of μ_q with respect to the CCH angles in the meta- and para-positions relative to this CH bond);

$$A_{2u}: \quad p'_{\zeta k} = \frac{\sqrt{6}\,\mu_q}{a} L_k^{\rho A_{2u}}; \qquad p'_{\xi k} = p'_{\eta k} = 0;$$

for p-$C_6H_4D_2$

$$B_{2u}: \quad p'_{\eta k} = -A\left(L_k^{q'} + \sqrt{2}\,L_k^{q''}\right) + \frac{3}{2s}(B+C)\,L_k^{\varrho} + \frac{\sqrt{3}}{a} C\left(\frac{1}{\sqrt{2}} L_k^{\gamma} - L_k^{\beta}\right);$$

$$p'_{\xi k} = p'_{\zeta k} = 0;$$

$$B_{3u}: \quad p'_{\xi k} = -\sqrt{3}\,AL_k^{q} + \frac{(3B-C)}{s\sqrt{6}}\left(\frac{1}{\sqrt{2}} L_k^{Q'} + L_k^{Q''}\right) + \frac{C}{a}\left(L_k^{\beta'} + L_k^{\beta''}\right);$$

$$p'_{\eta k} = p'_{\zeta k} = 0;$$

$$B_{1u}: \quad p'_{\zeta k} = \frac{\sqrt{6}\,\mu_q}{a} L_k^{\rho A_{2u}};$$

$$p'_{\xi k} = p'_{\eta k} = 0;$$

for C_6H_5D

$$A_1: \quad p'_{\eta k} = -A\left[L_k^6 - L_k^7 + \frac{1}{\sqrt{2}}\left(L_k^5 - L_k^4\right)\right] + \frac{3}{2\sqrt{2}\,s}(B+C)\left(L_k^2 - L_k^3\right) + \frac{\sqrt{3}}{2a} C\left[\sqrt{2}\left(L_k^{10} - L_k^{11}\right) + L_k^8 - L_k^9\right];$$

$$p'_{\xi k} = p'_{\zeta k} = 0;$$

$$B_1: \quad p'_{\xi k} = -\sqrt{\frac{3}{2}}\,A\left(L_k^3 + L_k^4\right) - \frac{1}{2\sqrt{2}\,a}(3B+C)\left(L_k^5 + L_k^6\right) - \frac{C}{\sqrt{2}\,a}\left(L_k^7 + L_k^8 - L_k^9 - L_k^{10}\right);$$

$$p'_{\eta k} = p'_{\zeta k} = 0;$$

$$B_2: \quad p'_{\zeta k} = \frac{\sqrt{6}\,\mu_q}{a} L_k^{\rho A_{2u}};$$

$$p'_{\xi k} = p'_{\eta k} = 0.$$

In all the expressions presented above s = 1.39 A and a = 1.09 A (the length taken as a unit[3]). The numerical values of the dimensionless normalized vibration form coefficients, L, are presented in Table 1.

The intensities are determined by the expression $(\pi g/3mc)(p'_k)^2$, in which m is the "spectroscopic" mass of the hydrogen atom, equal to 1.088 (in units of 1/16 of the mass of the oxygen atom); c is the velocity of light, g the degree of degeneracy, and p'_k the derivative of the dipole moment with respect to the k-th normal coordinate, taken at the equilibrium position of the atoms. From the experimental intensity values of the lines corresponding to nonplanar vibrations, the actual values of μ_q have been determined. Their average value equals ±0.65D, which agrees very well with the analogous quantity found for ethylene in the first work[2] and characteristic for the C—H bond formed by a carbon atom with sp^2 hybridization. The sign of μ_q cannot in principle be determined within the framework of this calculation. It is well known[1,2,8] that the negative and positive ends of the C—H bond dipole are located respectively on the C and H atoms.* We assume that the first-approximation corrections in B and C cannot be so large that the signs of B and C should be opposite to the sign of μ_q. Therefore the values of B and C must be positive. Taking this into consideration and using all the experimental intensity values from ref. 1, and also those for C_6D_6 from ref. 9, we have found that the best agreement between the calculated and observed intensities is attained with A = −0.48D/A, B = 0.40D, and C = 0.34D. The values obtained possess the property established in ref. 2, according to which μ_q and A must have opposite signs.

*$\mu_q > 0$ corresponds to this orientation of the dipole.

A comparison of the experimental and calculated intensity values (in units of 10^{-7} cm^2 $mole^{-1}$ sec^{-1} ln) is presented in Table 2. It can be seen from this table that the intensities computed by us are very close to those calculated in ref. 1, in consequence of which we have not carried out an advance calculation of the intensities for sym-$C_6H_3D_3$ and p-$C_6H_2D_4$.

Table 2. Comparison of Experimental and Calculated Intensity Values (units of 10^{-7} cm^2 $mole^{-1}$ sec^{-1} ln)

Substance	Symmetry type	$\nu_{obs.}$ (cm^{-1})	Intensity: Observed (ref. 1)	Calculated (ref. 1)	Calculated in the present work
C_6H_6	A_{2u}	673	4.39	4.65	4.64
	E_u^{-I}	1038	0.44	0.44	0.44
		1486	0.65	0.69	0.68
		3080	2.99	3.19	2.90
p-$C_6H_4D_2$	B_{1u}	367	—	0.05	0.05
		597	3.17	3.20	3.20
		874	0.74	0.67	0.69
	B_{2u}	992	0.02	0.03	0.03
		1034	0.21	0.19	0.19
		1475	0.31	0.31	0.31
		2278	0.55	0.54	0.54
		3065 *	—	0.47	0.49
	B_{3u}	823	0.15	0.15	0.16
		1107	0.05	0.05	0.05
		1301 *	< 0.01	0.00	0.00
		1414	0.22	0.18	0.18
		3080	—	1.40	1.44
		J (3065) + + J (3080)	1.85	1.87	1.93
C_6H_5D	B_2	380	—	0.02	0.02
		607	2.84	2.69	2.73
		698	0.68	0.66	0.70
		778	0.81	0.83	0.76
		926	0.08	0.08	0.08
		995	< 0.01	0.00	0.00
	A_1	601	—	0.00	0.00
		973	< 0.02	0.01	0.01
		1000	< 0.02	0.01	0.00
C_6H_5D	B_1	1032	0.21	0.21	0.22
		1178	< 0.01	0.00	0.00
		1475	—	0.32	0.32
		1590	—	0.00	0.00
	A_1	2277	0.26	0.26	0.26
		3070	—	0.10	0.05
		3070	—	0.14	0.01
		3070	—	0.71	0.92
	B_{2u}	603	—	0.00	0.00
		859	0.10	0.11	0.11
		1078	0.10	0.10	0.10
		1159	< 0.01	0.00	0.00
		1291	< 0.01	0.00	0.00
		1315 *	< 0.01	0.00	0.00
	B_{3u}	1462	—	0.26	0.26
		1590	—	0.01	0.01
		3044	—	0.00	0.00
		3079	—	1.44	1.45
		J (1462) + + J (1475)	0.58	0.58	0.58
		J (1590) + + J (1590)	0 02	0.01	0.01
		CH ($A_1 + B_1$)	2.35	2.39	2.43
C_6D_6	A_{2u}	497	—	2.50	2.55
	E_u^{-I}	813	—	0.42	0.43
		1333	—	0.14	0.13
		2294	—	1.58	1.62

*Frequency values computed by us.

The fundamental conclusion of the present work is the confirmation of the fact that carrying out the calculation in the first approximation of the valence-optical theory[3] enables one to interpret in a consistent way all the intensities in the infrared spectra of benzene and its deuterio derivatives. At the same time, we have succeeded in finding the actual value of the dipole moment of the CH bonds in benzene to be equal to 0.65D.

REFERENCES

1. H. Spedding and D. H. Whiffen, Proc. Roy. Soc. **A238**, 245 (1956).
2. L. M. Sverdlov, Opt. i Spektr. **4**, 697 (1958); Ibid. **6**, 729 (1959); Ibid. **7**, 21 (1959); Ibid. **7**, 600 (1959), Optics and Spectroscopy **6**, 477 (1959); Ibid. **7**, 11 (1959); Ibid. **7**, 368 (1959).
3. M. V. Vol'kenshtein, M. A. El'yashevich, and B. I. Stepanov, "Kolebaniya molekul" (Molecular Vibrations), Vol. 2. Gosudarst. Izd. Tekh.-Teoret. Lit., Moscow-Leningrad, 1949.

4. M. A. Kovner, Zhur. Eksptl. i Teoret. Fiz. 26, 598 (1954); Doklady Akad. Nauk SSSR 97, 65 (1954).
5. M. A. Kovner and A. M. Bogomolov, Opt. i Spektr. 4, 301 (1958).
6. M. A. Kovner and B. N. Snegirev, Opt. i Spektr. 7, 487 (1959), Optics and Spectroscopy 7, 309 (1959).
7. B. N. Snegirev and M. A. Kovner, Opt. i Spektr. 8, 880 (1960), Optics and Spectroscopy 8, 462 (1960).
8. T. Anno and A. Sadô, J. Chem. Phys. 29, 1170 (1958).
9. C. R. Bailey, J. B. Hale, C. K. Ingold, and J. W. Thompson, J. Chem. Soc. 931 (1936).

THE THEORY OF THE VIBRATIONAL SPECTRA OF POLYMERS
III. The Calculation and Interpretation of the Vibrational Spectrum of Polyethylene

Yu. Ya. Gotlib and L. V. Kudinskaya (pp. 335-342)

Received 12 May 1960

Using the method of Stepanov-El'yashevich we have worked out the matrices of the kinematic and dynamic coefficients for an infinitely long planar trans-chain $(-CR_2-)_n$ for the vibrations which are active in infrared absorption spectra and Raman spectra. The symmetry coordinates are introduced and the corresponding block matrices are obtained. The force constants were varied to give the best agreement with the experimental data. The assignment of the frequencies according to vibrational type is discussed. The infrared active frequencies of polydeuteroethylene are calculated and it is shown that there is a very good agreement between the calculated results and the experiment.

1. Recently there has appeared a series of studies devoted to a detailed investigation of infrared[1-3] and Raman[3,24] spectra of polyethylene and high molecular weight normal paraffins. The experimental data show that the differences in frequencies of infrared spectra for samples with different degrees of crystallinity for highly crystalline samples and for molten amorphous samples is generally not large. They lead to the appearance in the crystalline polymers and normal paraffins of resolved lines (doublets) and to some changes in the intensity, and also to the appearance of "amorphous" bands.[1-6] The presence of doublets in the spectrum of polyethylene is generally related to intermolecular interactions,[1,6-8,26] and the appearance of "amorphous" bands is explained by rotational isomers or by violation of the strict selection rules applicable to the ordered crystalline regions of the polymer.

The interpretation of the fundamental frequencies, which are not dependent on the degree of crystallinity in the infrared spectrum of polyethylene, has been made, up to the present[1-3,9-11] on the basis of the selection rules on the basis of the selection rules and classification according to vibrational type for an isolated chain of maximum extension. Such an approximation appears natural for the crystalline portions of a polymer. As regards the amorphous portions, in them there can exist a significant degree of close order responsible for the crystalline form[12] which follows, for example, from the large magnitude of the statistical element of the chain determined from data on its dimensions in solutions[13] and on double light refraction for amorphous polyethylene produced by the action of radiation.

The selection rules for infinite polyethylene chains have been examined by Tobin.[11] Calculation of the fundamental frequencies for different simplifying assumptions, relative to the form of the force field, have also been carried out in a series of studies (cf., e.g., refs. 15-17). The most accurate calculations have been made by Kellner,[10] and Mizushima and Simanouti.[9,18] In ref. 10 the simplest valence force scheme is applied, taking account only of the diagonal terms in the expression for the potential energy as a function of the natural coordinates (the valence angles and bonds). Moreover, two torsional force constants are introduced, determining the nonplanar, skeletal, torsional vibration, and the "twisting" of the C—C bond during the rocking vibration of the CH_2 group at the ends of the given bond. In refs. 9, 18 the expression for the potential energy in the Urey-Bradley form is used in the calculation.

The investigations of El'yashevich, Stepanov, and Vol'kenshtein[19-21] show that for a complete interpretation of the data for the spectra of normal paraffins (ethane, propane, butane, pentane, and the others) it is necessary to use the valence force scheme, taking account of the nondiagonal terms in the expression of the potential energy by the natural coordinates.

The system of force constants introduced in refs. 19-21 has recently been applied successfully (with slight changes of form) for the accurate calculation and interpretation of the vibrational spectra of the different rotational isomers of normal butane[22] and of 2-3 dimethyl butane.[23] Therefore, it is natural to use the system of force constants applied in refs. 19-23 for the calculation of the fundamental vibrational frequencies of the polyethylene and polydeuteroethylene chains. Such a calculation will allow us to determine the degree of suitability of the system of force constants obtained from the data in the spectra of the low molecular weight paraffins for the calculation of the spectra of polymeric chains. The results obtained can be further used in the calculation and interpretation of spectra of other polymeric chains of similar structure (polymers of the polyvinyl series and others).

2. The calculation carried out refers to an infinite isolated chain of polyethylene (or of polydeuteroethylene) in which all of the links are located in the transconfiguration. The chain can be considered as a one-dimensional crystal with a factor group isomorphic with the point group V^h.[11] The repeating unit of the chain consists of two CH_2 groups and of two C—C bonds. It is convenient to introduce a subunit $C—CH_2$ in which each subunit is transformed into the following (or preceding) by rotation around the axis of the chain and translation by 1/2 unit (a screw axis of the second order).

The vibrations which are active in the infrared and Raman spectra will be those in which the equivalent part

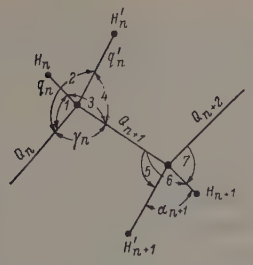

The symbols of the natural coordinates taken in the study. q_n, q'_n, and Q_n are the changes of the lengths of the corresponding CH and CC bonds; γ_n are the angles between adjacent CC bonds; the angles between CC and CH bonds are: 1—β_{nn}, 2—β'_{nn}, 3—$\beta_{n+1,\,n}$, 4—$\beta'_{n,\,n+1}$, 5—$\beta'_{n+1,\,n+1}$, 6—$\beta_{n+1,\,n+1}$, 7—$\beta_{n+2,\,n+1}$.

(bonds, angles) in adjacent units vibrate in phase. The equivalent coordinates in the subunits can then vibrate both in phase ($\theta = 0$) and in opposite phase ($\theta = \pi$) where θ is the phase difference between vibrations of equivalent coordinates in adjacent subunits.

In the construction of the equations of motion in the natural coordinates we used the method of Vol'kenshtein-El'yashevich-Stepanov[19] (the symbols of the coordinates are introduced in the Figure; the symbols of the force constants coincide with those introduced in ref. 19 on page 360). We will take the interactions of any two angles having a common vertex and adjoining one vertex to be identical [for example, $(\alpha_n, \beta_{nn}), (\beta_{nn}, \gamma_n)$]. The interaction of the angles γ lying next to a particular C—C bond is assumed equal to the interaction of the angles β lying adjacent to the same bond and located in the same plane.

Each subunit is characterized by nine natural coordinates with one condition linking them ($\alpha + \gamma + \sum_i \beta_i = 0$).

The solution of the equations of motion can be found in the form $q_{nr} = q_r^{(0)} e^{in\theta}$, where q_{nr} is the r-th natural coordinate of the n-th subunit. In the case of the vibrations active for an infinite chain we limit ourselves to $\theta = 0$ and $\theta = \pi$.

Using the symmetry properties of each subunit we introduce the following coordinates of approximate symmetry:*

*We will henceforth omit the number of the subunit.

$$\left.\begin{aligned}
q_C &= \left(\frac{1}{\sqrt{2}}\right)[q_n + q'_n],\\
q_A &= \left(\frac{1}{\sqrt{2}}\right)[q_n - q'_n],\\
\tau_{CC} &= \left(\frac{1}{2}\right)[(\beta_{nn} + \beta'_{nn}) + (\beta_{n+1,\,n} + \beta'_{n+1,\,n})],\\
\tau_{CA} &= \left(\frac{1}{2}\right)[(\beta_{nn} + \beta'_{nn}) - (\beta_{n+1,\,n} + \beta'_{n+1,\,n})],\\
\tau_{AC} &= \left(\frac{1}{2}\right)[(\beta_{nn} - \beta'_{nn}) + (\beta_{n+1,\,n} - \beta'_{n+1,\,n})],\\
\tau_{AA} &= \left(\frac{1}{2}\right)[(\beta_{nn} - \beta'_{nn}) - (\beta_{n+1,\,n} - \beta'_{n+1,\,n})].
\end{aligned}\right\} \qquad (1)$$

The matrices of the kinematic and dynamic coefficients are broken down into block matrices $G_B(q_1, \ldots, q_n)$ and $F_B(q_1, \ldots, q_n)$, where the subscript B denotes an irreducible representation of the symmetry group,[9,11] and in the brackets are shown the symmetry coordinates. In the further rearrangements are used the supplementary relations among the natural coordinates

$$2\tau_{CC} + \alpha + \gamma = 0 \qquad (2)$$

and

$$Q + \frac{1}{2\sqrt{2}\,\sigma}\gamma = 0. \qquad (3)$$

Condition (2) (cf. ref. 19) is valid for any small vibrations of tetrahedral valence angles. Condition (3), establishing a relation among the changes of Q and γ, is fulfilled only for vibrations of the type A_g, when all of the carbon atoms are shifting perpendicularly to the axis of the chain.

We will introduce a distribution of the symmetry coordinates according to symmetry type. For a phase change between subunits of $\theta = 0$

$$\left.\begin{aligned}
&B_{1g}: q_A(0);\ \tau_{AC}(0); \quad B_{1u}: \tau_{CA}(0);\\
&A_u: \tau_{AA}(0); \quad A_g: q_C(0);\ \alpha(0);\ \gamma(0);
\end{aligned}\right\} \qquad (4)$$

for $\theta = \pi$

$$\left.\begin{aligned}
&B_{2g}: \tau_{CA}(\pi);\ Q(\pi); \quad B_{2u}: q_A(\pi);\ \tau_{AC}(\pi);\\
&B_{3g}: \tau_{AA}(\pi); \quad B_{3u}: q_C(\pi);\ \alpha(\pi).
\end{aligned}\right\} \qquad (5)$$

The matrices of the kinematic coefficients (G_{ik}) for $\theta = 0$

$$G_{B_{1g}} = \begin{pmatrix} 1+\frac{4}{3}\varepsilon & -4\varepsilon\sigma - \frac{2}{3}\varepsilon \\ -4\varepsilon\sigma - \frac{2}{3}\varepsilon & \frac{1}{2} + \frac{1}{3}\varepsilon + 4\varepsilon\sigma + 12\varepsilon\sigma^2 \end{pmatrix}; \quad G_{B_{1u}} = \frac{3}{2} + 3\varepsilon;$$

$$G_{A_u} = \frac{3}{2}; \quad G_{A_g} = \begin{pmatrix} 1+\frac{2}{3}\varepsilon & -\frac{4}{3}\varepsilon & \frac{8}{3}\varepsilon\sigma \\ -\frac{4}{3}\varepsilon & 2+\frac{8}{3}\varepsilon & -\frac{16}{3}\varepsilon\sigma \\ \frac{8}{3}\varepsilon\sigma & -\frac{16}{3}\varepsilon\sigma & \frac{32}{3}\varepsilon\sigma^2 \end{pmatrix}; \qquad (6)$$

for $\theta = \pi$

$$\left.\begin{aligned}
G_{B_{2g}} &= \begin{pmatrix} \frac{8}{3}\varepsilon & -2\sqrt{2}\varepsilon - \frac{4\sqrt{2}}{3}\varepsilon\sigma \\ -2\sqrt{2}\varepsilon - \frac{4\sqrt{2}}{3}\varepsilon\sigma & \frac{3}{2} + 3\varepsilon + 4\varepsilon\sigma + \frac{4}{3}\varepsilon\sigma^2 \end{pmatrix};\\
G_{B_{2u}} &= \begin{pmatrix} \frac{1}{2}+\frac{1}{3}\varepsilon & -\frac{2}{3}\varepsilon \\ -\frac{2}{3}\varepsilon; & 1+\frac{4}{3}\varepsilon \end{pmatrix};\\
G_{B_{3g}} &= \frac{3}{2}; \quad G_{B_{3u}} = \begin{pmatrix} 1+\frac{2}{3}\varepsilon & -\frac{4}{3}\varepsilon \\ -\frac{4}{3}\varepsilon & 2+\frac{8}{3}\varepsilon \end{pmatrix},
\end{aligned}\right\} \qquad (7)$$

where ε is the ratio of the spectroscopic masses of hydrogen (or deuterium) and carbon in the polyethylene (polydeuteroethylene) chain, or of the corresponding atoms in the trans-chain having an analogous structure $(-CX_2-)_n$, and σ is the ratio of the lengths of the CX and CC bonds.

The matrices of the dynamic coefficients (the symbols of the force constants, as has been stated above, coinciding with those chosen in ref. 19) have the form:

for $\theta = 0$

$$\left.\begin{aligned}
F_{B_{1g}} &= \begin{pmatrix} K_q - h & a\sqrt{2} \\ a\sqrt{2} & K_\beta + m - n \end{pmatrix}; \quad F_{B_{1u}} = K_\beta - m - n;\\
F_{A_u} &= K_\beta - 2l + n - m;
\end{aligned}\right\} \qquad (8)$$

$$F_{A_g} = \left\| \begin{array}{ccc} K_q + h & \frac{a}{\sqrt{2}} & -\frac{a}{\sqrt{2}} \\ \frac{a}{\sqrt{2}} & K_\alpha + \frac{K_\beta}{4} - \frac{3}{2}l + \frac{m+n}{4} & \frac{A}{2\sqrt{2}\sigma} + \frac{K_\beta}{4} - \frac{3}{2}l + \frac{m+n}{4} - n \\ -\frac{a}{\sqrt{2}} & \frac{A}{2\sqrt{2}\sigma} + \frac{K_\beta}{4} - \frac{3}{2}l + \frac{m+n}{4} - n & K_\gamma + \frac{K_Q}{8\sigma^2} - \frac{A}{\sqrt{2}\sigma} + \frac{K_\beta}{4} - \frac{3}{2}l + \frac{9m-7n}{4} \end{array} \right|;$$

for $\theta = \pi$

$$F_{B_{2g}} = \begin{pmatrix} K_Q & 2A \\ 2A & K_\beta + m + n \end{pmatrix}; \quad F_{B_{2u}} = \begin{pmatrix} K_\beta - m + n & a\sqrt{2} \\ a\sqrt{2} & K_q - h \end{pmatrix};$$

$$F_{B_{3g}} = K_\beta - 2l + m - n; \quad F_{B_{3u}} = \begin{pmatrix} K_q + h & \frac{a}{\sqrt{2}} \\ \frac{a}{\sqrt{2}} & K_\alpha + \frac{K_\beta}{4} - \frac{3}{2}l - \frac{m+n}{4} \end{pmatrix}. \qquad (9)$$

On substitution of the numerical values of the force constants from ref. 19 the values of the fundamental frequencies of polyethylene were obtained as shown in column VII of Table 1. The assignments of the frequencies in the infrared and Raman spectra made by a series of authors differ somewhat from one another. These differences concern not only the fundamental frequencies active in the infrared spectrum but also some of the combination frequencies. The assignment of the symmetric and antisymmetric CH_2 stretching vibrations with the frequencies 2848 and 2920 cm^{-1} to B_{2u} and B_{3u}, carried out in ref. 2, appears evidently to be a misunderstanding since it contradicts almost all of the data occurring in the literature (refer to, for example, refs. 25, 26). We will take as our base the assignments made in the later studies,[3,24] which are in fundamental coincidence with the data of ref. 9, and will discuss below some possible changes in the assigned frequencies.

Comparison with the experimental data (Table 1) shows that the calculated values of seven out of the fourteen frequencies disagree significantly with the experimental values. Accordingly, the set of force constants calculated from the data from the spectra of low molecular weight compounds is not completely justified for a description of the spectra of polyethylene and of high molecular weight normal paraffins. In particular, the chosen set of force constants leads to an increase of the value of the frequencies of the CH_2 stretching vibrations (an analogous increase was obtained in ref. 22).

Variation of the force constants K_q and h in correspondence with the experimental values of the frequencies $\nu_{q_A}(\pi) = 2925$ cm^{-1} and $\nu_{q_C}(\pi) = 2853$ cm^{-1} (refer to Table 1, columns III and IV) leads to the new values

$$K_q = 7.69 \text{ and } h = 0.03 \qquad (10)$$

instead of $K_q = 8.08 \pm 0.05$ and $h = 0.05 \pm 0.01$ taken earlier (the force constants are expressed in units of 10^6 cm^{-2}). The set of frequencies calculated with the variational values of K_q and h, but with the initial values of the remaining force constants, is given in column VIII of Table 1. The magnitudes of the stretching frequencies $(CH_2)q_C(0)$ and $q_A(0)$ for the variational values of K_q and h also agree well with the experimental data.[3,24] The remaining frequencies differ very slightly from those calculated without the variations of K_q and h.

In correspondence with the experimental values of the frequencies $\nu_{\tau_{AC}}(\pi) = 719$ cm^{-1} and $\nu_{\tau_{CA}}(0) = 1370$

Table 1

Symmetry type	Form of the vibration*	Symbol assumed in the current study	Experimental values of the frequencies (cm^{-1})**								Calculated values of the frequencies (cm^{-1})		
											Calculated without variation of the constants	Calculated with the varied K_q and h	Calculated with the new set of constants
			I		II	III		IV	V	VI	VII	VIII	IX
B_{1g}	CH_2 (stretch)	q_A (0)	—		2934	2934	B_{2g}	2883	2886	2877	2965	2894	2894
	CH_2 (rock)	τ_{AC} (0)	—		1058	1295	B_{2g}	1168	—	—	1144	1144	1151
B_{1u}	CH_2 (wag)	τ_{CA} (0)	1369	B_{3u}	1372	1375	B_{1u}	1367	1372	—	1205	1206	1370 ***
A_u	CH_2 (twist)	τ_{AA} (0)	—		1173	—	A_{2u}	1306	—	—	1129	1129	1270
A_g	CH_2 (stretch)	q_C (0)	—		2862	2846—2878	A_{1g}	2848	2850	2843	2926	2852	2848
	CH_2 (deformation)	α (0)	—		1456	1471	A_{1g}	1440	1453	1446	1434	1433	1444
	CC (deformation)	γ (0)	—		1135	1135	A_{1g}	1060	1060	1065	1105	1105	1069
B_{2g}	CH_2 (wag)	τ_{CA} (π)	—		150	1442	B_{1g}	1415	—	(151)	1426	1426	1426
	CC (stretch)	Q (π)	—		1058	1058	B_{1g}	1130	—	(175) 1128	1068	1068	1133
B_{2u}	CH_2 (stretch)	q_A (π)	2926	B_{1u}	2848	2926	B_{2u}	2919	—	—	2997	2924	2924 ***
	CH_2 (rock)	τ_{AC} (π)	725	B_{1u}	719	728	B_{2u}	720	—	—	609	655	720 ***
B_{3g}	CH_2 (twist)	τ_{AA} (π)	—		1300	—	A_{2g}	1295	1297	1296	1302	1302	1309
B_{3u}	CH_2 (stretch)	q_C (π)	2853	B_{2u}	2920	2853	A_{1u}	2851	—	—	2928	2852	2852 ***
	CH_2 (deformation)	α (π)	1460	B_{2u}	1465	1475	A_{1u}	1473	1476	—	1466	1467	1470 ***
			—		—	—		—	955	494	—	—	—

*The description of the vibrational types are in the commonly accepted terms (see ref. 25).

**The experimental data (columns I-VI) are borrowed from the following references: column I – ref. 1; column II – ref. 2; column III – ref. 9; column IV – ref. 3; column V – refs. 24, 27; column VI – ref. 24. In columns I and III are given, on the right, the symmetry types assumed in the corresponding studies.

***Frequencies which are infrared active.

cm^{-1} we varied the constants $(K_\beta - m + n)$ and $(K_\beta - m - n)$. The initial value of the constant $(K_\beta + m + n)$ was taken. We obtained the following values of the constants

$$\left.\begin{array}{lll} K_\beta = 1.040, & & K_\beta = 0.92 \pm 0.05, \\ m = 0.006, & \text{instead of} & m = 0.12 \pm 0.01, \\ n = -0.026 & & n = -0.02 \pm 0.01. \end{array}\right\} \quad (11)$$

For the system of constants given in (11) and (10), with the initial values of the remaining force constants, we have excellent agreement with experiment for all of the frequencies with the exception of $\nu_\alpha(\pi)$ and $\nu_\alpha(0)$. In order to obtain satisfactory results for these frequencies we introduced a new force constant of interaction of the angles $\alpha-\alpha$ adjacent to neighboring carbon atoms. We took the value of this constant κ as 0.02. Thus, finally we take the following selection of force constants (in units of 10^6 cm^{-2})

$$\left.\begin{array}{lll} K_Q = 8.07, & K_\gamma = 1.10, & m = 0.006, \\ K_q = 7.69, & A = 0.50, & n = -0.026, \\ K_\beta = 1.04, & a = 0.35, & h = 0.03, \\ K_\alpha = 0.69, & l = -0.03\text{э}, & \varkappa = 0.02. \end{array}\right\}$$

With this is obtained the set of frequencies given in column IX of Table 1.

With the set of constants (12) a calculation of the infrared active frequencies of polydeuteroethylene was carried out. The results obtained, as follows from Table 2, agree well with experiment.

Table 2

Frequency	Experimental (cm^{-1})	Calculated (cm^{-1})
$\nu_{\tau_{AC}}(\pi)$ . . .	520	526
$\nu_{\tau_{CA}}(0)$ . . .	1060	1050
$\nu_e(\pi)$	1100	1100

For the CH stretching vibrations active in the infrared the values $\nu_{q_C}(\pi) = 2093$ cm^{-1} and $\nu_{q_A}(\pi) = 2190$ cm^{-1} were obtained.

We note that a monotonic change of the constant K_q is observed on transition from the CH_4 group to the CH_2 group:

$$K_q(CH_4) = 8.34 \cdot 10^6 \text{ см}^{-2}\ [19]; \quad K_q(CH_3) = 8.08 \cdot 10^6 \text{ см}^{-2}\ [19] \text{ and } K_q(CH_2) = 7.69 \cdot 10^6 \text{ см}^{-2} \text{ (this work)}. \quad (13)$$

For the skeletal vibrations $\nu_Q(\pi)$ and $\nu_Q(0)$ there are some possible variations in the assignment of the frequencies according to the vibrational type

$$\begin{array}{l} \nu_Q(\pi) = 1131 \text{ см}^{-1} \text{ and } \nu_Q(0) = 1061 \text{ см}^{-1}\ [3], \\ \nu_Q(\pi) = 1058 \text{ см}^{-1} \text{ and } \nu_Q(0) = 1135 \text{ см}^{-1}\ [9], \\ \nu_Q(\pi) = 1059 \text{ см}^{-1} \text{ and } \nu_Q(0) = 1135 \text{ см}^{-1}\ [2]. \end{array} \quad (12)$$

If we take the assignment of the frequencies in refs. 2 and 9 then $K_Q < K_q$. Such a relationship between K_Q and K_q occurs in the low molecular weight compounds.[19] For the assignment in ref. 3 $K_Q = 8.07 > K_q = 7.69$.

The assignment of the 150 cm^{-1} frequency to $B_{2g}[\tau_{CA}(\pi)]$ in ref. 2 should be considered an error since with this value of $\nu_{\tau_{CA}}(\pi)$ we have to set the force constant K_Q equal to 1.4×10^6 cm^{-2} instead of 7.02×10^6 cm^{-2} or 8.07×10^6 cm^{-2}.

The set of force constants obtained in the present work can be used as a first approximation in the calculation of the vibrations for polymeric chains $(-CH_2-CHR-)_n$.

The use of the valence force model with variation of the force constants in correspondence with the observed values of the frequencies is more convenient than the application of a force field of the Urey-Bradley type[9] which leads to a more complex form of the matrix of the dynamic coefficients.

In conclusion the authors express their thanks to M. V. Vol'kenshtein for his interest in the current study and for valuable discussion.

REFERENCES

1. C. Y. Liang, S. Krimm, and G. B. B. M. Sutherland, J. Chem. Phys. **25**, 543, 549 (1956).
2. M. C. Tobin and M. J. Carrano, J. Chem. Phys. **25**, 1044 (1956).
3. J. Rud Nielsen and A. H. Woollett, J. Chem. Phys. **26**, 1391 (1957).
4. I. I. Novak, Zhur. Tekh. Fiz. **24**, 18 (1954); **25**, 1854 (1955).
5. I. I. Novak and E. S. Solov'ev, Opt. i Spektr., **2**, 62 (1957).
6. I. I. Novak, Izvest. Akad. Nauk SSSR, Ser. Fiz. **22**, 1114 (1958).
7. R. S. Stein, J. Chem. Phys. **23**, 734 (1955).
8. R. S. Stein and G. B. B. M. Sutherland, J. Chem. Phys. **22**, 1993 (1954).
9. S. Mizushima, "Stroenie Molekul i Vnutrenee Vrashchenie" (Structure of Molecules and Internal Rotation). Izd. Inostrannoi Lit., Moscow, 1957. Academic Press, New York, 1954.
10. L. Kellner, Proc. Roy. Soc. **A64**, 521 (1951).
11. M. C. Tobin, J. Chem. Phys. **23**, 891, 1955.
12. O. B. Ptitsyn and Yu. A. Sharonov, Zhur. Tekh. Fiz. **27**, 2762 (1957); Soviet Phys.-Tech. Phys. **2**, 2561 (1957).
13. Q. Trementozzi, J. Polymer Sci. **36**, 113 (1959).
14. D. W. Saunders, Trans. Faraday Soc. **52**, 1414 (1956); Ibid. **53**, 860 (1957).
15. E. Bartholme and E. Teller, Z. physik. Chem. **B19**, 336 (1932).
16. J. G. Kirkwood, J. Chem. Phys. **7**, 506 (1939).
17. K. S. Pitzer, J. Chem. Phys. **8**, 711 (1940).
18. T. Simanouti, J. Chem. Phys. **17**, 734 (1949).
19. M. V. Vol'kenshtein, M. A. El'yashevich, and B. I. Stepanov, "Kolebaniya Molekul" (Molecular Vibrations). Gosudarst. Izd. Tekh. and Teoret. Lit., Moscow-Leningrad, 1949.
20. M. A. El'yashevich and B. I. Stepanov, Doklady Akad. Nauk SSSR **32**, 481 (1941); Zhur. Fiz. Khin. **17**, 145 (1943).
21. B. I. Stepanov, Acta Phys. Chim. **22**, 238 (1947).
22. R. I. Podlovchenko and M. M. Sushchinskii, Opt. i Spektr. **2**, 49 (1957).
23. R. I. Podlovchenko, L. M. Sverdlov, and M. M. Sushchinskii, Opt. i Spektr. **6**, 146 (1959), Optics and Spectroscopy **6**, 96 (1959).
24. A. Simon and G. Heintz, Kurzmitteilungen, Symposium uber Makromolekule in Wiesbaden, Sekt. I. Physik. makromolekularer Stoffe I C6.
25. "Primenenie Spektroskopii v Khimii" (Monografiya) (The Application of Spectroscopy to Chemistry. A Monograph). GLIV, IL, Moscow, 1959.
26. Ergeb. exakt. Naturw. **31**, 270-331 (1959).
27. B. Schrader, G. Kresz, and F. Nerdel, Z. physik. Chem. **12**, 132 (1957).

THE HYDROGEN BOND IN ACID GERMANATES
I. The Infrared Spectrum of Strontium Dihydrogermanate

G. P. Stavitskaya and Ya. I. Ryskin (pp. 343-347)

Received 11 May 1960

The infrared spectra of powder samples of acid strontium monogermanate and its deuterium analogue were measured over the region 400-3000 cm^{-1} and interpreted. It is shown that the germanate is capable of participating in strong hydrogen bonds through formation of $p\pi$-$d\pi$ bonding between the hydroxylic oxygen and germanium.

Earlier investigations[1-3] have shown that the ability of $(O_3SiOH)^{-3}$ ions and molecules of the type R_3SiOH (R = C_2H_5, C_6H_5) to participate in strong hydrogen bonds can be explained by the presence of vacant 3d-orbitals in the silicon atom and an increase in the role of $p\pi$-$d\pi$ bonding between the O and Si atoms.

In order to explore the possibility of similar changes in the Ge-O bond, we investigated the infrared absorption spectra of acid germanates. In this communication we discuss the spectra of acid strontium monogermanate SrH_2GeO_4 and its deuterium analogue SrD_2GeO_4.

Muller and Gulezian[4] obtained a gel of strontium germanate by neutralizing a solution of germanic acid with strontium hydroxide. Schwarz and Heinrich[5] showed that a compound having the formula $SrGeO_3 \cdot H_2O$ crystallizes out on prolonged boiling of the gel. According to Nowotny and Szekely[6] this compound is the acid salt of orthogermanic acid SrH_2GeO_4. On the basis of powder x-ray diagrams, these authors were able to determine the parameters of an elementary cell of the compound and the possible space groups C_{2v}^{11} and D_{2d}^{12}. Assuming that strontium germanate and potassium dihydrophosphate are isomorphous,[1] i.e., assuming the tetragonal space group D_{2d}^{12}, they obtained good agreement between the calculated and experimental intensities. Short hydrogen bonds (O—H $\cdots$ O = 2.54 A) were assumed to exist between the tetrahedra of GeO_4 in a crystal of SrH_2GeO_4 (by analogy to potassium dihydrophosphate). The bond lengths calculated from the model were: Ge-O = 1.73 A (tetrahedral environment), Sr—O = 2.65 and 2.67 A (coordination number = 8), O—O = 2.71 and 2.87 A.

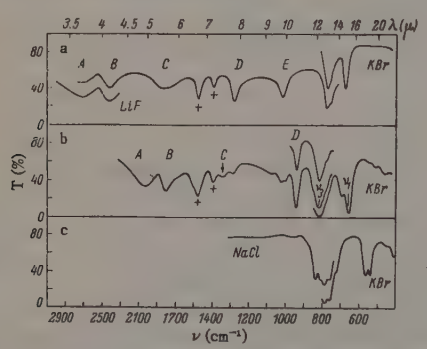

Fig. 1. Absorption spectra of powdered samples of strontium dihydrogermanate (a), its deuterium analogue (b), and of the product obtained on its thermal degradation at 550°C (c). The O—H valence and deformation modes are indicated by the letters A, B, C, D, and E; the signs + and – indicate the absorption bands of the paraffinic matrix.

INFRARED ABSORPTION SPECTRUM OF STRONTIUM DIHYDROGERMANATE

Figure 1 shows the spectra of powdered samples of the germanate and its deuterium analogue. The interpretation of the spectra is given in Table 1 and Fig. 2. On the basis of the magnitude of the isotopic shift, the bands A, B, C, D, and E must be assigned to vibrations which include the O—H group. The frequencies of these vibrations in this case are characteristic of compounds whose hydroxyl groups are bound to electronegative atoms and which participate in strong hydrogen bonds.[2,3] Since there is no absorption in the interval 2800 $cm^{-1} < \nu < 3700$ cm^{-1} it must be concluded that the crystalline lattice of the germanate does not contain any OH^- ions and water molecules. Moreover, since the stoichiometric composition of the compounds is $SrO \cdot GeO_2 \cdot H_2O$ the most probable structure is the one consisting of $(H_2GeO_4)^{-2}$ anions. This conclusion is also in agreement with the spectrum of the stretching vibrations of the Ge—O bonds.

Considering the mass of the hydroxyl group as concentrated in one point, we can assign the symmetry C_{2v} to the $O_2'GeO_2$ ion (O′ = OH). There are nine simple vibrations (all active in absorption) which correspond to

Molecules (ions)	Frequencies			
GeO_4 (T_d)	ν_1 (a_1)	ν_2 (e)	ν_3 (f_2)	ν_4 (f_2)
$O_2'GeO_2$ (C_{2v})	ν_1 (a_1)	ν_{2a} (a_1), ν_{2b} (a_2)	ν_{3a} (a_1), ν_{3b} (b_1), ν_{3c} (b_2)	ν_{4a} (a_1), ν_{4b} (b_1), ν_{4c} (b_2)

this symmetry. The frequencies of these vibrations must be grouped around four points corresponding to the frequencies of the tetrahedral (T_d) GeO_4^{-4} ion as shown in the table above.

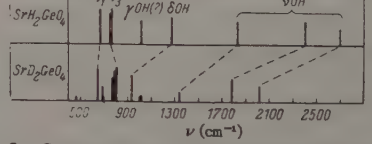

Fig. 2. Comparison of the fundamental frequencies of the $(H_2GeO_4)^{-2}$ and $(D_2GeO_4)^{-2}$ ions.

It is not difficult to evaluate the frequencies of the tetrahedral ion GeO_4^{-4}. It is easy to calculate the frequency ν_1 once the force constant f(Ge—O) is determined from Siebert's formula[8] and assuming a peripheral force constant $f_1 = 0.1f$. In this way we obtain $\nu_1 \approx 700$ cm^{-1}. The upper limit for the frequency ν_3 can be evaluated by comparison with the analogous frequency of the SiO_4^{-4} ion (~870 cm^{-1}). The frequency of the germanate ion

must be considerably smaller than 870 cm^{-1} as a result of the increase in mass of the central atom and lowering of the force constant f(Ge—O).* The lowest frequency in this range must be the totally symmetric stretching vibration $\nu_1(GeO_4^{-4})$.*

*Siebert's formula gives: f(Ge—O) = 3.6×10^5 dynes/cm; f(Si—O) = 3.73×10^5 dynes/cm.

*Only very rarely is the frequency ν_1 slightly higher than ν_3.

Table 1. Absorption Band Frequencies in the Infrared Spectra of SrH_2GeO_4 and SrD_2GeO_4 (in cm^{-1})

Approximate assignment	νOH, νOD	δOH, δOD	γOH (?)	νGeO	
				B_1, B_2, A_1	A_1
SrH_2GeO_4	2700, 2410, 1835	1278	1018	773, 752	676
SrD_2GeO_4	2025, 1790, 1340	939	?	815	656, 693

From the spectrum of the dihydrogermanate [Fig. 1(a)] it is seen that only two bands occur in the region 420-900 cm^{-1}. One, narrow and symmetrical is at 676 cm^{-1} and the other, broader and obviously composite, has its main maximum at 770 cm^{-1}. We assign the first band to the vibration ν_1 of the ion $O_2'GeO_2$ (in the absence of hydrogen atoms in the anion this vibration would have been inactive). We consider the second band to be the sum of overlapping bands ν_{3a}, ν_{3b}, and ν_{3c}. Our interpretation is supported by analysis of the absorption spectrum of the dehydration product of the dihydrogermanate [the sample was kept at 550°C for 2 hr; Fig. 1(c)]. Removal of a water molecule from SrH_2GeO_4 must result in condensation polymerization of the anion skeleton, i.e., formation of infinitely long chains $(GeO_3)_\infty$ [or rings $(GeO_3)_n$], composed of GeO_4 tetrahedra. The characteristic spectral manifestation of this process is the splitting of the breathing vibration $\nu_1(a_1)$.[9,10]

In the spectrum of the dehydrated strontium germanate the band at 676 cm^{-1} must be replaced by bands of higher and lower frequencies. This is exactly what is observed: the maxima at 540 and 563 cm^{-1} correspond to the low-frequency components of the split vibration ν_1, while the high-frequency components apparently overlap the absorption due to the second group of valence vibrations νGeO (band with maxima at 830, 808, 784, 760, and 726 cm^{-1}).

The frequencies of the deformation vibrations of the GeO_4^{-4} ion (ν_2 and ν_4) and the corresponding frequencies of the "acid" ion $(O_2Ge(OH)_2)^{-2}$ lie outside the spectral region investigated by us, i.e., lower than 420 cm^{-1} since there are no bands of appreciable intensity in the region 670-420 cm^{-1} of the dihydrogermanate spectrum.

INTERACTION OF BONDS IN THE $(O_2Ge(OH)_2)^{-2}$ ION

Comparing the valence vibration frequencies νOH of strontium dihydrogermanate and a number of known compounds with strong hydrogen bonds (Table 2), it can be concluded that the hydrogen bonds in the germanate are also strong. The position of the main maximum B permits one to evaluate the length of the O—H ··· O bonds.[11] It is found to be 2.5-2.6 A, in complete agreement with the assumptions of Nowotny and Szekely.

The ability of the germanate to participate in such strong hydrogen bonds is to us a sufficient reason for proposing the formation of pπ-dπ bonding between the hydroxylic oxygen and germanium (see refs. 1,3). Additional evidence in favor of this hypothesis can be obtained from the spectra of the valence vibrations Ge—OH and Ge—OD. Comparing the spectra of the dihydrogermanate and its deuterium analogue (Figs. 1 and 2), it can be seen that the main maximum of the ν_3 band has a higher frequency in the deuterium compounds. This phenomenon cannot be explained by variation in the kinematic interactions of ions since all the parameters of the crystalline lattice remain unchanged on D substitution: the interplanar distances and the intensities of the Debye rings of the crystals SrH_2GeO_4 and SrD_2GeO_4 are equal within experimental error (Table 3). The increase in the mass of the anion on deuteration cannot be the reason either for an increase in the frequency of one of its vibrations. The only conclusion then is that the force constants of the bonds Ge—O and Ge—O′ change on deuteration. This can be expected on the basis of the following argument. In an "isolated"* $(O_2GeO_2')^{-2}$ ion the presence of a formal positive charge on the Ge atom and of a formal negative charge on the O atom facilitate the formation of pπ-dπ bonding between the two atoms (ions) O and Ge. The formation of hydrogen bonds increases the probability of the formation of pπ-dπ bonding between the hydroxylic oxygens (O′) and germanium, causing a weakening in the corresponding bonds between O and Ge.[12] Thus when, on deuteration, the strength of the hydrogen bond changes, we must expect a change in the force constants f(Ge—O) and f(Ge—O′) and, hence, in the vibration frequencies of the germanate ion.

Table 2. Vibration Frequencies of Strongly Hydrogen-Bonded Hydroxyl Groups in Crystals (in cm^{-1})

Band	SrH_2GeO_4	SrD_2GeO_4	KH_2PO_4 [13]	KD_2PO_4 [13]	$C_5SH—\alpha^*$ [2]	$C_5SD—\alpha^*$ [2]
A	2700	2025	2750	2050	2847 2594	1790 1910
B	2410	1790	2400**	1770	2450	2115
C	1835	1340	1580	1200	—	—
D	1278	939	1300	942	1282	910

*Complete formula: $Ca_3(HSiO_4)OH$ and $Ca_3(DSiO_4)OD$
**According to ref. 11 this frequency is 2320 cm^{-1}.

*By an "isolated" ion we mean a nonhydrogen-bonded ion.

EXPERIMENTAL WORK

The strontium dihydrogermanate was prepared by a known method.[5,6] The deuterated analogue was synthe-

Table 3. Interplanar Distances and Relative Intensities of the Debye Lines of Strontium Dihydrogermanate and the Product of its Dehydration at 550°C

SrH_2GeO_4		SrD_2GeO_4		$SrGeO_3$	
$\frac{d}{n}$ (n Å)	$\frac{I}{I_0}$	$\frac{d}{n}$ (n Å)	$\frac{I}{I_0}$	$\frac{d}{n}$ (n Å)	$\frac{I}{I_0}$
3.68	9	3.68	10	3.35	2
2.95	1	2.94	1	3.22	10
2.82	10	2.81	10	3.11	10
2.61	4	2.60	4	2.75	7
2.48	1	2.48	1	2.17	1
2.31	2	2.31	2	2.08	1
2.14	2	2.13	1	1.93	3
1.96	1	1.96	1	1.78	3
1.92	10	1.91	10	1.71	1
1.85	2	1.85	3	1.64	1
1.68	1	1.67	1	1.60	1
1.65	5	1.65	6	1.55	1
1.55	5	1.55	5	1.49	2
1.53	5	1.52	5		
1.41	5	1.41	4	Other lines are washed out	
1.33	5	1.33	6		
1.31	1	1.31	1		
1.245	3	1.241	3		
1.236	1	1.232	1		
1.191	3	1.188	2		
1.181	4	1.178	3		
1.172	2	1.168	1		
1.097	2	1.092	2		
1.025	2	1.021	2		
1.009	3	1.007	3		
0.998	4	0.997	4		

sized in a similar fashion from solutions of GeO_2 and SrO in heavy water.

X-ray analysis shows that the compounds synthesized in the present investigation were identical to the ones prepared by Nowotny and Szekely.[6] There was good agreement with the values of $10^3 \cdot \sin^2\theta$ and the relative intensities of all Debye lines (copper radiation) given in ref. 6. Table 3 gives the interplanar distances and relative intensities of Debye lines of SrH_2GeO_4, SrD_2GeO_4, and strontium metagermanate $SrGeO_3$ obtained by dehydration of the dihydrogermanate at 550°C for a period of two hours.

The samples for infrared spectroscopic measurements were suspended in paraffinic or fluorinated oils.

Certain samples of strontium dihydrogermanate were contaminated with strontium carbonate. In the spectra of these samples additional bands are observed due to the vibrations of the CO_3^{-2} ion (1463, 1073, 815, and 693 cm^{-1}).

REFERENCES

1. Ya. I. Ryskin, Opt. i Spektr. 4, 532 (1958).
2. Ya. I. Ryskin, Opt. i Spektr. 7, 278 (1959), Optics and Spectroscopy 7, 177 (1959).
3. Ya. I. Ryskin, Opt. i Spektr. 8, 606 (1960), Optics and Spectroscopy 8, 320 (1960).
4. I. H. Müller and C. E. Gulezian, J. Am. Chem. Soc. 51, 2029 (1929).
5. R. Schwarz and F. Heinrich, J. anorg. allgem. Chem. 205, 43 (1932).
6. N. Nowotny and G. Szekely, Monatsh. Chem. 83, 568 (1952);
H. Nowotny, Uspekhi Khim. 27, 996 (1958).
7. J. West, Z. Kristallogr. 74, 306 (1930).
8. H. Siebert, Z. anorg. allgem. Chem. 273, 170 (1953).
9. H. Siebert, Z. anorg. allgem. Chem. 275, 225 (1954).
10. A. N. Lazarev, Opt. i Spektr. 9, 195 (1960), Optics and Spectroscopy 9, 103 (1960);
A. N. Lazarev and T. F. Tenisheva, Opt. i Spektr. 10, 79 (1961), Optics and Spectroscopy 10, 37 (1961).
11. K. Nakamoto, M. Margoshes, and R. E. Rundle, J. Am. Chem. Soc. 77, 6480 (1955).
12. H. H. Jaffe, J. Phys. Chem. 58, 185 (1954); Uspekhi Khim. 26, 1060 (1957).
13. R. Blinc and D. Hadzi, Molec. Phys. 1, 391 (1958).

SECOND ORDER RAMAN SPECTRA OF ALKALI-HALIDE MIXED CRYSTALS

A. I. Stekhanov and M. B. Eliashberg (pp. 348-353)

Received 14 May 1960

The second order spectrum of KBr is studied in detail. For the first time spectra of mixed time spectra of mixed crystals of KBr-KCl are obtained and investigated. On the basis of the results obtained conclusions are drawn about the particulars of the elastic spectra of the crystals investigated. It is discovered that, together with a second order spectrum, there is present in the mixed crystals a first order spectrum connected with defects of the crystalline lattice.

Study of the vibrational spectra of crystals is important for an understanding of a whole series of phenomena in solid-state physics. One of the most effective methods of studying the vibrational frequencies of crystals is the investigation of their Raman spectra.

For many crystals, until the present time, only the usual Raman spectra—the so-called first order Raman spectra—have been adequately studied. But in these spectra are revealed only the limiting frequencies of the optical branches corresponding to the long waves of the elastic spectrum.

A much more complete representation of the elastic spectrum of crystals is provided by Raman spectra of the second order in which all of the frequencies of the elastic spectrum appear, including also the frequencies of the acoustic branches. In spite of the great experimental difficulty of observing Raman spectra of the second order related with its low intensity there has been undertaken a systematic study of the second-order spectra of crystals of alkali-halide salts.[1-4] In this study it has been discovered that the Raman spectra of NaCl, NaBr, KCl, KBr, and KI have a continuous spectrum with maxima in the intensity.

In the current study we undertook the detailed investigation of the Raman spectrum of KBr and of the mixed crystal KBr-KCl.

Second order spectra of potassium bromide were first obtained by Stekhanov.[3] It was a continuous spectrum, on the background of which appeared four broad bands occupying the frequency intervals: 80-100, 120-165, 180-220, 240-290 cm^{-1}. Afterwards it was noted that some of the bands evidently have a structure. The second order spectra of mixed crystals have not been investigated until the present time, but they are of considerable interest since they provide the possibility of a deeper explanation of some important aspects of the phenomena of light scattering by alkali-halide crystals.

For the current experiments we grew, using the method of Kiropulos, large homogeneous single crystals of KBr and KBr-KCl, from which were cleaved samples having the form of a parallelepiped $15 \times 15 \times 70$ mm.

The investigations of the Raman spectra were carried out on a high intensity apparatus[3] which allowed us to obtain second order spectra from the mercury line 2537 A. The photographing of the spectra was carried out on a Zeiss Q-24 quartz spectrograph with a dispersion in the region of low frequencies of 8 A/mm. The slit of the spectrograph was 0.02 mm in the case of the KBr crystal and 0.03 mm for KBr-KCl. The second order spectrum of potassium bromide was obtained in 8 hr, and the spectrum of the mixed crystals in 10 to 11 hr. In the study of the state of polarization the exposure time of the spectra was approximately 28 hr.

In Fig. 1 is presented a microphotogram of the Raman spectrum of crystalline KBr. As is seen from the figure the second order spectrum of KBr is continuous with sharply separated maxima. Particularly characteristic is an intense maximum which consists of three

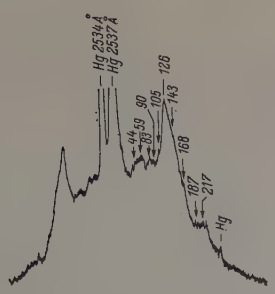

Fig. 1. Microphotogram of the Raman spectrum of the KBr crystal.

sharp peaks with the frequencies 126, 143, and 168 cm^{-1}. The structure of this maximum is clearly seen in the photograph of the spectrum.

In the region of the gap in the intensity between the Rayleigh line and the 126 cm^{-1} peak are discovered maxima with the frequencies 44, 59, 83, 90, and 105 cm^{-1}. On the high frequency side maxima at 187 and 217 cm^{-1} are observed. They form steps sharply defined on the background of the rapidly falling intensity of the 126 cm^{-1} peak. Further, at the end of the spectrum occur weak broad maxima of the intensity with frequencies 229, 240, 281, and 304 cm^{-1}. The extent of the complete spectrum is about 380 cm^{-1}.

The Raman spectra of the KBr-KCl mixed crystals were obtained for the cases of three different concentrations of the components:

(1) 80 mole % KBr + 20 mole % KCl,
(2) 40 mole % KBr + 60 mole % KCl,
(3) 20 mole % KBr + 80 mole % KCl.

Microphotograms of the spectra of these crystals are presented in Fig. 2.

In general, for all three of these spectra there appears a continuous character of the Raman spectrum,

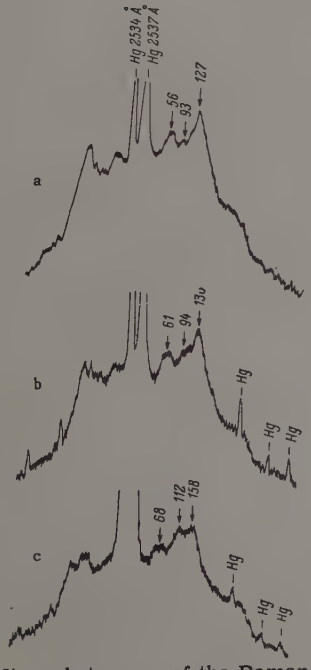

Fig. 2. Microphotogram of the Raman spectra of mixed crystals. a—80% KBr + 20% KCl; b—40% KBr + 60% KCl; c—20% KBr + 80% KCl.

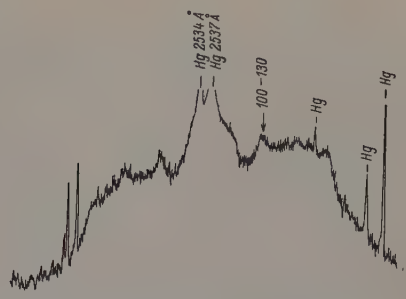

Fig. 3. Microphotogram of the Raman spectrum of the KBr crystal.

with maxima of the intensity. However, they differ substantially from one another regarding the distribution of the intensity, and differ particularly from the spectra of the pure crystals of KBr and KCl. Here (Fig. 3) we will introduce the spectrum of the pure KCl crystal as given by Stekhanov.[5] Comparing the Raman spectra it is possible to follow the changes in the intensity distribution which occur with an increase of the KCl concentration in the KBr-KCl crystal. First of all, attention is drawn to the filling of the region of the intensity gap in the transition from pure KBr to the first mixed crystal containing comparatively little KCl. Further, there arises a gradual leveling of the maxima in intensity which gives the spectrum a smoother character. In particular one can evaluate the broadening of the spectrum by the magnitude of the frequencies of the more characteristic maxima observed in the Raman spectra of the KBr-KCl crystals with different KCl concentrations (cf. Table).

Concentration of KCl (mole %)	Frequencies of the maxima (cm^{-1})		
Pure KBr	52	83	126
20% KBr	56	93	127
60% KBr	61	94	138
80% KBr	68	112	158
Pure KCl	—	100—130	—

In a more detailed comparison of the spectra we note that the difference in the intensity of the 83 cm^{-1} and 126 cm^{-1} maxima, which was very large in the spectrum of the KBr crystal, gradually decreases and finally in the spectrum of the 20% KBr + 80% KCl crystal both maxima have approximately the same intensity (their frequencies in the spectrum of this crystal are 112 and 158 cm^{-1}). The 112 cm^{-1} maximum, on a further increase of the KCl concentration, evidently transforms into the broad maximum at 100-130 cm^{-1} observed in the spectrum of crystalline KCl.

We note also that the shoulder observed on the high frequency side of the spectrum becomes more distinct on transition from the KBr crystal to the mixed crystals. In the comparison of the spectra of the mixed crystals with the spectra of the pure components we consider it to be particularly characteristic that even for KCl concentrations approaching 80% the Raman spectrum in its form is closer to the spectrum of KBr than to the spectrum of KCl. This is related to the fact that the scattering of alkali-halide crystals is governed principally by the electronic cloud of the halogen ions.[3] In this specific case the polarizability of the bromide ion is almost twice the polarizability of the chloride ion.

With the purpose of a deeper study of the scattering of the mixed crystals we obtained the spectra of mixed crystals heated to 350°C, and also we studied the state of polarization of the spectrum of one of the mixed crystals (80% KBr + 20% KCl).

The results of these investigations consist of the

following: The character of the intensity distribution in the spectrum of the heated mixed crystals proves to be somewhat smoother than the spectrum of the cold crystals, but generally speaking, the heating does not have a substantial influence on the intensity distribution. The study of the state of polarization showed that the second order spectrum of the mixed crystals is markedly polarized but the intensity distribution in the spectra of the two different components of the polarized light has a similar character.

An exposition of the above results, we feel, can be interpreted on the basis of the Born theory of the crystalline lattice. However, at the present time there do not exist any theoretical data on the second order spectrum of the KBr crystal and of KBr-KCl mixed crystals. Also, their elastic spectra are not known. Therefore, it is of interest to obtain from the second-order spectra some information about the elastic spectrum of these crystals.

It is known that the second order Raman spectrum is produced in the form of a spectrum of octaves of sum and difference combinations of the frequencies of the entire elastic spectrum of the crystal. If the elastic spectrum of the crystal is quasi-continuous then the second order spectrum should be continuous itself, but when there occurs in some narrow frequency interval of the elastic spectrum a high density of frequencies, then this inevitably appears in the region of the octave frequencies of the second order spectrum in the form of a corresponding maximum of the intensity. Similarly, two maxima in different portions of the elastic spectrum will give maxima of the intensity in the scattering of the Raman spectra in places corresponding to the sum and difference frequencies. Taking this into consideration we will examine the results of our investigations.

First of all, it is considered significant that the Raman spectra of KBr and of KBr-KCl mixed crystals appear to be spectra of a single type. They appear as continuous spectra with maxima of intensity which indicates, evidently, the existence of a quasi-continuous character of their elastic spectra, in which the frequency distribution has a continuous form. But on a comparison of the spectra of the mixed crystals with one another and with the spectra of the pure KBr and KCl crystals it is not difficult to note a significant difference in the spectra. The spectra of all of the crystals differ both in their extent and in the distribution of the intensity. This indicates that the elastic spectra of the crystals must differ in form in spite of their similar type of lattice.

The presence in the second order spectrum of KBr of extraordinarily sharp maxima of the intensity, the width of which does not exceed 5 cm^{-1}, and the presence of narrow maxima also in the spectrum of NaCl[6,3] and of KCl,[5] evidently bears witness to the presence of very sharp peaks in their elastic spectra. At the same time the elastic spectra of NaCl and KCl, presently known,[7,8] do not contain such sharp maxima. For example, in the elastic spectrum of NaCl the narrowest maximum resulting from the superposition of the transverse optical branch and the longitudinal acoustic branch has a width of approximately 80 cm^{-1}.

The absence of sharp maxima in the calculated elastic spectra appears, evidently, to be due to an inadequate accuracy of the calculations.

In connection with this it should be noted that in the theoretical studies[9-11] proposals have been advanced on the possibility of the existence in the elastic spectrum of a lattice of particular points at which the frequency density can be very large.

In the investigation of the Raman spectrum of mixed crystals we have seen that it is not possible to study their spectra as a simple superposition of the spectra of pure KBr and KCl. Each of the mixed crystals has its second order spectrum which differs from the spectrum of both the components. This evidently indicates that the KBr-KCl crystal has its own structure, possessing, for a given percentage composition, its own lattice and its own characteristic elastic spectrum. In spite of the fact that the lattice of the mixed crystals substantially differs from the lattice of the pure components it remains essentially a lattice of the NaCl type. On an increase of the KCl concentration in the KBr-KCl crystal the high frequency limit of its elastic spectrum gradually shifts in the direction of larger frequencies, corresponding with the fact that the eigenfrequencies in KCl, on the average, are larger than KBr as a result of the smaller mass of the anion. In addition to the shift of the elastic spectrum there also arises a substantial change in the distribution of the frequencies. It is possible that some of the peaks in the spectrum of the elastic vibrations become broader and some generally are smoothed out; this is indicated by a certain washing-out of the form of the second order spectrum of the mixed crystals.

On comparing the spectrograms of the KBr and KBr-KCl crystals we note the significant shift in the spectrum in the transition from pure KBr to the first mixed crystal containing 80% KBr and 20% KCl, which is inferred from the evidence that the gap of the intensity, observed in the region of low frequencies for KBr (Fig. 1), becomes less deep in the spectrum of the mixed crystal (Fig. 2).

Taking account of the circumstance that the Raman spectra of the mixed crystals, including even the crystal containing 80% KCl and 20% KBr, undoubtedly preserve the lines of the KBr spectrum, one can assume that the spectrum of a KBr crystal containing small amounts of additive should be very close to the KBr spectrum. From this viewpoint the difference discovered in the low frequency region proves to be somewhat unexpected. It appears to us that it is not possible to explain such a strong difference in the distribution of intensity in the Raman spectra by a sharp change in the elastic spectrum: the elastic spectrum of the crystal can scarcely change so strongly for a comparatively small concentration of KCl. This is emphasized by the fact that a further increase of the KCl concentration, while it influences the Raman spectra of the crystals, does so to a much lesser degree. In agreement with this their elastic spectra should also change gradually.

Thus we may conclude that in the Raman spectrum of the mixed crystals we have discovered a new phenomenon which, in its properties, differs from the second order scattering of the pure crystals.

We will examine a possible explanation of this phenomenon. It is known that, as a result of the central symmetry characteristic for the pure crystals of the alkali-halide salts, first order Raman spectra are absent for them and the observed scattering must be only second order scattering. On transition from the pure crystal to the mixed crystal there arises a substantial breaking-down of the crystalline lattice. Indeed, in the KBr-KCl crystal Cl^- ions are located side-by-side with Br^- ions on the anion sites of the lattice. Moreover, part of the sites of the lattice prove to be generally not occupied.[12] Near the additive ion (Cl^-) the symmetry of the field is changed; this leads to a displacement of the ions. As a result, while the sites of the mixed crystal (just as the sites of the pure crystal) are separated from one another by a distance determined by the minimum of mutual potential energy, this distance must be different in different parts of the crystal.

The particulars of the microstructure of mixed crystals of the MBr-MCl type (M is a metal) have been examined theoretically.[13] The authors calculate the mean

magnitude of the displacement of the ions of the metal under the action of changes of the symmetry of the field, and arrive at the conclusion that it is not possible to assign a definite lattice constant to the mixed crystal.

Thus, if a lattice contains an impurity then its structure undoubtedly is altered. The degree of alteration obviously will be maximum for an identical concentration of the components.

As a result of the perturbations of the symmetry of the sites in the defect lattice we can expect lifting of the restrictions for the first order spectra. Consequently, first order spectra, together with the second order spectra, should appear in the Raman spectrum of the mixed crystal. Therefore we consider it possible to explain the anomalous radiation observed in the low frequency region in the second order spectra of the mixed crystals as first order scattering from the defects of the crystalline lattice.

The first order spectra of the mixed crystals will be completely dissimilar in form to the first order spectra of those crystals in which it is allowed, where there appear only the limiting frequencies of the optical branches of the elastic spectrum. As a result of the fact that in mixed crystals the translational symmetry of the lattice is also disturbed to a known degree, their first order spectra should be continuous. Indeed, the radiation we have discovered appears as a continuous spectrum which is located in the low frequency region, i.e., in that part of the spectrum where there should appear a first order Raman spectrum.

However, the spectrum of the anomalous radiation in mixed crystals differs markedly from the spectra of the elastic vibrations in both the distribution of the frequencies and in its extent. Thus in the second order spectrum of the 80% KBr + 20% KCl crystal it is observed that the extent of its elastic spectrum is not less than 200 cm^{-1}, while the anomalous radiation occupies a frequency interval from 20 to 100 cm^{-1}; i.e., in the first order continuous spectrum, frequencies of the elastic vibrations from 0 to 20 cm^{-1} and from 100 to 200 cm^{-1} are not revealed.

This peculiarity of the first order anomalous scattering finds an explanation in the theoretical investigations of Pavinskii.[14] These investigations have shown convincingly that, in the first order spectra connected with defects of the crystalline structure, there should appear only those frequencies of the elastic spectrum for which the length of the elastic wave is comparable with the dimensions of the scattering center. In correspondence with this diffraction condition the observed first order spectrum of the mixed crystal is cut off both on the low and on the high frequency sides.

It should be noted that the first order spectrum in the mixed crystals differs in its properties from the first order spectrum observed in heated rock salt.[15]

In the mixed crystals we did not observe such a strong temperature dependence of the intensity of the anomalous radiation as was observed in rock salt. This is understandable since in the mixed crystals there is already at room temperature a concentration of defects responsible for the appearance of the first order spectrum, which is sufficiently large, and the heating of the crystals increases it only insignificantly. Further, our investigations of the state of polarization showed that the anomalous radiation in the mixed crystals is nonpolarized while, at the same time, in the heated rock salt the low frequency region is more strongly polarized than the remaining portion of the scattering spectrum. The latter circumstance we consider to be connected with a different nature of the defects in the heated rock salt and the mixed crystals causing, respectively, polarized and nonpolarized first order spectra. Evidently, weakly-bonded electrons are responsible for the anomalous first order scattering in rock salt.[14,15] The appearance of anomalous first order scattering in the Raman spectrum of the mixed crystals is connected with those substantial alterations which arise in the crystalline lattice on the introduction of impurities, and which are not accompanied by the appearance of weakly-bonded electrons.

REFERENCES

1. E. Fermi and F. Rasetti, Z. Physik **71**, 689 (1931).
2. E. Gross and A. Stekhanov, Izvest. Akad. Nauk SSSR, Ser. Fiz. **11**, 364 (1947).
3. A. I. Stekhanov, Kand. Diss., Leningrad, 1948.
4. A. Stekhanov and M. Petrova, Zhur. Eksptl. i Teoret. Fiz. **19**, 1108 (1949).
5. A. Stekhanov, Zhur. Eksptl. i Teoret. Fiz. **20**, 330 (1950).
6. R. S. Krishnan, Nature **159**, 266 (1947).
7. E. W. Kellermann, Phil. Trans. Roy. Soc. **238**, 513 (1940).
8. M. Jona, Phys. Rev. **60**, 824 (1941).
9. E. W. Montroll, J. Chem. Phys. **15**, 575 (1947).
10. W. V. Houston, Revs. Modern Phys. **20**, 161 (1948).
11. M. Smollet, Proc. Phys. Soc. **A65**, 109 (1952).
12. M. S. Ivankina, Izvest. Vysshikh Ucheb. Zaved. No. 1, 101 (1958).
13. G. S. Durham and J. A. Hawkins, J. Chem. Phys. **19**, 149 (1951).
14. P. P. Pavinskii, Vestnik Leningrad. Gosudarst. Univ. No. 22, **4**, 51 (1957).
15. E. F. Gross, P. P. Pavinskii, and A. I. Stekhanov, Doklady Akad. Nauk SSSR, **68**, 27 (1949).

EXCITATION ENERGY TRANSFER IN RIGID SOLUTIONS OF ORGANIC SUBSTANCES

I. M. Rozman (pp. 354-361)

Received 3 May 1960

We have measured the efficiency of the transfer of electronic excitation energy from p-terphenyl to 1,3,5-triphenyl-Δ^2-pyrazoline in polystyrene, and the fluorescence yield of p-terphenyl as a function of the concentration of the energy acceptor. For an acceptor concentration ≥ 0.01 mole/liter, transfer by means of resonance interaction of the molecules plays the principal role. It is proposed that the deviation from the Förster-Galanin theory is associated with the migration of energy via the solvent.

INTRODUCTION

The present work was undertaken for the purpose of verifying the adequacy of the Förster-Galanin theory[1,2] to describe energy transfer in solutions of organic substances. As is well known, this theory is based on the idea of inductive resonance interaction of the molecules. On the assumptions that the molecules are motionless (during the lifetime of the excited state) and statistically distributed in the solution, and that the interaction between them is of dipole-dipole character, the dependence of the quantum yield of the fluorescence of the energy donor M_1 on the concentration of the acceptor M_2 is determined by the formula

$$\eta_l = \eta_{l0}\left\{1 - 2qe^{q^2}\int_q^\infty e^{-x^2}dx\right\}, \qquad (1)$$

where

$$q = 1.55\,(2\pi n)^{-2}\left(\frac{\tau_0 \bar{\lambda}^4}{\tau_e N_A}\right)^{1/2} n_2. \qquad (2)$$

Here n is the refractive index of the medium, n_2 is the number of molecules of M_2 per cm^3, τ_0 is the lifetime of the excited state of M_1 in the absence of M_2, τ_e is the "natural" lifetime of the excited state of M_1, N_A is Avogadro's number, and

$$\bar{\lambda}^4 = \int f_Q(\lambda)\, k(\lambda)\, \lambda^4 d\lambda, \qquad (3)$$

where f_Q is the normalized quantum emission spectrum of M_1, k is the (decimal) absorption coefficient for M_2 in cm^2/mole, and λ is the wavelength in cm. In the derivation of formula (1), it is also assumed that the excitation energy for M_1 may be either transferred to one of the M_2's, or emitted in the form of a photon, or dissipated within M_1. Now the presence of M_2 will not affect the rate of the latter two processes. Therefore the quantum yield of the radiationless transfer of excitation energy from M_1 to M_2 will be

$$\eta_t = 1 - \frac{\eta_l}{\eta_{l0}}. \qquad (4)$$

The experiments of Belikova and Galanin[3] and Cohen and Weinreb[4] have given a considerably larger efficiency of energy transfer from a solvent (toluene, xylene, anisole) to a dissolved substance (p-terphenyl, anthracene) than follows from formula (4). As a possible explanation, these authors introduce diffusion of the molecules within the lifetime of the excited state. This conclusion agrees with the results of Kuznetsova and Sveshnikov[5] on the influence of solvent viscosity, and also with the ideas of Furst and Kallmann[6] on energy transfer in liquid solutions by means of collisions. However, there are experiments which indicate an insignificant role for molecular diffusion. Thus, according to Hardwick's data,[7] the energy transfer efficiency from naphthalene to anthracene in toluene or methyl methacrylate is even somewhat lower than in polymethyl methacrylate. Comparing the concentration dependence of the duration of luminescence in solutions of anthracene in benzene and in polystyrene under excitation by electrons, Knau[8] comes to the conclusion that diffusion of the molecules does not play a substantial role in the energy transfer process, but that there is diffusion of the excitation energy via the solvent. This possibility had also been pointed out previously.[3] Cohen and Weinreb[4] suppose the role of diffusion of the excitation energy via the solvent to be insignificant. Thus, on 1400-fold dilution of toluene by cyclohexane, the transfer efficiency to p-terphenyl changes by only a few percent.

Lipsky and Burton have shown in a recently published work[9] that introducing molecular diffusion or diffusion of the excitation energy via the solvent by means of dipole-dipole interaction is insufficient to explain the experimentally-obtained high efficiency of energy transfer from toluene and benzene to p-terphenyl or from benzene to diphenylhexatriene. They consider that in liquid hydrocarbons there are regions of high local ordering, in which exciton migration is possible. Energy transfer takes place on collision of the solute molecules with these regions as a whole.

Thus it follows, from the totality of the experimental data, that the Förster-Galanin theory does not give a complete description of the energy transfer process in liquid solutions of organic substances, and the fundamental cause of this lies in the presence of diffusion of the molecules and of the excitation energy. Furthermore, Birks and Cameron[10] and Birks[11] consider that the energy transfer in such solutions takes place only by means of a radiative mechanism, i.e., through emission and absorption of photons.[12]

We chose plastic scintillators as our object of study. The experimental data on energy transfer from the matrix substance (solvent) to the luminescent solutes in these scintillators are in qualitative agreement with the Förster-Galanin theory.[13-16] In order for there to be a possibility of establishing the degree of quantitative agreement, it is necessary to exclude not only diffusion of the molecules, but also diffusion of energy via the solvent. Accordingly, we have measured the energy transfer efficiency not from the matrix substance to the solute, but between two different solutes. p-Terphenyl (3Ph) served as energy donor, and 1,3,5-triphenyl-Δ^2-pyrazoline (3PhP) as acceptor. Scintillators with various concentrations of 3Ph and 3PhP were prepared by thermal polymerization of styrene solutions.[17] The samples measured were formed into cylinders (diameter 16 mm, height 10 and 1 mm) with a polished surface.

PROCEDURE AND EXPERIMENTAL RESULTS

The efficiency of excitation energy transfer from the donor M_1 to the acceptor M_2 (that is, the number of M_2 molecules excited by the transfer, calculated for one excited M_1 molecule) was determined by comparison of the fluorescence intensities of M_2 on excitation by ultraviolet radiation in the absorption band of the donor (λ_1) and in a band where the acceptor absorbs and the donor is transparent (λ_2). If the fraction of λ_1 absorbed in M_1 equals α_{11} and that in M_2 equals α_{21}, then the transfer efficiency will be[14]

$$T_{12}=\frac{\frac{I_{21}}{I_{22}}-\alpha_{21}}{\alpha_{11}}, \qquad (5)$$

where I_{21} and I_{22} are the respective fluorescence intensities of M_2 under equal fluxes of exciting photons (complete absorption is assumed).

The energy transfer takes place both by means of a photon mechanism and by means of a radiationless transfer, i.e.,

$$T_{12}=\eta_l+\eta_1 R_{12}^{*}, \qquad (6)$$

where R_{12}^{*} is the average probability of absorption of photons from M_1 by M_2, and depends on the nature of the molecules, their concentration, and the conditions of the experiment.

Let the exciting photons fall perpendicularly on a planar slab of isotropic luminor of thickness H, containing c_1 gm/gm of M_1 and c_2 gm/gm of M_2. If the absorption coefficient of these photons equals κ, and the absorption coefficient of the photons from the fluorescence of M_1 equals $\mu(\lambda)$, then the probability of absorption of an M_1 photon within the slab will be (for $\kappa H \gg 1$)*

*The computations are analogous to ref. 18. At the "entrance" boundary of the slab, complete internal reflection takes place at an angle $\theta_0 = \text{arc sin}\,(1/n)$. All the photons falling on the second boundary leave the slab.

$$P_\lambda=\frac{1}{2}\left\{1-e^{-\mu H}+\frac{1-e^{-\mu H\psi}}{\psi}+\frac{\mu}{\varkappa}\ln\frac{\mu+\varkappa}{\mu+\varkappa/\psi}\right.$$

$$\left.-\mu H\,[Ei(-\mu H)+Ei(-\mu H\psi)]+\frac{\mu}{\varkappa}\,[Ei(-\mu H)-Ei(-\mu H\psi)]\right.$$

$$\left.-\frac{\mu}{\varkappa}\,e^{-\varkappa H}\,Ei\,[H(\varkappa-\mu)]\right\},$$

where

$$\psi=\frac{n}{(n^2-1)^{1/2}}.$$

The average probability of self-absorption of the primary fluorescence of M_1 is

$$R_{11}=\int P_\lambda \alpha_1(\lambda)\, f_Q d\lambda, \qquad \alpha_1=\frac{c_1k_1}{c_1k_1+c_2k_2},$$

where k_1 and k_2 are the absorption coefficients of M_1 and M_2. If, furthermore, we assume that for the secondary fluorescence of M_1 the quantity P_λ remains as before,[19] then it is easy to obtain*

*Here it is assumed that the quantum yield of M_1, namely η_1, does not depend on λ over the whole reabsorption interval. This cannot lead to substantial error in the case of 3Ph, since the fundamental contribution to R_{11} is given by $\lambda < 3450$ A.

$$R_{12}^{*}=\frac{\int P_\lambda \alpha_2(\lambda)\, f_Q d\lambda}{1-\eta_1 R_{11}}\equiv\frac{R_{12}}{1-\eta_1 R_{11}}. \qquad (7)$$

Under the same assumptions, the fluorescence intensity of M_1, measured from the excitation side and in the direction normal to the slab, will be proportional to the quantity

$$I_1=\frac{\eta_1\alpha_{11}}{1-\eta_1 R_{11}}\int\frac{f_Q\sigma(\lambda)\,d\lambda}{1+\alpha_{11}\frac{c_1k_1(\lambda)+c_2k_2(\lambda)}{c_1k_1(\lambda)}}\equiv\frac{\eta_1 B_1}{1-\eta_1 R_{11}}, \qquad (8)$$

where σ is the quantum sensitivity of the recording apparatus (photomultiplier + filters). Designating I_1 ($c_2 = 0$) as I_{10}, we have

$$\frac{\eta_1}{\eta_{10}}=\frac{\frac{I_1B_{10}}{I_{10}B_1}}{1-\eta_{10}R_{10}\left(1-\frac{I_1R_{11}B_{10}}{I_{10}R_{10}B_1}\right)}. \qquad (9)$$

The measuring apparatus is shown in Fig. 1. An SF-4 monochromator separated individual lines out of the spectrum of a mercury lamp. The exciting light was directed onto the upper surface of the luminor at an angle of 14° to the normal. The dimensions of the spot amounted to about 3×5 mm with a sample diameter of 16 mm. The fluorescence intensity was measured in the direction of the normal through appropriate filters by an FEU-19m photomultiplier. The fundamental results were obtained for samples 1 mm in thickness, the lower surfaces of which were in optical contact (paraffin oil) with sooty ebonite. The measurements were carried out on two series of samples. In the first series, the concentration of 3Ph was 5×10^{-3} gm/gm and that of 3PhP ranged from 0 to 5×10^{-3}. During the second series, $c_1 = 2 \times 10^{-2}$ gm/gm and $c_2 = 0$ to 2×10^{-2} gm/gm. The results of the measurements for $\lambda_1 = 2894$ A and $\lambda_2 = 3650/63$ A are presented in Fig. 2. The 3Ph fluorescence was isolated by a filter made up of UFS-2 and BS-6, which transmitted about 50% in the region $\lambda\lambda$3400-3700 A and less than 1% for $\lambda < 3200$ A or $\lambda > 3900$ A. The 3PhP fluorescence was measured through a ZhS-16 filter (this transmits $\lambda > 4600$ A, the maximum of the emission spectrum being 4350 A). During λ_2 excitation, corrections for incomplete absorption were made in I_{22}. At $c_2 = 1 \times 10^{-4}$ gm/gm and H = 1 mm, the absorption is 72%, and at $c_2 = 3 \times 10^{-4}$ gm/gm it is 98%. The relative intensity of the exciting lines was measured with the help of three quantum counters placed in the sample holder. Plastic scintillators 16 mm in diameter and 10 mm in height, with polystyrene bases and different luminescent solutes, served as counters: (a) 2-phenylchrysene-2,5-oxazole, 2% by weight; (b) 3,5-diphenyl-1-(β-naphthyl)-Δ^2-pyrazoline, 2% by weight; and (c) 1,1,4,4-tetraphenyl-1,3-butadiene, 3% by weight. Their fluorescence intensity was measured through a ZhS-16 filter.*

*The properties of the quantum counters were tested according to Solomin's method,[20] by comparison with solutions of 3PhP in dioxane (1 gm/liter) and of 1,5-diphenyl-3-(4-phenylbutadienyl)-Δ^2-pyrazoline in dioxane (5 gm/liter).

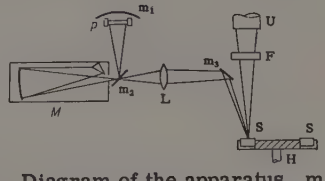

Fig. 1. Diagram of the apparatus. m_1, m_2, m_3—mirrors; P—PRK-8 mercury lamp; M—monochromator; L—quartz lenses; S—samples being measured; H—12-position sample holder; F—filter; U—FEU-19m photomultiplier.

The absorption spectra of 3Ph and 3PhP in polystyrene were measured in the following way. For $\lambda > 3000$ A, we compared the transmission of identically-dimensioned samples of pure polystyrene and of polystyrene with a varying concentration of 3Ph or 3PhP. The thickness of the samples lay within the limits of 10 to 1 mm. For smaller λ, direct comparison is not suitable because of strong absorption in the polystyrene itself. Therefore, the spectra were measured in dioxane and a polystyrene correction was made for the overlap regions. The results are presented in Fig. 3, where the quantum fluorescence spectrum of 3Ph is also shown. It is important to note that Beer's law is observed over the entire concentration range (up to 2×10^{-2} gm/gm).

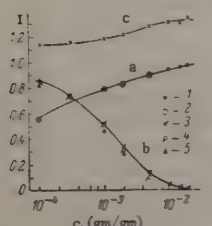

Fig. 2

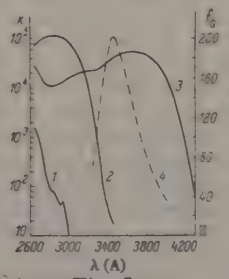

Fig. 3

Fig. 2. Fluorescence intensity of 3Ph and 3PhP as a function of concentration. Curve a—I_{21}/I_{22}, I_{21} under excitation by the 2894 A mercury line, I_{22} at 3655 A; curve b—I_1/I_{10} under excitation by λ 2894 A; curve c—I_{22} for c_1 2×10^{-2} gm/gm. Points 1 and 3: $c_1 = 2 \times 10^{-2}$ gm/gm; points 2, 4, and 5: $c_1 = 5 \times 10^{-3}$ gm/gm; point 5: at sample thickness 10 mm.

Fig. 3. Absorption spectra of polystyrene (curve 1) 3Ph (curve 2), and 3PhP (curve 3) in polystyrene. k is the decimal absorption coefficient in cm^2/gm. Curve 4 is the normalized quantum fluorescence spectrum of 3Ph—f_Q (photons) $\times 10^4$ A.

As the concentration of 3PhP increases, I_{21}/I_{22} approaches 1 (Fig. 2). Differences in the spatial distribution of the excited molecules for λ_1 and λ_2 can not have exerted a substantial influence on this quantity. Thus for $\lambda_2 = 4078$ A, I_{21}/I_{22} proved to be the same as for $\lambda_2 = 3650$ A, although the absorption coefficients differ by a factor of 7.5 (Fig. 3). In Table 1 are presented the results of a computation of the transfer efficiency T_{12} according to formula (5). For each λ_1, four series of measurements were carried out. The reproducibility was not worse than 2%. Coincident values of T_{12} were obtained for both λ_1's and c_1's. The computations show that the absorption probabilities R_{11} and R_{12} likewise do not depend on λ_1. The results are presented in Table 2. Since

Table 1. Efficiency of Excitation Energy Transfer from 3Ph to 3PhP

c_2 (gm/gm)	$\lambda_1 = 3022/26$ Å, $c_1 = 2 \cdot 10^{-2}$ gm/gm			$\lambda_1 = 2894$ Å, $c_1 = 2 \cdot 10^{-2}$ gm/gm			$c_1 = 5 \cdot 10^{-3}$ gm/gm, $\lambda_1 = 2894$ and 3022.26 Å
	$\frac{I_{21}}{I_{22}}$	a_{11}	T_{12}	$\frac{I_{21}}{I_{22}}$	a_{11}	T_{12}	T_{12}
$1 \cdot 10^{-4}$	0.55	0.00	0.55	0.55	0.00	0.55	0.56
$3 \cdot 10^{-4}$	0.71	0.00	0.71	0.71	0.00	0.71	0.71
$1 \cdot 10^{-3}$	0.79	0.01	0.79	0.78	0.00	0.78	0.80
$2 \cdot 10^{-3}$	0.82	0.02	0.82	0.83	0.01	0.83	0.83
$5 \cdot 10^{-3}$	0.89	0.05	0.88	0.89	0.03	0.89	0.90
$1 \cdot 10^{-2}$	0.94	0.09	0.93	0.94	0.05	0.94	—
$1.5 \cdot 10^{-2}$	0.96	0.13	0.95	0.96	0.07	0.96	—
$2 \cdot 10^{-2}$	0.97	0.17	0.96	0.97	0.09	0.97	—

Table 2. Absorption of the Fluorescence of 3Ph by 3Ph (R_{11}) and by 3PhP (R_{12})

c_1 (gm/gm)	$c_1 = 5 \cdot 10^{-3}$ gm/gm		$c_1 = 2 \cdot 10^{-2}$ gm/gm	
	R_{11}	R_{12}	R_{11}	R_{12}
0	0.132	—	0.197	—
$1 \cdot 10^{-4}$	0.076	0.68	0.128	0.62
$3 \cdot 10^{-4}$	0.048	0.83	0.089	0.73
$1 \cdot 10^{-3}$	0.027	0.87	0.054	0.84
$2 \cdot 10^{-3}$	0.02	0.89	0.036	0.86
$5 \cdot 10^{-3}$	0.01	0.92	0.02	0.90
$1 \cdot 10^{-2}$	—	—	—	0.92
$2 \cdot 10^{-2}$	—	—	—	0.93

η_{10}, the quantum yield of the fluorescence of 3Ph in polystyrene, equals 0.75,[21] then, as is easily seen, the relation $T_{12} > \eta_{10} R_{12}^*$ is fulfilled over the entire range of c_2 concentrations; i.e., radiationless energy transfer takes place.

Let us now consider the results of measurements of the fluorescence intensity of 3Ph (Fig. 2, curve b). The quotient I_1/I_{10} depends only slightly on c_1 and on the sample thickness. The somewhat smaller value of I_1/I_{10} for thick samples is governed by the effect of secondary fluorescence of 3Ph. It is easy to show that the quantum yield of 3Ph, η_1, diminishes as the concentration of 3PhP increases. In fact, if there were no such diminution, then, according to (8),

$$\frac{I_1}{I_{10}} > \frac{a_{11}}{1 + a_{11} \frac{c_2 k_2(\lambda_m)}{c_1 k_1(\lambda_1)}},$$

where $k_2(\lambda_m)$ is the maximum absorption coefficient of 3PhP in the luminescence region of 3Ph. For $c_1 = 2 \times 10^{-2}$ gm/gm and $c_2 = 1 \times 10^{-2}$ gm/gm, we obtain (Table 1, Fig. 3) $I_1/I_{10} > 0.78$. Experimental results give $I_1/I_{10} = 0.045$; i.e., a significant diminution of η_1 takes place.

The quantity B_{01}/B_1, which is necessary for calculations according to formula (9), has been evaluated for $c_1 = 5 \times 10^{-3}$ gm/gm (Table 3). From this it is easy to obtain data for other concentrations, since c_1 and c_2 enter into B_1 only in the form of ratios.

Table 3. B_{10}/B_1 at a 3Ph Concentration of 5×10^{-3} gm/gm

c_2 (gm/gm)	Calculated		Experiment		Experiment $c_1 = 2 \cdot 10^{-2}$ gm/gm	
	λ 2894	λ 3022/26	λ 2894	λ 3022/26	λ 2894	λ 3022/26
$1 \cdot 10^{-4}$	1.01	1.01	1.01	1.01	1.00	1.00
$3 \cdot 10^{-4}$	1.03	1.04	1.03	1.04	1.00	1.01
$1 \cdot 10^{-3}$	1.10	1.15	1.09	1.14	1.01	1.03
$2 \cdot 10^{-3}$	1.21	1.30	1.19	1.27	1.02	1.06
$5 \cdot 10^{-3}$	1.50	1.74	1.47	1.67	1.11	1.18
$1 \cdot 10^{-2}$	—	—	—	—	1.22	1.33
$1.5 \cdot 10^{-2}$	—	—	—	—	1.33	1.50
$2 \cdot 10^{-2}$	—	—	—	—	1.43	1.67

The experimental values of B_{01}/B_1 presented in Table 3 were obtained in the following way. The fluorescence intensity of 3Ph for $c_2 = 0$ (i.e., I_{10}) was measured on the apparatus sketched in Fig. 1, under the conditions that a polystyrene disc with 3PhP was placed before the BS-6 and UFS-2 filters. The thickness of the disc amounted to 1 mm and the 3PhP concentration varied from 1×10^{-5} gm/gm to 3×10^{-4} gm/gm. With an increase in 3PhP concentration, I_{10} diminishes according to an exponential law (Fig. 4) with an absorption coefficient (decimal) $c_2 \bar{k} = 3.8 \times 10^4 c_2$ cm^{-1}. B_{10}/B_1 was computed according to the formula

$$\frac{B_{10}}{B_1} = \frac{1}{a_{11}} + \frac{c_2 \bar{k}}{c_1 k_1}.$$

DISCUSSION OF RESULTS

The data obtained undoubtedly testify to the great role of radiationless transfer of excitation energy from 3Ph to 3PhP. Thus, for example, when $c_2 = 1 \times 10^{-2}$ gm/gm, the transfer efficiency $T_{12} = 0.93$ (Table 1) and the quantum yield of the fluorescence of 3Ph $\eta_1 = 0.05$ (Fig. 2 and Table 3). With an increase in c_2, the transfer efficiency approaches 100%, which agrees with the concepts of the theory of inductive resonance. A quantitative comparison is carried out in Fig. 5. The theoretical values of the quantum yield of radiationless transfer (curve a) were calculated according to formulas (1)-(4). On the assumption that $\tau_0/\tau_e = \eta_{10}$, we obtained $q = 7.78 \times 10^{-20}$ n_2. The experimental values of η_t, computed on the basis of T_{12} (Table 1) and formulas (6) and (4) (points 1 and 2), agree satisfactorily with the theoretical in the

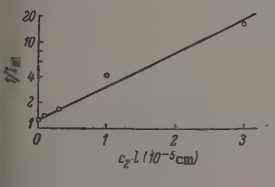

Fig. 4

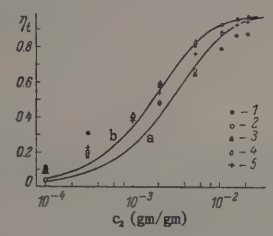

Fig. 5

Fig. 4. Reduction in the fluorescence intensity of 3Ph (I_{10}) on filtration through 3PhP in polystyrene (c_2 gm/gm).

Fig. 5. Quantum yield of excitation energy transfer from 3Ph to 3PhP. Curves a and b are theoretical. Points 1, 3, and 5: $c_1 = 2 \times 10^{-2}$ gm/gm; points 2 and 4: $c_1 = 5 \times 10^{-3}$ gm/gm. For further explanation, see text.

region of intermediate concentrations. For the characteristic constant R_0, the theory gives 27 A, the experiment 30 A. The fact that η_t does not depend on the donor concentration* also agrees with the theory. For $c_2 \gtrsim 1 \times 10^{-2}$, the experimental points lie below the curve. One may suppose that this is associated with an increase in the probability of internal quenching in the 3Ph molecules on account of the presence of 3PhP.[10] In such a case, relation (4) is invalid and η_1 must be taken from experiment for the calculation of η_t according to (6). The results (points 5) agree well with theory for $c_2 \gtrsim 5 \times 10^{-3}$.

*For $c_2 \lesssim 2 \times 10^{-3}$, the precision of the determination of η_t according to (6) is very low on account of the large fraction of photon transfer.

However, one must bear in mind that, for values of I_{21}/I_{22} close to 1, the error in η_t significantly exceeds the error in I_{21}/I_{22}. Thus for $c_2 = 2 \times 10^{-2}$, one obtains $I_{21}/I_{22} = 0.97$ and $\eta_t = 0.88$. If we take $I_{21}/I_{22} = 0.99$ (which lies within the limits of error), then $\eta_t = 0.97$. For a further test of the hypothesis of additional quenching, let us turn to the magnitude of the quantum yield of 3Ph. The experimental results, treated according to formula (9), are presented in Fig. 5 (points 3 and 4). In the entire concentration range of 3PhP, η_1/η_{10} is less than the value given by (4) and the theoretical value of η_t. If we assign this difference to the quenching of 3Ph by 3PhP molecules, then we can compute the probability of this process. Let k_e and k_i be the probabilities of transitions with emission and with quenching within the 3Ph molecule; let $K_t(c_2)$ be the probability of a transition of the excitation energy from the 3Ph molecule to 3PhP, and let $K_q(c_2)$ be the probability of a transition with quenching within 3Ph on account of the presence of 3PhP. By definition,

$$\eta_1 = \frac{k_e}{k_e + k_i + K_t + K_q}, \quad \eta_t' = \frac{K_t}{k_e + k_i + K_t + K_q}.$$

Since the transfer quantum yield determined by formulas (1)-(4) equals

$$\eta_t' = \frac{K_t}{k_e + k_i + K_t},$$

it is easy to obtain

$$\tau_0 K_q = \frac{\eta_{10}}{\eta_1} - \frac{1}{1 - \eta_t'}.$$

The right-hand side of this formula is known: η_{10}/η_1 from experiment, and η_t from calculation. The computations show that $K_q \approx K_t$ (Table 4); i.e., $\eta_t' \lesssim 0.5$, which contradicts the results of the measurements (Fig. 5, points 1 and 2). It is easy to see that the assumption of a static character for the quenching does not take away this contradiction.

Table 4

c_1 (в г/г)	η_t' theory	$\frac{\eta_1}{\eta_{10}}$ experiment	$\tau_0 K_t$	$\tau_0 K_q$
$1 \cdot 10^{-4}$	0.029	0.91	0.030	0.07
$3 \cdot 10^{-4}$	0.085	0.82	0.093	0.13
$1 \cdot 10^{-3}$	0.24	0.61	0.32	0.32
$2 \cdot 10^{-3}$	0.41	0.41	0.70	0.74
$5 \cdot 10^{-3}$	0.70	0.18	2.34	2.22
$1 \cdot 10^{-2}$	0.87	0.064	6.70	7.9
$1.5 \cdot 10^{-3}$	0.927	0.034	12.7	15.7
$2 \cdot 10^{-2}$	0.958	0.022	22.8	21.6

For $c_2 \geq 2 \times 10^{-3}$, the experimental values of η_1/η_{10} agree well with those calculated according to (1), if we take $q = 12 \times 10^{-20}$ n_2 (curve b). However, such a value of the coefficient in (2) cannot be obtained from the experimental data. The error in the measurement of the absorption coefficients was known to be less than 10%. Even in the case $\tau_0/\tau_e = 1$, the coefficient cannot exceed 9.5×10^{-20}. Furthermore, for $c_2 \lesssim 10^{-3}$ there remain too-large differences between curve b and the results of experiment. We are inclined to consider as the cause of the differences between the experimental values of $(1 - \eta_1)/\eta_{10}$ and the calculated η_t the fact that the energy transfer did not take place only by means of a direct interaction of the 3Ph and 3PhP molecules. It is possible that migration of energy via the solvent played a certain part. In this connection, it is important to note that the quantum yield of the fluorescence of polystyrene in our experiments does not depend on the wavelength of the exciting radiation clear down to $\lambda \approx 3000$ A. Moreover, according to Agranovich's hypothesis, energy transfer from 3Ph to 3PhP may take place with the help of virtual excitons propagating along the polymer chain.

Returning once more to Fig. 5, we may state the following conclusion. In a rigid solution of 3Ph and 3PhP in polystyrene, there is radiationless transfer of electronic excitation energy from 3Ph to 3PhP. The quantum yield of the transfer is somewhat larger than that computed according to the Förster-Galanin theory. In the region of high 3PhP concentrations ($\gtrsim 1.5 \times 10^{-2}$ moles/liter), the differences do not exceed 15%. In the region of low 3PhP concentrations ($\lesssim 3 \times 10^{-3}$), the differences are greater. It is possible that some other mechanism of radiationless transfer plays a substantial part here.

The author is grateful to V. M. Shoniya for preparation of the samples and to V. S. Viktorova for her help in the measurements.

REFERENCES

1. Th. Förster, Z. Naturforsch. **4a**, 321 (1949).
2. M. D. Galanin, Zhur. Eksptl. i Teoret. Fiz. **28**, 485 (1955), Soviet Phys.-JETP **1**, 317 (1955).
3. T. P. Belikova and M D. Galanin, Opt. i Spektr. **1**, 169 (1956).
4. S. G. Cohen and A. Weinreb, Proc. Phys. Soc. **B69**, 593 (1956).
5. L. A. Kuznetsova and B. Ya. Sveshnikov, Opt. i Spektr. **4**, 55 (1958).
6. M. Furst and H. Kallmann, Phys. Rev. **94**, 503; **96**, 902 (1954).
7. R. Hardwick, J. Chem. Phys. **26**, 323 (1957).
8. H. Knau, Z. Naturforsch. **12a**, 881 (1957).
9. S. Lipsky and M. Burton, J. Chem. Phys. **31**, 1221 (1959).
10. J. B. Birks and A. J. W. Cameron, Proc. Phys. Soc. **72**, 53 (1958).
11. J. B. Birks, J. Chem. Phys. **28**, 730 (1958).
12. J. B. Birks, Phys. Rev. **94**, 1567 (1954).
13. R. K. Swank and W. L. Buck, Phys. Rev. **91**, 926 (1953).
14. I. M. Rozman, Opt. i Spektr. **2**, 480 (1957).
15. T. P. Belikova and M. D. Galanin, Izvest. Akad. Nauk SSSR, Ser. Fiz. **22**, 48 (1958).
16. I. M. Rozman and S. F. Kilin, Uspekhi fiz. nauk **69**, 459 (1959), Soviet Phys.-Uspekhi **2**, 856 (1959).
17. E. A. Andreeshchev, E. E. Baroni, K. A. Kovyrzina, I. E. Pani, I. M. Rozman, and V. M. Shoniya, Pribory i Tekh. Ekspt. No. 1, 32 (1956).
18. M. D. Galanin, Trudy Fiz. Inst. Akad. Nauk SSSR **5**, 340 (1950).
19. A. Budo and J. Ketskemety, Acta Phys. Acad. Sci. Hung. **7**, 207 (1957).
20. S. S. Solomin, Doklady Akad. Nauk SSSR **31**, 741 (1941).
21. E. A. Andreeshchev and I. M. Rozman, Opt. i Spektr. **8**, 828 (1960), Optics and Spectroscopy **8**, 435 (1960).

NATURE OF BONDING IN THE ASSOCIATED MOLECULES OF RHODAMINS 3B AND 6G IN AQUEOUS SOLUTION AND THE EFFECT OF CONCENTRATION AND TEMPERATURE ON MIGRATION QUENCHING*

*Presented on October 27th, 1959 at the VIII Conference on Luminescence.

E. G. Baranova and V. L. Levshin (pp. 362-367)

Received 3 May 1960

The luminescence quenching of aqueous solutions of rhodamins 3B and 6G was investigated in relation to the association of dye molecules and migration of energy to the associated molecules. The effect of larger associates on quenching was determined and it was shown that the effect of the monomers is small. The energy of dissociation of the dimers was determined.

INTRODUCTION

In the large majority of cases an increase in the concentration of the luminescent dye in solution leads to a large decrease in the luminescence yield. This effect is due to several factors: inactive absorption by nonluminescing associates formed in concentrated solutions,[1,2] migration of excitation energy from luminescing monomers to the polymeric associates,[3-7] and possibly quenching occurring in the migration of excitation energy from one monomer to another.[8-11]

The authors have previously investigated this phenomenon in great detail for aqueous, glycerin, and alcoholic solutions of rhodamins 6G and 3B at room temperature and were able to separate the quenching due to inactive absorption from that caused by migration of energy from the monomers to the polymeric associates.[7,12]

In the present investigation our aim was to determine the nature of the bonding between the polymeric associates in aqueous solutions of the two dyes and to study migration quenching as a function of temperature and dimer concentration in the solution.

DETERMINATION OF THE ENERGY OF DISSOCIATION OF DIMERS AND THE NATURE OF THE BONDING BETWEEN THE POLYMERIC ASSOCIATES

The association of molecules in solution can occur either through van der Waals interaction where the heats of dissociation are 2-3 kcal/mole or through hydrogen bonding where the heats of dissociation are 3.5-10 kcal/mole. In order to determine the nature of the bonding in the dimers of rhodamins 3B and 6G in aqueous solutions, we determined the energies of dissociation of the dimers.

The energies of dissociation of the dimers of rhodamins 3B and 6G in aqueous solutions were determined using the Vant-Hoff's relation

$$\ln K = \ln A - \frac{Q}{R}\frac{1}{T}, \qquad (1)$$

where Q is the energy of dissociation of the dimers in kcal/mole, K is the dissociation equilibrium constant, R is the gas constant, and T is the absolute temperature.

The values of K at different temperatures T were determined from the well-known relationship

$$K = \frac{2Cx^2}{1-x}, \qquad (2)$$

where Cx and C(1 – x)/2 are the molar concentrations of the monomeric and dimeric molecules respectively.

Thus, in order to calculate Q it was necessary to measure x as a function of temperature.

In order to determine the concentration of the monomeric molecules Cx in aqueous solutions at different temperatures, the absorption spectra of aqueous solutions of the rhodamins were measured using spectrophotometers SF-2m and SF-4 over the temperature range 20° to 85-100°C (in 10-15°C intervals). It was found that in all cases the shape of the absorption curves on heating approached the absorption curve of the monomer. At λ =

508 mμ all curves passed through a common point (thus, the curve for 85°C in Fig. 6 of our previous paper[6] must be considered incorrect).

The degree of association x of solutions at different temperatures was determined from calibration graphs such as the one in Fig. 1.

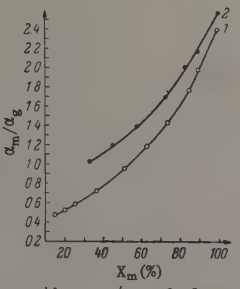

Fig. 1. The ratio a_m/a_d of absorptivities from monomer and dimer band maxima as a function of monomer concentration in aqueous solutions of rhodamins 6G (curve 1) and 3B (curve 2) at room temperature.

Figure 2 shows the weight content of monomers (in %) in aqueous solutions of rhodamin 6G as a function of temperature. The values of K were then calculated with the help of Eq. (2).

The energy of dissociation Q was determined from the slope of $\ln K = f(1/T)$. The linear relationship between $\ln K$ and $1/T$ is well obeyed in the interval from 20° to 80-90°C. Figure 3 shows such a plot for an aqueous solution of rhodamin 6G at $C = 4 \times 10^{-4}$ mole/liter ($Q = 8.6$ kcal/mole).

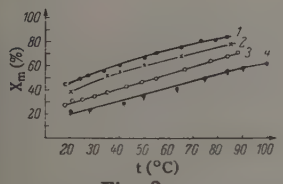

Fig. 2

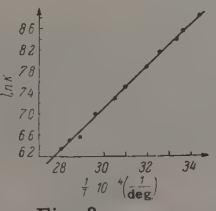

Fig. 3

Fig. 2. Concentration of monomers in aqueous solutions of rhodamin 6G as a function of temperature. Concentration of the solution (in moles/liter); curve 1—4×10^{-4}; curve 2—10^{-3}; curve 3—2×10^{-3}; curve 4—4×10^{-3}.

Fig. 3. Determination of the energy of dissociation of dimers in aqueous solutions of rhodamin 6G (concentration $C = 4 \times 10^{-4}$ mole/liter).

The energy of dissociation was determined for different concentrations of the dye (the results are given in the Table).

THE ENERGY OF DISSOCIATION (IN KCAL/MOLE) OF DIMERS IN AQUEOUS SOLUTIONS OF RHODAMINS 6G AND 3B AT DIFFERENT CONCENTRATIONS

It can be seen from the Table that the magnitude of dimer dissociation energy in rhodamin 3B is smaller than in rhodamin 6G and that it, moreover, increases with increase in concentration. Such an increase in Q may be due to the formation of higher associates as the concentration is increased. Hence the values of Q at high concentrations are unreliable since Eq. (1) does not hold for concentrated solutions and the approximate values of the heats of dissociation become only a qualitative indication of the presence of higher associates.

$C \cdot 10^4$ (mole/liter)	Rhodamin 6G		Rhodamin 3B
	I	II	III
4	7.0	8.6	4.605
10	6.32	—	5.17
20	(8.16)	(10.3)	(6.24)
40	(8.7)	—	(7.82)
66.5	(11)	—	—

Note: The columns I and II refer to two series of experiments.

The heats of dissociation of dimers obtained by us exceed the magnitude for molecules associated through van der Waals forces, thus indicating that association of the dye molecules occurs through hydrogen bonding. The molecule of rhodamin 6G has the following structural formula:

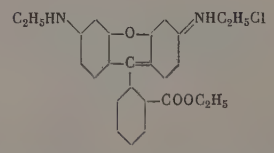

Rhodamin 3B is identical to 6G except that the hydrogen in the N—H group is substituted by C_2H_5 groups. Since molecules of both rhodamins are capable of hydrogen bonding, it is likely that water molecules take part in the association.

We observe experimentally that rhodamin 6G is more strongly associated than rhodamin 3B. Let us examine more closely the reasons for such behavior.

According to the theory of color, a deepening in the color of dyes can be explained either by an increase in the total length of conjugated bonds or by the presence of a constant shift in electron density in the conjugated system, resulting in a decrease in the excitation energy of the molecule and a shift of the absorption spectrum to longer wavelengths.[13] These factors would tend to make the association of rhodamin 3B molecules stronger than that of rhodamin 6G molecules, which is contrary to experimental observation. Thus, apparently, the increased tendency towards association between rhodamin 6G molecules must be due to the presence of the polar N—H bonds. Thus the difference in the association of molecules of the two rhodamins is not determined by the length of their conjugated chains.

EFFECT OF TEMPERATURE ON LUMINESCENCE YIELD OF CONCENTRATED SOLUTIONS AND ITS RELATION TO THE DISSOCIATION OF DIMERS

It has been determined in a number of previous papers[1,2,6,7,12,14] that an increase in temperature led to an increase in the luminescence intensity of concentrated solutions notwithstanding the effect of temperature quenching. This phenomenon was explained qualitatively by the dissociation of associates which decreased the inactive absorption and the energy migration to dimers. In the present investigation quantitative measurements and calculations have led to a complete elucidation of the relative contribution of each one of the two factors. Aqueous solutions of rhodamin 6G were studied. These solutions when monomeric at $C < 2 \times 10^{-6}$ mole/liter do not exhibit temperature quenching in the temperature interval 12-120°C.

Figure 4 shows the development of luminescence at

various concentrations. Excitation was achieved by means of 366 mμ radiation which is absorbed equally by associated as well as nonassociated solutions. The initial intensity at 20°C was considered to be unity. It can be seen from Fig. 4 that luminescence in very concentrated solutions, starting with 2×10^{-3} mole/liter, increases very slowly in the beginning; this was observed by us earlier.[6] This phenomenon could be due to the presence of higher associates.

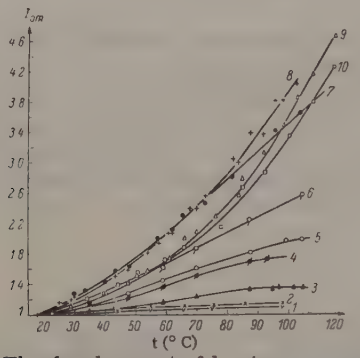

Fig. 4. The development of luminescence as a function of temperature for aqueous solutions of rhodamin 6G. Concentration of solutions (in moles/liter): Curve 1—2×10^{-6}; curve 2—4×10^{-6}; curve 3—2×10^{-5}; curve 4—1×10^{-4}; curve 5—2×10^{-4}; curve 6—4×10^{-4}; curve 7—1×10^{-3}; curve 8—2×10^{-3}; curve 9—4×10^{-3}; curve 10—8×10^{-3}.

Figure 5 compares the curves of luminescence development and concentration of monomers both as functions of temperature for a 2×10^{-3} mole/liter aqueous solution of rhodamin 6G.

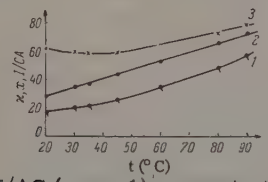

Fig. 5. I/AC (curve 1), concentration of monomers x (curve 2) and κ the coefficient of migration quenching (curve 3), as functions of temperature for a 2×10^{-3} mole/liter aqueous solution of rhodamin 6G. x is expressed as %.

It can be seen from Fig. 5 that the shape of the curve representing the concentration of monomeric molecules (curve 2) is different from that of the curve representing the development of luminescence. The initial rate of increase of luminescence intensity (at relatively low temperatures) is small and then increases with increase in temperature. At the same time the rate of increase of monomeric molecule concentration is constant with increase in temperature.

Using curves 1 and 2 of Fig. 5 we determined the effect of temperature on migration quenching. We started with the following formula for the intensity of luminescence for a thin layer of solution

$$I = ACx\kappa, \qquad (3)$$

where κ is the coefficient of quenching due to migration. The values of I/CA and x (fraction of monomers in the solution) were obtained from curves 1 and 2 of Fig. 5.*

*I/CA is the intensity of luminescence of an infinitely thin layer reduced to unit thickness, unit monomer concentration, unit absorptivity, and unit intensity of excitation. The measurements of I necessary for the determination of κ were performed in thin cells of three different thicknesses. For concentrations up to 2×10^{-3} mole/liter where higher associates are absent the error in κ is 10-20%. For higher concentrations, the error becomes much larger.

From curve 3 in Fig. 5 it can be seen that migration quenching of the excitation energy increases slightly up to 35°C and then decreases (κ increases) with further increase in temperature. Such behavior could be due to the presence of higher associates in solutions at $C \geq 2 \times 10^{-3}$ mole/liter. These higher associates possess a smaller energy of dissociation and an absorption spectrum different from that of the dimers. Increasing the temperature to 30-35°C dissociates primarily the higher associates and thus the consequent increase in the number of separate quenching centers compensates to a certain extent the effect due to the dissociation of the dimers. This provides an explanation for the very small change in migration quenching in the region 20-40°C. The shape of curve 3 in Fig. 5 in this temperature range is not accurate since the values of x (curve 2) calculated from the absorption spectra can be in error due to the difference between the absorptions of the dimers and the higher associates, respectively, in the region of maximum absorption by the higher associates.

Thus the sum total of observed phenomena indicates that in aqueous solutions at low temperatures and at concentrations $C \geq 2 \times 10^{-3}$ mole/liter, higher associates are formed.

Next, in order to elucidate the role of the monomers in excitation energy transfer and the effect of temperature on resonance transfer of energy, we plotted the coefficient κ of migration quenching as a function of $C(1 - x)$—the absolute concentration of dimers—for solutions of different total concentrations C of the dye at different temperatures (Fig. 6). The values of κ obtained for different total concentrations and temperatures all fall very satisfactorily on a smooth curve. Thus it follows from Fig. 6 that migration quenching is primarily a function of the dimer concentration and is almost independent of temperature and total concentration of the solution.

Fig. 6. The coefficient of migration quenching κ as a function of dimer concentration in aqueous solutions of rhodamin 6G at total concentrations of 4×10^{-4}, 1×10^{-3}, 2×10^{-3}, and 4×10^{-3} mole/liter at different temperatures. Abcissa: $C(1 - x) \times 10^4$ mole/liter. Temperatures in °C: 1—30; 2—35; 3—45; 4—60; 5—80; 6—85.

CONCLUSIONS

1. The associated species in the aqueous solutions of rhodamins 3B and 6G in the concentration interval

10^{-6} to 2×10^{-3} mole/liter are dimers. At higher concentrations and at temperatures lower than 30-35°C, higher associates are formed.

2. The high energy of dissociation of the dimers ($Q > 5$ kcal/mole) shows that the molecules of rhodamins 3B and 6G in aqueous solutions are associated through hydrogen bonds.

3. Migration quenching in aqueous solutions of rhodamine 6G depends primarily on the dimer concentration and is relatively independent of temperature and total concentration. Hence it follows that (a) variation in temperature has only a small effect on resonance transfer of energy from excited molecules to the dimers; (b) migration of energy through monomers plays a small role when the energy is transferred to the dimers; and (c) the probability of quenching during transfer of excitation energy to monomers is negligibly small.

REFERENCES

1. V. L. Levshin, Z. Physik **43**, 230 (1927).
2. V. L. Levshin, Zhur. Fiz. Khim. **6**, 1 (1935); Ibid. **1**, 185 (1935).
3. F. Perrin, Ann. phys. **17**, 283 (1932).
4. F. Dushinskii, Doklady Akad. Nauk SSSR **14**, 73, 179 (1937).
5. V. L. Levshin, Izvest. Akad. Nauk SSSR, Ser. Fiz. **20**, 397 (1956).
6. V. L. Levshin and E. G. Baranova, Izvest. Akad. Nauk SSSR, Ser Fiz. **20**, 424 (1956).
7. V. L. Levshin and E. G Baranova, Opt. i Spektr. **6**, 55 (1959), Optics and Spectroscopy **6**, 31 (1959); Ibid. **5**, 869 (1958).
8. J. Perrin, II Congr. de Chim. Solvay, Paris, 1925.
9. S. I. Vavilov, Zhur. Eksptl. i Teoret. Fiz. **13**, 13 (1940); Collected Works, Vol. 2, p. 240. Izd. Akad. Nauk SSSR, 1951.
10. Th. Forster, "Fluoreszenz organischer Verbindungen," Gottingen, 1951.
11. M. D. Galanin, Zhur. Eksptl. i Teoret. Fiz. **28**, 485 (1955), Soviet Phys.—JETP **1**, 317 (1955).
12. V. L. Levshin and E. G. Baranova, Izvest. Akad. Nauk SSSR, Ser. Fiz. **22**, 1058 (1958).
13. B. I. Stepanov, Zhur. Fiz. Khim. **29**, 2173 (1955).
14. V. L. Levshin, E. G. Baranova, L. D. Derkacheva, and L. V. Levshin, Trudy Soveshchaniya Termod. i Stroeniiu Rastvorov, p. 275, Moscow, 1959

BAND SPLITTING IN THE LUMINESCENCE SPECTRA OF ANISOTROPIC CENTERS IN LiF AND CaF_2-Eu CRYSTALS SUBJECTED TO ORIENTED DEFORMATION

A. A. Kaplyanskii, N A. Moskvin, and A. K. Przhevuskii (pp. 368-373)

Received 20 April 1960

The dependence of the spectral band splitting of anisotropic luminescence centers in LiF and CaF_2-Eu^{3+} on uniaxial compression is investigated experimentally. The results of the investigation confirm the theoretical expressions for the magnitude of the splitting of bands due to anisotropic centers during oriented deformation of crystals. Values are given for the "piezospectroscopic" parameters which characterize the splitting of the spectral bands of centers in LiF and CaF_2-Eu^{3+}.

The present paper describes further experimental investigation of the polarized splitting of spectral bands of anisotropic centers in cubic crystals subjected to oriented deformation.[1-2] A calculation of the splittings of the bands produced by anisotropic centers under deformation was performed in ref. 3, and it was shown that these quantities must be determined by two independent parameters for an orientation of centers along C_4 and C_3 axes, and by three parameters for an orientation of centers along C_2 axes. The primary purpose of the present work was to obtain an experimental check of the relationships obtained in ref. 3, which must be satisfied by the splitting, and to obtain new data about centers in the crystals which were investigated. Colored crystals of LiF and crystals of CaF_2 activated by trivalent europium were chosen for the investigation. Polarized splitting of the bands under deformation was observed previously[2] in the luminescence spectra of these crystals.

The experimental method was approximately that described in ref. 2. The samples were elongated, right parallelepipeds. Two plane-parallel faces were normal to crystallographic symmetry axes of different orders. The samples were subjected to uniaxial compression in a press at $T = 77°K$; the spectra were studied at right-angles to the axis of compression P. Luminescence was excited by unfiltered light from a SVDSH-1000 mercury lamp incident perpendicular to the direction of observation. The spectra were photographed with a spectrograph (ISP-51 with autocollimating camera) having a dispersion of about 6 A/mm in the working region of the spectrum. With the aid of a diaphragm placed at the slit, the spectra of uniaxially stressed samples were photographed in juxtaposition with the spectra of unstressed crystals.

SPLITTING IN THE LINE LUMINESCENCE SPECTRUM OF COLORED LiF CRYSTALS UNDER UNIAXIAL COMPRESSION

A peculiar line structure is observed in the visible region of the absorption spectra[4] and the luminescence spectra[5] of colored LiF crystals at low temperatures. The line luminescence spectrum of LiF consists of a series of equidistant lines and an adjoining series of irregularly located lines.[5] An investigation of the effect of uniaxial compression of LiF single crystals on the luminescence lines[2] showed that the splitting is the same for all of the lines. When the crystal is compressed along a fourfold symmetry axis ($P \parallel C_4$) a doublet arises; when compressed along a twofold axis ($P \parallel C_2$), a triplet is obtained. The components of the splitting are polarized. From the character of the splitting it was established that the centers of the line luminescence in LiF are anisotropic and are oriented in the lattice along the six axes

of twofold symmetry (this result agrees with a determination of the orientation of centers by investigating the angular dependence of the degree of polarization of the line luminescence[6]).

In the present investigation, we studied the effect of deformation on the main line (5698 A) of the equidistant series of emission lines from x-rayed LiF. The line evidently corresponds to a purely electronic transition. First, the splitting of the line produced by compression of the crystal along a threefold symmetry axis was studied; this had not been studied previously. It was established that for $P \parallel C_3$ the line splits into a polarized doublet, the short wavelength component of which is observed in both components of polarization ($E \parallel P$ and $E \perp P$); the long wavelength part is observed only in the $E \perp P$ component. This type of splitting corresponds[1] perfectly to the established orientation of luminescence centers along the $6C_2$-axes and the electric dipole (π_e) nature of the radiation.

The general splitting scheme of 5698 A for all directions of compression ($P \parallel C_4$, $P \parallel C_3$, $P \parallel C_2$) and transverse observation is given in Fig. 1. The total number of components for the three directions of compression is seven. The polarization ($E \parallel P$ or $E \perp P$) is indicated for completely polarized components of the splitting. The polarization of these components permits each of them to be referred uniquely to a C_2 axis (or several C_2 axes) which is the orientation axis of a group of centers; transitions in these centers make up the given component. It is convenient to designate these axes by means of the angle PN which they form with the direction of the compression P (in Fig. 1 the values of the corresponding cos PN are given near the components). The shift $(\nu - \nu_0)$ of the component for compression along a k-fold axis ($P \parallel C_k$), measured in cm^{-1}, is designated as $\Delta_{k,\cos PN}$. This component is connected with a group of centers oriented along a C_2 axis which forms an angle PN with the axis of the compression P (in Fig. 1, the meaning of the quantity $\Delta_{4,1/\sqrt{2}}$ is shown as an example).

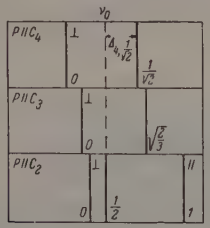

Fig. 1. Splitting scheme of the line 5698 A in the luminescence spectrum of colored LiF for uniaxial compression of the crystal in different directions. The position of the line in the unstressed crystal is indicated by the dashed line.

The measurements of the dependence of the shift on the directions of uniaxial compression P are presented in Fig. 2 for all seven components of the splitting. These $\Delta(p)$ functions were obtained from two samples for each direction of P ($P \parallel C_4$, $P \parallel C_3$, $P \parallel C_2$). A large number of points were obtained, except in the cases of $\Delta_{2,0}$ and $\Delta_{2,1/2}$. The $\Delta_{2,1/2}$ shift is practically zero for maximum stress; $\Delta_{2,0}$ is small and difficult to measure in view of its proximity to the component $\Delta_{2,1/2}$ (therefore, only an estimate of the quantity $\Delta_{2,0}$ for maximum stress is given). As is evident from Fig. 2, $\Delta(p)$ is linear for small stresses; it is only with large stresses that one observes deviations from linearity for certain components.* From the slope of the linear portions of the curves $\Delta(p)$ one can compute "specific" shifts per unit ($1\ kg/mm^2$) stress for all components (these values for the seven splitting components are given in Table 1).

*These deviations from linearity begin at significantly smaller stresses P than the deviations from the linear shift of spectral bands usually observed under hydrostatic compression (see, for example, ref. 7).

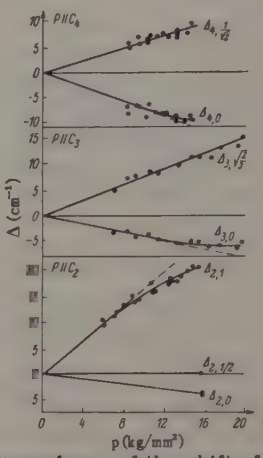

Fig. 2. Dependence of the shift of the components of the split line 5698 A on the degree of uniaxial compression of colored LiF crystals.

Furthermore, a comparison was made between the experimental δ values for the magnitudes of splitting of bands due to centers oriented along twofold axes and the computed values.[3] It turned out that the seven δ values agree very well with the expression containing three independent parameters derived in ref. 3 for the shifts of bands. Values of δ, computed by the formulas of ref. 3 for $A_1 = -0.72$, $A_2 = 0.65$, and $A_3 = 1.83\ cm^{-1}/kg/mm^2$, are given in Table 1. Table 1 shows that these values practically coincide with the experimental values of δ. Thus the frequency change for an electronic transition between the levels of a center of the line luminescence of LiF, for an elastically deformed lattice, is expressed to a high degree of accuracy by the formula[3]

$$\Delta(cm^{-1}) = -0.72\sigma_{zz} + 0.65(\sigma_{xx} + \sigma_{yy}) + 1.83\sigma_{xy}$$

Here the stresses σ are computed in a coordinate system which is referred to the center according to ref. 3, and are measured in kg/mm^2.

It is also easy to verify that the specific shift of the center of mass of the split band 5698 A is practically the same for all directions of compression, and amounts to $\bar{\delta} = 0.19\ cm^{-1}/kg/mm^2$. From this it is possible to predict the shift of a luminescence line from colored LiF for hydrostatic (isotropic) compression ($\delta' = 3\bar{\delta}$)[3], which for pressure p is $\Delta'(cm^{-1}) = 0.0058\ p(atm)$.*

*The shift for isotropic compression of M-absorption bands is about $0.024\ cm^{-1}/atm$; for an F-band of alkali halide crystals it is about $0.1\ cm^{-1}/atm$.[7] Thus, our value of $0.0058\ cm^{-1}/atm$ is nearer, by an order of magnitude, to the shifts for the more complicated centers in alkali halide crystals. This agrees with the fact that the centers of the line luminescence of LiF are undoubtedly complex.

From the known values of the parameters A and the

Table 1

δ (cm^{-1}/kg/mm^2)	$\delta_{4,\frac{1}{\sqrt{2}}}$	$\delta_{4.0}$	$\delta_{3,\sqrt{\frac{2}{3}}}$	$\delta_{3.0}$	$\delta_{2.1}$	$\delta_{2,\frac{1}{2}}$	$\delta_{2.0}$
Experimental	0.65	−0.72	0.80	−0.42	1.58	∼0	−0.28
Calculated	0.65	−0.72	0.80	−0.42	1.58	0.03	−0.27

elastic constants of LiF the coefficients describing the dependence of the band shifts on the magnitude of the deformation of an elastically deformed lattice[3] can be determined. If one uses the values of the elastic constants of LiF at 77°K, then the dependence of the frequency change of a transition on the relative elongation of the lattice along an axis of the center u_{110} and the two directions $u_{1\bar{1}0}$ and u_{001} perpendicular to it is expressed by the formula

$$\Delta(cm^{-1}) = 20100u_{110} - 4400u_{1\bar{1}0} - 3500u_{001}.$$

It is evident from this that the energy of a transition in a center is significantly more sensitive to distortions along the axis of the center than to distortions in a plane perpendicular to the axis. This probably indicates the strong anisotropy and "elongated" form of the center.

SPLITTING IN THE LUMINESCENCE SPECTRUM OF CaF_2-Eu^{3+} CRYSTALS UNDER UNIAXIAL COMPRESSION

The luminescence spectrum of Eu^{3+} in CaF_2 consists of a group of narrow lines in the visible region. It follows from the results of investigations of polarized luminescence,[9] the Zeeman effect,[10] and the splitting for uniaxial deformation[2] that the luminescence centers in CaF_2-Eu^{3+} are anisotropic and are oriented along the four threefold axes. According to ref. 11, the possibility of anisotropy of the centers is connected with the asymmetry of the surroundings of the Eu^{3+} ion (a neighboring F^- ion is replaced by an O^{2-} ion, which compensates for the excess Eu^{3+} charge).

In the present investigation, a study is made of the effect of uniaxial compression on the most intense "zero" luminescence line 5735 A, which corresponds to a transition between the nondegenerate levels ($^7F_0 \rightarrow {}^5D_0$). It was shown earlier[2] that when the crystals are compressed along C_2, the line splits into a polarized doublet; for compression along C_4 there is no splitting. From this the orientation of the centers was determined, and the electric dipole character of the emission was established. The present study of the effect of compression along C_3 on the line showed that the line is split into a doublet polarized in such a way that the short wavelength part is observed only in the E ∥ P component, but the long wavelength part is observed in both components of polarization. This type of splitting for P ∥ C_3 is in complete agreement with the established orientations of the centers along $4C_3$ and the multipole order of the transition (π_e).

A combined schematic diagram of the splitting of the 5735 A line for different directions of compression of the crystals CaF_2-Eu^{3+} is given in Fig. 3. The notation in Fig. 3 has the same meaning as that in Fig. 1 for LiF. The total number of components of the splitting for P ∥ C_4, P ∥ C_3, and P ∥ C_2, is five. Results of measurements of the dependence of the shift $\Delta(p)$ on the pressure p for four components of the splitting with P ∥ C_3 and P ∥ C_2 obtained in two samples for each direction of P is shown in Fig. 4. The shift of the line for P ∥ C_4 is not shown, since it is extremely small; one can only state that the

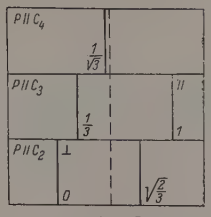

Fig. 3

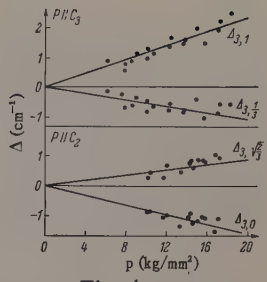

Fig. 4

Fig. 3. Splitting scheme of the line 5735 A in the luminescence spectrum of CaF_2-Eu^{3+} for uniaxial compression of the crystal in different directions.

Fig. 4. Dependence of the shift of the components of the split line 5735 A on the amount of uniaxial compression of CaF_2-Eu^{3+} crystals.

long wavelength shift for deformation $\Delta_{4,1/\sqrt{3}} < 0$.

Figure 4 shows that $\Delta(p)$ is a straight line for all components. The specific magnitudes of the shifts δ for different components, determined from the slopes of the lines, are given in Table 2. These experimental values of δ were compared with the calculated data[3] for the case of centers oriented along $4C_3$. Table 2 gives five δ values calculated according to the formulas of ref. 3 for N ∥ C_3, using the following values of the two coefficients in the formulas: $A_1 = -0.012$ and $A_2 = 0.123$ cm^{-1}/kg/mm^2.

Table 2

δ (cm^{-1}/kg/mm^2)	$\delta_{4,\frac{1}{\sqrt{3}}}$	$\delta_{3.1}$	$\delta_{3,\frac{1}{3}}$	$\delta_{2,\sqrt{\frac{2}{3}}}$	$\delta_{2.0}$
Experimental	<0	0.114	−0.050	0.046	−0.076
Calculated	−0.012	0.111	−0.053	0.049	−0.073

A comparison of the experimental and calculated data shows good agreement. The five δ values agree well with the expression containing two independent parameters. Thus the dependence of the frequency shift of a transition in Eu^{3+} on deformation is given by the expression

$$\Delta(cm^{-1}) = -0.012(\sigma_{xx} + \sigma_{yy} + \sigma_{zz}) + 0.123(\sigma_{xy} + \sigma_{yz} + \sigma_{zx}).$$

Here the components of stress, given in a system of cubic axes,[3] are measured in kg/mm^2. It is clear from the expression that the greatest effect on the transition frequency is that of the shear stresses in the lattice.

With the aid of the formula, one can determine the magnitude of the line shift which would be expected for isotropic compression of the crystals (i.e., $\sigma_{xx} = \sigma_{yy} = \sigma_{zz} = p$, $\sigma_{xy} = \sigma_{yz} = \sigma_{zx} = 0$). This shift equals $\Delta'(cm^{-1}) = -0.00036$ p(atm).

One can also express this shift in terms of the relative volume change $\Delta v/v$ under isotropic compression if one makes use of the value of the bulk modulus of CaF_2. Then $\Delta'(cm^{-1}) = 320\ \Delta v/v$.

Although no data for the effect of isotropic compression are available, it is interesting to compare the value obtained with the shift of the line 5735 A when the crystals are heated, assuming that the temperature shift of the line is caused by the thermal expansion of the crystal. The relative volume change of a CaF_2 crystal upon heating from T = 77°K to room temperature can be computed from the known value of the coefficient of thermal expansion of the crystal, and is about 9×10^{-3}, which gives $\Delta' = 2.9$ cm^{-1}. Experiment shows that heating the

crystal from 77°K to 20°C shifts the 5735 A line about 3.2 cm^{-1} toward the blue, which is in good agreement with the results of a calculation of this shift from data obtained from a study of the line shift for uniaxial compression of the crystals.*

*The possibility (noted in ref. 3) of a combination of a small band shift for uniform compression with large shifts for uniaxial compression is well illustrated by the example of the line 5735 A.

CONCLUSIONS

The experimental data on the magnitude of the splitting of spectral bands due to anisotropic centers in the cubic crystals LiF and CaF_2 under uniaxial compression agree well with the relationships obtained in ref. 3. Experimental and calculated values also agree for centers of widely different types and orientations, such as the luminescence centers of colored LiF ($N \parallel C_2$) and rare earth ions in CaF_2 ($N \parallel C_3$). This verifies the correctness of the assumptions underlying the theoretical investigation in ref. 3 and indicates, in particular, the extreme importance of the symmetry of the centers in determining the character of their interaction with the lattice. It is shown experimentally that, for small deformations, the frequency change of the spectral bands (energy levels) of anisotropic centers in an elastically deformed crystal is a linear function of the deformation components or stresses. The function contains two ($N \parallel C_3$) or three ($N \parallel C_2$) independent parameters. The "piezospectroscopic" coefficients which characterize the interaction of the corresponding centers with the lattice were determined for the bands investigated in the spectra of LiF and CaF_2-Eu. Their values can be used for the theoretical calculation of the centers and for determining th behavior of the spectra under isotropic compression and changes in temperature.

In conclusion, the author thanks E. F. Gross for his interest in this work.

REFERENCES

1. A. A. Kaplyanskii, Opt. i Spektr. 7, 677 (1959), Optics and Spectroscopy 7, 406 (1959).
2. A. A. Kaplyanskii, Opt. i Spektr. 7, 683 (1959), Optics and Spectroscopy 7, 409 (1959).
3. A. A. Kaplyanskii, Opt. i Spektr. 10, 165 (1961), Optic and Spectroscopy 10, 83 (1961).
4. P. Pringsheim and C. Delbecq, J. Chem. Phys. 21, 794 (1953); Z. Physik 136, 573 (1954).
5. A. A. Kaplyanskii, Opt. i Spektr. 6, 424 (1959), Optics and Spectroscopy 6, 267 (1959).
6. P. P. Feofilov, Opt. i Spektr. 6, 426 (1959), Optics and Spectroscopy 6, 268 (1959).
7. W. Maisch and H. Drickamer, J. Phys. Chem. Solids 5, 328 (1958).
8. C. Briscoe and C. Squire, Phys. Rev. 106, 1175 (1957
9. P. P. Feofilov, Doklady Akad. Nauk SSSR 99, 731, 975 (1954).
10. V. A. Arkhangel'skaya and P. P. Feofilov, Opt. i Spektr. 4, 602 (1958).
11. I. V. Stepanov and P. P. Feofilov, Doklady Akad. Naul SSSR 108, 615 (1956), Soviet Phys.-Doklady 1, 350 (1957).

DETERMINATION OF ELECTRON TRAP DEPTH IN ZnS PHOSPHORS BY FLASH UNDER THE ACTION OF INFRARED LIGHT

L. A. Vinokurov and M. V. Fok (pp. 374-378)

Received 21 April 1960

The depths of electron traps in the phosphors ZnS-Cu, Co (0.40 ev); ZnS-Cu, Ni (0.56 ev); ZnS-Cu (0.3 and 1.1 ev), and in the crystal ZnS-Cu (0.66 ev) were determined from the temperature dependence of the intensity of the infrared induced flash in the late states of afterglow.

The most widely used methods for determining the depth of electron traps in powdered crystal phosphors are based on thermal de-excitation.[1,2] These methods, however, have a number of basic faults. First of all, it is not possible to use thermal de-excitation to study deep traps, whose maximum glow range lies in the region of temperature quenching. Furthermore, a reliable determination of trap depth can only be made if the trap depths differ from each other by large amounts. If a phosphor contains several closely spaced levels, only a rough determination of trap depth is possible from the temperatures of the maxima in the thermally stimulated emission. Moreover, this method requires a knowledge of the frequency factor, which is usually unknown and can vary over a wide range. Also, for any method based on thermally stimulated luminescence, one needs an apparatus which can heat the phosphor at a constant rate.

All of these considerations prompted us to undertake a search for a method which would be useful for investigating deep traps and which, to some extent, would be free of the remaining deficiencies of the thermal de-excitation method. It seemed to us that a comparison of the probability of thermal liberation of electrons from a given set of traps to the probability of liberation from the same traps by infrared light might prove to be the method we were seeking. If one determines how the ratio of these probabilities changes with temperature, it should be possible to find the depth of the traps ε_1, since temperature has a much smaller effect on the probability of photoliberation of electrons than on the probability of thermal liberation.

The probability of photoliberation of electrons will show the strongest temperature dependence when the liberation of electrons by infrared light requires an activation energy ε (thermo-optical liberation). In this case, the probability of liberation of an electron by infrared light will also be a function of temperature in accordance with Boltzmann's equation, and we will only be able to determine the difference $\varepsilon_1 - \varepsilon$, rather than ε_1 itself. Usually, however, ε is much smaller than ε_1, and neglecting it will not lead to a large error.

Getting ahead of our story somewhat, we would like

to point out that in those two cases for which it was possible to compare the trap depths determined by our method with the values known previously from other experiments, it turned out that our data were approximately 10% lower. It is possible that this disagreement results from neglecting ε, but the accuracy of our method is not great enough to assert this with complete confidence.

In order to determine the ratio of the two probabilities, it is sufficient to expose the phosphor to infrared light during its afterglow period. The resulting increase in the brightness of the afterglow indicates how much the probability of liberating electrons changes under the action of infrared light. By measuring the intensity of the flash at the same brightness of afterglow, but at a second temperature, and comparing the ratio of these flash intensities, we can determine the effective trap depth from which the electrons were liberated under the two sets of conditions.

In fact, if the main light sum is concentrated in levels at a single trap depth, then the brightness of the afterglow is given by the equation

$$J_a = \frac{\beta w_1 n^2}{\delta_1 + \beta n}, \qquad (1)$$

where β is the recombination coefficient for free electrons and ionized centers, δ_1 and w_1 are, respectively, the probabilities of capture and liberation of electrons by traps, and n is the concentration of ionized centers which is equal to the concentration of trapped electrons.

Under the action of red light, it is only the probability of liberating electrons, w_1, which changes

$$w_{1,\,ir} = w_1 + PI, \qquad (2)$$

where I is the intensity of the red light and P is a constant. The brightness of the afterglow in this case will be equal to

$$J_{a,\,ir} = \frac{\beta (w_1 + PI)}{\delta_1 + \beta n} n^2. \qquad (3)$$

If the stored light does not have time to change very much during the flash, then

$$\frac{J_{a,\,ir}}{J_a} = 1 + \frac{PI}{w_1}, \qquad (4)$$

but

$$w_1 = w_{10} e^{-\frac{\varepsilon_1}{kT}}. \qquad (5)$$

If the ratio (4) is measured at several temperatures, we can determine ε_1. In order to do so, it is necessary to construct a plot of the parameter $\ln(J_{a,ir} - J_a)$ as a function of 1/T. The slope of the lines obtained yields the desired parameters.

Let us now consider the main factors which limit the applicability of this method. First of all, it is necessary that either red or infrared light be capable of producing flashes (de-excitation); i.e., electrons must be liberated by such light from the traps in question. Furthermore, it is known from experiments that electrons are usually localized at levels of various depths, albeit in comparable numbers. This is caused in particular by the de-exciting action of the exciting light (see, for example, ref. 3) which prevents the accumulation of electrons in the deep traps. It is therefore necessary to measure the flashes during late stages of the afterglow, when thermal equilibrium has been established in the distribution of electrons among the various levels. In this case it is only the deepest level which plays a significant role. In order to see whether such a distribution has been achieved, the measurements must be made at several temperatures, rather than at two temperatures as stipulated above; these temperatures should cover as wide a temperature interval as possible. If an equilibrium distribution has not been established at the time of the measurement, then the amount by which the distribution differs from the equilibrium value will of necessity be different at different temperatures. Therefore, the plot will not yield a straight line. If we obtain a series of parallel lines after the flashes have been measured at several temperatures and several afterglow intensities and the data have been plotted in suitable coordinates, then we can assume that the method can be applied with confidence.

Finally, the condition that the stored light sum be constant while the flash is initiated also sets a limit, especially at high temperatures, when decay occurs more rapidly. Here, however, we are able to introduce correction factors by extrapolating the decay curves, thus relating the flash intensity to the afterglow intensity which would have existed when the flash was at its maximum, rather than to the afterglow intensity at the beginning of the flash.

As is evident from the calculation, external quenching does not interfere with the applicability of this method, since the migration of the holes changes only the time rate of decrease of the stored light sum, but does not affect the brightness at a given value of the stored light sum.

We studied a series of zinc sulfide phosphors activated by copper and other activators. We chose the Hg 365 mμ line for excitation; this line gives reasonably uniform excitation throughout the volume of the sample. The light of a 25 watt incandescent lamp covered by an RG-9 Schott light filter was used for de-excitation; this filter has a transmission maximum in the vicinity of 0.8μ. The luminescence light was recorded with the aid of a photomultiplier covered by a heat-absorbing filter (BG-18 Schott) to guard against red light, and a light filter (OG-4 Schott) which passes the long wavelength part of the green luminescence band and absorbs the blue bands. Separate experiments showed that the intensity of the blue band is small in comparison with that of the green bands. This means that the blue luminescence centers did not play an important role and that, as far as the over-all picture was concerned, they could be ignored. It was also established that the intensity of the flash J_f, i.e., the parameter $[(J_{a,ir}/J_a) - 1]$ was proportional to the intensity of the infrared light to a reasonable degree of accuracy.

Figure 1 shows the dependence of $\log (J_{a,ir} - J_a)$ on 1/T for different stages of afterglow (i.e., for various values of J_a) for the phosphor ZnS-Cu(3×10^{-5}),Co(5×10^{-6}), Cl. It is evident that as the brightness of the afterglow decreases, the points lie closer and closer to a straight line. For the two lowest brightness values, the deviations from the straight line are still within the limits of accuracy. The slope of these lines indicates a trap depth

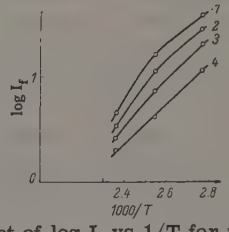

Fig. 1. Plot of log I_f vs 1/T for powdered ZnS-Cu(3×10^{-5}), Co(5×10^{-6}),Cl. I_f—intensity of the flash; T—absolute temperature. Curves 1, 2, 3, and 4 refer to different stages of quenching in the order of decreasing afterglow intensity.

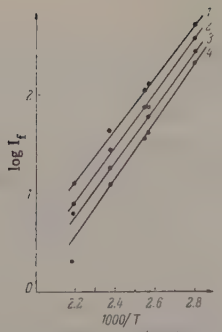

Fig. 2. Plot of log I_f vs 1/T for powdered ZnS-Cu(3×10^{-5}), Ni(5×10^{-6}),Cl. The symbols have the same meaning as they do in Fig. 1.

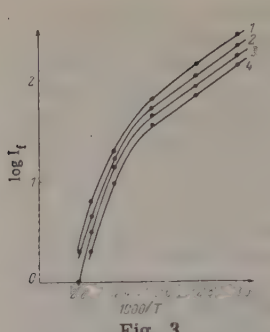

Fig. 3

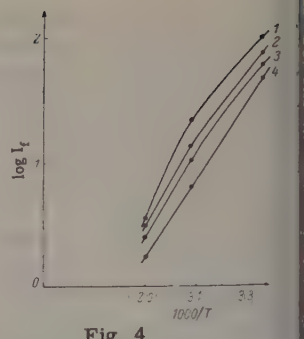

Fig. 4

Fig. 3. Plot of log I_f vs 1/T for powdered ZnS-Cu (3×10^{-5})Cl. The symbols have the same meaning as they do in Fig. 1.
Fig. 4. Plot of log I_f vs 1/T for a ZnS-Cu,Cl crystal. The symbols have the same meaning as they do in Fig. 1.

of 0.40 ev. This value agrees with the known depth of electron traps in this phosphor, which is 0.44 ev.[4]

Figure 2 shows similar data for the phosphor ZnS-Cu(3×10^{-5}),Ni(5×10^{-6}),Cl. It is seen here that the points lie on straight lines over a rather wide range of temperatures and afterglow intensities. The value of trap depth computed from these lines is 0.56 ± 0.03 ev. In ref. 5, one of us showed that this phosphor has electron traps which are so deep that they could not be studied by the thermal de-excitation method. This conclusion was based on the fact that even though this phosphor does not have a high temperature, thermal de-excitation peak, it can retain its light sum even at +120°C, whereas the maximum for the thermal de-excitation of the phosphor ZnS-Cu,Co,Cl occurs at +90°C. The trap depth which is now found is indeed considerably greater than that in ZnS-Cu,Co,Cl.

Figure 3 shows data for the phosphor ZnS-Cu(3×10^{-5})Cl. It is evident that the points fall on two lines with different slopes, rather than on a single line. The low temperature part, which has the smaller slope, corresponds to a value of 0.3 ev. This is the depth of a well-known level of the ZnS-Cu,Cl phosphor. It is usually considered to be equal to 0.33 to 0.35 ev. The rest of the curve shape can be explained if one assumes that the phosphor ZnS-Cu,Cl also has a small number of very deep traps. If their depth is such that there can be virtually no release of electrons from these traps at temperatures up to +100°C, then at the onset of quenching they are completely filled with electrons which fall into them after their release from shallower traps. At the same time, if the number of these levels is very small, then the stored light sum for these levels will not play an important role in the total balance—at least in the stages of afterglow of interest to us. At higher temperatures, the stored light sum cannot be maintained for very long at the shallow levels. Therefore, the instant at which the stored light sum concentrates in the deep traps arrives somewhat sooner. The probability of liberating electrons from these traps also increases markedly. Thus at higher temperatures, the deep traps can be readily observed in the afterglow. At +130°C, they are already playing the principal role. Infrared light is clearly capable of releasing electrons from these traps in exactly the same way as from the shallow traps. As a result of all these factors, the slopes of the lines correspond to these deep levels at high temperatures. Their depth turns out to be approximately 1.1 ev. The accuracy with which the trap depth can be determined in this case is considerably lower, since the absolute magnitude of the flashes is very small. It is interesting to note that as early as 1937-1938, Antonov-Romanovskii,[6,7] analyzing decay curves for a similar phosphor, at various temperatures, concluded that the trap depths were 0.3 and 1.1 ev.

There also were previous indications of the existence of deep traps in the phosphor ZnS-Cu,Cl. In the first place, it was known that the small light sum of this phosphor could be retained for a very long time: two days after the excitation is cut off, a rather bright flash appears under the action of infrared light. Secondly, in ref. 4, it was hypothesized that such levels existed in order to explain why the photoluminescence decreases with decreasing excitation intensity in the low excitation intensity range. The explanation went as follows: Even at room temperature, for sufficiently low excitation intensities the main light sum is concentrated in the deep traps, since the total number of ionized centers under these conditions is such that the number of electrons removed from them is not sufficient to fill these levels completely. At the same time, the de-exciting action of the exciting light on the deep levels can also be quite small, so that they will not prevent the accumulation of electrons in these traps. Under these conditions, the luminescence will experience strong external quenching, since the electron trap depth is considerably greater than the depth of the activator levels (hole traps). When the excitation intensity is increased, as has been stated already, the role played by the deep traps decreases and the external quenching also decreases, i.e., the luminescence yield increases.

Figure 4 shows how the flash intensity in a ZnS-Cu,Cl crystal with a Cu concentration of about 10^{-4} depends on 1/T. As is evident in the figure, the lines do not behave as they did for powdered ZnS-Cu,Cl. The depth of the levels in this case turns out to be 0.66 ev. Experiments on the dependence of light flash intensity on afterglow time described in ref. 3 showed that this crystal also has a level at about 0.3 ev. Clearly, we did not observe this level by the same method as in the case of powdered phosphors because there were many more deep traps in the crystal. The difference between their depths, which of course lies beyond the limits of experimental error, can be explained by a difference in the mode of preparation. The fact is that the crystal was grown at a temperature of about 1400°C, close to the softening point of quartz, and may have been contaminated by impurities contained in the walls of the quartz ampoule. The powder phosphor was prepared at considerably lower temperatures, and therefore was probably less contaminated.

REFERENCES

1. V. V. Antonov-Romanovskii, Izvest. Akad. Nauk SSSR, Ser. Fiz. 10, 477 (1946).
2. Ch. B. Lushchik, Trudy Inst. Fiz. i Astron., Akad. Nauk Eston.SSR No. 3 (1955).
3. L. A. Vinokurov and M. V. Fok, Opt. i Spektr. 10, 225 (1961), Optics and Spectroscopy 10, 112 (1961).
4. V. V. Antonov-Romanovskii and L. A. Vinokurov, Opt. i Spektr. 1, 71 (1956).
5. L. A. Vinokurov, Opt. i Spektr. 1, 901 (1956).
6. V. V. Antonov-Romanovskii, Doklady Akad. Nauk SSSR 17, 95 (1937).
7. V. V. Antonov-Romanovskii, Doklady Akad. Nauk SSSR 20, 361 (1938).

COTTON-MOUTON EFFECT IN THE REGION OF THE IMPURITY ABSORPTION OF LIGHT

A. F. Lubchenko (pp. 379-383)

Received 21 May 1960

Formulas are obtained which define the birefringence in the region of the impurity absorption of light in the presence of a constant external magnetic field; the dependence of this birefringence upon temperature and other parameters characterizing the solvent and its interaction with the impurity centers is established.

ABSORPTION AND DISPERSION OF LIGHT BY A SOLUTION IN THE PRESENCE OF A CONSTANT EXTERNAL MAGNETIC FIELD

As was shown in a preceding work,[1] in the presence of a constant external magnetic field directed along axis OZ, the polarization of the solution caused by the light wave can be written in the form

$$\mathbf{p}_1=\frac{\varepsilon-1}{4\pi}\mathbf{E}_1+\frac{1}{Zh}\sum_{jm m_0}e^{-H\zeta_{m_0}/kT}\langle l_1m\,|\,\mathbf{p}^j\,|\,l_0m_0\rangle(\langle l_0m_0\,|\mathbf{p}^j\,|\,l_1m\rangle \times\chi^j\mathbf{E}_1)(F^j_m-iS^j_m). \quad (1)$$

Here ε is the dielectric permeability of the solution, caused by all virtual transitions except the one under consideration (it is assumed that ε depends weakly on the frequency of the incident light), $\mathbf{E}_1$ is the intensity of the field of light flux, H is the Z component of the intensity of the external magnetic field

$$Z=\sum_{m_0}\exp\left(\frac{-H\zeta_{m_0}}{kT}\right),$$

$H\zeta_{m0}$ is the increment to the energy of the ground state of the solution caused by the external magnetic field; m, m_0 are magnetic quantum numbers,* $\langle l_1m\,|\mathbf{p}^j\,|\,l_0m_0\rangle$ are

*The field in which an impurity center is located is considered as a perturbation.

matrix elements of the dipole moments of the j-th impurity center; and F^j_m and S^j_m are functions defining, respectively, the course of the refractive index and the coefficient of absorption by the impurity centers. (For the remaining symbols see ref. 1.)

In the present paper we shall confine ourselves, for simplicity, to the case of isotropic solvents, and will consider that the light in the solution is propagated along axis OX, perpendicular to the magnetic field. Then, taking into account that the matrix elements $\langle l_1m\,|\mathbf{p}\,|\,l_0m_0\rangle$ are different from zero only for $m = m_0 \pm 1$ and $m = m_0$, and neglecting the dependence of χ upon H, we can rewrite (1) in the form

$$\mathbf{p}_1=\frac{\varepsilon-1}{4\pi}\mathbf{E}_1+\frac{N\chi}{Zh}\sum_{m_0}{}'e^{-H\zeta_{m_0}/kT}$$
$$\times\{(l_1m_0+1\,|\,\mathbf{p}\,|\,l_0m_0)(l_0m_0\,|\,\mathbf{p}\mathbf{E}_1\,|\,l_1m_0+1)(F_{m_0+1}-iS_{m_0+1})$$
$$+(l_1m_0-1\,|\,\mathbf{p}\,|\,l_0m_0)(l_0m_0\,|\,\mathbf{p}\mathbf{E}_1\,|\,l_1m_0-1)(F_{m_0-1}-iS_{m_0-1})$$
$$+(l_1m_0\,|\,\mathbf{p}\,|\,l_0m_0)(l_0m_0\,|\mathbf{p}\mathbf{E}_1\,|\,l_1m_0)(F_{m_0}-iS_{m_0})\}.$$

Here N is the number of impurity centers per unit volume of solution; the prime on the summation sign indicates summation only for those values of m_0 for which $m = m_0 \pm 1$ in the excited state.

Further, using the general characteristics of the expressions for the matrix elements $\langle l_1m\,|\mathbf{p}\,|\,l_0m_0\rangle$ [2] and introducing the relationship

$$R=\frac{1}{Z}\sum_{m_0}{}'e^{-H\zeta_{m_0}/kT}[|A_{m_0}|^2(F_{m_0+1}-iS_{m_0+1})$$
$$+|B_{m_0}|^2(F_{m_0-1}-iS_{m_0-1})],$$

$$\theta=\frac{1}{Z}\sum_{m_0}{}'e^{-H\zeta_{m_0}/kT}[|A_{m_0}|^2(F_{m_0+1}-iS_{m_0+1})$$
$$-|B_{m_0}|^2(F_{m_0-1}-iS_{m_0-1})],$$

$$\theta'=\frac{1}{Z}\sum_{m_0}{}'e^{-H\zeta_{m_0}/kT}|D_{m_0}|^2(F_{m_0}-iS_{m_0}),$$

where

$$\alpha(l_1m_0+1\,|\,P_x\,|\,l_0m_0)=\mp A^*_{m_0},\qquad \alpha(l_0m_0\,|\,P_x\,|\,l_1m_0)=0,$$
$$\alpha(l_1m_0+1\,|\,P_y\,|\,l_0m_0)=\mp(iA_{m_0})^*,\qquad \alpha(l_0m_0\,|\,P_y\,|\,l_1m_0)=0,$$
$$\alpha(l_1m_0\pm1\,|P_z\,|\,l_0m_0)=0,\qquad \alpha(l_0m_0\,|\,P_z\,|\,l_1m_0)=D_{m_0},$$
$$\alpha(l_1m_0-1\,|\,P_x\,|\,l_0m_0)=\pm B^*_{m_0},\qquad \alpha=\sqrt{4\pi h^{-1}N\chi}.$$
$$\alpha(l_1m_0+1\,|\,P_y\,|\,l_0m_0)=\pm(-iB_{m_0})^*,$$

we can write an expression for the induction vector component in the form

$$\left.\begin{aligned}D_x&=(\varepsilon E)_x+RE_y+i\theta E_y,\\ D_y&=(\varepsilon E)_y-i\theta E_x+RE_y,\\ D_z&=(\varepsilon E)_z+\theta' E_z.\end{aligned}\right\} \quad (2)$$

The dielectric permeability tensor ε, as was shown in ref. 1, has the form

$$\varepsilon=\begin{vmatrix}\varepsilon' & i\varepsilon''_{12} & 0\\ -i\varepsilon''_{12} & \varepsilon' & 0\\ 0 & 0 & \varepsilon_{33}\end{vmatrix},$$

so that Eqs. (2) can be rewritten in the form

$$\left.\begin{aligned} D_x &= (\varepsilon' + R) E_x + i(\theta + \varepsilon''_{12}) E_y, \\ D_y &= (\varepsilon' + R) E_y - i(\theta + \varepsilon''_{12}) E_x, \\ D_z &= (\varepsilon_{33} + \theta') E_z. \end{aligned}\right\} \quad (3)$$

System (3) together with the equation for plane waves in the medium

$$\mathbf{D} = N^2 [\mathbf{E} - \mathbf{s}(\mathbf{sE})], \quad (4)$$

where $N = n - i\kappa$, the complex refractive index, and s is the unit vector of the wave normal, define the propagation of light in the solution in the presence of a constant external magnetic field. If the light is propagated along axis OX, then Eq. (4) can be written by components along the respective axes in the form

$$D_x = 0, \quad D_y = N^2 E_y, \quad E_z = N^2 E_z. \quad (5)$$

From (3) and (5) we find

$$\left.\begin{aligned} & D_z [N^2 - (\varepsilon_{33} + \theta')] = 0, \\ & D_y \left[N^2 - (\varepsilon' + R) + \frac{(\theta + \varepsilon''_{12})^2}{\varepsilon' + R} \right] = 0. \end{aligned}\right\} \quad (6)$$

The system (6) has the solution

$$D_y = 0, \quad D_z = 1, \quad N^2 = \varepsilon_{33} + \theta', \quad (7)$$

$$D_y = 1, \quad D_z = 0, \quad \frac{1}{N^2} = \frac{\varepsilon' + R}{(\varepsilon' + R)^2 - (\theta + \varepsilon''_{12})^2}. \quad (8)$$

The first solution corresponds to a wave polarized along axis OZ, the second to a wave polarized along axis OY.

We further take into account that $N = n - i\kappa$, so that we get from (7)

$$\left.\begin{aligned} & n_2^2 - \varkappa_2^2 = \varepsilon_{33} + \frac{1}{Z} \sum_{m_0}' e^{-H\zeta_{m_0}/kT} |D_{m_0}|^2 F_{m_0}, \\ & 2n_2\varkappa_2 = \frac{1}{Z} \sum_{m_0}' e^{-H\zeta_{m_0}/kT} |D_{m_0}|^2 S_{m_0}. \end{aligned}\right\} \quad (9)$$

Since $\kappa_2^2 \ll n_2^2$, we find from the first relationship of (9) that

$$n_2 = \sqrt{\varepsilon_{33}} + \frac{1}{2Z\sqrt{\varepsilon_{33}}} \sum_{m_0}' e^{-H\zeta_{m_0}/kT} |D_{m_0}|^2 F_{m_0}.$$

The expression for the refractive index for a wave polarized along axis OY, as is easy to see, can be written in the form

$$\frac{1}{N_1^2} = \frac{1}{2}\left[\frac{1}{N_+^2} + \frac{1}{N_-^2}\right], \quad (10)$$

where N_+ and N_- are complex indices of refraction for left and right circularly polarized waves, respectively.[1] Separating the real and imaginary parts of (10), we get

$$\frac{n_1^2 - \varkappa_1^2}{(n_1^2 + \varkappa_1^2)^2} = \frac{1}{2}\left[\frac{n_+^2 - \varkappa_+^2}{(n_+^2 + \varkappa_+^2)^2} + \frac{n_-^2 - \varkappa_-^2}{(n_-^2 + \varkappa_-^2)^2}\right], \quad (11)$$

$$\frac{n_1\varkappa_1}{(n_1^2 + \varkappa_1^2)^2} = \frac{1}{2}\left[\frac{n_+\varkappa_+}{(n_+^2 + \varkappa_+^2)^2} + \frac{n_-\varkappa_-}{(n_-^2 + \varkappa_-^2)^2}\right]. \quad (12)$$

In the latter expressions one can neglect κ^2 in comparison with n^2; if also we use the approximation $n_1 = \sqrt{\varepsilon'}$, we get

$$\frac{1}{n_1^2} = \frac{1}{2}\left[\frac{1}{n_+^2} + \frac{1}{n_-^2}\right], \quad \varkappa_1 = \frac{1}{2}[\varkappa_+ + \varkappa_-]. \quad (13)$$

On substituting the expression for κ_+ and κ_- from ref. 1, we finally obtain

$$n_1\varkappa_1 = \sum_m' e^{-H\zeta_{m_0}/kT} \{|A_{m_0}|^2 S_{m_0+1} + |B_{m_0}|^2 S_{m_0-1}\} \frac{1}{2Z}. \quad (14)$$

Formula (14) defines the form of the absorption curve for light polarized along the axis OY by a solution in the presence of a constant external magnetic field.

For calculation of the refractive index n_1, we write (13) in the form

$$n_1 = \frac{2n_+n_-}{n_+^2 + n_-^2}.$$

Substituting n_+^2 and n_-^2 from ref. 1 into this expression and extracting the square root, we find

$$n_1 = \sqrt{\varepsilon'} + \frac{1}{2Z\sqrt{\varepsilon'}} \sum_{m_0}' e^{-H\zeta_{m_0}/kT} \{|A_{m_0}|^2 F_{m_0+1} + |B_{m_0}|^2 F_{m_0-1}\}.$$

BIREFRINGENCE IN THE REGION OF IMPURITY ABSORPTION OF LIGHT

Making use of the above-derived expressions for n_1 and n_2, it is easy to compute the magnitude of the birefringence in the region of impurity absorption of light in the presence of a constant external magnetic field:

$$\Delta = n_1 - n_2 = \sqrt{\varepsilon'} - \sqrt{\varepsilon_{33}} + \frac{1}{2Z} \sum_{m_0}' e^{-H\zeta_{m_0}/kT} \times \left\{ \frac{|A_{m_0}|^2}{\sqrt{\varepsilon'}} F_{m_0+1} + \frac{|B_{m_0}|^2}{\sqrt{\varepsilon'}} F_{m_0-1} - \frac{|D_{m_0}|^2}{\sqrt{\varepsilon_{33}}} F_{m_0} \right\}. \quad (15)$$

From (15) it follows that in the region of impurity absorption of light, the magnitude of the birefringence, generally speaking, is not proportional to H^2, but depends on the intensity of the magnetic field in a more complex manner. In addition, the magnitude of the birefringence depends upon temperature. The temperature dependence Δ is defined not only by the exponential, but also by the dependence of the functions F_m upon temperature. Furthermore, from the expression for F_m[1] it follows that the magnitude of the birefringence, even for a normal triplet, will not be, in the general case, a symmetrical function with respect to the point $\omega = \Omega_{11}^{n_s}{}_0 + A$ (the maximum of absorption for the central line of the triplet); from the behavior of $F_m(\omega)$ it follows that the asymmetry will increase with decrease in temperature.

For more detailed investigation of expression (15) it is necessary to be more specific about the solvent and the impurity center. We will consider, for simplicity, the case of an isotropic solvent and an impurity center having central symmetry and singlet terms; we will also consider that the site-group of the field of the solution in which the impurity center is located does not have less symmetry than that of the impurity center.* In such a field the degenerate levels of the impurity fields will not split: all splitting will be caused by the external magnetic field. The function F_m will not depend in this case upon the quantum number m_0; F_{m_0} will not depend sensibly upon the intensity of the magnetic field, and the argument of F_{m_0} will have the same form as in the absence of the field H ($x_{m_0} = [\Omega_{11}^{n_s}{}_0 + A - \omega]/\Gamma$) and the arguments of functions F_{m_0+1} and F_{m_0-1} can be written respectively in the form

$$x_{m_0+1} = x_0 + \eta H \text{ and } x_{m_0-1} = x_0 - \eta H,$$

where η is proportional to the Bohr magneton. Still neglecting the difference between ε_{33} and ε' within the braces

*If H_0 is the Hamiltonian of the impurity center, and V is the perturbation field of the solution, the symmetry of $H_0 + V$ must coincide with that of H_0.

in (15), and setting $\sqrt{\varepsilon_{33}} \simeq \sqrt{\varepsilon'} = n$, we write the expression for birefringence in the form

$$\Delta = \sqrt{\varepsilon'} - \sqrt{\varepsilon_{33}} + \frac{1}{2Zn}$$

$$\times \sum_{m_0}' e^{-H\zeta_{m_0}/kT} [|A_{m_0}|^2 F_+ + |B_{m_0}|^2 F_- - |D_{m_0}|^2 F_{m_0}].$$

Far from the region of absorption, where transformations (17) of ref. 1 are correct, we get the following expression for the magnitude of the birefringence: when $x > 0$

$$\Delta_1 = \sqrt{\varepsilon'} - \sqrt{\varepsilon_{33}} + \frac{1}{x^3 Z_0 n}$$

$$\times \sum_{m_0}' \left\{ \frac{1}{2} [|A_{m_0}|^2 + |B_{m_0}|^2] H^2\gamma_1^2 + H\gamma_1 [|A_{m_0}|^2 \beta_2 - |B_{m_0}|^2 \beta_1] \right\}$$

$$+ \frac{1}{2x^2 Z_0 n} \sum_{m_0}' \left\{ \frac{H^2 \zeta_{m_0} \eta}{kT} [|A_{m_0}|^2 - |B_{m_0}|^2] \right.$$

$$\left. + \frac{H\zeta_{m_0}}{kT} [|A_{m_0}|^2 \beta_2 + |B_{m_0}|^2 \beta_1] \right\},$$

when $x < 0$

$$\Delta_2 = \sqrt{\varepsilon'} - \sqrt{\varepsilon_{33}} - \frac{1}{|x|^3 Z_0 n}$$

$$\times \sum_{m_0}' \left\{ \frac{1}{2} [|A_{m_0}|^2 + |B_{m_0}|^2] H^2\gamma_1^2 + H\gamma_1 [|A_{m_0}|^2 \beta_2 - |B_{m_0}|^2 \beta_1] \right\}$$

$$+ \frac{1}{2x^2 Z_0 n} \sum_{m_0}' \left\{ \frac{H^2 \eta \zeta_{m_0}}{kT} [|A_{m_0}|^2 - |B_{m_0}|^2] \right.$$

$$\left. + \frac{H\zeta_{m_0}}{kT} [|A_{m_0}|^2 \beta_2 + |B_{m_0}|^2 \beta_1] \right\},$$

where Z_0 is the zero order term in the series expansion of Z in powers of H.

From (16) it follows that in the neighborhood of the impurity absorption, and at low temperatures, the dependence of the birefringence upon the intensity of the magnetic field is defined, generally speaking, by the sum of two members: one linear with the field, and one quadratic. The linear member vanishes at $\beta_1 = \beta_2$, that is, when the transition of electrons from states corresponding to various m_0 to excited states with $m = m_0 \pm 1$ is accompanied by interaction with the same types of oscillations of the solvent (in this case the half-width of the limiting bands of absorption in the triplet will be identical). If $\beta_1 \neq \beta_2$, the member which is linear with the field differs from zero; however, its contribution to Δ falls off with increased temperature. At temperatures at which the absorption band becomes symmetrical (bell-shaped) one can neglect the contributions of the members proportional to H. The magnitude of the birefringence at these temperatures will be proportional to H^2, while the temperature dependence of Δ will be defined by the member proportional to 1/T. From (16) it also follows that the magnitude of the birefringence at identical distances from the point $\omega_0 = \Omega^{n_s}_{l_1 l_0} + \Delta$ (the maximum absorption for the central line of the triplet) will be different: the curve of Δ goes higher on the side of smaller frequencies than ω_0 than on the side of greater frequencies.

When the connection between electron excitation and oscillations of the atoms of the solvent is weak, the magnitude of the birefringence, as is seen from the expression for F_m, appears in the form of a sum of curves, analogous to those which are obtained for a classical oscillator.[3]

In conclusion, I express my gratitude to A. S. Davidov for valuable discussions and for his interest in the work.

REFERENCES

1. A. F. Lubchenko, Opt. i Spektr. 10, No. 4 (1961), Optics and Spectroscopy 10, No. 4 (1961), to be published.
2. E. V. Condon and G. H. Shortley, "Theory of Atomic Spectra." Cambridge Univ. Press, 1935.
3. M. Born, "Optik." Springer, Berlin, 1933.

THEORY OF MULTILAYER ASYMMETRIC REFLECTORS

P. G. Kard (pp. 384-389)

Received 20 May 1960

Theoretical considerations are given to the problem of synthesizing multilayer coatings which, for a given transmission coefficient, have small reflection and large absorption coefficients when light is incident from one side, and have large reflection and small absorption coefficients when light is incident from the other side. The conditions necessary for this are determined, and formulas are obtained which characterize the properties of such coatings.

INTRODUCTION

We shall define an asymmetric reflector as a two-sided mirror whose transmission coefficient differs from zero and whose reflection coefficients from the two sides are not the same. Such mirrors can be constructed using multilayer interference coatings. It is well known that the coefficients of energy transmission D and D′ of any multilayer coating (the prime means that light falls on the coating from the reverse side) are always identical independently of whether the coating is transparent or has absorbing layers (see, for example, ref. 1). The analogous equation $R = R'$ for the energy reflection coefficients is true, on the other hand, only for nonabsorbing coatings and for absorbing ones in certain special cases (e.g., in the case of a symmetric coating). In the general case $R \neq R'$, i.e., the coating is an asymmetric reflector. The inequality of the reflection coefficients implies the inequality of the absorption coefficients A and A′. For the side whose reflection coefficient is the larger, the absorption coefficient is the smaller, and vice versa. Here

$$R - R' = A' - A. \qquad (1)$$

A semitransparent metallic layer deposited on a glass substrate can serve as the simplest example of an

asymmetric reflector (however, R – R′ in this case is small). An asymmetric reflector having, say, R′ and A close to zero could be of practical interest. For example, let D = 0.5 and A be small. Such a reflector from the reverse side would have an absorption coefficient close to 0.5, but from the front (for the same transmission) the absorption would be insignificant. For nonidentical illumination (and partly even for identical illumination) such a reflector would behave like an asymmetric transmitter, i.e., it would be to a considerable degree transparent in one direction and practically nontransparent in the other.

In ref. 2 Pohlack presents some considerations of a qualitative character which refer to conditions necessary for constructing an asymmetric reflector. However, he does not give a precise quantitative theory which could show the limits attainable in this direction and could serve for the calculation of this sort of system.

The purpose of the present article is to state the basis of a precise theory of asymmetric reflectors in which a recently proposed method of calculating absorbing multilayer coatings is used (see refs. 3-6).

STATEMENT OF THE PROBLEM

We shall consider a multilayer absorbing coating consisting of three subcoatings (see Figure) separated by two intermediate layers. The boundary media (which we shall take to be nonabsorbing) we designate by the indices 0 and 3, and the intermediate layers by the indices 1 and 2. All quantities referring to the whole coating will be designated by the indices 03 or 30 (depending on the direction of incidence of the light); analogously, we shall designate quantities which refer to the subcoatings by two indices (for example, 01, 12, 32, 02, 31). The indices 12 and 21, however, will frequently be omitted (using primes for the designation of quantities which refer to the subcoating 21 in contrast with quantities which refer to the subcoating 12).

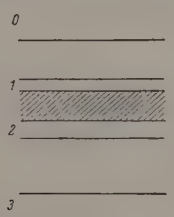

The extreme outer subcoatings of the three, and the intermediate layers, should be made transparent, whereas the middle subcoating should be absorbing (this does not mean that all layers in the middle subcoating should be absorbing, but at least one should). In the simplest case the middle subcoating consists of a single absorbing layer. Of course, the transparency condition on the outer subcoatings is not restrictive, since the middle subcoating can always be formed in such a way that it includes all absorbing layers. In special cases, however, one or the other transparent subcoating can be missing.

Let us introduce the following notation (it agrees with that used by the author in previous works):[4-6]

$$\left.\begin{aligned} \alpha_1 &= kn_1h_1, \\ \alpha_2 &= kn_2h_2, \end{aligned}\right\} \tag{2}$$

where k is the wave number in vacuum, and n_1, h_1 and n_2, h_2 are the refractive indices and thicknesses of the intermediate layers. Further,

$$a = \frac{r}{d}, \quad b = \frac{1}{d}, \tag{3}$$

where r and d are the amplitude coefficients of reflection and transmission of the (ε·b)coatings. In addition, let

$$\left.\begin{aligned} a &= \sqrt{\frac{R}{D}}\, e^{i\mu}, \\ b &= \frac{1}{\sqrt{D}}\, e^{i\nu}. \end{aligned}\right\} \tag{4}$$

We recall also the basic formulas, which we will need later,

$$a' = -\bar{a}^*, \tag{5}$$

$$b\bar{b}^* - a\bar{a}^* = 1, \tag{6}$$

where the asterisks denote complex-conjugate quantities, and the superscript ~ designates that a given quantity refers to a conjugate coating, i.e., one in which the refractive indices of all layers have complex-conjugate values. In addition, we shall use the Vlasov formulas in the new form (see ref. 3). Finally, let us define

$$P = \frac{1}{2}\left(\frac{A}{D} + \frac{\bar{A}}{\bar{D}}\right) = \frac{1}{2}\left(b\bar{b}^* + \bar{b}b^* - a\bar{a}^* - \bar{a}a^*\right) - 1, \tag{7}$$

$$S = \frac{1}{2}\left(\frac{A}{D} - \frac{\bar{A}}{\bar{D}}\right) = \frac{1}{2}\left(b\bar{b}^* - \bar{b}b^* - a\bar{a}^* + \bar{a}a^*\right), \tag{8}$$

$$Ue^{i\varphi} = \bar{a}b - a\bar{b}, \quad U \geqslant 0, \tag{9}$$

where the following relationships occur:

$$S^2 - U^2 = \operatorname{sh}^2\varphi, \tag{10}$$

$$\operatorname{ch}\varphi = 1 + P, \quad \varphi > 0. \tag{11}$$

In all cases we shall consider the light to be incident normally.

Our problem is to find the conditions under which the quantity $D_{03} = D_{30}$ has a preassigned value, and A_{03} and R_{30} are as small as possible. The solution of this problem can be approached in two ways: We can require, first, that A_{03} be a minimum, or, secondly, that R_{30} be a minimum. The ideal case would be that in which both of these requirements would be satisfied independently of one another. However, as will be shown below, this is impossible. The better of these two alternatives seems to be the second. However, for completeness, to begin with, we shall consider briefly the first alternative.

ASYMMETRIC REFLECTOR CHARACTERIZED BY A MINIMUM VALUE OF A_{03}

Now, let us require a minimum for A_{03} or, what is the same thing (since D_{03} is considered fixed), a minimum for A_{03}/D_{03}. In refs. 4 and 5 it is shown that the condition

$$\left(\frac{A_{03}}{D_{03}}\right)_{\min} = e^{\varphi} - 1 \tag{12}$$

is attained for

$$\cos\left(2\alpha_2 + \sigma - \mu_{23} + \nu_{23}\right) = -1 \tag{13}$$

and

$$R_{23} = \frac{S - \operatorname{sh}\varphi}{S + \operatorname{sh}\varphi}. \tag{14}$$

The condition (13) determines the thickness of the second intermediate layer, and (14) determines the reflection coefficient of the back (second) transparent subcoating. Assuming these conditions to be fulfilled, we can calculate all the coefficients of reflection, transmission, and absorption. Not quoting here all the results, we mention only the following noteworthy relationship:

$$R_{30} = e^{-2\varphi} R_{03}. \qquad (15)$$

This equation together with Eq. (12) shows that this approach gives a significant degree of symmetry only when the transmission coefficient D is small. Otherwise, in order that A_{03} be sufficiently small, φ must also be small [see Eq. (12)]. But, on the other hand, for the reflection coefficient R_{30} to be as small as possible in comparison with R_{03}, φ must be, according to Eq. (15), rather large. Thus, contradictory requirements are placed on φ which can be satisfied only by a compromise.

ASYMMETRIC REFLECTOR WITH $R_{30} = 0$

Let us consider the other alternative, based on the requirement of a minimum for R_{30}, i.e., for the condition $R_{30} = 0$.

Considering our coating to consist of subcoatings 01 and 13, let us write the Vlasov formulas in the form

$$\left.\begin{aligned} a_{03} &= a_{01} b_{13} e^{i\alpha_1} + a_{13} b_{01}^* e^{-i\alpha_1}, \\ a_{30} &= -\tilde{a}_{13}^* b_{01} e^{i\alpha_1} - a_{01}^* \tilde{b}_{13}^* e^{-i\alpha_1}, \\ b_{03} &= b_{30} = b_{01} b_{13} e^{i\alpha_1} + a_{13} a_{01}^* e^{-i\alpha_1}. \end{aligned}\right\} \qquad (16)$$

Multiplying each of these quantities by the complex-conjugate, we get

$$\frac{R_{03}}{D_{03}} = \frac{1}{D_{01} D_{13}}$$

$$[R_{01} + R_{13} + 2\sqrt{R_{01} R_{13}} \cos(2\alpha_1 + \mu_{01} - \mu_{13} + \nu_{01} + \nu_{13})], \qquad (17)$$

$$\frac{R_{30}}{D_{30}} = \frac{1}{D_{01} \tilde{D}_{13}}$$

$$[R_{01} + \tilde{R}_{13} + 2\sqrt{R_{01} \tilde{R}_{13}} \cos(2\alpha_1 + \mu_{01} - \tilde{\mu}_{13} + \nu_{01} + \tilde{\nu}_{13})], \qquad (18)$$

$$\frac{1}{D_{03}} = \frac{1}{D_{30}} = \frac{1}{D_{01} D_{13}}$$

$$[1 + R_{01} R_{13} + 2\sqrt{R_{01} R_{13}} \cos(2\alpha_1 + \mu_{01} - \mu_{13} + \nu_{01} + \nu_{13})]. \qquad (19)$$

Now we must set

$$R_{30} = 0. \qquad (20)$$

For this it is necessary that

$$R_{01} = \tilde{R}_{13} \qquad (21)$$

and

$$\cos(2\alpha_1 + \mu_{01} - \tilde{\mu}_{13} + \nu_{01} + \tilde{\nu}_{13}) = -1. \qquad (22)$$

The first of these conditions fixes the reflection coefficient of the front transparent subcoating, and the second, the thickness of the first intermediate layer.

Calculating the values of R_{03}/D_{03} and $1/D_{03}$ with the use of these conditions, we find

$$\frac{R_{03}}{D_{03}} = \frac{\tilde{D}_{13}}{1 - \tilde{R}_{13}} (\tilde{a}_{13} b_{13} - a_{13} \tilde{b}_{13})(\tilde{a}_{13}^* b_{13}^* - a_{13}^* \tilde{b}_{13}^*) = \frac{U_{13}^2}{\operatorname{ch}\varphi - S_{13}}$$

and

$$\frac{1}{D_{03}} = \frac{\tilde{D}_{13}}{1 - \tilde{R}_{13}} \left[\frac{1}{D_{13} \tilde{D}_{13}} + \frac{R_{13} \tilde{R}_{13}}{D_{13} \tilde{D}_{13}} - \frac{2\sqrt{R_{13} \tilde{R}_{13}}}{D_{13} \tilde{D}_{13}} \cos(\mu_{13} - \tilde{\mu}_{13} - \nu_{13} + \tilde{\nu}_{13}) \right]$$

$$= \frac{1}{1 + \frac{A_{13}}{D_{13}}} (b_{13} \tilde{b}_{13}^* - a_{13} \tilde{a}_{13}^*)(\tilde{b}_{13} b_{13}^* - \tilde{a}_{13} a_{13}^*) = \frac{1}{\operatorname{ch}\varphi - S_{13}}.$$

Thus,

$$\left.\begin{aligned} R_{03} &= U_{13}^2 = S_{13}^2 - \operatorname{sh}^2\varphi, \\ D_{03} &= \operatorname{ch}\varphi - S_{13}, \\ A_{03} &= (\operatorname{ch}\varphi - S_{13})(\operatorname{ch}\varphi + S_{13} - 1) \end{aligned}\right\} \qquad (23)$$

and

$$\left.\begin{aligned} R_{30} &= 0, \\ D_{30} &= \operatorname{ch}\varphi - S_{13}, \\ A_{30} &= 1 + S_{13} - \operatorname{ch}\varphi. \end{aligned}\right\} \qquad (24)$$

In connection with these formulas we must pay attention, first of all, to the fact that condition (21) can be satisfied only if $\tilde{R}_{13} < 1$. And since $\tilde{R}_{13} = 1 - \tilde{A}_{13} - \tilde{D}_{13}$, we must have $\tilde{A}_{13} + \tilde{D}_{13} > 0$, from which it follows that $\cosh\varphi - S_{13} > 0$ and $S_{13}^2 - \sinh^2\varphi < 1$. Equations (23) themselves give reasonable expressions for D_{03} and R_{03}. Consequently, as a condition in addition to (21) and (22) it is necessary to consider the requirement

$$U_{13} < 1, \qquad (25)$$

which must be satisfied by the choice of the subcoating 13.

CONSIDERATION OF RESULTS

We shall limit ourselves here to a consideration of the latter alternative, which has obvious advantages over the first. From the first of Eqs. (23) it is clear that by choosing U_{13} in a suitable manner, we can obtain any value for R_{03} theoretically as close to unity as is desired, with R_{30} always equal to zero. The value of U_{13} depends, according to Eq. (10), on S_{13} and φ, while φ depends only on the absorbing subcoating 12, and S_{13} depends, in addition, on the back transparent subcoating 23 and on the second intermediate layer according to the formula

$$S_{13} = \frac{1 + R_{23}}{1 - R_{23}} S + 2U \frac{\sqrt{R_{23}}}{1 - R_{23}} \cos(2\alpha_2 + \sigma - \mu_{23} + \nu_{23}). \qquad (26)$$

In order to obtain, for a given value of D_{03}, as small an A_{03} as possible (and, correspondingly, as large an R_{03} as possible), it is obviously necessary to make φ as small as possible. If the subcoating 12 is a single metallic layer, this means that this layer must be made as thin as possible. In this case not only φ will be small, but also S and U. However, according to Eq. (26), S_{13} can be made arbitrarily large (in spite of the smallness of S and U). In order to do this it is only necessary to choose the value of R_{23} sufficiently close to unity. Thus, a suitable choice of the value of S_{13} [observing the condition (25)] guarantees any predetermined value of D_{03} for any value of φ theoretically as small as may be desired.

In the light of what we have just said, it is expedient to rewrite Eqs. (23) and (24), expressing S_{13} in terms of D and φ, in the form

$$\left.\begin{aligned} R_{03} &= 1 - 2D\operatorname{ch}\varphi + D^2, \\ A_{03} &= D(2\operatorname{ch}\varphi - 1 - D), \\ R_{30} &= 0, \\ A_{30} &= 1 - D, \end{aligned}\right\} \qquad (27)$$

where we have omitted the index on D. The smallness of φ makes it possible to take $\cosh\varphi \approx 1$, after which Eqs. (27) are even more simplified. Of course, in practice the reduction in thickness of the absorbing layer must have some limit, if only because of the necessity of satisfying condition (21), according to which R_{01} can take on a value ideally close to unity.

We note the following remarkable circumstance: If

we choose D close to zero (in order to do this for small φ it is necessary to make S_{13} equal to or even larger than unity, provided that condition (25) is satisfied), then according to Eq. (27) we get A_{03} close to zero and A_{30} close to unity. This latter result is surprising because it does not depend on the thickness of the absorbing layer, which, at least theoretically, can be chosen as small as is desired. Nevertheless, the absorption (for light incident from the reverse side) appears to be almost complete. In practice, as was indicated above, the absorbing layer should in all cases have a thickness no less than some limit.

Thus, in this report we have shown that a highly effective asymmetric reflector actually can be synthesized. However, conditions (21) and (22) and also the values of φ and S_{13} depend on the wavelength. Therefore, the question of achromaticity of asymmetric reflectors arises. This question deserves special consideration, and in this article we have not touched upon it. We note only that, along with achromaticity, the case of more or less sharply expressed chromaticity is also of interest as it may be of value in the construction of light filters.

REFERENCES

1. K. Ishiguro and T. Kato, J. Phys. Soc. Japan 8, 77 (1953).
2. H. Pohlack, "Optik aller Wellenlangen," p. 363. Berlin, 1959.
3. P. G. Kard, Opt. i Spektr. 9, 95 (1960), Optics and Spectroscopy 9, 49 (1960).
4. P. G. Kard, Opt. i Spektr. 9, 248 (1960), Optics and Spectroscopy 9, 129 (1960).
5. P. G. Kard, Izvest. Akad. Nauk Eston. SSR, Ser. Tekh. i Fiz.-Mat. Nauk 9, 250 (1960).
6. P. G. Kard, Opt. i Spektr. 9, 386 (1960), Optics and Spectroscopy 9, 200 (1960).

ON THE SENSITIVITY OF EMISSION SPECTRAL ANALYSIS

S. L. Mandel'stam and V. V. Nedler (pp. 390-397)

Received 6 June 1960

The sensitivity limit of spectral analysis is discussed theoretically. The smallest content of an element in a sample that can be determined is defined as that content which gives a spectral line signal which is several times greater than the mean fluctuation of the background signal caused by the radiation detector. The electronic excitation of atoms is discussed, and the signal-to-noise ratio investigated as a function of the electron concentration in the luminous cloud in the source, the parameters of the spectral apparatus, and other factors. Numerical estimations of the sensitivity of spectral analysis are given for the arc and the hollow cathode as excitation sources. It is shown that the loss of sensitivity is due mainly to the inefficient transfer of atoms of the sample into the luminous cloud of the source and to the poor retention of atoms in that region.

The sensitivity required in emission spectral analysis has been increasing very rapidly in recent years. A sensitivity of about 10^{-3} to 10^{-4}% was sufficient 15 or 20 years ago for the main problems of production control. The development of the atomic materials industry demanded methods having a sensitivity of 10^{-5} to 10^{-6}%. At present, the technology of semiconductors needs analytical methods with a sensitivity of about 10^{-8} to 10^{-9}%.

Sensitivities of 10^{-3} to 10^{-4}% were achieved mainly by using classical methods; i.e., introducing the sample directly into the excitation source (flame, arc, or spark). Sensitivity was increased two or three orders of magnitude by developing new procedures, mostly based on various physical and physicochemical methods of enriching the sample, utilization of fractional evaporation, and, to some extent, on new excitation sources (e.g., the hollow cathode).[1,2]

A theoretical estimation of the limits of sensitivity of spectral analysis seems to be of interest. The results of these calculations are given below.

It is important to point out that many processes in the excitation sources, which vitally influence the intensity of spectral lines, have not yet been studied sufficiently; the values of many quantities entering the calculations are also unknown. Therefore it is not possible at present to expect accurate—that is, quantitative—estimations of sensitivity. The purpose of our calculation is mainly to clarify the relative importance of the basic physical factors which determine the sensitivity of spectral analysis. This should enable one to develop a reasoned approach to the increase of sensitivity. The majority of the methods now in use certainly have not reached the limits of their potentialities; for instance, the use of purer carbon electrodes, chemicals, etc., will make it possible to increase the sensitivity of these procedures considerably. However, these methods of increasing sensitivity are obvious and need not be elaborated.

We will choose the following scheme for spectral analysis:

The sample is placed in the excitation source. The radiation emitted by the source is dispersed by a spectrometer and the intensity of the line of the element to be analyzed is recorded photoelectrically. The photocurrent due to this line is denoted by I_1, and the photocurrent in the absence of this element in the sample by I_b (this photocurrent is caused by the continuous spectrum of the source and by the dark current of the photoelectric detector). In order to determine whether the element under investigation is present in the sample, we must make essentially two kinds of measurements: we must measure the intensity of the signal due to the line in the spectrum of the sample ($I_1 + I_b$) and the intensity of the signal from a sample not containing this element, or the signal from the spectral region adjacent to the line (I_b). The intensities of both signals are subject to fluctuation, so that we can recognize the presence of the line in the spec-

trum only if the condition

$$\overline{I_1 + I_b} - \overline{I_b} > \sqrt{\Delta^2 (I_1 + I_b) + \Delta^2 I_b}. \quad (1)$$

is fulfilled. When the fluctuations of the signals ΔI are known, it is possible to determine the smallest signal intensity of the line I_1 that can be detected, and thus the limit of sensitivity of the analysis.

The value of ΔI consists of fluctuations caused by the instability of the light source, errors of signal measurement, and fluctuations of the signal caused by the photoelectric detector itself. The fluctuations of the light source can be neglected if I_b is measured simultaneously with $(I_1 + I_b)$, either in the vicinity of the line, or by selecting a line which is homologous with the background. In the first approximation, the errors of signal measurement can be ignored. In the following calculations it can be assumed that for practical purposes, the sensitivity limit—the smallest amount of the element in the sample that can be detected—is the amount for which the signal from the line of this element is 10 times greater than the mean fluctuation of the background signal caused by the photoelectric detector itself, that is,

$$I_{1(\min)} \sim 10 \Delta I_b. \quad (2)$$

It should be mentioned that the situation is quite similar in the case of photographic recording of the spectrum. By measuring the optical density by means of a sufficiently sensitive microphotometer in the region of the plate where the line is expected, and in the neighboring region of the plate which has only the background, we can detect a line when the optical density at this location exceeds the density at the neighboring location by an amount which is larger than the mean fluctuation of the density. This was first pointed out by Kaiser.[3]

Let us now consider the factors affecting the signal-to-noise ratio $(I_1/\Delta I_b)$.

The photocurrent from a spectral line is

$$I_1 = \alpha \gamma F_1', \quad (3)$$

where F_1' is the light flux from the line incident on the photoelectric detector, γ is the sensitivity of the detector expressed in amp/lum, and α is the mechanical equivalent of light ($\alpha = 0.68$ lum/erg · sec^{-1}). The light flux from a spectral line has the value

$$F_1' = \frac{j_\nu}{4\pi} lsb\Omega, \quad (4)$$

where j_ν is the line intensity in the luminous cloud of the source, l is the diameter of the luminous cloud, s and d are the width and length of the entrance slit, respectively, and Ω is the speed of the collimator (it is assumed that the exit slit transmits the image of the entrance slit in its entirety).

We shall now give the expression for the intensity of the lines j_ν in a general form, assuming electronic excitation, for a wide range of electron concentrations. The balance between the processes of excitation and deactivation in the luminous cloud can be represented by the equation

$$N_0 N_e \langle \sigma v \rangle - N_i N_e \langle \sigma' v' \rangle - N_i A = 0. \quad (5)$$

where N_0 is the concentration of the unexcited atoms of the element in question in the luminous cloud, N_i is the concentration of excited atoms, and N_e is the electron concentration. A is the probability of spontaneous emission, σ and σ' are the cross sections for collisions of the first and second kind, respectively, and v and v' are the electron velocities before and after collision, related to each other by the equation $mv^2/2 = \chi + mv'^2/2$, where χ is the excitation energy of a given line. The velocity distribution of electrons is assumed to be the Maxwellian, corresponding to a temperature T_e (the angular brackets indicate averaging the values of σv over a Maxwellian velocity distribution).

The first term in Eq. (5) represents the number of atomic excitations in unit time due to electronic collisions of the first kind; the second term is the number of deactivations of excited atoms due to electronic collisions of the second kind, and the third term is the number of deactivations of excited atoms due to spontaneous emission.

From (5) we obtain

$$N_i = \frac{\frac{\langle \sigma v \rangle}{\langle \sigma' v' \rangle}}{1 + \frac{A}{N_e \langle \sigma' v' \rangle}} N_0.$$

By using the Klein-Rosseland relationship, we obtain

$$\frac{\langle \sigma v \rangle}{\langle \sigma' v' \rangle} = e^{-\frac{\chi}{kT_e}}.$$

Consequently, we obtain the following expression for the line intensity:

$$j_\nu = h\nu A N_i = \frac{h\nu N_0 A e^{-\frac{\chi}{kT_e}}}{1 + \frac{A}{N_e \langle \sigma' v' \rangle}}. \quad (6)$$

If the electron concentration in the luminous cloud of the course is high, the second term in Eq. (5) is considerably larger than the third term: the deactivation of the excited atoms is due mainly to collisions of the second kind. In this case, the fraction in the denominator of Eq. (6) is considerably smaller than unity, and Eq. (6) becomes

$$j_\nu = h\nu A N_0 e^{-\frac{\chi}{kT_e}}. \quad (7)$$

In the other extreme case (N_e small), the deactivation of the excited atoms is due mainly to spontaneous emission. The second term in Eq. (5) is now considerably smaller than the third term, and the fraction in the denominator of Eq. (6) is much greater than unity. Expression (6) then becomes

$$j_\nu = h\nu N_0 N_e \langle \sigma v \rangle. \quad (8)$$

Substituting (6) and (4) into (3), we obtain the following expression for the photocurrent from the line of the element being determined:

$$I_1 = \frac{\alpha \gamma lsb\Omega}{4\pi} \cdot \frac{h\nu N_0 A e^{-\frac{\chi}{kT_e}}}{1 + \frac{A}{N_e \langle \sigma' v' \rangle}}. \quad (9)$$

Let us now calculate the value of ΔI_b. The photocurrent I_b consists of the dark current of the photomultiplier I_d and the photocurrent from the continuous spectrum I_c. The mean fluctuation of the photocurrent from the background is given by the well-known relationship

$$\Delta I_b = \sqrt{2eB\mu\tau^{-1}(I_d + I_c)}, \quad (10)$$

where B is a constant (approximately 2.5), μ is the coefficient of amplification of the photomultiplier, and τ is the recording time.

The photocurrent from the continuous spectrum is connected with the light flux and with the intensity of the continuous spectrum by the relationships

$$I_c = \alpha \gamma F_c' \quad (11)$$

and

$$F_c' = \frac{\varepsilon_\nu}{4\pi} lsb\Omega d\nu, \quad (12)$$

where ε_ν is the intensity of the continuous spectrum; l, s, and Ω have the same meaning as before, and $d\nu$ is the

width of the spectral interval defined by the exit slit of the spectrometer ($d\nu = s'(c/\lambda^2)10^{-7}D$, where s' is the width of the exit slit, D is the dispersion in A/mm).

To determine the value of ε_ν, we shall assume that the continuous spectrum has the smallest value for a given source; i.e., that it is caused only by the interaction of electrons and ions in the luminous cloud of the source, that is, by the recombination of electrons and ions, and by the bremsstrahlung of electrons in the ionic fields (free-bound and free-free transitions). Usually there are additional sources of background (in the arc, for instance, there is background caused by the luminescence of the electrode tips and graphite particles in the arc column, etc.). It should be possible to eliminate these additional sources of background, for instance, by screening off the images of the electrode ends, by using graphite which does not disintegrate, etc.

For the intensity of the continuous spectrum caused by the free-bound and free-free electron transitions we shall use Unsöld's expression, which has been thoroughly confirmed experimentally

$$\varepsilon_\nu = \frac{128\pi^3}{3\sqrt{3}} \frac{Z^2e^6}{c^3(2\pi m)^{\frac{3}{2}}} \frac{N_e N_j}{(kT_e)^{\frac{1}{2}}}$$

$$= 8 \cdot 10^{-46} \frac{Z^2 N_e^2}{(kT_e)^{\frac{1}{2}}} \text{ (erg/sec., frequency un.)}, \quad (13)$$

where Z is the ionic charge, assumed henceforth to be unity, and N_j is the concentration of ions, assumed to be equal to the electron concentration.

Expression (13) is valid for relatively large N_e ($\geq 10^{15}$), in which case there is a Boltzmann distribution of atoms among the excited states corresponding to Eq. (7) for the line intensity. Apparently, no large error is involved if this expression is also used for smaller values of N_e, especially if it is assumed that for $N_e < 10^{14}$ the main contribution to I_b is made by the dark current I_d.

By using Eqs. (10)-(13) we obtain the following relationship for ΔI_b

$$\Delta I_b = \left[2eB\mu\tau^{-1} \left(I_d + \frac{\alpha\gamma lsb\Omega d\sqrt{8} \cdot 10^{-46} N_e^2}{4\pi (kT_e)^{\frac{1}{2}}} \right) \right]^{\frac{1}{2}} \quad (14)$$

We shall consider first the dependence of I_1, ΔI_b, and $I_1/\Delta I_b$ on N_e—the electron concentration in the luminous cloud of the source.

We assume the following numerical values for the quantities entering into these expressions: for the line under consideration $\lambda = 3000$ A, $\chi = 4$ ev, $A = 10^8$ sec^{-1}, $\langle \sigma v \rangle \approx 10^{-10}$, $\langle \sigma' v' \rangle \approx 10^{-7}$; for the luminous cloud in the source, $T_e = 7000°$, $l = 10^{-1}$ cm; for the spectral apparatus, $s = s' = 5 \times 10^{-3}$ cm, $b = 1$ cm, $\Omega = 10^{-2}$, $D = 20$ A/mm. For the detector, we assume a photomultiplier with the following parameters: $\gamma = 1$ amp/lum, $\mu = 10^5$, $I_d = 10^{-9}$ amp; recording time $\tau = 10$ sec. The calculated dependence of I_1, ΔI_b, and $I_1/\Delta I_b$ on N_e (on a logarithmic scale and in arbitrary units) is given in the Figure (curves 1, 2, and 3, respectively).

It follows from the Figure that for the chosen values of the constants, the greatest sensitivity (highest value of $I_1/\Delta I_b$) is obtained at $N_e \approx 10^{14}$ to 10^{15} electrons/cm^3. At lower N_e values, the line intensity is given by Eq. (8) and decreases proportionally to N_e, whereas the intensity of the background signal is determined by the dark current of the photomultiplier and remains practically constant. For higher N_e values, the line intensity reaches a constant value [Eq. (7)] because of the increasing influence

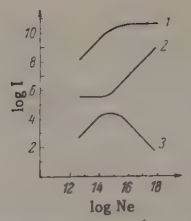

Dependence of the values I_1 (curve 1), ΔI_b (curve 2) and $I_1/\Delta I_b$ (curve 3) on the electron concentration in the luminous cloud of the source.

of quenching collisions with electrons, whereas the background intensity increases rapidly, being determined by the interaction of electrons with ions.*

*When the recording is done photographically, the mean fluctuation of the optical density discussed previously is given by $\sqrt{n_f + n_c}$, where n_f is the number of developed grains caused by the fog, and n_c is the number of grains produced by the continuous background. Thus, when the intensity of the continuous spectrum is low, the sensitivity is given by the square root of the fog density, and when it is high, by the square root of the intensity of the continuous spectrum.

It must be mentioned that in the above calculations the electronic temperature of the discharge was assumed to be constant. Actually, of course, sources with different electron concentrations also have different temperatures. The influence of the source temperature on the sensitivity of analysis must be considered separately.

The next parameter influencing the sensitivity of analysis is the exposure time τ. Increasing τ reduces the value of ΔI_b proportionally to $\tau^{1/2}$, but as we shall see later, the number of atoms leaving the source is increasing at the same time proportionally to τ. Thus, an increase in τ is, on the whole, unfavorable.

Changing the parameters of the spectral apparatus —increasing the width and length of the slit and the optical speed, and increasing the sensitivity of the photomultiplier—increases the sensitivity of analysis: the latter is proportional to the product $\gamma sb\Omega$ for small N_e, and proportional to $(\gamma sb\Omega)^{1/2}$ for large N_e. Using a high dispersion instrument is advantageous, unless it involves a decrease of speed, as it usually does.

We shall now illustrate the above calculations by numerically estimating the limit of the spectral sensitivity for two typical excitation sources: the carbon arc and the low pressure hollow cathode discharge. N_e is approximately 10^{15} in the column of a free burning arc in air between carbon electrodes. In this case, Eq. (6) for the line intensity goes over into Eq. (7). With the numerical values assumed earlier, we obtain from (4)*

*In these and in the following calculations the results are rounded off to the nearest order of magnitude.

$$F_1' \approx 10^{-12} N_0 \text{ erg/sec.}$$

and from (3)

$$I_1 \approx 10^{-16} N_0 \text{ amp.}$$

For the continuous spectrum, (12) and (13) give us

$$F_c' \approx 10^{-4} \text{ erg/sec.}$$

and (11) gives us

$$I_c \approx 10^{-6} \text{ amp.}$$

The photocurrent from the continuous spectrum is

considerably greater than the dark current of the multiplier. For $\tau = 10$ sec, from (10), $\Delta I_b \approx 10^{-11}$ amp. In accordance with (2), we shall assume that for the line detection, $I_{1(min.)}$ must be about $10\Delta I_b$. From this we obtain: $N_{0(min.)} \approx 10^6$ atoms/cm³.

Taking the value 10^{-2} cm³, for the volume of the luminous cloud, we obtain $N_{min.} \approx 10^4$ for the smallest number of atoms. Thus with our assumptions, in order to detect a line, it is necessary to maintain an atomic concentration of 10^6 atoms/cm³ of the element to be analyzed for 10 sec.

We shall now attempt to estimate the number of atoms in the sample M which is necessary for this condition. It is apparent that M must be able to replace the losses of atoms of the element in the arc column during the time τ in order to maintain the concentration N_0. The removal from the arc column of the impurity atoms apparently occurs mainly in two ways: (1) by diffusion of atoms through the main gas filling the column, from the central parts of the column toward the periphery, and the formation at the periphery of molecules of various kinds, which subsequently escape into the atmosphere; (2) by removal of atoms of the main gas and the impurities by convection currents. We shall assume that the latter factor is somehow eliminated (for instance, by external stabilization of the column, etc.), so that there remains only atomic diffusion, which cannot be eliminated and which therefore determines the lower limit for atomic losses.

We shall consider an arc column in the form of a cylinder of diameter l and length L, and shall assume that all atoms of the impurity which diffuse to the walls of cylinder are removed from the discharge and do not participate further in the emission of light. The number of atoms which are lost by the column in unit time is then

$$q = S\beta\Delta N,$$

where S is the surface of the side of the column ($S = \pi lL$), $\beta = \mu_0^2 D/l^2$ ($\mu_0 = 2.4$ is the first root of the Bessel function of the zero order), D is the diffusion coefficient, and ΔN is the difference between the concentration of atoms at the axis and at the surface of the column. The diffusion coefficient is given by the well-known expression $D = u\lambda_c/3$, where $u = \sqrt{8kT/\pi m}$, m is the atomic mass of the impurity element, and λ_f is the mean free path ($\lambda_c = 1/\sqrt{2}\pi nd^2$, where n is the concentration of molecules of the main gas in the column, and d is the diameter of the gas molecule). Assuming that $n = 10^{18}$ cm^{-3}, $d^2 = 10^{-15}$ cm², and $m = 10^{-22}$ gm, we obtain $D = 10$ cm²/sec^{-1}.* Assuming for simplicity that the atomic concentration decreases linearly from the cylinder axis toward the surface, we obtain $\Delta N/2 = N_0$, where N_0 is the mean concentration in the volume.

According to the aforesaid, the smallest number of atoms in the sample must be equal to the number of atoms leaving the column during the time τ, that is, $M = q\tau = 4 \times 10^4 N_0 = 10^{10}$ atoms. Assuming the weight of one atom $m = 10^{-22}$ gm, we obtain for the minimum weight of the impurity element $P = 10^{-12}$ gm. Making the further assumption that the weight of the sample is 100 mg, the lowest detectable concentration C must be about 10^{-9}%.

*See the note added in proof at the end of the article.

Let us now consider the other example. The mechanism of the excitation of atoms in a hollow cathode discharge is not yet well known. However, one may assume that the excitation of neutral atoms is due essentially to collisions with electrons, if there are no secondary processes, so that the line intensity is given by (8).

Assuming $N_e = 10^{13}$ electrons/cm³, and using the previous values for the excitation cross section and the parameters of the spectral apparatus, Eq. (4) gives us

$$F_1' \approx 10^{-14} N_0 \text{ erg/sec.}$$

and

$$I_1 \approx 10^{-18} N_0 \text{ amp.}$$

for the flux from the line and the photocurrent.

For the flux from the continuous spectrum, (12) and (13) give us $F_c' = 10^{-8}$ erg/sec; that is, the intensity of the continuous spectrum is so low that the photocurrent caused by it is smaller than the dark current of the photomultiplier. In this case, the lowest detectable line intensity is determined by the mean fluctuation of the dark current of the multiplier. Taking the recording time $\tau = 100$ sec, we get from (10)

$$\Delta I_b \approx 10^{-12} \text{ amp.}$$

Assuming as before that the lowest detectable line intensity satisfies the condition,

$$I_{1(min)} = 10\Delta I_b,$$

we get: $N_{0(min.)} = 10^7$ atoms/cm³.

Taking the volume of the luminous cloud as 10^{-2} cm³, we obtain

$$N_{(min)} \approx 10^5 \text{ atoms.}$$

In order to estimate the total number of atoms in the sample M that are necessary for maintaining the concentration N_0 in the luminous volume of the hollow cathode, it can be assumed that the concentration N_0 must be maintained throughout the volume of the tube (atoms deposited on the walls can be returned to the tube volume by heating the walls). Taking $V = 10^2$ cm³, we obtain $M = VN_0 = 10^9$ atoms. Therefore, with $m = 10^{-22}$ gm, the smallest detectable quantity of the element is $P = 10^{-13}$ gm. If the weight of the sample is 100 mg, the smallest concentration is $C = 10^{-10}$%.

A summary of the results obtained is given in the Table.

Thus, despite the difference in the excitation sources, the sensitivity of detection is very similar in the two cases.

The estimations of the limits of sensitivity given in the table exceed the values obtainable at present in the usual analytical procedures by approximately two or three orders of magnitude.

However, it should be pointed out once more that the physical situation on which the above calculations are based is highly idealized, and that the numerical values of the quantities used in the calculations (such as, for instance, the transition probabilities, excitation cross sections, conditions for evaporation of samples, and so forth) can vary considerably in actual cases. Therefore, as was pointed out in the beginning of this article, these estimations of sensitivity should not be taken quantita-

Excitation source	Arc	Hollow cathode
Minimum number of impurity atoms in the luminous cloud of the source N (atoms)	10^4	10^5
Minimum concentration of impurity atoms in the luminous cloud of the source N_0 (atoms/cm³)	10^4	10^7
Minimum number of impurity atoms in the sample M (atoms)	10^{10}	10^9
Minimum detectable weight of impurity P (gm)	10^{-12}	10^{-13}
Minimum detectable concentration of the impurity C (%)	10^{-9}	10^{-10}

tively, but should be considered essentially from the qualitative point of view.

The data given above show that a relatively small number of atoms of the element in the luminous cloud of the source is sufficient to give a detectable line. Comparison of the values of N and M shows that the main loss of sensitivity, which amounts to several orders of magnitude, is due to the unfavorable transfer of atoms from the sample into the luminous cloud of the source and to the poor retention of atoms in that region. It appears, as mentioned in ref. 1, that the main potentialities for increasing the sensitivity of spectral analysis lie in improving these stages of the procedure and in improving methods for enriching the samples.

Note added in proof: In a recently published paper, Ya. D. Raikhbaum and V. M. Malykh [Opt. i Spektr. 9, 425 (1960), Optics and Spectroscopy 9, 223 (1960)] obtained D ~ 10-20 cm^2/sec for the diffusion coefficient of atoms in the arc column.

REFERENCES

1. L. V. Lipis, Uspekhi Fiz. Nauk 68, 71 (1959), Soviet Phys.-Uspekhi 3, 393 (1959).
2. L. N. Filimonov, Zavodskaya Lab. 25, 936 (1959).
3. H. Kaiser, Spectrochim. Acta 3, 40 (1947).
4. A. Unsöld, Ann. Physik 33, 607 (1938).
5. W. Lochte-Holtgreven, Repts. Progr. Phys. 21, 312 (1958).

THE PLASMATRON (PLASMA JET) AS A LIGHT SOURCE FOR SPECTROSCOPY

F. A. Korolev and Iu. K. Kvaratskheli (pp. 398-402)

Received 5 May 1960

The excitation conditions of the spectrum in the plasma jet obtained with a gaseous plasmatron have been studied. It was found that when argon is used, a temperature of over 10,000°K is obtained in the plasma jet and temperature equilibrium prevails. The plasmatron was shown to be highly efficient as a light source for the spectral analysis of refractory specimens (slags). The possibility was indicated of determining the transition probabilities of a broad class of substances with the plasmatron.

INTRODUCTION

One of the basic problems of applied spectroscopy and spectral analysis is improving the sensitivity of spectroscopic determinations, enhancing their precision, broadening the class of substances which can be studied and analyzed and, finally, automating analytical methods. The disadvantages of the majority of light sources for emission analysis must be overcome. These disadvantages include the variation of the arc temperature with electrode material and ambient conditions (atmosphere, electrode shape, etc.). It is well known that blowing the arc gap reduces these disadvantages to some extent.[1]

Recently, several papers have been published showing that a special electrode shape combined with the use of a rapid stream of inert gas gives a considerable increase in the temperature of a dc arc.

The first of these devices—plasmatrons—was used in supersonic aerodynamics.[2-8] They were then applied to welding and cutting metals[9,10] and finally to spectral analysis.[11,12] The present paper is devoted to an investigation of some of the characteristics of the plasmatron as a light source for spectroscopy.

APPARATUS AND EXPERIMENTAL METHOD

We used the plasmatron arrangement shown in Fig. 1. It consists of a closed chamber formed by the metal rings 1 and 2 and the insulator 3. The arc is struck between the anode 5 and the graphite cathode 4; the latter is an annulus. When argon at a pressure of 0.3 to 5 atm is passed into the chamber, the discharge takes the form of a jet I which is joined to the cathode by a thin discharge column II and is surrounded by a corona of vapor of easily ionized material III.

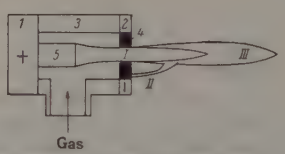

Fig. 1. Diagram of the plasmatron.

We studied the possibility of exciting the spectrum of refractory and difficultly excited substances. For the test specimen we used powdered slags mixed with Co_2O_3 and powdered graphite, which were fed into an opening in the cup-shaped anode. The electrode spacing was 3 mm. The spectrograms were taken with an ISP-22 spectrograph. Reference 13 gives a detailed description of the construction and operation of the plasmatron.

RESULTS

Figures 2a, b, and c show the external characteristics of the discharge. Fig. 3 gives a plot of the ratio of the intensity of the spectral lines to the transition probability as a function of the energy of the upper level. These graphs show that thermal equilibrium exists at both the base (Fig. a) and the tip (Fig. b) of the jet. Consequently, Ornstein's method may be used for determining the temperature. For this purpose, we used the Fe I and Fe II lines whose transition probabilities were given by Sobolev.[14] The temperature proved to be greatly dependent on the gas pressure in the plasmatron (see Table 1). Figure 4 gives the variation of temperature along the jet. We used four standard samples (slags) with known Fe_2O_3 contents to determine the effect of the electrode material and the nature of the gas on the temperature.

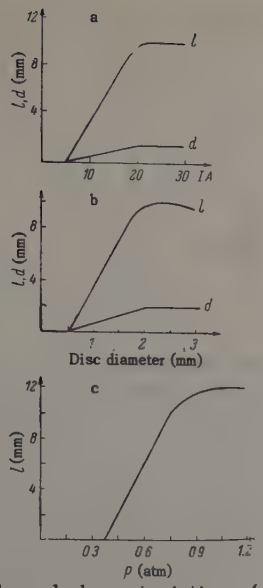

Fig. 2. External characteristics. (a) Length l and diameter d of the plasma plotted against current I. Pressure—0.7 atm; diameter D of the aperture—1.6 mm. (b) l and d plotted against diameter D of the aperture. Current—20 amp; pressure—0.7 atm. (c) l plotted against pressure p.

Two sets of standards were prepared:

(1) 1 part by weight slag, 1 part by weight Co_2O_3, 2 parts by weight powdered graphite.

(2) 1 part by weight slag, 1 part by weight Co_2O_3, 2 parts by weight powdered graphite, 2 parts by weight $KMnO_4$.

Calibration curves (Fig. 5) were plotted from these two sets of standards.

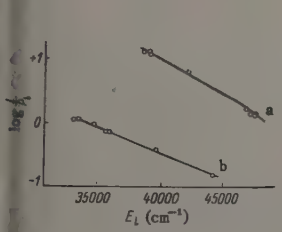

Fig. 3

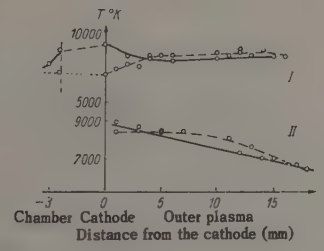

Fig. 4

Fig. 3. Log I/p_i plotted against energy of the upper level E_i ($p_i = h\nu_i A_i g_i / g_0$, where ν_i is the frequency of the line under study, A_i is the transition probability, g_i, g_0 are the statistical weights of the upper and normal states). Curve a—base of the jet; curve b—tip of the jet.

Fig. 4. Temperature distribution along the jet. I—Argon pressure p = 0.5 atm; D = 1.6 mm. II—Argon pressure p = 0.16 atm; D = 3.5 mm. Solid curves—temperatures obtained from spark lines; dotted curves—temperatures obtained from arc lines.

Figure 5 shows that the type of gas, the diameter of the aperture, and the pressure greatly affect not only the discharge temperature, but also the dependence of the temperature on the electrode material. The absolute intensity of the lines is greater when argon is used than when nitrogen is used. It is interesting also to note that when the test specimen was mixed with powdered Co_2O_3 and graphite in the ratio 1 : 1 : 2, there was hardly any fractionation, as Fig. 6 shows.

Table 1. Variation of Temperature with Pressure

Excess pressure in the chamber atm	Temperature of the plasma jet (° K)	
	From Fe I lines	From Fe II lines
0.4	9600 ± 300	9000 ± 300° K
1.0	9200 ± 300	9500 ± 300° K
1.7	9200 ± 300	11000 ± 500° K
2.4	8100 ± 300	11400 ± 500° K

Since the diameter of the jet is very small, the pressure within it is low (the flow velocity of the gas reached 200-300 meters/sec) and the discharge occurred in almost pure argon. Self-absorption was consequently very low. Figure 7 shows the contour of the Mg 2852 A line across four cross sections of the plasma jet.

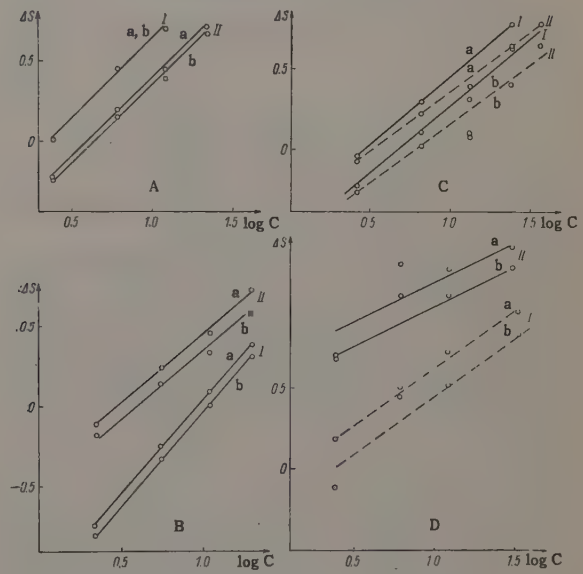

Fig. 5. Calibration curves for (I) the first and (II) the second system of standards. (a) Fe II 2628 A line; (b) Fe II 2562 A line; comparison line Co I 3044 A. ΔS—density differences; C—concentration. (''Spektral'nye type 1'' plates; ISP-22 spectrograph). A—Diameter of the cathode aperture D = 1.6 mm; argon pressure in the chamber p = 0.6 atm; current I = 20 amp; distance between the electrodes l = 3 mm. B—D = 3.5 mm; p(argon) = 0.16 atm; I = 20 amp; l = 3 mm. C—D = 1.6 mm, p(nitrogen) = 0.6 atm; I = 15 amp; l = 3 mm. D—D = 3.5 mm; p(nitrogen) = 0.16 atm; I = 20 amp; l = 3 mm.

From what has already been said, it follows that when argon is used at a chamber pressure above 0.4 atm with a cathode aperture of 1.6 mm, the plasmatron has many advantages: the temperature is independent of the electrode material and is uniform along the length of the plasma; temperature equilibrium prevails over the whole outer volume of the plasma; negligible self-absorption occurs in the outer part of the plasma; finally, fractionation is almost absent.

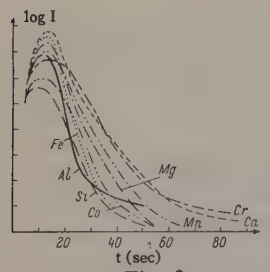

Fig. 6

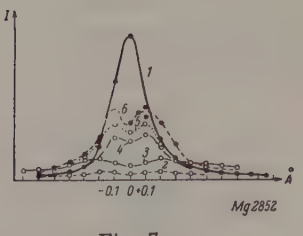

Fig. 7

Fig. 6. Evaporation curves.

Fig. 7. Contour of the Mg 2852 A line. Curve 1—outer part of the jet; curve 2—at the anode; curve 3—between the anode and the cathode inside the chamber; curve 4—at the inner surface of the cathode; curve 5—contour of the line in the jet when nitrogen is used in the plasmatron (cathode aperture 3.5 mm, chamber pressure 0.16 atm); curve 6—contour of the line in the activated ac arc.

These properties enabled us to apply the plasmatron successfully to the spectral analysis of a wide range of refractory substances, in particular, to slags. A precision of 4 to 5% was obtained from the combined graphs (see refs. 13 and 14). The plasmatron was also applied to determining relative oscillator strengths. We determined relative oscillator strengths from the shifts of the calibrating graphs for corresponding Fe, Ca, Mn, Al lines. The graphs were constructed with the aid of 10 to 12 standard specimens. Table 2 gives the results. They show that the accuracy of determining f is fully comparable with that of such laborious methods as the "hook" method.

Table 2. Relative Oscillator Strengths f

Line (A)	Author		Plasmatron	Line (A)	Author		Plasmatron
Fe II	King[15]	Sobolev[13]		MnI	Theory[16]		
2983	40	40	40	4034.5	4	—	4
2994	48	49	46	4033.1	6	—	5.8
3001	51	50	48	4030.7	8	—	7.8
3025	18	27	28	Ca II		Nikonov and Prokov'ev[16]	
3037	38	41	40				
3047	50	52	56	3933.7	—	1.96	1.90
3059	42	45	51	3968.5	—	1.00	1.00
3057	500	595	595	Al I		Nikonov and Prokov'ev[16]	
3067	520	360	380				
3075	490	220	240	3961.5	—	1.00	1.00
				3044.0	—	0.98	1.05

REFERENCES

1. F. A. Korolev and Zh. Zheenbaev, Izvest. Vyssh. Uchenye Zaved., Fiz. No. 5, 134 (1959).
2. Missiles and Rockets **2**, No. 3, 29 (1957).
3. The Christian Science Monitor **3**, No. 108, 6 (1957).
4. Amer. Aviation **20**, No. 21, 28 (1957).
5. Aviation Week **66** No. 10, 31 (1957); Ibid. **66**, No. 12, 30-31 (1957).
6. G. Giannini, Sci. American **197**, No. 2, 80, 86 (1957).
7. G. N. Paterson, Can. Aeronaut. J. **4**, No. 1/3, 3, 39, 79 (1958).
8. I. Stone, Aviation Week **69**, No. 15, 48 (1958).
9. I. D. Kulagin and A. V. Nikolaev, Svarochnoe Proizvodstvo No. 9, 1 (1958).
10. K. V. Vasil'ev and A. A. Isachenko, Svarochnoe Proizvodstvo No. 9, 5 (1958).
11. B. F. Scribner, Spectrochim. Acta No. 2, 133 (1959).
12. F. A. Korolev and Vainshtein, Zhur. Anal. Khim. **14**, 618 (1959).
13. Iu. K. Kvaratskheli, Zavodskaya Lab. No. 5, 537 (1960).
14. N. N. Sobolev, Zhur. Eksptl. i Teoret. Fiz. **13**, 131 (1943).
15. R. B. King and A. S. King, Astrophys. J. **87**, 24 (1938).
16. E. I. Nikonova and V. K. Prokov'ev, Opt. i Spektr. **1**, 290 (1956).

AN ATOMIC BEAM AS LIGHT SOURCE FOR STUDYING SPECTRA OF GASES

V. I. Odintsov (pp. 403-409)

Received 14 May 1960

An atomic beam arrangement has been constructed which makes it possible to obtain extremely narrow spectral lines of elements which are gaseous under ordinary conditions.

INTRODUCTION

Since the first experiments of Dobretsov and Terenin[1] atomic beams have been repeatedly used in a variety of spectroscopic problems; however, up to the present no apparatus has been constructed in which the atomic beam method could be used for studying elements (gases) which are difficult to condense. Attempts to do this have been made by several authors[2-4] but have not been crowned with success.

As is well-known the essential feature of a gaseous atomic beam[2,5] is that the substance being studied in this case cannot be condensed on cooled surfaces inside the apparatus and must be removed by pumping. This creates the condition that, in the region in which the excitation of the atomic beam takes place, along with the beam atoms there exist also "scattered" atoms having large velocity components in the direction of observation. The total emission of these "scattered" atoms gives a broad spectral line which is superposed on the narrow line given by the atomic beam.

If the width of the line emitted by the atoms of the beam is much less than the width of the line emitted by the "scattered" atoms, the radiation from the "scattered" atoms leads essentially to the development of "wings" on the profile of the line under study or to the appearance of a more or less strong background.

SPECIAL FEATURES OF THE EXCITATION OF A GASEOUS ATOMIC BEAM

The formation of an atomic beam for the case in which two slits are used is illustrated in Fig. 1. Atoms

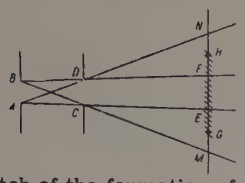

Fig. 1. Sketch of the formation of an atomic beam.

which issue from the "oven" through the first slit AB and which pass without undergoing collisions through the second (collimator) slit CD form the atomic beam.

In order to reduce the intensity of the radiation from the "scattered" atoms in the case of a gaseous atomic beam it is necessary, as Mack and Barkofsky[2] have pointed out, to use a sufficiently narrow beam of electrons to excite the atomic beam.* If the emission of the atomic beam is observed along the straight line MN, perpendicular to the axis of the beam, the width of the electron beam GH exciting the atomic beam* should not substantially exceed the geometrical dimensions of the atomic beam MN.

*We will restrict ourselves to the discussion of beams with electron excitation of the light emission.

*It is assumed that the electron beam used to excite the atomic beam has a direction perpendicular to the plane of the diagram, and that it has a uniform density and is positioned symmetrically with respect to the axis of the atomic beam.

Mack and Barkofsky[2] recommend in their paper that the excitation should not extend at all to the region of the penumbra, EM and FN; we cannot however agree with this. A more detailed consideration of the question shows that there exists a certain optimal degree of limitation of the region of excitation; this depends on the ratios h/l and s_1/s_2, where h is the distance between the beam slits, l is the distance from the first slit to the point of observation of the emission, and s_1 and s_2 are the widths of the first and second slits of the beam.* If the degree of limitation of the region of excitation of the beam is specified by the ratio $\zeta = EG/EM$, then for most practical designs the optimal value of ζ is 0.5-0.6.

*Here and in what follows we will assume that $s_1 \leq s_2$.

In connection with the necessity of limiting the region of excitation in gaseous atomic beams it was of interest to determine how this limitation affects the width of the spectral line emitted by the atoms of the beam. For this purpose we carried out a calculation on the intensity distribution of the emission of an atomic beam for the case in which the electron beam which produces excitation of the atomic beam can have any given width; this is a more general case than that considered in the study by Minkowski and Bruck.[6]* As in the calculation of Minkowski and Bruck, we did not take into account the small effect of the size of the first slit in the direction perpendicular to the line of observation of the beam emission on the distribution on the emission intensity.

*Minkowski and Bruck assumed that the excitation of the beam occurs along its whole width, that is, GH ≥ MN (Fig. 1). It is obvious that the case for which GH ≤ EF is also included in the expression of Minkowski and Bruck.

From the expression obtained for the intensity distribution it was found that, if $s_2/h \leq 1$, the Doppler width $\delta\nu$ of the line emitted by the atomic beam can be given in the form

$$\delta\nu = K(\xi, \eta, \zeta)\frac{s_2}{h}\delta\nu_0,$$

where $\xi = h/l$, $\eta = s_1/s_2$, and $\delta\nu_0$ is the Doppler width of the line emitted by atoms at the temperature of the "oven." This formula remains valid to a very high degree of accuracy even in cases when the ratio s_2/h is not very small, i.e., up to values of s_2/h equal to 0.3-0.5. The coefficients $K(\xi, \eta, \zeta)$ can be determined by a graphical procedure. As an example, Fig. 2 shows the dependence of K on $\zeta (0 \leq \zeta \leq 1)$ with $\eta = 1$ for several values of ξ; curves like these permit the determination of the Doppler width of the line for any values of ξ. Figure 3 shows the dependence of K on η for $\zeta = 1$; this is valid for all values of ξ.

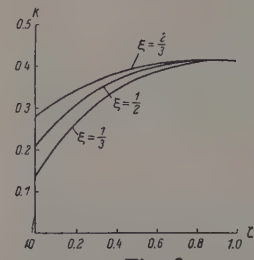

Fig. 2

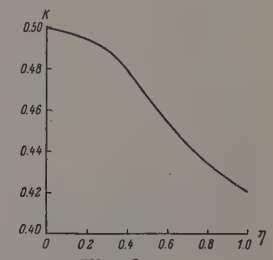

Fig. 3

Fig. 2. Variation of K with ζ for $\eta = 1$.
Fig. 3. Variation of K with η for $\zeta = 1$.

DIMENSIONS AND POSITIONING OF THE BEAM SLITS

An approximate calculation of the density of "scattered" atoms was carried out for various apparatus designs. The calculation showed that good results can be achieved if two slits (Fig. 1) are used to form the atomic beam, provided that observation of the beam emission takes place at a considerable distance from the second slit and that a sufficiently narrow beam of electrons is used for the excitation of the beam.

In our arrangement the ratio h/l is equal to 1:3, the beam slits being placed perpendicular to the line of observation of the emission, as in the arrangement used by Mack and Barkofsky; the length of the first slit a_1 was ~0.6 l.

A calculation showed that for small ratios s_1/s_2 it is possible to achieve a better ratio of the emission intensity of the atomic beam to the emission intensity of the "scattered" atoms. Moreover, it is convenient to work with a first slit of small width in view of the fact that it is unnecessary to replace it in going over to a higher degree of collimation of the beam.

On the other hand, if s_1 is decreased the ratio a_1/s_1 increases and this leads to an increase in the number of collisions between the atoms issuing from the first slit* (we assume that the density of the atoms in the "oven" increases proportionally to $1/s_1$).[6] If the density of the atoms in the "oven" is such that the mean free path λ of the atoms in the "oven is equal to s_1, then, according to our approximate estimate, for $a_1/s_1 = 15$ about 20% of the atoms issuing from the first slit collide with each other; for $a_1/s_1 = 100$ this number increases to 33% and for $a_1/s_1 = 333$ to 39%. In the case of a circular aperture of diameter d the number of colliding atoms for $\lambda = d$ amounts to only 10%. Collisions of atoms issuing from the "oven" constitute one of the sources of "scattered" atoms in the excitation chamber; "scattered" atoms of

*This question is closely related to that of the formation of a "cloud" of atoms behind the "oven" slit.[7,8]

this kind are present even in atomic beams of metal atoms. The increase in the number of such collisions which occurs when the width of the first slit is reduced does not lead, however, to an increase in the Doppler width of the line emitted by the atomic beam, since it arises as a result of an increase of the number of collisions near the first slit.

In our arrangement the ratio s_1/s_2 for not very highly collimated beams is considerably less than 1.

In cases where the width of the electron beam exciting the atomic beam is considerably greater than the geometrical dimensions of the atomic beam, better results can be obtained by using an arrangement with three slits. In our design three slits are used when working with high collimations, when the width of the atomic beam in the direction of observation is small.

We have not yet said anything about the relation between the dimensions of the slit system and the capacity of the pumps used for evacuating the apparatus chamber. Let us assume that there is a proportionate change in the absolute dimensions of only that part of the apparatus*

*It is not difficult to convince oneself that, if there is a proportionate decrease in the absolute dimensions of the whole arrangement by factor k, the density of atoms with given velocity components at any point in the apparatus increases by the factor k, provided that the speed of evacuation by the pumps decreases at the same time by the factor k^2, and the atom density in the "oven" increases by the factor k. Thus, for a proportionate decrease in the width of the electron beam and a constant current density of electrons, such a change in the absolute dimensions of the apparatus does not affect the intensity distribution of the emission nor its brightness.

which is situated near the slits of the atomic beam and which is related to the formation and excitation of the beam (that is, there is a proportionate change in h, l, the dimensions of the slits, the cross section of the electron beam, and the dimensions of the separating partitions near the slits). The absolute dimensions of this part of the apparatus or, as we will say, the absolute dimensions of the slit system, can be specified for example, by the value of l, that is, the distance from the first slit to the point of observation of the beam emission. For a change in l (if we assume that the atom density in the "oven" changes as 1/l), the atom density in the beam, n, will change as 1/l. The density of "scattered" atoms, n*, can be divided into two parts: $n^* = n_1^* + n_2^*$; the first part n_1^* is due to atoms which, on issuing from the "oven" slit, did not leave the region near the beam slits which we have isolated, and the second part n_2^* is due to the atoms which have left this region. Obviously n_1^* is proportional to 1/l, so that the ratio n_1^*/n remains constant when l changes. Consequently the efficiency of any given set of absolute dimensions of the slit system (for the same set of pumps) is determined by the ratio n_2^*/n. A calculation shows that if the pumping speeds used for the evacuation of the apparatus chamber are less than certain values, which depend on the dimensions and shape of the tubes connecting the pumps to the space near the slits, it is always advantageous to decrease the absolute dimensions of the slit system, since n* decreases or increases more slowly than 1/l. We note that for most designs which are feasible in practice the pumping speeds are much less than the values referred to. Thus it is advantageous to decrease the absolute dimensions of the slit system as long as n_2^* is not significantly smaller than n_1^*. In practice, in decreasing the dimensions, one has to take account of the feasibility of obtaining a sufficiently narrow electron beam for exciting the atomic beam, and also the increasing technical difficulties involved in decreasing the absolute dimensions of the slit system and with decreasing the luminous part of the beam. In this connection the use of more powerful pumps has considerable advantages.

In our apparatus evacuation of all the chambers is carried out with TsVL-100 pumps; the value of 1 is 3-5 mm.

ARRANGEMENT OF THE APPARATUS

In Fig. 4 the arrangement of the apparatus is schematically portrayed (apart from some subsidiary details). The essential part of the apparatus is the metal chamber 1, evacuated by four TsVL-100 pumps.* It can be divided

*To improve the evacuation of the apparatus the addition of the more powerful N-5S pump has been provided for.

into several chambers with independent pumping by means of partitions with rectangular slits for the passage of the beam. Figure 4 shows the variant of the apparatus in which three slits are used to obtain the atomic beam.

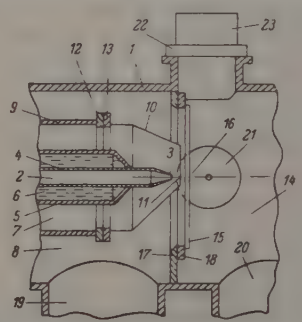

Fig. 4. Diagram of the gaseous atomic beam apparatus.

In working with monatomic gases* the gas to be stud-

*In studying diatomic gases the necessity of preliminary dissociation of the gas molecules arises. We propose to use an ultrahigh frequency discharge for this purpose. The apparatus for this has not yet been tested.

ied is admitted through a needle valve into a vessel provided with an oil manometer; it is then introduced through a narrow capillary into the first chamber ("oven") 2, which ends in the first slit 3. The first chamber consists of the metal tube 4 which passes through the cylindrical reservoir 5 which can be filled with liquid nitrogen 6. To facilitate heat exchange between the gas and the walls of the tube a piece of wire gauze is inserted in the tube. Cooling of the gas in the first chamber gives an additional reduction in the Doppler width of the spectral lines and also reduces the consumption of the substance being studied.

By regulating the gas input the required pressure can be established in the first chamber; this pressure is usually chosen so that the mean free path of the gas atoms in the first chamber is approximately equal to the width of the first slit.

The second chamber 7 is separated from the third chamber 8 by the cylinder 9 with a removable end-piece 10 which carries the second slit 11. A vacuum seal between the cylinder and the removable end-piece is made by means of the two flat-ground flanges 12 and 13. The second chamber is evacuated by a diffusion pump which is connected with it by a side-tube (the pump and side-tube are not shown in the diagram). The third chamber 8 and the fourth chamber (excitation chamber) 14 are

separated from each other by the removable partition 15 with the third slit 16. The vacuum seal here is also made by means of two flat-ground flanges 17, 18. The third chamber is evacuated by the pump 19. The fourth chamber is evacuated by two pumps, only one of which (20) is shown on the diagram.

If beam atoms constitute the greater part of all the gas atoms which penetrate into the excitation chamber from the preceding chamber, then, in order to lower the gas pressure in the excitation chamber it is advantageous to divide the latter into two parts with independent pumping by a partition with a slit which allows the beam atoms to pass through. This division, which was provided in the apparatus of Mack and Barkofsky,[6] can also be realized in our arrangement.

The width of the first slit of the atomic beam is approximately equal to 0.05 mm and its length is about 2 mm; the width of the second and third slits is chosen with regard to the beam collimation required, and their length is approximately equal to the length of the first slit. To change the slits, for example, in going over to a different beam collimation, the partitions 10 and 15 along with the flanges 13 and 18 are taken out.

All the slits of the atomic beam are positioned horizontally (i.e., parpendicular to the plane of the diagram in Fig. 4). The alignment of the slits is carried out by moving the second and third slits, which together with the flanges 13 and 18 can be displaced by special attachments.

Excitation of the atomic beam is affected by an electron gun (the gun anode is seen at 21 in Fig. 4) mounted on a special holder, which allows it to be brought into the required position with respect to the axis of the atomic beam. The electron current which excites the beam emission is directed perpendicular to the plane of the diagram. The beam emission is observed through the optical window 22 by means of the reflecting prism 23.

All the diffusion pumps used for evacuating the apparatus are provided with liquid nitrogen traps which prevent the penetration of oil vapor into the volume being evacuated. Another liquid nitrogen trap is situated in the excitation chamber. The ultimate vacuum attainable in the apparatus is at least 5×10^{-7} mm Hg.

In cases in which two slits are used to obtain the atomic beam the partition 15 is removed.

If elimination of the background is not important and if a certain line width can be tolerated, experiments have shown that it is possible to work in general without a collimator slit. To do this both partitions 10 and 15 are taken away.* In this case the "collimation" of the atomic "beam" is determined by the width of the electron beam and its distance from the first slit. One of the disadvantages of this arrangement, which cannot be eliminated by increasing the pumping speed, is the copious scattering of atoms issuing from the "oven" slit on the anode of the electron gun and on other components situated near the point where the excitation of the emission takes place.

Excitation of the atomic beam emission is effected by an axially symmetrical single-potential electron gun with a spherical cathode,* designed according to the method of Pers.[10] The spherical oxide-coated cathode (Fig. 5), made of nickel, has a radius 7 mm. The bifilar spiral 2 is used to preheat the cathode. The shapes of the cathode electrode 3 and of the anode 4 are patterned after the electrolytic bath.[10] The gun was assembled using the quartz rings 5 and 6. The diameter of the electron beam at its minimal cross section was not more than 0.4 mm. The current density in this cross section was approximately 6 amp/cm² for a potential difference of 600 volts between the anode and cathode. This rather high density of the exciting current, due to good focusing and the small absolute dimensions of the gun, gave efficient excitation of the atomic beam.

*If it is necessary the electron gun can be moved into a special chamber with separate pumping.

*An electron gun with an elliptical cathode, as described by Heil and Ebers,[9] was also prepared; however, it proved less satisfactory for exciting the atomic beam since the electron beam diverged rapidly after leaving the anode.

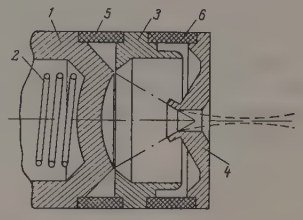

Fig. 5. The electron gun.

Figure 6 shows the optical arrangement for projecting the beam emission on the slit of the spectrograph. In this diagram 1 is the luminescent portion of the beam, 2 a cylindrical lens which elongates the image of the luminescent portion of the beam on the slit of the spectrograph,* 3 the optical window of the vacuum chamber, 4 a reflecting prism, 5 a condensing lens, and 6 the slit of the spectrograph.* The diagram also shows a lens 7 and a plane mirror 8 which also allows use to be made of light emitted from the atomic beam in the opposite direction, i.e., downwards from the luminous portion of the beam 1. The distance from the mirror to the lens [sic: translator] and from the lens to the luminous part of the beam is equal to the focal length of the lens.

*It is obvious that on going away from the central portion of this elongated image the Doppler width of the line increases.

*This system of illumination could be improved by mounting a second cylindrical lens between the cylindrical lens 2 and the lens 5. It is also possible to use a system of two cylindrical lenses only.

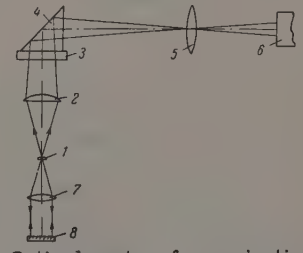

Fig. 6. Optical system for projecting the radiation on the spectrograph slit.

Figure 7 shows two interferograms of the green helium line at 5016 A; these illustrate the possibilities of a gaseous atomic beam in decreasing the Doppler width of spectral lines.

Fig. 7. Interferograms of the yellow helium line at 5016 A obtained with (a) the atomic beam and (b) a hollow-cathode discharge tube.

In the first case (a) the source of light used was an atomic beam of helium with 1:8 collimation. The spacing of the Fabry-Perot etalon was 70 mm. The exposure time on a plate with isopanchromatic (?: translator) sensitivity of 180 units GOST' was 5 min with a spectrograph camera of relative aperture 1:10.

In the second case (b) the source of light was a hollow-cathode discharge tube cooled with liquid nitrogen. As a consequence of the large Doppler width of the line emitted by the hollow cathode, this photograph had to be made with a smaller etalon spacing (50 mm).

The gaseous atomic beam apparatus described above will be used in the near future in the study of the structure of lines of some of the rare gases.

In conclusion the author wishes to express his gratitude to F. A. Korolev for proposing the problem and supervising its execution.

REFERENCES

1. L. N. Dobretsov and A. N. Terenin, Naturwissenschaften **16**, 656 (1928).
2. J. E. Mack and E. C. Barkofsky, Revs. Modern Phys. **14**, 82 (1942).
3. J. W. Drinkwater, O. Richardson, and W. E. Williams, Proc. Roy. Soc. (London) **A174**, 164 (1940).
4. W. E. Williams, Revs. Modern Phys. **14**, 94 (1942).
5. R. G. J. Fraser, "Molecular Rays." Cambridge Univ. Press, 1931.
6. R. Minkowski and H. Bruck, Z. Physik **95**, 274 (1935).
7. F. Knauer and O. Stern, Z. Physik **39**, 755 (1926).
8. M. Kratzenstein, Z. Physik **93**, 289 (1935).
9. O. Heil and J. J. Ebers, Proc. I.R.E. **38**, 645 (1950).
10. Dj. R. Pers, Teoriya i raschet elektronnykh puchkov (Theory and design of electron guns). Moscow, 1956.

SHORT COMMUNICATIONS

THE DISTRIBUTION OF ATOMS AMONG THE EXCITED LEVELS IN A LOW PRESSURE ARC

I. M. Belousova and D. B. Gurevich (pp. 410-412)

Received 25 July 1960

It is frequently important to investigate the validity of Boltzmann's law for describing spectral line intensities. In the simplest case, when the atoms are excited by collisions of the first kind with electrons and fall back to the unexcited state by collisions of the second kind or by spontaneous emission, the criterion for the existence of a Boltzmann distribution is:[1,2]

$$\frac{N_e p_q}{A_i} > 1, \qquad (1)$$

where N_e is the concentration of electrons per cm³, $A_i = \sum_k A_{ik}$ is the probability of a transition from a given level to all possible lower levels;

$$p_q \approx \bar{s}_i \bar{v} \frac{g_0}{g_i} e^{\frac{E_i}{kT_e}} \qquad (2)$$

Here $\bar{s}_i$ is the mean effective excitation cross section, v is the mean electron velocity at the given temperature, T_e is the electron temperature, E_i is the excitation energy of the upper level, and g_0 and g_i are the statistical weights of the ground and excited states. At high electron concentrations, for example, in discharges at atmospheric pressure and fairly high current densities, this relationship is satisfied. At low pressures or low current densities, the population of certain levels may vary considerably from the Boltzmann distribution and must be estimated for each individual case. This very difficult in practice since the effective cross sections are largely unknown. Experimental verification of the existence of a Boltzmann distribution for the levels $^3P_1$, $^3P_2$, $^1P_1$, $^3S_1$ of mercury atoms was obtained by Kagan and Penkin and by Semenova for individual lines of Sr and Zn.

We have confirmed the existence of a Boltzmann distribution for certain lines of Fe I and Ba II at pressures ranging from 760 to 20 mm Hg. The test was made by comparing the "excitation temperatures" obtained by measuring the relative intensities of these lines. If all of the temperature values agreed, this would indicate that the population of the levels followed a Boltzmann distribution. If we determine the conditions under which the individual levels no longer have a Boltzmann population, knowing the electron concentration, we can estimate the effective excitation cross sections.

The spectrum was excited in an arc between cored carbon electrodes, placed in a special chamber. The arc current was maintained constant at 5 amp. The spectral line intensities were measured with an SP-64 four-channel photoelectric spectrometer.[5] The detector was calibrated with a ribbon-filament lamp of known brightness temperature. A correction for reabsorption was made by the line absorption method, by superimposing an image of the source on the source itself.[6]

The Figure shows a graph of "excitation temperature" and gas temperature plotted against pressure. The "excitation temperature" was measured for different Fe I and Ba II lines and the gas temperature was determined from CN bands. Up to 100 mm Hg, the temperature

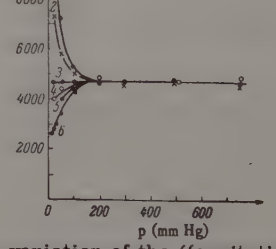

Pressure variation of the "excitation temperature" measured by means of Fe I and Ba II lines, and the gas temperature measured by means of CN. Curve 1—FeI(I_{5167}/I_{5371}); curve 2—BaII(I_{4899}/I_{4934}); curve 3—FeI(I_{4325}/I_{5371}); curve 4—CN; curve 5—FeI(I_{5233}/I_{5167}); curve 6—FeI(I_{4325}/I_{5167}).

values all agree; that is, the levels under consideration (see the table) have a Boltzmann population distribution and the electron temperature and the gas temperature are identical. At pressures below 100 mm Hg, the gas temperature begins to fall and the "excitation temperature" behaves differently for different lines; that is, the population of the levels does not conform to the Boltzmann distribution.

With decreasing pressure, the electron temperature should, in general, increase.[7] Fe I 5233 and 4325.8 were used as the lines of higher excitation potential, the "excitation temperature" began to fall at pressures below 100 mm (curves 5 and 6). We therefore conclude that the e^7D_5 and z^3G_3 levels, at which these lines originate, no longer have a Boltzmann population.

Element	λ	Transition	gf	E_i	$A_i = \sum_k A_{ik}$	$\frac{N_e P_q}{A_i}$	Si (cm²) estimate
Fe I	5233.95	$zP^0 - e^7D_5$	3.83	5.29	$3 \cdot 10^8$	$7 \cdot 10^{17} \cdot S_i$	$\sim 10^{-18}$
Fe I	4325.77	$a^3F - z^3G_3$	3.6	4.45	$2 \cdot 10^8$	$3 \cdot 10^{17} \cdot S_i$	$\sim 5 \cdot 10^{-18}$
Fe I	5167.5	$a^3F - {}^3D_3$	2.46	3.87	$8 \cdot 10^8$	$2.8 \cdot 10^{17} \cdot S_i$	$> 10^{-17}$
Fe I	5371.5	$a^5F - z^5D_2$	1.9	3.25	$5 \cdot 10^8$	$1.3 \cdot 10^{18} \cdot S_i$	$> 5 \cdot 10^{-18}$
Ba II	4934.06	$^2S'_{1/2} - {}^2P^0_{1/2}$	1.00	2.52	10^8	$4 \cdot 10^{16} \cdot S_i$	$> 5 \cdot 10^{-16}$
Ba II	4899.97	$^2S'_{1/2} - {}^2P^0_{3/2}$	1.55	5.25	$2 \cdot 10^8$	$1 \cdot 10^{16} \cdot S_i$	$> 5 \cdot 10^{-18}$

The Table gives data for the lines used in the temperature measurement. The values of gf were taken from King and Aartz.[8] Our estimates of the values of A_i are based on Crosswhite's results.[9] The conversion to absolute values was made according to Allen.[10] In the same Table we include values of $N_e p_q / A_i$; the value of the effective excitation cross section Si is not known. The electron concentration was obtained by measuring the ratio of the intensities of an atomic and an ionic barium line (Ba I 5535 A and Ba II 4554 A), at atmospheric pressure and at 100 mm Hg; that is, under conditions where Saha's equation applies. The measurements showed that at 760 mm Hg the concentration was $N_e = 9 \times 10^{14}$ cm^{-3} and at 100 mm Hg, $N_e = 3 \times 10^{14}$ cm^{-3}.

Equation (1) was evaluated for pressures a little below 100 mm Hg. We assumed that the electron concentration was approximately 10^{14} cm^{-3} and the electron temperature ~5500°K. Knowing the pressure range at which the Boltzmann distribution begins to break down, we can estimate the effective cross section. In fact, for the levels from which the 5233 and 4325.8 A lines are emitted, at $N_e = 10^{14}$ cm^{-3}, Eq. (1) should be approximately unity, that is, the effective cross section for the e^7D_5 level should be 10^{-18} cm², and for the z^3G^3 level somewhat higher, about 5×10^{-18} cm². For the levels from which the 5167 and 5371 A Fe and the 4934 and 4900 A Ba II lines are emitted, we can assume that Eq. (1) should be greater than unity under the same conditions, since these levels apparently still have a Boltzmann distribution (curves 1 and 2). This gives the values listed for the effective excitation cross sections of these levels. It is interesting to note that the effective excitation cross section of the resonance line of the barium ion is very large —greater than 5×10^{-16} cm². It is thus of the same order of magnitude as the excitation cross section of the alkali element resonance lines.

The authors take pleasure in expressing their gratitude to V. K. Prokof'ev for discussions concerning these results.

REFERENCES

1. A. D. Sakharov. Izvest Akad. Nauk SSSR, Ser. Fiz. 12, 372 (1948).
2. S. L. Mandel'shtam and N. K. Sukhodrev, Zhur. Eksptl. i Teoret. Fiz. 24, 6 (1953).
3. Yu. M. Kagan and N. P. Penkin, Izvest. Akad. Nauk SSSR, Ser. Fiz. 14, 721 (1950).
4. O. P. Semenova and V. V. Kokhanenko, Izvest. Akad. Nauk SSSR, Ser. Fiz. 14, 727 (1950).
5. D. B. Gurevich, V. K. Prokov'ev, and Iu. A. Snegirev, Trudy Vsesoyuz. Nauch.-Izzledovatel. Inst. Metrol., Sbornik 1, 51 (1958).
6. I. B. Podmoshenskii and L. D. Kondrasheva, Trudy X Konf. po spektr. (Proc. 10th Conf. on Spectroscopy), Vol. 2. Lvov, 1958.
7. A. Engel and M. Steenbeck, "Fizika gasovogo razryada" (The Physics of Gas Discharges). Moscow, 1936.
8. J. Aartz, Physica 20, 1250 (1954).
9. H. M. Crosswhite, Spectrochim. Acta 4, 122 (1950).
10. C. W. Allen, "Astrophysical Quantities." Univ. of London, Athlone Press, 1955.

A NEW DERIVATION OF EXPRESSIONS FOR INTERNAL VIBRATIONAL COORDINATES IN TERMS OF ATOMIC DISPLACEMENTS IN POLYATOMIC MOLECULES

L. A. Gribov (pp. 412-414)

Received 23 August 1960

In the theory of the vibrations of polyatomic molecules, a knowledge of the matrix for going over from the displacements of the atoms of the molecule from their equilibrium positions to the internal vibrational coordinates is required for the evaluation of the kinematic constant matrix T^{-1}, and also for the evaluation of the intensities of the normal vibrations and the atomic displacements in a vibration of a given form. The corresponding expressions have been repeatedly derived by various authors (see, for example, refs. 1 and 2) and have been partly gathered into tables. However, the existing derivations of these formulas, especially for the nonplanar and rotational coordinates, are marked by excessive complexity and insufficient perspicuity. It is therefore of definite procedural interest to give simpler derivations of the relationships just cited.

All vibrational motions of polyatomic molecules may be described, as is well known, with the help of the following vibrational coordinates: change in the bond lengths, change in the angles between bonds and between a bond and a plane, and change in the dihedral angles between planes passed through the atoms of the molecule. Thus it is necessary to express the stretching of a bond its rotation in space, and the rotation of a plane in terms of the displacements of the corresponding atoms. Let a bond be formed by two atoms 1 and 2, the positions of which are characterized by the radius vectors $\mathbf{a}_1$ and $\mathbf{a}_2$ drawn from a fixed coordinate origin. Let the length of the bond in the equilibrium state be $\bar{s}_{12}$, and its direction vector be $\mathbf{e}_{12}$. As is well known,

$$\mathbf{a}_2 - \mathbf{a}_1 = s_{12}\mathbf{e}_{12}.$$

Considering the atomic displacements during the vibrations to be small (we denote them respectively by $\mathbf{r}_1$ and $\mathbf{r}_2$) and differentiating, we obtain

$$\Delta\mathbf{a}_2 - \Delta\mathbf{a}_1 = \mathbf{r}_2 - \mathbf{r}_1 = \Delta\mathbf{r}_{21} = \Delta s_{12}\mathbf{e}_{12} + s_{12}\Delta\mathbf{e}_{12}. \qquad (1)$$

We find the stretching of the bond, $\Delta\bar{s}_{12}$, by scalar multiplication of the right and left sides of formula (1) by $\mathbf{e}_{12}$, and its angle of rotation within the plane of the equilibrium angle in the $\mathbf{f}_{23}$ direction ($\mathbf{f}_{23}$ is, as usual, the unit vector perpendicular to the bond and lying in the plane of the equilibrium angle) by scalar multiplication of the equality (1) by $\mathbf{f}_{23}$. Then (since $\Delta\mathbf{e}_{12} \perp \mathbf{e}_{12}$ and $\gamma_1 = \Delta\mathbf{e}_{12}\mathbf{f}_{23}/|\mathbf{e}_{12}|$)

$$\Delta s_{12} = q_{12} = \Delta\mathbf{r}_{21}\mathbf{e}_{12};$$
$$\Delta\mathbf{r}_{21}\mathbf{f}_{23} = s_{12}\Delta\mathbf{e}_{12}\mathbf{f}_{23} = s_{12}\gamma_1; \qquad \gamma_1 = \frac{\Delta\mathbf{r}_{21}}{s_{12}}\mathbf{f}_{23}. \qquad (2)$$

The total change in the equilibrium angle formed by the atoms 2, 1, 3 will equal

$$\gamma - \gamma_1 + \gamma_2 = \frac{\Delta\mathbf{r}_{21}}{s_{12}}\mathbf{f}_{23} + \frac{\Delta\mathbf{r}_{31}}{s_{31}}\mathbf{f}_{32}.$$

We shall characterize the position of the plane passing through the three atoms 1, 2, 3 by the vector $\mathbf{h} = [\mathbf{e}_{12} \times \mathbf{e}_{13}]$ normal to it. On displacement of these atoms from their equilibrium positions, the plane turns and the vector $\mathbf{h}$ changes its direction. The corresponding change in the vector is

$$\Delta\mathbf{h} = [\Delta\mathbf{e}_{12} \times \mathbf{e}_{13}] + [\mathbf{e}_{12} \times \Delta\mathbf{e}_{13}].$$

Hence, substituting $\Delta\mathbf{e}_{12}$ and $\Delta\mathbf{e}_{13}$ from relation (1), we obtain

$$\Delta\mathbf{h} = \frac{1}{s_{12}}[\Delta\mathbf{r}_{21} \times \mathbf{e}_{13}] - \frac{1}{s_{13}}[\Delta\mathbf{r}_{31} \times \mathbf{e}_{12}] - \left(\frac{q_{12}}{s_{12}} + \frac{q_{13}}{s_{13}}\right)\mathbf{h}. \qquad (3$$

Formula (3) for the vector of the rotation of the plan serves as a basis for the derivation of expressions for the nonplanar vibrational coordinates in terms of the displacements of the atoms which form them. The angle of rotation of the plane around some axis, κ, will evidently be equal to the scalar product of $\Delta\mathbf{h}$ by the unit vector $\mathbf{g}$ perpendicular to $\mathbf{h}$ and to the axis of rotation of the plane, divided by $|\mathbf{h}|$. We shall choose the direction of the vector $\mathbf{g}$ such that it forms an acute angle wit the projection of $\Delta\mathbf{h}$ on the plane 1, 2, 3.

Then

$$|\mathbf{h}|\varkappa = \frac{1}{s_{12}}\mathbf{g}[\Delta\mathbf{r}_{21} \times \mathbf{e}_{13}] - \frac{1}{s_{13}}\mathbf{g}[\Delta\mathbf{r}_{31} \times \mathbf{e}_{12}]$$
$$= \frac{\Delta\mathbf{r}_{21}}{s_{12}}[\mathbf{e}_{13} \times \mathbf{g}] - \frac{\Delta\mathbf{r}_{31}}{s_{13}}[\mathbf{e}_{12} \times \mathbf{g}].$$

Expanding the vector products and introducing the unit vector $\mathbf{n} \parallel \mathbf{h}$, we finally obtain (taking into account that $\sin(\widehat{\mathbf{e}_{12}\mathbf{e}_{13}}) = \sin\theta_{23}$)

$$\varkappa = \frac{\Delta\mathbf{r}_{21}}{s_{12}}\frac{\sin(\widehat{\mathbf{e}_{13}\mathbf{g}})\,\mathbf{n}}{\sin\theta_{23}} - \frac{\Delta\mathbf{r}_{31}}{s_{13}}\frac{\sin(\widehat{\mathbf{e}_{12}\mathbf{g}})\,\mathbf{n}}{\sin\theta_{23}}. \qquad (4$$

Formula (4) provides a possibility of easily finding expressions for all possible nonplanar coordinates in terms of the atomic displacements. Let us illustrate this by a series of examples.

Change in the dihedral angle between planes when the axis of rotation (the edge of the dihedral angle) **coincides with the direction of one of the bonds** (Fig. 1). In this case the axis of rotation coincides with the direction of the 3—2 bond. The change in the dihedral angle formed by planes I and II during shifts of the corresponding atoms (coordinate χ) will be equal to the sum of the rotations of the two planes. Introducing the vectors $\mathbf{g}_1$ and $\mathbf{g}_2$ (Fig. 1), we obtain, according to formula (4),

$$\chi = \frac{\Delta\mathbf{r}_{12}}{s_{12}}\frac{\mathbf{n}_1}{\sin\theta_{13}} - \frac{\Delta\mathbf{r}_{32}}{s_{32}}\cot\theta_{13}\mathbf{n}_1 + \frac{\Delta\mathbf{r}_{43}}{s_{43}}\frac{\mathbf{n}_2}{\sin\theta_{24}} - \frac{\Delta\mathbf{r}_{23}}{s_{32}}\cot\theta_{24}\mathbf{n}_2$$

since

$$\sin(\widehat{\mathbf{e}_{23}\mathbf{g}_1}) = \sin(\widehat{\mathbf{e}_{32}\mathbf{g}_2}) = 1$$

and

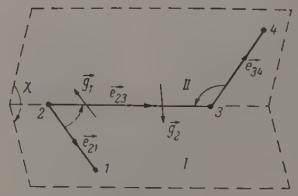

Fig. 1

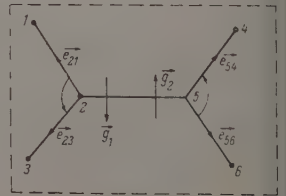

Fig. 2

$$\sin(\widehat{e_{21}g_1}) = \cos\theta_{23}$$

and

$$\sin(\widehat{e_{34}g_2}) = \cos\theta_{24}].$$

In a special case, all the bonds may lie in one plane. Then we obtain the coordinate of the out-of-plane bending of the 3—4 bond by setting $n_1 = n_2$ and $g_1 = g_2$.

Coordinate of the rotation of two planes around a common axis which coincides with none of the bonds. The coordinates of the rotation of the CH_2 planes around the C=C bond in the ethylene molecule are a common case of this sort. According to formula (4), we obtain (Fig. 2)

$$= \frac{\Delta r_{12}}{s_{12}} \frac{\cos\theta_{35}}{\sin\theta_{13}} n - \frac{\Delta r_{32}}{s_{32}} \frac{\cos\theta_{15}}{\sin\theta_{13}} n + \frac{\Delta r_{65}}{s_{65}} \frac{\cos\theta_{24}}{\sin\theta_{46}} n - \frac{\Delta r_{45}}{s_{54}} \frac{\cos\theta_{26}}{\sin\theta_{46}} n$$

[since $\sin(\widehat{e_{21}g_1}) = \cos\theta_{15}$ etc.].

Bending of the 0—1 bond out of the 3—0—2 plane. The angle between the 3—0—2 plane and 0—1 bond during shifts of all the atoms is made up of the rotation of the plane around an axis perpendicular to the 0—1 bond and lying in the 3—0—2 plane, and the rotation of the 0—1 bond around the same axis. In this case, the vector g

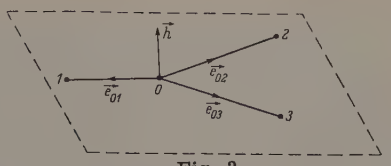

Fig. 3.

coincides with the direction of the 0—1 bond. Then the corresponding coordinate will equal (Fig. 3)

$$\rho' = \frac{\Delta r_{30}}{s_{30}} \frac{\sin\theta_{12}}{\sin\theta_{23}} n - \frac{\Delta r_{20}}{s_{20}} \frac{\sin\theta_{13}}{\sin\theta_{23}} n + \frac{\Delta r_{10}}{s_{10}} n.$$

REFERENCES

1. M. V. Vol'kenshtein, M. A. El'yashevich, and B. I. Stepanov, "Kolebaniya molekul" (Molecular Vibrations), Vol. 1. Gosudarst. Izd. Tekh.-Teoret. Lit., Moscow-Leningrad, 1949.
2. E. Wilson, J. Decius, and P. Cross, Molecular Vibrations: Theory of Infrared and Raman Spectra. Izd. Inostrannoi Lit., Moscow, 1960. McGraw-Hill, New York, 1955.

INFRARED ABSORPTION SPECTRA OF SYNTHETIC ALUMINATES OF THE ALKALI AND ALKALINE-EARTH METALS

V. A. Kolesova (pp. 414-417)

Received 10 September 1960

One of the manifestations of the amphoteric nature of aluminum is the ability of this element to enter, on the one hand, into the anionic framework of silicate crystals, isomorphously replacing Si atoms therein, and, on the other hand, to enter the lattice of many silicates in the capacity of a cation, replacing in this case atoms of the alkali and alkaline-earth elements.[1]

Study of the infrared absorption spectra of crystalline and glassy Al-containing silicates, and also of some aluminates,[2-4] has led us to the conclusion that the partially covalent Al—O bond which exists in the case when Al atoms isomorphously replace Si atoms in the crystal lattice or the glass network appears in the spectrum in the region 760-800 cm^{-1}. In view of the fact that the number of Si^{4+} ions replaced by Al^{3+} ions does not exceed one-half in the aluminosilicate lattice, it is easy to understand that, in this case, we are dealing with manifestations of the Al—O—Si link in the vibrational spectrum: Al—O—Al bonds do not arise in such crystal lattices and the AlO_4 tetrahedra are, so to speak, separated from one another by Si—O bonds. Among natural minerals, no compounds are known in whose crystal lattice a complex anion formed by linked AlO_4 tetrahedra would exist. However, such crystals can easily be synthesized in the laboratory. The investigation of crystalline aluminates with complex polymeric three-dimensional anions of the type $(AlO_4)_\infty$ should give a possibility of studying the spectroscopic manifestation of the Al—O—Al bond, which would enable us to establish more reliably the manifestation of the Al—O bond in the spectra of Al-containing crystals of more complex composition, especially in the spectra of aluminosilicates.

We have synthesized monoaluminates of the following compositions: $LiAlO_2$, $KAlO_2$, $RbAlO_2$, $CaAl_2O_4$, $BaAl_2O_4$. All the compounds were identified on the basis of their known interplanar distances.[5,6] We did not find in the literature any data on the interplanar distances of rubidium monoaluminate, in which connection we present here a table of the d values obtained by us for $RbAlO_2$ (Table 1).

Table 1. Interplanar Distances, d, and Intensities, I, in the Reflections of Crystalline $RbAlO_2$

No.	d (A)	I	No.	d (A)	I
1	4.597	w	10	1.825	w
2	3.468	w	11	1.797	w
3	3.11	m	12	1.617	vs
4	2.828	vs	13	1.526	w
5	2.79	vs	14	1.403	m
6	2.669	w	15	1.252	m
7	2.392	vs	16	1.143	vw
8	2.282	w	17	1.058	m
9	1.985	m	18	0.936	w

The crystal lattices of sodium, potassium, calcium, and barium monoaluminates are formed by AlO_4 tetrahedra joined at the corners by shared oxygen atoms. The uninterrupted linkage of such tetrahedra produces a three-dimensional structure analogous, in the spatial location of the atoms, to the structure of cristobalite or tridymite.[7-10] The Al—O distances amount to: 1.66 A in $KAlO_2$,[7] from 1.68 to 1.82 A in $CaAl_2O_4$, and 1.79 A in $BaAl_2O_4$, and consequently the dimensions of the AlO_4 tetrahedra exceed, in the general case, the dimensions of SiO_4 tetrahedra (the Si—O distance equals 1.60 A). We have found no information in the literature on the spatial location of the atoms and the interatomic distances in the crystal lattices of $LiAlO_2$ and $RbAlO_2$.

The infrared absorption spectra of all the aluminates

synthesized, and also of sodium monoaluminate, the spectrum of which has previously been presented,[2] were obtained in the region 420-1500 cm^{-1} on a VIKS-M3 vacuum spectrometer with an NaCl prism and an ISP-14b spectrometer with a KBr prism. The samples for study were prepared either in the form of transparent discs pressed from a mixture of the investigated substance with KBr, or in the form of a suspension in paraffin oil. The spectra obtained by us are presented in the Figure, and the spectral frequencies are collected in Table 2.

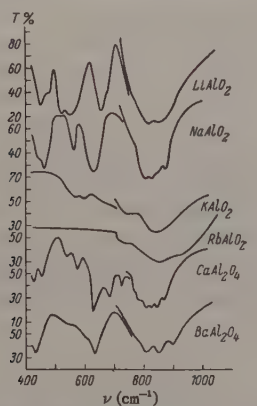

Infrared absorption spectra of the crystalline aluminates of Li, Na, K, Rb, Ca, Ba.

It is noteworthy that the highest-frequency band in the spectra of all the aluminates studied is a band in the 800-900 cm^{-1} region which possesses in every case, except for potassium and rubidium aluminates, a well-marked structure with sharp maxima (in the spectra of $KAlO_2$ and $RbAlO_2$, the band is very much "washed out" and the maxima on it are weakly marked.)* This intense and complex band is apparently the band of a vibration of the $(AlO_4)_\infty$ framework which is genetically associated with the trebly degenerate valence vibration $\nu_3(F_2)$ of the AlO_4 tetrahedron. In the case of the aluminosilicates, we associate the corresponding vibration with the characteristic absorption in the 760-800 cm^{-1} region,[2] and we assume that the elevation of the frequency in the spectra of the aluminates is brought about by the transition from the Al—O—Si bond system to the Al—O—Al system.

The circumstance that the highest-frequency bands in the spectra of lithium and rubidium aluminates lie in the same frequency range as the bands of the other aluminates investigated in this work permits us to propose a structure with highly polymerized aluminum-oxygen $(AlO_4)_\infty$ frameworks for $LiAlO_2$ and $RbAlO_2$ also.

*In addition to the bands presented, one also observes in the spectra of certain aluminates bands due to vibrations of the NO_3^- or CO_3^{2-} ions (1380 and 1450 cm^{-1} respectively) of the starting materials (nitrates or carbonates) which have remained partially undecomposed in the course of the synthesis. These bands are not considered here.

Table 2. Frequencies (in cm^{-1}) of the Bands in the Infrared Absorption Spectra of Crystalline Aluminates

$LiAlO_2$	$NaAlO_2$	$KAlO_2$	$RbAlO_2$	$CaAl_2O_4$	$BaAl_2O_4$
452	443	—	—	426	430
474	464	—	—	454	—
520	518	—	—	536	—
550	562	568	—	574	550
—	—	596	—	628	610
—	628	—	—	635*	634
653	638	—	—	685	—
675*	—	680	—	724	—
770*	768*	750	740	768	780
815	804	—	—	785	—
—	826	—	—	806	810
855	840	842	850	822	—
—	874	—	920	842	850
—	—	—	—	868	900

Note. Unresolved maxima on the slopes of the bands are designated by an asterisk.

In conclusion, we note that the difference in the position of analogous bands in the spectra of aluminates and silicates with the same degree of polymerization of the anionic frameworks (1190-1200 cm^{-1} for the highly polymeric silicates—quartz, cristobalite, and tridymite[11]—and 800-900 cm^{-1} for the aluminates) may be laid principally to the account of the difference in the force constants f(Si—O) and f(Al—O). Here the higher value of the constant for the Si—O bond in comparison with the constant for the Al—O bond is in accordance with the known data on the degree of covalency in the bonds under discussion.

REFERENCES

1. A. G. Betekhtin, "Mineralogiya" (Mineralogy). Gosgeolizdat, Moscow, 1950.
2. V. A. Kolesova, Opt. i Spektr. 6, 38 (1959), Optics and Spectroscopy 6, 20 (1959).
3. V. A. Kolesova and Ya. I. Ryskin, Opt. i Spektr. 7, 261 (1959), Optics and Spectroscopy 7, 165 (1959).
4. V. A. Kolesova, Stroenie stekla (The structure of glass), Trudy III Soveshchaniya po stekloobraznomu sostoyaniyu (Proc. III Conf. on the Glassy State). Izd. Akad. Nauk SSSR, Moscow-Leningrad, 1960.
5. F. Hummel, B. Sastry, and D. Wotring, J. Am. Ceram. Soc. 41, 88 (1959).
6. Alphabetical and numerical indexes of x-ray diffraction patterns, American Society for Testing Materia 1953.
7. T. F. Barth, J. Chem. Phys. 3, 323 (1935).
8. S. Wallmark and A. Westgren, Arkiv Kemi, Mineral. Geol. 12B, 1 (1937).
9. M. J. Buerger, Am. Mineralogist 39, 600 (1954).
10. M. W. Dougill, Nature 180, 292 (1957).
11. V. A. Florinskaya and R. S. Pechenkina, Doklady Akad. Nauk SSSR 85, 1265 (1952);
N. A. Sevchenko and V. A. Florinskaya, Doklady Akad. Nauk SSSR 109, 1115 (1956).

THE INFRARED ABSORPTION SPECTRUM OF SILVER OXIDE

E. F. Gross and F. I. Kreingold (pp. 417-418)

Received 23 September 1960

It is well known that silver oxide Ag_2O is isomorphous with cuprous oxide, and that the lattice constants of the two materials are nearly the same, namely, 4.69 and 4.26 A respectively. Ag_2O, like Cu_2O, is a p-type semiconductor; we can therefore expect similarities in the properties of the two substances. The literature does not contain much information on the physical and, in particular, on the optical properties of Ag_2O, whereas Cu_2O has been studied extensively. This can be explained by the great difficulty encountered in obtaining single crystals of Ag_2O. It is well known that Ag_2O begins to decompose even at 300°C and normal pressure; the melting point of the material is 815°C. At this temperature, the oxygen pressure should be 4625 atm.[2]

The work reported here is an investigation of the infrared absorption spectrum of Ag_2O. An investigation in the infrared region enjoys the advantage that powders can be used[3] and here the samples can be prepared by compressing Ag_2O powder. The actual samples studied were between 10 and 100μ thick. The Ag_2O powder was obtained by the reaction of silver nitrate with alkali.[4] The Ag_2O precipitate which resulted from this reaction was washed in running distilled water and dried at 80°C. In order to prevent photodecomposition of Ag_2O, this reaction and all the subsequent operations were performed under red light. We also used chemically pure, commercial grade Ag_2O. The measurements were made in the 410 to 1500 cm^{-1} region with the help of the IKS-6 and IKS-14 infrared spectrometers.

Three absorption bands were found in the infrared spectrum of Ag_2O in the spectral region under study: there were two narrow bands at 1073 cm^{-1} (9.3μ) and 802 cm^{-1} (12.5μ) and a broad band with a maximum at 530 cm^{-1} (19μ). We compared these results with the infrared absorption spectrum of Cu_2O, which had been studied in detail by Pastrnyak.[5] Since the Ag_2O spectrum should be displaced toward longer wavelengths with respect to the Cu_2O spectrum, the bands at 1073 and 802 cm^{-1} could be compared to the 1124 and 848 cm^{-1} bands of Cu_2O, respectively. In fact, a calculation of the position of the absorption bands of Ag_2O corresponding to the 1124 and 848 cm^{-1} bands of Cu_2O leads to the values 1080 and 812 cm^{-1}. The disagreement with the experimental data is insignificant and can probably be explained by the fact that the lattice constants of Ag_2O and Cu_2O differ. It must be noted that the absorption bands of Ag_2O are considerably narrower than the corresponding bands in Cu_2O. The wide Ag_2O absorption band with a maximum at 530 cm^{-1} has an absorption constant greater than 10^3 cm^{-1} and can therefore be compared to the intense Cu_2O absorption bands whose center of gravity is at 630 cm^{-1}. The band at 530 cm^{-1} is displaced further toward the longer wavelengths than the bands at 802 and 1073 cm^{-1}.

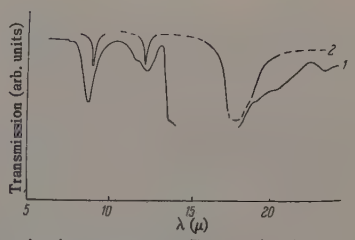

Transmission curves. Curve 1—Cu_2O; curve 2—Ag_2O.

Thus from this comparison of the Ag_2O and Cu_2O spectra (see the Figure) it is evident that the various absorption bands are displaced to different extents as a result of the transition from one material to the other. Furthermore, it is abundantly clear that in going from Cu_2O to Ag_2O, the absorption bands are narrowed considerably. Our results can be explained by assuming that there are nonpolar bonds in both Ag_2O and Cu_2O, but that the fraction of bonds with homeopolar components is larger in Ag_2O. This result is in agreement with the results in other publications.[6,7] In the previously cited work of Pastrnyak, special attention was given to the band at 8.9μ. On the basis of a series of experiments, Pastrnyak came to the conclusion that this band was associated with lattice vibrations. When we compare the absorption spectra of Cu_2O and Ag_2O, we see that the absorption 8.9μ band in Cu_2O corresponds to the 9.3μ band in Ag_2O, if the mass of Cu is replaced by that of Ag, which is direct proof of the vibrational nature of these bands.

REFERENCES

1. R. G. Wyckoff, Am. J. Sci. **3**, 184 (1922).
2. H. Hennig, Z. Erzbergbau u. Metallhüttenw. **8**, 117 (1955).
3. Zh. Lekont, "Infrakrasnoe izluchenie" (Infrared Radiation). Moscow, 1958.
4. M. M. Pavlyuchenko and E. Gurevich, Zhur. Obshchei Khim. **21**, 467 (1951).
5. I. Pastrnyak, Opt. i Spektr. **6**, 107 (1959), Optics and Spectroscopy **6**, 64 (1959).
6. J. Sherman, Chem. Revs. **11**, 107 (1932).
7. F. Weichman, Phys. Rev. **117**, 998 (1960).

THE RAMAN SPECTRUM OF TITANITE (SPHENE) $CaTiOSiO_4$

Ya. S. Bobovich (pp. 418-420)

Received 29 September 1960

Structural determinations of glassy substances can often be substantially simplified by a simultaneous study of their crystalline analogues. For this reason, this investigation was devoted to obtaining the Raman spectrum of titanite, which so far as is known, has not been described in the literature to date. The samples of the mineral were comparatively small, translucent, yellowish crystals from various sources.* This made it necessary to use experimental cells specially constructed for studies of powders, as shown schematically in Fig. 1. The crystals of the mineral were glued to the outer surface of a glass cone covered with picein. In order to decrease parasitic scattering at the "sample-air" boundary, the cone was immersed in water, which filled the cylindrical glass cell. The spectrum was intensified somewhat by silvering the front part of the glass tube in order to increase internal reflection. The spectral apparatus consisted of a double monochromator and a photoelectric recorder (DFS-12). The spectrum of titanite is shown in Fig. 2a. The Table gives the precise values of the frequencies and the relative intensities of the bands.

*The author is very much indebted to O. M. Rimskii-Korsakov for kindly giving him crystals from the museum of the mineralogy department of Leningrad State University for this investigation.

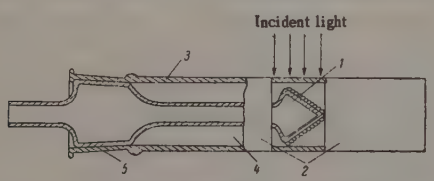

Fig. 1. Schematic diagram of the experimental cell for observing the Raman spectra of powders. 1—Cone with the material under study; 2—external silvering; 3—glass tube; 4—immersion; 5—joint.

According to Schiebold,[1] titanite is related to the silicates which have the so-called island structure. On the basis of this hypothesis, Schaffer, Matossi, and Wirtz[2] in turn hypothesized that vibrations of isolated SiO_4 tetrahedra should be evident in the vibration spectrum of titanite. These workers attributed the bands which they found in the 945-875 and 570 cm^{-1} regions to two such vibrations (triply degenerate and active in the infrared spectrum).

If the interpretation offered in ref. 2 is correct, then by analogy with known tetrahedral molecules and ions, the totally symmetrical vibration band should occupy an intermediate position between 945-875 and 570 cm^{-1}. As is evident from Fig. 2 and the Table, the most intense band in the Raman spectrum actually has a frequency of 605 cm^{-1}, i.e., it satisfies the requirements indicated above. Nevertheless, such an agreement should not in any case be taken as proof of Schiebold's hypothesis. This follows from the almost complete identity between the spectra of titanite and rutile,[3] indicating that all of the observed bands, including the one at 605 cm^{-1}, are associated mainly with vibrations of the Ti—O bonds. The latter are

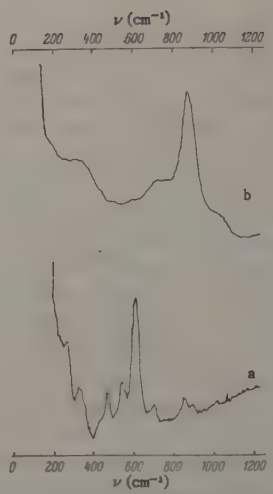

Fig. 2. Raman spectra of titanite $CaTiOSiO_4$ (a) and a glass whose composition is 37 Na_2O-25 TiO_2-38 SiO_2 (b).

caused by the unusually high relative intensity of the Raman lines associated with titanium, and agree well with observations on the tetrachlorides of elements in Group IV of the periodic table.

Frequency and Intensity of Raman Lines of Titanate

Frequency (cm^{-1})	Intensity (rel. un.)
150—170	10
240	15
308	15
420	3
460	20
540	25
605	65
855	10
885	5

As an indication of how transition into the vitreous state affects the structure of a solid, Fig. 2b shows the spectrum of a glass which has a composition similar to titanite but which contains Na_2O in place of CaO. Judging for example, from the data for danburite and the corresponding borate glass,[4] which were similarly investigated this difference should not be important. As can be seen in Fig. 2, the spectra of the titaniferous glass and titanite do not coincide with each other. Consequently, there is no question but that the structures of these two materials are different. One should not be surprised at this. The x-ray investigation in ref. 5 showed that titanite consists of SiO_4, CaO_7, and TiO_6 polyhedra partially connected at the edges. According to Zachariasen's rules,[6] however, the polyhedra in a glass can only be connected at the corners. This means that the transition from titanite to glass is accompanied by a fundamental structural reorganization of the substance.

It is difficult to say anything definite about the nature of this structural reorganization at this time. In any case the data given in this paper do not contradict our previous

nterpretation of the spectrum of titaniferous glass;[7] this as based on the assumption that titanium has a coordiation number of 4 with respect to oxygen.

EFERENCES

. E. Schiebold, Ergeb. exakt. Naturw. 11, 560 (1932).
. C. Schafer, F. Matossi, and K. Wirtz, Z. Physik 89, 210 (1934).
3. P. S. Narayanan, Proc. Indian Acad. Sci. A32, 279 (1950); Ibid. A37 411 (1953).
4. Ya. S. Bobovich and T. P. Tulub, Proc. III All Union Conf. on Vitreous Substances, p. 138, Leningrad, 1959; Optiko-Mekh. Prom. No. 2, 9 (1960).
5. W. H. Zachariasen, Z. Kristallogr. 73, 7 (1930).
6. W. H. Zachariasen, J. Am. Chem. Soc. 54, 3841 (1932).
7. Ya. S. Bobovich and T. P. Tulub, Opt. i Spektr. 5, 663 (1958).

THE CONNECTION BETWEEN THE ABSORPTION SPECTRUM AND THE DEPENDENCE OF THE RAMAN SPECTRUM ON THE FREQUENCY OF THE INCIDENT LIGHT

L. N. Ovander (pp. 420-421)

Received 10 October 1960

Earlier the author,[1] using a specific model, established the proportionality between the intensity of Raman spectra, studied as a function of the frequency of the incident light, and the ordinate of the absorption spectrum. In the present study an example is chosen where this conclusion is not valid; i.e., it is not possible to extend the result obtained previously[1] to arbitrary systems.

The intensity of Raman scattering close to an absorption band is determined by the tensor

$$a_{xy} = \sum_{n'} \frac{M_{n_0}^{n'} M_{n'}^{n+1}}{\omega_n^{n'} - \omega + i\gamma}. \qquad (1)$$

Here we take only those terms which are significant close to the absorption band, and also the factor containing ω is omitted since it is assumed that within the limits of the absorption band the relative change of the frequency is not large. In order not to complicate the examination of the polarization properties we will assume that a_{xy} is a scalar quantity.

We will examine here complex molecules exhibiting continuous absorption bands. Having this in mind, it is expedient to examine $\omega_n^{n'} = \omega_1$ as a continuously changing quantity, and we will let $M_n^{n'} = M_c(\omega_1)$ and $M_n^{n+1} = M_1(\omega_1)$ be continuous functions of ω_r. If the motion of the electrons and the nuclei is examined in the adiabatic approximation then it is easy to show with a known degree of accuracy that $M_1(\omega_1) = kM_0(\omega_1)$, where k is a constant.

The frequency dependence of the Raman spectrum will be determined by the square of the quantity

$$a = k \int_{-\infty}^{\infty} \frac{M_0^2(\omega)\, d\omega}{\omega_1 - \omega + i\gamma} \qquad (2)$$

(keeping in mind that, within the absorption band $M_0(\omega_1) = 0$, the integration can be expanded to infinite limits) and the intensity of the absorption spectrum will be proportional to

$$I \sim M_0^2(\omega) \qquad (3)$$

(For simplicity M_0 is considered to be a large quantity.)

Already, from expressions (2) and (3), it is seen that there is no proportionality between the quantities I and a^2. We will pick as the simplest example of an absorption spectrum that depicted in part (a) of the Figure.

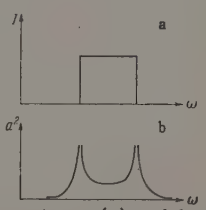

Absorption spectrum (a) and frequency dependence of the intensity of the Raman spectrum (b).

Assuming that γ is much smaller than the width of the absorption spectrum we will examine the limits of expression (2) for γ going to zero. Using the formula

$$\lim_{\gamma \to 0} \frac{1}{x + i\gamma} = P\frac{1}{x} - i\pi\delta(x),$$

where P is the symbol of the principle value and δ is a delta-function, we obtain the dependence of a^2 on ω as shown in part (b) of the Figure.

The example studied shows that, generally speaking, there is not proportionality between absorption and the intensity of Raman spectra.

REFERENCES

1. L. N. Ovander, Opt. i Spektr. 4, 555 (1958).
2. G. Placzek, "Releevskoe Rasseyanie i Raman-effekt" (Rayleigh Scattering and the Raman Effect). Ob'ed. Nauch.-Tekh. Izd., Narod. Komiss. Tyazh. Prom., Moscow, 1935.

EVENTS

CONFERENCE IN EAST GERMANY ON OPTICS AND SPECTROSCOPY AT ALL WAVELENGTHS

(pp. 423-424)

The annual conference on spectroscopy, "Optics and Spectroscopy at All Wavelengths," took place in Jena (East Germany) from 27 to 31 October 1960. The Conference was conducted by the Physical Society of East Germany.

Besides a considerable number of scientific workers from East Germany, scholars from Bulgaria, Hungary, Poland, Rumania, the USSR, Czechoslovakia, Yugoslavia, England, France, West Germany, and other countries were present at the Conference. From the Soviet Union, a delegation composed of P. A. Bazhulin, S. L. Mandel'shtam, A. R. Striganov, and S. E. Frish took part in the work of the Conference.

The Conference proceeded very actively and was of considerable scientific interest. At the opening, Prof. P. Görlich delivered a speech entitled "In Memory of Abbe, on the 55th Aniversary of His Death." Thereafter sessions were conducted in two sections in parallel, the first of which was devoted to spectroscopy, the second to various problems of physical and applied optics.

In the spectroscopy section, six sessions were held, covering some 35 papers devoted to various branches of atomic and molecular spectroscopy, Raman scattering of light, construction of spectral apparatus, etc. Some of the papers were reviews; some were accounts of individual experimental and theoretical work. The papers of workers at the Institute of Optics and Spectroscopy in Berlin (East Germany) on sensitized fluorescence and collisions of the second kind (R. Seiwert, G. Bunke, et al.) contained interesting new data. P. Jacquinot (France) gave an extensive and very interesting report on the Fourier method in spectroscopy, and B. Vodar (France) gave one on spectroscopic studies in the region of short ultraviolet rays. In T. A. Hoffman's paper (Hungary), the results of new investigations with the phototron by the author and his collaborators were presented (this is a device for amplification by means of "negative absorption" in the radiofrequency region around 10 mc). The report of H. Bartels (West Germany) was devoted to the problems of diagnosis of a plasma on the basis of spectroscopic data.

Soviet scientists gave the following papers: P. A. Bazhulin: "Shape and Width of Raman Lines"; S. L. Mandel'shtam: "Diagnosis of a Plasma by the Width and Shift of Spectral Lines"; A. R. Striganov: "Anomalies in the Isotopic Shift"; and S. E. Frish: "Spectroscopic Investigation of a High-Frequency Discharge in Neon."

Several papers were devoted to new spectral apparatus and methods of measurement in the infrared and ultraviolet regions. M. Schubert (Jena), together with his collaborators, presented a paper in which a description of a new spectrometer for work in the far infrared region was given. Schubert also discoursed on the influence of receiver noise on the accuracy of measurements. G. Geppert (Leipzig) reported on a new double-beam infrared spectrometer. R. Ritschl and L. Gutjahr (Berlin, East Germany) discussed the measurement of intensities in infrared vibrational bands.

There are very few papers devoted to spectral analysis. W. Körber and G. R. Rölling (East Germany) considered the question of the determination of minor impurities by photographic broadening of the image of spectral lines. A. C. Menzies (England) gave a long paper on the solution of analytical problems by the methods of flame photometry. A few papers relating to the x-ray region were given.

In the second section, a highly diverse set of problems was considered: microscopy, image contrast, geometrical optics, interferometry, optics of thin layers, photometry, and meterorological and physiological optics. A considerable number of these papers was given by workers at the Zeiss factory in Jena. Among the papers devoted to optics of thin layers, one should note the general paper of G. Polak (Jena) on the present state of theory and practice in the optics of thin layers, and two papers by G. Koch (Jena), one on the use of thin-layer interference phenomena in infrared spectrometry, and the second on the use of thin layers in multiple-beam interferometric devices.

During the Conference, there were several unofficial meetings which took place in a friendly and unconstrained atmosphere. At the end of the Conference, there was an excursion to Tautenburg (near Jena), where a large reflecting telescope with a mirror 2 meters in diameter, made by the Zeiss works, had been set up. The mounting of the telescope in a special well-arranged pavilion has been completed, and at the present time its adjustment is underway.

The proceedings of the Conference will be issued by the Physical Society of the German Democratic Republic (East Germany) in the form of a special collection.

The members of the Soviet delegation met with a most cordial reception on the part of the organizers of the Conference and the East German physicists, and also participated in a number of friendly and interesting meetings with Conference delegates from other countries.

S. F.

BOOK REVIEW

L. MARTIN: TECHNICAL OPTICS

(Translated from the English by M. V. Leikin under the editorship of G. G. Slyusarev.) Fizmatgiz (State Publishers of Physical-Mathematical Literature), Moscow, 1960. 424 pages, 269 figures, bibliography.

(pp. 424-425)

In 1960 the Russian literature on applied optics was enriched by the publication of the translation of "Technical Optics" by L. Martin. The work consists of two volumes published in England in 1948 and 1950, respectively. These two volumes represent an expansion of Martin's book "Introduction to Applied Optics" published in 1930 and translated into Russian in 1935 under the editorship of S. E. Frish.

The first volume differs little from the well known "Introduction to Applied Optics." The second volume is more interesting. In it the author describes contemporary optical instruments, and an outline is given of the more important recent achievements in optics, for example, the new viewpoints on image formation in a microscope, phase contrast in microscopy, recent theories on the nature of image quality using ideas on contrast, etc. Characteristic of the book is the description of optical systems with a detailed treatment of the question of correction of aberrations.

The first chapter deals with the magnification of various optical systems and describes the more common types of magnifiers (i.e., simple microscopes). A shortcoming of this chapter is the absence of sufficient rigor in the development of the ideas of geometrical optics. For example, on page 9 the author, using paraxial optics, derives a relation for the image size and states that for larger field angles the angles appearing in this equation must be replaced by their tangents. In an annotation, the translation editor remarks, quite correctly, that it is not permissible to talk about "large angles" in the paraxial region since this can lead to misunderstandings, or even to errors.

The second chapter is devoted to telescopic systems. It deals, primarily, with astronomical refractors and reflectors. Periscopes, cystoscopes, and sighting instruments are described very briefly. Rotating prism systems are described in detail, and methods are indicated for the determination of their properties. Telescopic oculars are also described in detail, including their interaction with the eye of the observer.

The third chapter deals with the microscope. Among others, it discusses such topics as the design of microscope objectives and the question of magnification and resolving power of a microscope. The author discusses in detail the role of microscopic illumination in the formation of images of thin structures. The problem of viewing transparent phase objects is discussed in special detail and the phase contrast method is explained in popular terms. The conditions of dark field viewing are also described in detail. Ultraviolet microscopy and investigations in polarized light are discussed only very briefly.

It is regrettable that in the annotations to this chapter the translator and the translation editor did not report on the work of Russian scientists in the area of ultraviolet microscopy and the development of interference microscopes for viewing transparent objects.

The fourth chapter discusses questions of binocular vision and binocular instruments. The treatment includes a consideration of recent theories of stereoscopic vision.

The fifth chapter is devoted to photographic objectives. No really new material is included in this chapter, despite its large size. However, the data on recently developed types of photographic objectives are valuable. Also given are a large number of useful annotations by the translation editor, which are actually corrections and refinements of the original text.

The sixth chapter deals with photometry of optical systems and image projection. In addition to the conventional material the chapter discusses in detail the Stiles-Crawford phenomenon and the question of night vision. Numerical examples which are given in the chapter to illustrate the application of the derived formulas are very useful for the assimilation of the material. The fundamentals of beacon lights and projection systems are very clearly explained.

The seventh chapter is devoted to testing of optical instruments. It describes visual and photographic methods of testing of optical systems, and various test targets, and discusses the effect of the photosensitive layer in photographic testing of the quality of optical instruments. It also describes methods of measuring the scattered light in optical systems, a problem to which much attention has recently been given. Various methods for investigating the aberrations of optical systems, some of which are new, are also discussed and described in detail.

The eighth chapter is devoted to questions of the manufacture and application of aspheric surfaces. These questions are rarely discussed in the current literature although aspheric surfaces are more and more used in practice. A number of new optical systems are described in this chapter, for example, the systems of Maksutov, Schmidt, Baker, Gabor, and others. The theory of the Scmidt camera is discussed. Methods for making aspheric surfaces are indicated, and schematics of the required machines are given together with an explanation of the principles of their operation.

Included in the book are appendices on the theory of diffraction gratings, the theory of the longitudinal chromatic aberration of a thin lens system in air, and the design of components for certain photographic objectives.

The book does not attempt to include all optical instruments. Only an incomplete description is given of a large group of military instruments, terrestrial telescopes, binoculars, and others. Geodetic instruments are not mentioned at all, and too little is said about various types of microscopes. Descriptions of such important instruments as photometers, colorimeters, and spectroscopic systems are missing completely.

Inaccuracies are frequently encountered in the book. However, most of these are pointed out in the annotations by the editor of the translation.

Despite these shortcomings the book is of considerable interest to the Russian reader, since it contains a great deal of original and useful material which is, in part, little known. Martin's book should generally be considered as one of the better books on applied optics. The translation is excellent, and the work of both the editor and the translator is commendable.

A. N. Zakhar'evskii

ANNIVERSARY

SERGEI IVANOVICH VAVILOV

(24 March 1891-21 January 1951)

(pp. 426-428)

This year marks the 70th anniversary of the birth and the 10th anniversary of the death of the outstanding Soviet physicist Sergei Ivanovich Vavilov. Sergei Ivanovich's life was short but his contribution to science and his activities in the organizing of Soviet science will never be forgotten.

Vavilov's reputation was firmly established in science in 1912, when his first papers on luminescence received wide attention. Before that time, luminescence had been one of the least developed fields of optics, only casually mentioned in the most comprehensive textbooks of physics. While still quite young, Sergei Ivanovich was able to evaluate the scientific importance of luminescence and to foresee its practical value. On the basis of the quantum theory, just previously developed, Vavilov soon established several important laws of luminescence.

In those years, both in Russia and abroad, the optics of atoms and simple diatomic molecules was being successfully developed. By his luminescence studies, S. I. Vavilov initiated the development of the difficult field of the spectroscopy of complex molecules.

His characteristic energy attracted several young colleagues to his work, and in the early thirties he created two luminescence laboratories: in the State Optical Institute and in the P. N. Lebedev Physical Institute of the USSR Academy of Sciences. S. I. Vavilov was the head of these laboratories until his death, and in these, and in several others, important developments in the science of luminescence and its application to the nation's economy were completed during his lifetime.

S. I. Vavilov paid most attention to the kinetics of luminescence, that is, the study of the processes occurring during the lifetime of the excitation centers. In this work Sergei Ivanovich utilitzed several basic characteristics of luminescence: the yield, the lifetime, and the polarization of the light. Experimental studies were usually rounded off by the construction of a theory of the phenomenon. His ideas on energy migration in solutions and diffusive fluorescent quenching are firmly established in modern luminescence theory; and work on the kinetics of phosphorescence carried out by his colleagues under his direction was important in the creation of the modern conception of the kinetics of the phosphorescence of crystal phosphors. An intense program of work on the kinetics of luminescence was undertaken in the late thirties and the succeeding years, and led Sergei Ivanovich to the task of creating new methods and instruments for studying the kinetics of fast processes. The outcome was a group of first class instruments such as the fluorometer, the taumeter, the ultrataumeter, etc.

Although research on the kinetics of luminescence was a major part of the work of Vavilov himself and his students, perhaps the polarization of luminescence was closest to his heart. Vavilov created the well-known "polarization diagram" method which makes it possible to estimate the nature of the elementary radiators; he discovered polarization spectra giving important information on molecular structure and, as already mentioned, he made wide use of polarization methods for studying the kinetics of luminescence. It may be said that S. I. Vavilov, his colleagues, and his students founded the modern science of the polarization of the luminescence

of solutions and crystals. Among the early spectroscopic research by S. I. Vavilov, and from his laboratories, we should mention the comparison of the spectra of long-term and short-term luminescence of organic phosphors, the establishment of the law of mirror symmetry in luminescence and absorption spectra of complex molecules, and the study of the luminescence spectra under anti-Stokes excitation. Later, in connection with the theory of molecular spectra and the technique of spectroscopic measurements, Sergei Ivanovich prompted a large-scale study of uranyl salt spectra, phosphorescence spectra of benzol and its derivatives, rare-earth spectra, luminescence spectra of crystal phosphors, and the luminescence spectra of homologous series of organic compounds.

S. I. Vavilov did not recognize a distinction between "theoretical" and "applied" science. His role in organizing and leading the creation of a manufacturing technology for fluorescent lamps in the USSR and in bringing them into production is well known. It may be of interest to mention that Sergei Ivanovich had raised the question of creating a fluorescent lamp in the early thirties, when he had only a small group of workers at the Institute of Physics of Moscow State University.

Later, under S. I. Vavilov's leadership, luminescent compounds for fluorescent lamps and for many other purposes were developed in the laboratories and a great deal of work was done on luminescent analysis. Methods and apparatus for ultraviolet and luminescent microscopy were also developed as well as new methods and apparatus for the study of luminescence as already mentioned. S. I. Vavilov's work on the creation of the science of luminescence and the work of his group on producing fluorescent lamps were awarded Stalin prizes.

The Soviet school of luminescence founded by S. I. Vavilov continues to work in all the directions that he indicated. New trends, also, in the study and application of luminescence arise and develop rapidly. Without exaggeration we can say that, despite the great increase in the number of papers on luminescence appearing abroad, Soviet scientists continue to march with honor in the front ranks of luminescence research. Much credit for this is due to Sergei Ivanovich.

The Vavilov-Cherenkov effect was one of the most remarkable discoveries of the twentieth century. The history of this discovery is very instructive. Sergei Ivanovich drew attention to the fact that the universal fluorescence of liquids under the action of γ-rays, discovered by the Curies and called γ-luminescence by them, apparently did not obey the basic laws of luminescence. He assigned to his post-graduate student P. A. Cherenkov several experiments to elucidate the nature of this luminescence. These showed that the light observed was not in fact luminescence but was a new type of radiation caused, as was explained later, by electrons arising from the decay of the γ-rays and propagating in the medium with a velocity greater than the phase velocity of light. I. E. Tamm and I. M. Frank gave the complete theory of the phenomenon. The discovery of the Vavilov-Cherenkov effect was rewarded by the Stalin prize in 1944 and by the Nobel prize in 1958.

Sergei Ivanovich's great talent was concentrated on one branch of optics—luminescence. He personally, and others in his laboratory, carried out much work of basic importance to the science of light. Sergei Ivanovich examined critically the basic principles of physical optics: the superposition principle in the scattering of light beams and Bouger's law, stating that the absorption coefficient is independent of the incident light intensity. Searching for deviations from linear optics, he devised many incisive experiments. These experiments did not give clear indications of nonlinear effects in optics, although such indications were obtained later.

Research on the quantum nature of light with visual observations occupies a conspicuous place in the work of S. I. Vavilov and his students. This work was based on Sergei Ivanovich's theory of the phenomenon and two very interesting conclusions emerged: Firstly, the human eye is sensitive to a light flux of ten or twenty photons, when appropriately adapted; and secondly, in short period light flashes of mean brightness equal to the threshold sensitivity of the eye, it is possible to detect variations of the light flux caused by the quantum nature of light.

In discussing the work of S. I. Vavilov on physical optics, it is impossible to neglect the brilliant methods that he suggested for determining the nature of the elementary radiators by the interference of widely divergent light beams.

Sergei Ivanovich's work on quantum fluctuations of light, on nonlinear optics, and part of his work on luminescence, were included in his book "The Microstructure of Light," which won a Stalin prize.

S. I. Vavilov was one of the first natural scientists to be guided in his work by the method of Marxist-Leninist dialectic. His extraordinary ability, deep erudition in physics, high general culture, and intimate knowledge of the Marxist-Leninist classics enabled S. I. Vavilov to produce several papers devoted to philosophical analysis and based on the data of modern natural science.

A description of S. I. Vavilov's activities would be incomplete without mention of his many works on the history of science and his popular scientific papers and books. He translated into Russian Newton's "Optics" and "Lectures in Optics" and wrote a scientific biography of and several papers on this great scientist. Sergei Ivanovich also wrote many studies of the optical work of Lomonosov, Galileo, Euler, Petrov, and others. The brilliantly descriptive book "Eye and Sun" is still a model of popular scientific literature.

S. I. Vavilov's great work as president of the USSR Academy of Sciencies in organizing science in our country is well known. For many years he was the scientific head of the State Optical Institute, which now bears his name.

Sergei Ivanovich often repeated the well-known proverb "Ars longa, vita brevis." He himself strove to serve science every minute of his life. When he heard of his mortal illness his fear was that he would not be able to achieve what his knowledge and talents might have permitted.

S. I. Vavilov's whole life was a shining example of service to science and the Fatherland.

B. Sveshnikov

IMPORTANT NOTICE TO ALL READERS OF OPTICS AND SPECTROSCOPY

OiS CLUB SCHEME

The Optical Society of America has been translating Optika i Spektroskopiya and distributing this monthly journal free - thanks to an NSF grant - to all OSA members and subscribers to the Journal of the Optical Society of America. This free distribution was an experiment for three years, so that the individual reader might become accustomed to reading a translation journal not as an oddity but as a publication that is looked for each month in the same manner as is J. Chem. Phys., J. Am. Chem. Soc., etc. In December of this year the NSF grant ends, but the interest in Optics and Spectroscopy is now too lively for OSA to discontinue the translation, so they have evolved the OiS CLUB SCHEME.

Put simply, this is a special subscription rate for members of those societies who wish to take part in the OiS CLUB SCHEME, viz:

To OSA members ---------- $ 7.50
To members of the OiS Club ------- $11.00
To non-members ---------- $15.00

OSA is emphatic that if a translation journal is to be of real use (as is the case with any scientific journal) it should be read widely by all the people working in the field, and that these research results should be made available in the shortest possible time. OPTICS AND SPECTROSCOPY is published in English translation within three months of the Russian edition coming out e.g. the March 1961 issue will be published in English on June 10th. OSA is making this special offer to members of some sixty scientific societies across the English speaking world, and it asks the members of those Societies to write to their Society or directly to the Assistant Secretary, OSA, 1155 16th St., N.W., Washington 6, D.C. for further details or to send in their order. (see below)

ALL SUBSCRIBERS PLEASE NOTE that your subscriptions will start with the January 1962 issue which is published in English in March/April 1962 -- so don't start worrying when the January 1962 issue does not appear in that month!

ORDER FORM

To: OPTICS AND SPECTROSCOPY
Optical Society of America
1155 Sixteenth St., N.W.
Washington 6, D.C.

Please enter my/our subscription to OPTICS AND SPECTROSCOPY for one year commencing with the January 1962 issue (which will be published in April), at:

☐ Special OSA member rate $ 7.50

☐ Special rate to members of Societies cooperating in OiS Club Scheme $11.00

Name of your Society _____

☐ Non-members $15.00

☐ Please send OSA membership information

Membership no. _____

Name _____

Address _____

_____

FILLER MATERIAL - NOT IN RUSSIAN ORIGINAL

The Raman Spectrum of Titanite (Sphene) $CaTiOSiO_4$ . . . . . Ya. S. Bobovich 212 (418)
The Connection Between the Absorption Spectrum and the Dependence of the Raman Spectrum on the Frequency of the Incident Light . . . . . L. N. Ovander 213 (420)

EVENTS

Conference in East Germany on Optics and Spectroscopy at All Wavelengths 214 (423)

BOOK REVIEW

L. Martin: Technical Optics (Translated from the English by M. V. Leikin under the Editorship of G. G. Slyusarev.) . . . . . A. N. Zakhar'evskii 215 (424)

ANNIVERSARY

Sergei Ivanovich Vavilov . . . . . B. Sveshnikov 216 (426)

EDITOR'S NOTE

Comments on the scientific content of the translated Russian articles published in OPTICS AND SPECTROSCOPY are invited. They should be addressed as a Letter to the Editor of the Journal of the Optical Society of America and forwarded to the Editor of that journal, Dr. D. B. Judd, National Bureau of Standards, Washington 25, D. C.

UNIVERSITY OF ILLINOIS 3
LIBRARY
UNDERGRADUATE DIV
NAVY PIER GRAND AVE
CHICAGO 11 ILL

VOL. X, NO. 3 OPTICS AND SPECTROSCOPY MARCH 1961

CONTENTS

(Numbers in parentheses are original Russian page numbers.
These Russian page numbers are also quoted at the head of each paper.)

On the Quantum Theory of the Vavilov–Cherenkov Radiation Emitted by a Particle with a Magnetic Moment . . . A. B. Kukanov 147 (289)
Determination of the Nuclear Magnetic Moment of the Hg^{199} from the Hyperfine Structure of the HgI 5461 A Line . . . I. I. Agarbiceanu, L. Blanaru, V. Draganescu, N. J. Ionesco-Pallas, N. Komanichu, and V. Tatu 151 (297)
Determination of the Nuclear Magnetic Moment of Na^{23} from the Hyperfine Structure of the Absorption Lines D_1 and D_2 . . . V. Draganescu 152 (301)
Calculation of the Probability of Autoionization in He^- and Be^+ Ions . . . R. Kh. Propin 155 (308)
Study of the State of Krypton Behind a Shock Wave . . . A. P. Dronov, A. G. Sviridov, and N. N. Sobolev 157 (312)
Vibrational Spectra of Aromatic Compounds. VIII. Characteristic Vibrations of 1,2-Orthodisubstituted Benzenes . . . A. N. Bogomolov 162 (322)
Vibrational Spectra of Aromatic Compounds. IX. Theoretical Calculation of Intensities in the Infrared Spectra of Benzene and Certain Deuteriobenzenes . . . M. A. Kovner and B. N. Snegirev 165 (328)
The Theory of the Vibrational Spectra of Polymers. III. The Calculation and Interpretation of the Vibrational Spectrum of Polyethylene . . . Yu. Ya. Gotlib and L. V. Kudinskaya 168 (335)
The Hydrogen Bond in Acid Germanates I. The Infrared Spectrum of Strontium Dihydrogermanate . . . G. P. Stavitskaya and Ya. I. Ryskin 172 (343)
Second Order Raman Spectra of Alkali-Halide Mixed Crystals . . . A. I. Stekhanov and M. B. Eliashberg 174 (348)
Excitation Energy Transfer in Rigid Solutions of Organic Substances . . . I. M. Rozman 178 (354)
Nature of Binding in the Associated Molecules of Rhodamins 3B and 6G in Aqueous Solution and the Effect of Concentration and Temperature on Migration Quenching . . . E. G. Baranova and V. L. Levshin 182 (362)
Band Splitting in the Luminescence Spectra of Anisotropic Centers in LiF and CaF_2-Eu Crystals Subjected to Oriented Deformation . . . A. A. Kaplyanskii, N. A. Moskvin, and A. K. Przhevuskii 185 (368)
Determination of Electron Trap Depth in ZnS Phosphors by Flash Under the Action of Infrared Light . . . L. A. Vinokurov and M. V. Fok 188 (374)
Cotton-Mouton Effect in the Region of the Impurity Absorption of Light . . . A. F. Lubchenko 191 (379)
Theory of Multilayer Asymmetric Reflectors . . . P. G. Kard 193 (384)
On the Sensitivity of Emission Spectral Analysis . . . S. L. Mandel'stam and V. V. Nedler 196 (390)
The Plasmatron (Plasma Jet) as a Light Source for Spectroscopy . . . F. A. Korolev and Iu. K. Kvaratskheli 200 (398)
An Atomic Beam as Light Source for Studying Spectra of Gases . . . V. I. Odintsov 202 (403)

SHORT COMMUNICATIONS

The Distribution of Atoms Among the Excited Levels in a Low Pressure Arc . . . I. M. Belousova and D. B. Gurevich 206 (410)
A New Derivation of Expressions for Internal Vibrational Coordinates in Terms of Atomic Displacements in Polyatomic Molecules . . . L. A. Gribov 208 (412)
Infrared Absorption Spectra of Synthetic Aluminates of the Alkali and Alkaline-Earth Metals . . . V. A. Kolesova 209 (414)
The Infrared Absorption Spectrum of Silver Oxide . . . E. F. Gross and F. I. Kreingold 211 (417)

(Contents continued on inside back cover)